# DEVELOPMENT OF CARBON NANOTUBE INKS FOR PRINTED ELECTRONICS

# DEVELOPMENT OF CARBON NANOTUBE INKS FOR PRINTED ELECTRONICS

BY DIALIA RITAINE, M.Sc

A thesis submitted to the Department of Chemistry and Chemical Biology and the School of Graduate Studies of McMaster University in Partial Fulfilment of the Requirements for the degree of PhD in Chemistry

Ph.D. of Chemistry (2023) McMaster University
(Chemistry & Chemical Biology) Hamilton, Ontario, Canada

TITLE: Development of Carbon Nanotube Inks for Printed Electronics

AUTHOR: Dialia Ritaine

M.Sc., (Chemistry)

University of Strasbourg, France

SUPERVISOR: Professor Alex Adronov

PAGES: xxx, 228

## Lay Abstract

The objective of this thesis is to develop cleavable complexes between conjugated polymers and single-walled carbon nanotubes (SWNTs) to maximize the potential performance of printed devices post-processing. We functionalized a conjugated polymer with cleavable side-chains and investigated the impact on the conductivity after their removal. In addition, this work also focuses on dispersing SWNTs in green solvents that are compatible with printing processes such as inkjet printing. Lastly, we synthesized a degradable and water-soluble conjugated polymers to produce dispersant free-SWNTs.

## Abstract

Single-walled carbon nanotubes (SWNTs) have excellent electronic, mechanical, and optical properties that make them promising materials for various applications. However, SWNT production methods produce a mixture of semiconducting and metallic species and non-SWNT impurities limiting their incorporation into devices. Among the different purification methods, conjugated polymer sorting has proven to be a scalable and cost-effective method. Conjugated polymers can easily be tuned to disperse SWNT species and obtain solubility in target solvents. They are multifunctional structures that enable the purification and extraction of specific SWNTs while simultaneously enhancing their processability. Therefore, they are suitable as purification methods for the fabrication of SWNT-based devices, particularly for printed electronics. However, the polymer backbone and the non-conductive side-chains negatively impacts the performance of SWNT devices by preventing good contact between the nanotubes.

We first functionalized our polymer with thermally cleavable side-chains and demonstrated that the removal of the side-chains leads to a higher conductivity. We obtained stable dispersions in two green solvents compatible with inkjet printing. We also functionalized our polymer with photocleavable side-chains and showed efficient cleavage in solution. These investigations represent a proof-of-concept that could be used for the development of SWNT-based devices where the removal of the side-chains will improve the device performance.

Lastly, we synthesized a fluorene-based polymer that contains a photocleavable ortho-nitrobenzylether unit and is functionalized with hydrophilic side-chains. We demonstrated the degradation of the polymer in organic and aqueous solvents. These investigations highlight the challenges of dispersing SWNTs in aqueous solvents using conjugated polymer.

**Acknowledgements**

First, I would like to thank my supervisor Dr. Alex Adronov for the opportunity to work in his research group. The past five years have been a long and difficult challenge but Alex has always been an amazing support with my different projects but also on a personal level. He helped me to improve my skills and to be more confident. I am very grateful for these years in his lab.

I also would like to thank my committee members Dr. Jose Moran-Mirabal and Dr. Harald Stöver for their helpful feedback and advices during our meetings.

A special thanks to the Nierengarden group at the University of Strasbourg in France and particularly to Jean-François who recommended me for this Ph.D.

A big thanks to all my past and current coworkers. Dr. James Bodnaryk and Dr. Eric Meichsner for their help, guidance and training at the start of my Ph.D. Thank you to Dr. James Mayo for his help and precious advice on a professional and personal level. Thank you to Shagana Kukendran, Mokhamed Ranne, Anumta Amir, Dr. Sarah Salimi, Annika Yardy, Anumta Amir, Alexandra Ly, Ben Kertesz, Dora Yu, Daniel Hrabowyj, Billy Deng for their support and friendship.

Thank you to my parents, my siblings, my cousin Juliette, and my best friends Anaïs, Loane and Benoit. Being far from home is difficult but they were always supportive. I am lucky to have them in my life. I also want to thank my

little companion Yakko. A cute and lovely black cat that always wants to play and be petted between his naps. I am so happy to have him in my life. He helped me a lot during the stressful and anxious times.

## List of Abbreviations

| | |
|---|---|
| ALD | Atomic Layer Deposition |
| BWF | Breit Wigner Fano |
| CDI | Carbonyldiimidazole |
| $C_h$ | Chiral Vector |
| CoMoCAT | Cobalt-Molybdenum catalyst |
| Cm | Centimeter |
| cP | Centipoise |
| CP | Conjugated Polymer |
| CP-M | Metal-coordination polymer |
| CTAB | Hexadecyl(trimethyl)ammonium Bromide |
| CuAAC | Copper-catalyzed Azide-Alkyne Cycloaddition |
| CuO | Copper Oxide |
| CV | Column Volume |
| CVD | Chemical Vapour Deposition |
| Đ | Dispersity |
| Da | Dalton |
| DCM | Dichloromethane |
| DGU | Density Gradient Ultracentrifugation |
| DMF | Dimethylformamide |
| DMSO | DimethylSulfoxide |
| DNA | Deoxyribonucleic Acid |
| DOC | Sodium Deoxycholate |
| DOD | Drop-On-Demand |
| DOS | Density of States |
| DOSY | Diffusion-Ordered NMR spectroscopy |
| $D_t$ | Diameter |

| | |
|---|---|
| EDC.HCl | N-(3- dimethylaminopropyl)-N'-ethylcarbodiimide hydrochloride |
| $Et_2O$ | Diethyl Ether |
| EtOAc | Ethyl Acetate |
| FET | Field-Effect Transistors |
| FT-IR | Fourier - Transform Infrared spectroscopy |
| GO | Graphene oxide |
| GPC | Gel Permeation Chromatography |
| HCl | Hydrochloric Acid |
| HF | Hydrofluoric acid |
| HiPco | High-Pressure Carbon Monoxide Disproportionation |
| HOMO | Highest Occupied Molecular Orbital |
| HPLC | High-Performance Liquid Chromatography |
| IEC | Ion Exchange Chromatography |
| IoT | Internet of Things |
| Log | Logarithm |
| LUMO | Lowest Unoccupied Molecular Orbital Metallic |
| MeOH | Methanol |
| Min | Minute |
| mL | Mililiter |
| $M_n$ | Number-Average Molecular Weight |
| MS | Mass spectrometry |
| m-SWNT | Metallic Single-Walled Carbon Nanotube |
| $M_w$ | Weighted-Average Molecular Weight Multiwalled |
| MWNT | Multiwalled Carbon Nanotube |
| n,m | Integer Lattice Translations Indices for SWNTs |
| NBS | N-bromosuccinimide |
| nm | Nanometer |
| NMP | N-methyl-2-pyrrolidone |

| | |
|---|---|
| NMR | Nuclear Magnetic Resonance |
| OFET | Organic Field-Effect Transistor Organic |
| OPV | Organic Photovoltaic |
| P3HT | Poly(3-hexylthiophene) |
| PCPT | Poly(carbazole-co-terephthalate) |
| PDMS | Polydimethylsiloxane |
| PEDOT:PSS | Poly(3,4-ethylenedioxythiophene) Polystyrene sulfonate |
| PEG | Poly(ethylene glycol) |
| PEN | Polyethylene naphthalate |
| PE | Printed Electronics |
| PET | Polyethylene terephthalate |
| PF | Polyfluorene |
| PI | Polyimide |
| PL | Photoluminescence |
| PS | Polystyrene |
| R2R | Roll-to-roll |
| RBM | Radial Breathing Mode |
| RF | Radiofrequency |
| rGO | Reduced Graphene oxide |
| RT | Room Temperature |
| SCh | Sodium cholate |
| sc-SWNT | Semiconducting Single-Walled Carbon Nanotube |
| SDBS | Sodium Dodecylbenzenesulfonate |
| SDS | Sodium Dodecyl Sulfate |
| SEC | Size Exclusion Chromatography |
| SPAAC | Strain-Promoted Azide-Alkyne Cycloaddition |
| SWNT | Single-Walled Carbon Nanotube |
| TEGME | Triethylene glycol monomethyl ether |
| Tetraglyme | Tetramethylene glycol dimethyl ether |

| | |
|---|---|
| TFA | Trifluoroacetic Acid |
| TFT | Thin-Film Transistor |
| THF | Tetrahydrofuran |
| TTFV | Tetrathiafulvalene |
| UV-Vis-NIR | UltravioletVisible-Near-Infrared |

**Contents**

## List of Tables

## List of Figures

## List of Schemes

# Chapter 1

# The purification, characterization and application of Single-Walled Carbon Nanotubes

## 1.1 Introduction to carbon nanotubes

### 1.1.1 Geometry of SWNTs

Single-walled carbon nanotubes (SWNT) are cylindrical one-dimensional (1D) allotropes of carbon with diameters on the nanometer scale and lengths on the micrometer scale.[1] Their high aspect ratio and shape afford interesting thermal,[2–4] mechanical,[5,6] electronic[7,8] and optical properties[9–11] that can be used for multiple applications.[12–18] Depending on the production method, their dimensions can vary, resulting in diameters ($d_t$) ranging from ~0.4 to 3 nm.[1,19] In comparison to SWNTs, multi-walled carbon nanotubes (MWNTs), which are composed of multiple nested tubes or layers, are significantly larger with diameters up to ~30 nm.[19]

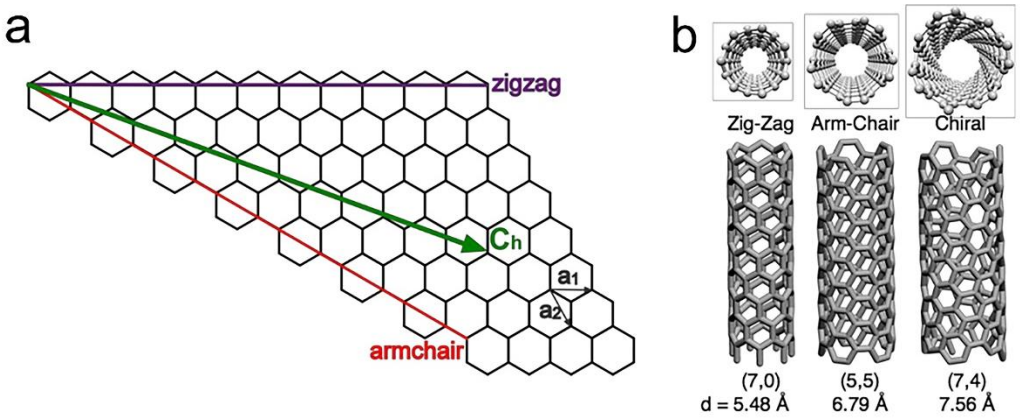


Figure 1.1. a) Graphene template with labelled unit vectors $a_1$ and $a_2$. b) Nanotube species and cross-sections with labelled chiral indices.

SWNTs can be pictured as a 2D graphene sheet that has been rolled up into a cylinder. Depending on how this graphene sheet is rolled up, different SWNT species can be formed as shown in Figure 1.1. These different species

are defined by their chiral vectors ($C_h$, green arrow) representing the circumference of a given SWNT species, and by their chiral angle (θ) which defines the angle between $a_1$ and $C_h$.[1] $C_h$ is generated by the addition of the unit vectors $a_1$ and $a_2$ on the graphene lattice and the SWNT species associated with this chiral vector can be specified using integer values (n,m) as shown in Equation 1.1.

$$C_h = na_1 + ma_2 = d_t\pi \quad (1.1)$$

The chiral angle of SWNTs is confined to values of 0 – 30°. The two extreme values of the chiral angle represent SWNTs that are achiral. If θ = 0° (m = 0), the SWNT is referred to as a "zig-zag" tube due to the zig-zag pattern around the periphery, while if θ = 30° (n = m), the SWNT is called "arm-chair". All the remaining SWNTs are chiral tubes.

### 1.1.2 Electronic structures of SWNTs

In comparison to 2D graphene which is a semimetal or zero-bandgap semiconductor,[20] the electronic structure of 1D SWNTs results in quantum confinement of their electron into discrete energy levels in the density of states (DOS) called van Hove singularities (Figure 1.2).[21] Depending on the π-overlap upon the "rolling", the valence π-band (HOMO) or the conduction π*-band (LUMO) may or may not possess an energy level barrier (band gap) resulting in SWNT species that are either semiconducting or metallic, respectively.[22]

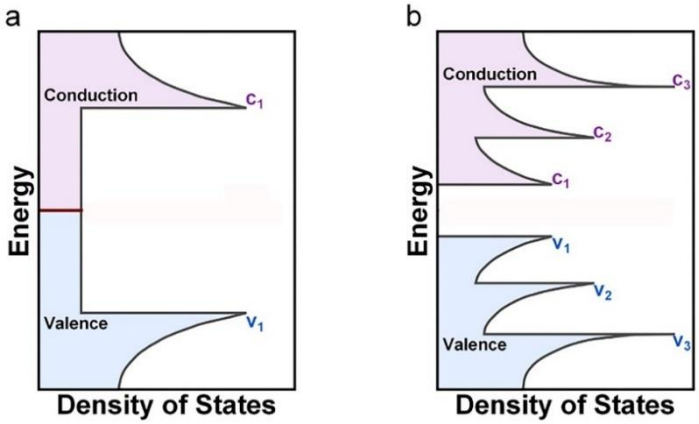


Figure 1.2. The density of states of a) metallic and b) semiconducting SWNTs.

The electronic and optical properties of SWNTs depend on their structure and vary with diameter and chiral angle.[22] Therefore, if the integer values (n,m) are known, it is possible to determine the electronic (semiconducting or metallic) nature of the tube.[23] Any SWNT species that satisfies the equation, $|n - m| = 3q$, where q = 0, 1, 2, 3, etc. are metallic tubes (m-SWNTs). Therefore, all the arm-chair tubes ($\theta = 30°$ and n = m) possess metallic character. For SWNTs where $n \neq m$, the tubes are referred to as semi-metallic because they have a small curvature-induced band gap (~1 – 100 meV).[24] However, to minimize the confusion and because these semimetallic SWNT species have similar electronic characteristics, they are considered metallic. Semiconducting SWNTs (sc-SWNTs) possess different band gaps (~ 0.5 – 1.0 eV)[22,25] that have an inverse relationship with the tube diameter. Overall, it can be stated that one-third of all SWNTs species are metallic, and the remaining two-thirds are semiconducting.

## 1.2 Synthesis of Carbon Nanotubes

The first carbon nanotube synthesis was achieved and published in 1991 by Sumio Iijima[26] who successfully prepared MWNTs using the arc-discharge method, followed by the synthesis of SWNTs two years later.[27] Significant progress has been made to improve and extend our knowledge of these carbon-based materials. Several methods are now used, including arc-discharge,[28] laser ablation,[29] chemical vapor deposition (CVD),[30] high-pressure carbon monoxide disproportionation (HiPco),[31] cobalt-molybdenum catalyst (CoMoCAT),[32] and plasma-torch growth.[33] These different techniques allow the production of SWNTs with various diameter ranges and therefore different thermal and electronic properties.[32] Ideally, the ultimate objective for the production of SWNTs would be the isolation of a single chirality, however, this objective is extremely difficult to achieve. The production of SWNTs using the different techniques mentioned above produces a heterogeneous mixture of SWNT along with impurities such as amorphous carbon and leftover metal catalysts.

### 1.2.1 Arc-discharge

This technique is one of the oldest ways to produce SWNTs. Two graphite electrodes are placed into a pressurized chamber filled with an inert gas (such as argon or helium). The cathode is impregnated with a metal catalyst such as iron, cobalt or nicked.[28] When the current is applied between the two electrodes, a carbon vapour is produced that can adsorb onto the metal catalyst, which subsequently results in the growth of SWNTs. SWNTs typically

produced using this technique have a diameter between 1.2 – 1.4 nm (matching catalyst dimensions) but tend to be shorter than those produced with other synthesis methods.[32]

### 1.2.2 Laser ablation

Laser ablation was first used in 1995 to produce SWNT.[29] In this method, a pulsed laser is used to vaporize a graphite substrate (containing small amounts of catalysts such as nickel or cobalt) in a high-temperature reactor filled with an inert gas. The vaporized carbon reaches the chilled surface of the reactor, allowing the condensation of carbon to form nanotubes. Variations in conditions such as the temperature or the catalyst used on the substrate can lead to different diameter ranges and lengths of SWNTs allowing a certain degree of control. However, it still generates a range of SWNT diameters.[34]

### 1.2.3 Chemical vapor deposition (CVD)

First reported in 1996,[35] CVD involves the use of a hydrocarbon gas (like $CH_4$, $C_2H_4$ or $C_2H_2$), a carrier gas (such as $NH_3$, $N_2$ or $H_2$) and a solid substrate containing catalyst particles (iron, cobalt or nickel) on the surface, which are heated together in a chamber at high temperature (700 – 900 °C). The carbon-based gas decomposes allowing the formation of the SWNTs on the metal catalyst.[36] The size of the metal catalyst is important as it controls the diameter of the SWNTs made.[30]

### 1.2.4 High-pressure carbon monoxide disproportionation (HiPco)

Developed in 1999, the HiPco method is a variation of the CVD technique[31] in which the metal catalyst is introduced into the gas phase rather

than the solid phase. This process allows large-scale production via a continuous process because the tubes are formed free from catalyst support. The method uses carbon monoxide as the carbon source and iron pentacarbonyl $(FeCO)_5$) as the catalyst placed into a high-temperature reactor. Aerosolized SWNTs can then be collected and are typically produced with a 0.7 – 1.3 nm diameter range.[37]

CoMoCat is a variation of the HiPco precess that also involves the disproportionation of carbon monoxide but in the presence of a cobalt-molybdenum (CoMo) catalyst.[38] The SWNTs obtained via this method have narrow diameters ranging from ~0.7 – 0.9 nm.

### 1.2.5 Plasma-torch growth

This process was first developed in 2000 by Olivier Smiljanie[39] and combines both the arc-discharge and laser ablation methods with a carbon-containing gas - typically a mixture of ethylene and ferrocene - instead of graphite. The carbon source and an argon carrier gas are introduced into a microwave plasma-torch to break down the carbon-source material. The resulting fumes contain SWNTs with diameters ranging from 1.1 to 1.5 nm as well as amorphous carbon and left over metal catalysts. This process can also work using carbon black/metal catalyst particle feedstock.

The 1D electronic nature of SWNTs affords interesting properties. m-SWNTs are known to be conductive[40] and sc-SWNTs possess high electron and hole mobility.[8,41] These characteristics are promising for the production of a variety of SWNTs-based devices such as organic-field effect transistors

(OFETs),[14,41] sensors,[17,42,43] organic photovoltaic devices (OPVs),[16,44] conductive inks,[45,46] and more.[23,47,48] However, the heterogenous mixture of as-synthesized SWNTs in terms of electronic species, diameters, and length[49] combined with their tendency to form bundles via van der Waals interactions and π-stacking lead to poor processability and dispersity.[50] This prevents the use of SWNTs for commercial applications. Purification of any non-SWNT impurities is therefore required as well as an effective solubilization to afford the processability for device fabrication. Moreover, the separation of the different electronic species or the isolation of a specific chirality can also be required for certain applications.[1]

### 1.3 Functionalization and purification of SWNTs

As mentioned above, SWNTs tend to aggregate into bundles due to van der Waals interaction and π-stacking. These bundles contain SWNTs with different diameters, lengths and electronic properties, as well as non-SWNT impurities resulting in a lack of purity and low solubility of SWNTs in most common organic and aqueous solvents. As a consequence, SWNTs cannot be processed for the fabrication of electronic devices. SWNTs must therefore be purified and dispersed to be spin-coated, printed, filtered etc. Moreover, the resulting SWNT dispersions should remain stable to avoid the reaggregation of bundles. Methodologies have therefore been developed to purify non-SWNT impurities from a raw-SWNT mixture but also techniques that can purify and discriminate SWNTs in terms of electronic type, diameter and (n,m) chiral indices. Theses methodologies can be broadly classified into two categories:

covalent and non-covalent functionalization.[51] Progress in both methodologies has been made over the past years to separate SWNTs by type, diameter and chirality.

### 1.3.1 Covalent functionalization of SWNTs

In this method, the functionalization of SWNTs involves the use of strong oxidizing conditions to covalently functionalize the surface of SWNTs.[51,52] Typically, raw SWNTs are sonicated in mixtures of either sulfuric acid and nitric acid or sulfuric acid and hydrogen peroxide.[51] This results in the formation of oxygenated functionalities such as carboxylic acids, esters, and quinones[53] at the tube ends or at the defect sites along the tubes. These covalently-bonded groups can further react to achieve good solubility of SWNTs in organic or aqueous solvents. Despite the effective solubility, the covalent functionalization disrupts the conjugated network of the tubes resulting in an alteration of the optical, mechanical and electrical properties of the SWNTs. Moreover, these harsh conditions tend to reduce the length of the tubes.[54]

### 1.3.2 Non-covalent functionalization of SWNTs

In contrast with the covalent functionalization technique mentioned above, the non-covalent functionalization does not alter the properties of the SWNTs.[55] In this method, SWNTs are sonicated in the presence of a dispersant to mechanically de-bundle the tubes. The dispersant interacts with the tubes via non-covalent interactions which do not impact the nanotube surface and therefore leave the optical, mechanical, and electrical properties of the tubes intact. Different dispersants including surfactants, biomolecules,

aromatic molecules and conjugated polymers have been used to successfully purify and disperse SWNTs in organic or aqueous solvents.

### 1.3.3 Dispersion of SWNTs using surfactants

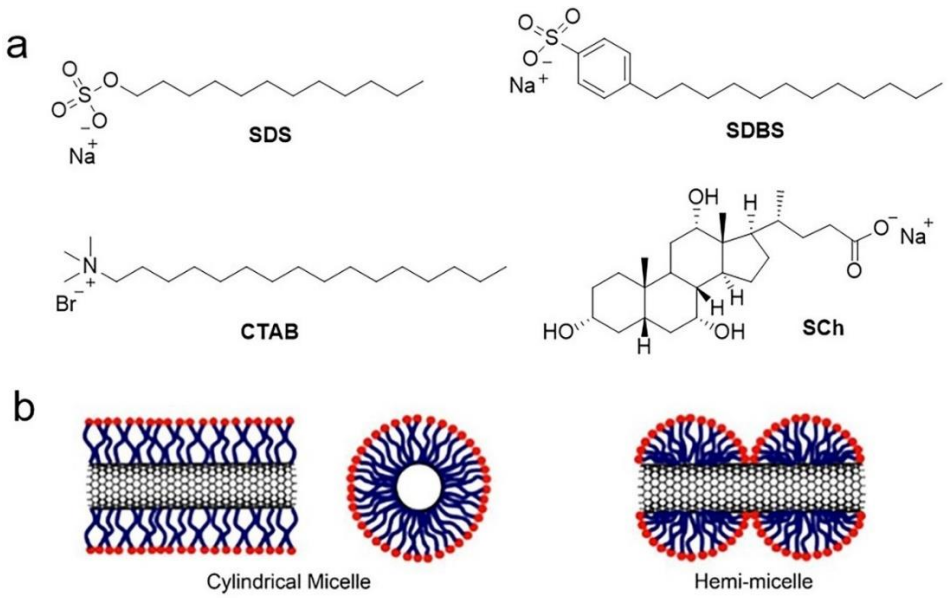


Figure 1.3. a) Common surfactant used for the dispersion of SWNTs in water forming supramolecular complexes in the form of b) cylindrical micelles and hemi-micelles.Reproduced with permission from Elsevier.[56] Copyright 2009.

In 2002, a method to successfully disperse SWNTs in water was published by researchers at Rice University.[25] In this method, an anionic surfactant, sodium dodecyl sulfate (SDS) was sonicated in the presence of SWNTs. When sonicated, SWNT bundles break apart allowing the surfactant to orient itself around the SWNT with the hydrophobic tails toward the tube sidewall and the anionic head toward the surrounding solvent. The formation of the micelle around the tube surface prevents the reaggregation into bundles resulting in a

stable suspension of isolated SWNTs. As shown in Figure 1.3b, different micelle orientations such as cylindrical or hemi-micelle can be obtained by varying the concentration of surfactant used.[56] Since this discovery, different surfactants including sodium dodecylbenzenesulfonate (SDBS), hexadecyl(trimethyl)ammonium bromide (CTAB), sodium cholate (SCh), and sodium deoxycholate (DOC) (Figure 1.3a) have been used to disperse SWNTs.[57,58] However, surfactants do not interact with a specific SWNT species.[59,60]

Following the discovery of the surfactant dispersion of SWNTs, additional purification methods have been developed to use in combination with the surfactant. The first method was the density gradient ultracentrifugation (DGU) technique. DGU was typically used for the separation of macromolecules such as DNA and large proteins based on molecular mass and chemical moiety and was first used for the separation of SWNTs in 2006 by Arnold et al.[61] The aqueous surfactant-SWNT dispersions were added dropwise into the density gradient and ultracentrifuged at ~200000 – 250000 g for at least 18 hours. Under the force of centrifugation, the surfactant-coated SWNTs travel through the density gradient allowing the different densities of SWNT species to migrate through the solvent. As shown in Figure 1.4, this results in localized coloured bands within the density gradient that corresponds to pure SWNT species.

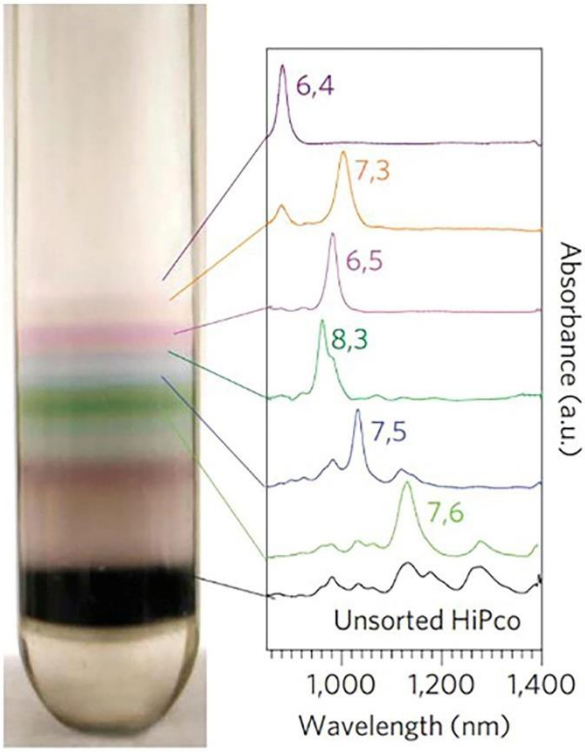


Figure 1.4. a) A centrifuge tube showing localized bands of colour indicating different SWNT species alongside their corresponding UV-Vis-NIR absorption spectra. Reproduced with permission from Springer Nature.[62] Copyright 2010, Springer Nature Limited.

In addition to the DGU technique, agarose gel columns have also been used to purify SDS-SWNT dispersions. It has been found that m-SWNTs elute first from the column, therefore by varying the eluent, it is possible to obtain pure sc-SWNT with narrow diameter distributions.[63] A variation of this method has also been developed where the SDS-SWNT mixture is absorbed into the agarose and squeezed like a sponge to expel SWNTs resulting in samples that contain up to 70% of m-SWNTs.[64,65] Sephacryl (a cross-linked copolymer of allyl dextran and N,N'-methylene bisacrylamide) size-exclusion chromatography (SEC)

has also been used to separate metallic and semiconducting species (Figure 1.5).[66–68]


Figure 1.5. Photograph of Sephacryl-packed columns loaded with SDS-dispersed SWNTs showing different bands containing semiconducting and metallic species. Reproduced with permission.[66] Copyright 2013, American Chemical Society.

Surfactant-dispersed SWNTs can also be purified via an aqueous two-phase technique. In this method, two water-soluble polymers, polyethylene glycol (PEG) and dextran are mixed at certain concentrations to form separate phases.[69,70] Dispersions of DOC-SWNTs and SCh-SWNTs have been added to these two-phase systems and it has been observed that SWNTs

spontaneously partition between the phases based on their diameter or electronic nature.

### 1.3.4 Dispersion of SWNTs using DNA

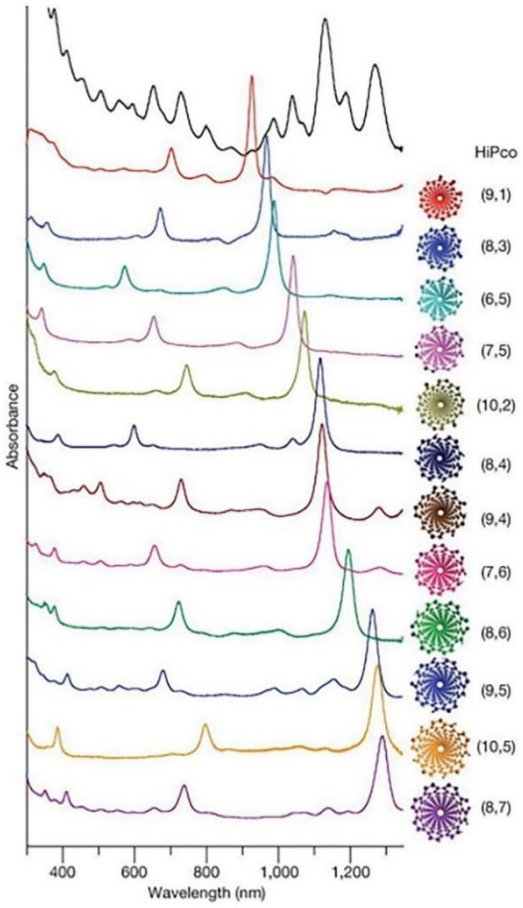


Figure 1.6. UV-Vis-NIR absorption spectra of raw HiPco SWNTs (top black) and 12 isolated sc-SWNT chiralities that were obtained using DNA and IEX. Reproduced with permission from Springer Nature.[71] Copyright 2009, Macmillan Publishers Limited.

DNA can also be used as a selective dispersant for purifying SWNTs.[71] The nucleobases interact with the surface of the tubes via π-stacking.[72]

Moreover, the helical structure of the DNA allows the molecule to helically wrap around the tubes and the hydrophilic charged functional groups of the DNA also provide stability to the dispersion.[73] The resulting DNA-SWNTs complexes can be further purified using ion exchange chromatography (IEC),[74] DGU[75] or two-phase extraction techniques.[76] In contrast to surfactant-SWNT dispersions, the DNA method can be highly selective toward specific electronic types or chiralities. Indeed it has been found that specific single-stranded DNA sequences preferentially wrap different groups of SWNT populations.[77] Therefore, a significant amount of work has been performed to find the proper DNA sequence required for the purification of different SWNT chiralities. As shown in Figure 1.6, Zheng et al.[71] were able to identify specific single-stranded DNA sequences to separate and purify sc-SWNTs containing single (n,m) species.

Despite the effectiveness of each technique described above for the dispersion and purification of SWNTs, these methods allow the production of sub-microgram quantities of SWNTs and usually after combining multiple steps and processes. As a result, these methods are very expensive and time-consuming and are therefore not suitable for large-scale commercial applications.

### 1.3.5 Dispersion of SWNTs using conjugated polymers

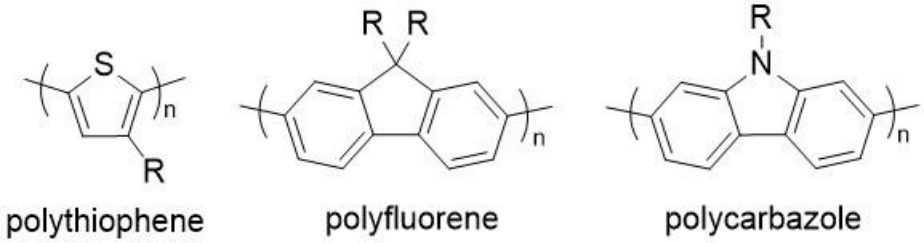


Figure 1.7. Common examples of conjugated polymers used for the dispersion of SWNTs in organic solvents.

Dispersion of SWNTs using conjugated polymers is one of the most promising methods that has been developed in terms of cost, time, and processability.[78] In this method, the π-conjugated backbone of the polymer interacts with the surface of the tubes via π-stacking.[79] This interaction disrupts the van der Waals interaction of the bundles and prevents reaggregation resulting in stable dispersions in organic solvents that are compatible with the polymer (typically THF or toluene).[79] Different types of conjugated polymers including homopolymers, alternating copolymers, random copolymers and block copolymers have all been developed and demonstrated to be suitable for the dispersion of SWNTs in both aqueous and organic solvents. Among the variety of polymer families, polyfluorenes,[80–84] polythiophene,[85–89] polycarbazole[90–93] and others[94–98] (Figure 1.7) are well known for their effective dispersion and purification of SWNTs. The wide library of monomer structures combined with the tuning of the polymer structure (molecular weight,[90,99,100] nature and length of the side-chains[89,101–103]) enables not only the dispersion of SWNTs but allows the processability in organic solvents that

can lead to a variety of potential applications of these polymer-SWNTs complexes such as in field-effect transistors (FETs),[41,104–106] chemical sensors,[17,107,108] conductive inks,[45,46] photovoltaic devices[16,44,109,110] and more.[13,15,23,47,48]

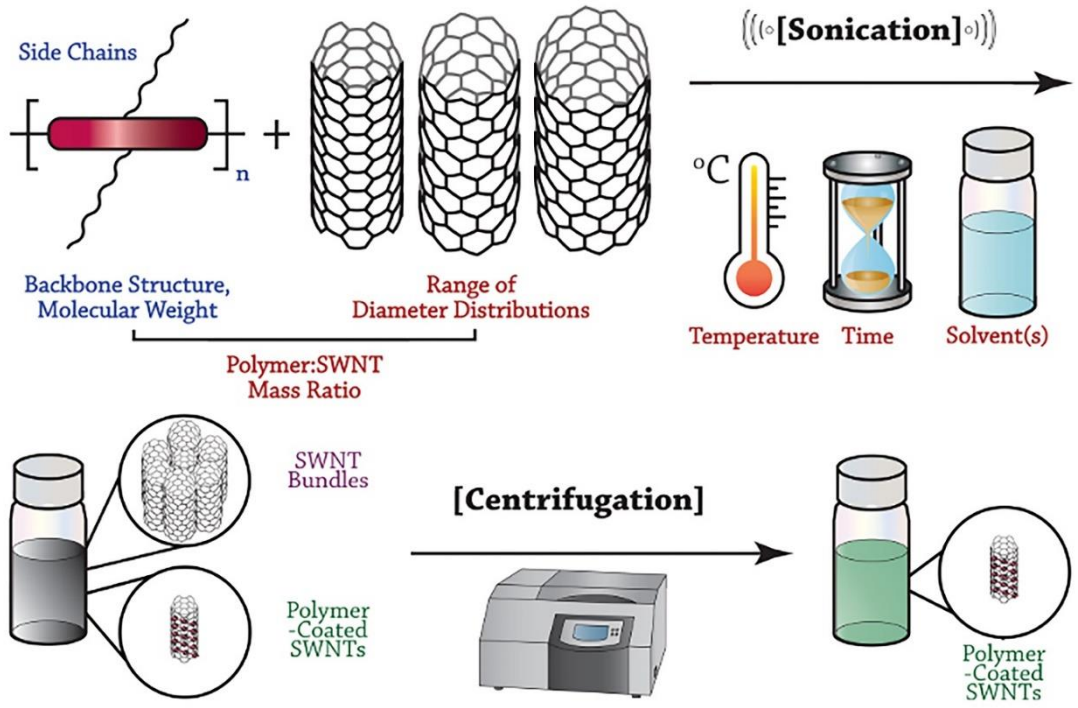


Figure 1.8. General view of the SWNT dispersion protocol showing the sonication and centrifugation steps. The polymer features are labelled in blue and preparation conditions are labelled in red. Reproduced with permission from Chemical Science.[111] Copyright 2017, Royal Society of Chemistry.

The preparation of polymer-SWNT complexes consists of a sonication step followed by a centrifugation step and a filtration step (Figure 1.8). Parameters such as sonication time and power,[112] temperature,[89,113,114] polymer: SWNT mass ratio,[90,102] solvent,[115–117] and centrifugation speed must be optimized for different polymer-SWNT systems to allow effective SWNT dispersions. Sonication is used to temporarily de-bundle the SWNTs to allow

the conjugated polymer to access and interact with the SWNT surface and prevent the re-bundling of the tubes. Some studies have demonstrated that increasing the sonication time decreases the bundling but can also decrease the average SWNT length.[112] The sonication temperature also impacts the effectiveness of SWNTs dispersion. A low sonication temperature prevents the polymer aggregates to dissociate and interact with the tubes while a high sonication temperature can disfavour the polymer-SWNT complex formation due to entropic penalties.[89] Therefore, the effective sonication temperature must be an intermediate temperature at which there is enough energy to overcome polymer-polymer interactions and allow the formation of the polymer-SWNT complex. The effective polymer: SWNT mass ratio depends on each polymer system[90,95] but in general, the ideal ratio is where there is enough polymer to interact with the SWNT surfaces but not enough polymer to saturate all SWNT surfaces and indiscriminately disperse all SWNTs.[90,116] It has been found that polymer-SWNT mass ratios of 0.5:1–1.5:1 produced the highest sc-SWNT purity.[102] Concerning the choice of solvent, the density must be lower than the buoyant density of SWNT bundles (~1.3 $g.cm^{-3}$), otherwise, the bundles cannot sediment upon centrifugation.[111] This excludes the use of solvents such as dichloromethane and chloroform that are too dense (densities of 1.3 and 1.5 $g.cm^{-3}$, respectively). Other parameters such as viscosity,[116] polarity[115] and dielectric constant[117] have been shown to affect SWNT dispersions. Solvents such as THF, toluene, *o*-xylene, *m*-xylene, tetralin and decalin have been used to produce stable dispersion of sc-SWNTs.[118]

## 1.4 Characterization of SWNTs

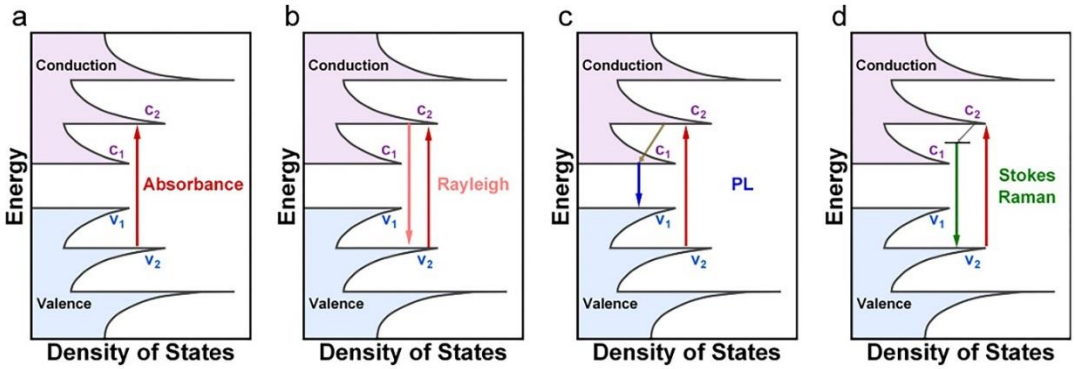


Figure 1.9. Generalizations of various optical processes that can occur for SWNTs, including a) absorbance, b) Rayleigh scattering, (c) photoluminescence (PL) and d) Stokes Raman processes.

Specific methods are used to characterize the electronic nature of SWNTs. Spectroscopy, including absorbance, resonance Raman spectroscopy, and photoluminescence, is a powerful tool to characterize SWNT species present in a dispersion. SWNTs can be excited to a higher energy level via thermal,[119] optical[10] or electronic[8] methods and relax to the ground state via the emission of a photon through different processes (Figure 1.9). The quantum confinement of the electrons in the form of van Hove singularities in the density of states gives SWNTs interesting optoelectronic characteristics.

### 1.4.1 UV-Vis-NIR absorption spectroscopy

The absorbance process (Figure 1.9a) occurs when an incident photon matches a corresponding excitonic energy difference ($E_{ii}$), promoting an electron to a higher energy state. Each SWNT species present in the dispersion possesses its own distinct electronic transitions,[120] resulting in multiple

absorption features in a UV-Vis-NIR absorption spectrum. Using this characterization technique, sc-SWNTs and m-SWNTs can be observed separately due to the difference in their density of states.[25] The diameter of SWNTs also has an impact on the absorption characteristics, resulting in different regions of interest in an absorption spectrum depending on the diameter range of the produced SWNTs. HiPco SWNTs with diameters ranging from 0.7 – 1.2 nm have four primary regions of interest: three semiconducting regions ($S_{11}$ at 830 – 1600 nm, $S_{22}$ at 600 – 800 nm, and $S_{33}$ 350 – 500 nm) and one metallic ($M_{11}$ at 440 – 645 nm),[9] where the $S_{33}$ region is typically not shown due to its overlap with the polymer absorption. Using HiPco SWNTs, the $M_{11}$ region overlaps with the $S_{22}$ region, increasing the difficulty in estimating the ratio between sc-SWNTs and m-SWNTs within a sample (Figure 1.10a). For dispersions that contain metallic SWNTs or SWNT bundles, a broad exponential background[121] is observed. It is therefore possible to make qualitative assumptions about the electronic character of SWNT species present in a sample, but other techniques such as photoluminescence mapping and resonant Raman spectroscopy are required for a more complete characterization.

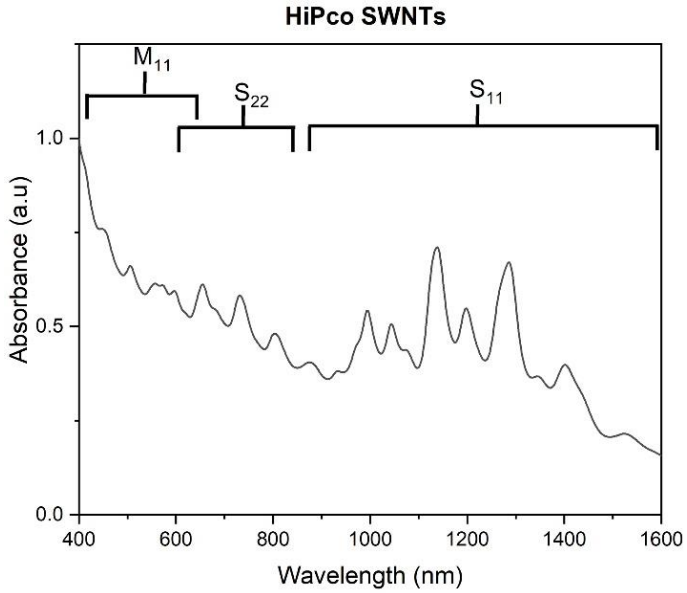


Figure 1.10. UV-Vis-NIR absorption spectrum HiPco dispersed SWNTs using a polyfluorene derivative in THF. The spectrum is labelled with regions that signify semiconducting ($S_{11}$, $S_{22}$) and metallic ($M_{11}$) SWNTs.

### 1.4.2 Photoluminescence mapping

Photoluminescence (PL) spectroscopy is used to observe the fluorescence of sc-SWNT species.[120] When sc-SWNTs are excited to a higher energy state, they can emit light upon relaxation. This phenomenon is only observed for sc-SWNTs as they have a band gap between their valence and conduction bands. When excited, an electron can radiatively relax from the $c_1$ to the $v_1$ energy levels and emit a photon[122] (Figure 1.10c). In contrast, m-SWNTs possess a continuous density of states between the valence and conducting bands, therefore, an electron excited to higher energy relaxes via non-radiative pathways. To obtain a complete characterization of a SWNT dispersion, multiple emission spectra using different excitation wavelengths are gathered into a “PL map” where each PL maximum indicates the presence of a

single SWNT species. PL maxima of all sc-SWNTs have been empirically determined and can be used to provide qualitative information on which SWNT species are present in the dispersion[123] (Figure 1.11).

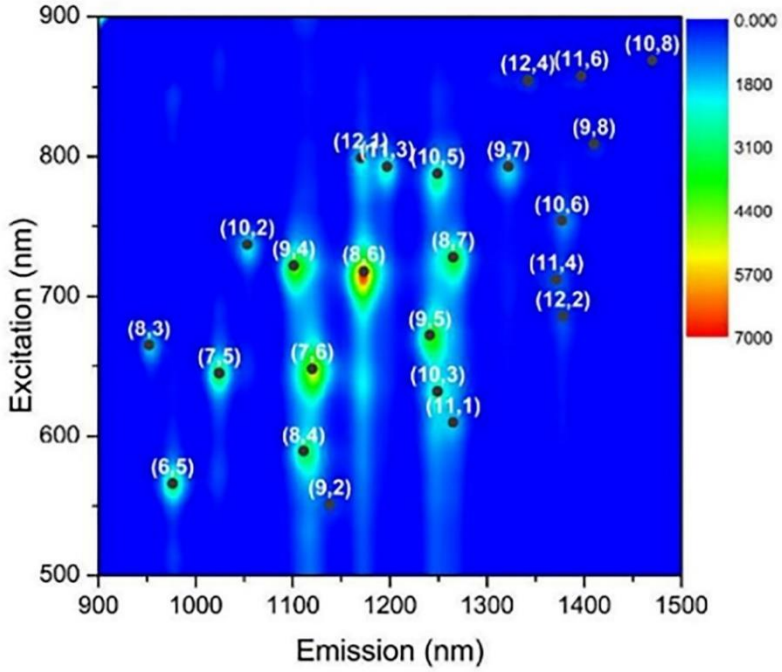


Figure 1.11. PL map of dispersed HiPco SDBS-SWNTs in $D_2O$. The map is overlapped with (n,m) chiral indices, for which excitation and emission energies have been empirically determined.[9]

The presence of m-SWNTs can also be indirectly evaluated using PL mapping due to their fluorescence quenching.[124,125] As mentioned above, the excited electron radiatively relaxes to a lower energy state level. That electron could also be accepted by a lower energy state of a nearby m-SWNT that effectively quenches the fluorescence. This can be used when comparing multiple samples by evaluating their relative fluorescence.[126,127] However, it should be noted that SWNT aggregates can also quench fluorescence. As one-

third of all SWNTs are metallic, any SWNT aggregates having three or more tubes statically contain a metallic SWNT that quenches fluorescence. To evaluate the degree of SWNT aggregation, techniques such as atomic force microscopy, UV-Vis-NIR absorption and resonant Raman spectroscopy can be used.

### 1.4.3 Resonant Raman Spectroscopy

In resonant Raman spectroscopy, the incident light is in resonance with the electronic transitions of SWNTs and the excited electron relaxes to a vibrational state with higher energy than the ground state (Stokes Raman scattering)[21] (Figure 1.9d). The intensity of the Stokes-Raman scattering is therefore measured and reported as a frequency difference (in $cm^{-1}$).[128,129] To completely characterize SWNT dispersions, multiple laser excitation wavelengths are required to match with the different van Hove singularities of the SWNTs, allowing the examination of both sc-and m-SWNTs. The laser wavelengths can be determined using a semiempirical Kataura plot[11] which plots the SWNT electronic transition energy as a function of the tube diameter (Figure 1.12)

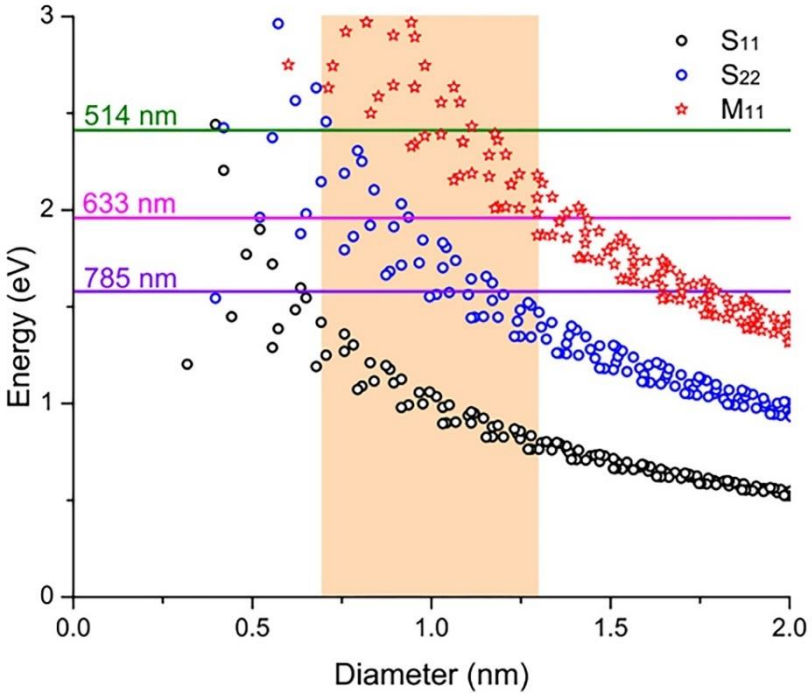


Figure 1.12. Semiempirical Kataura plot of optical transition energies $S_{11}$ (black circles), $S_{22}$ (blue circles), and $M_{11}$ (red stars) from the density of states of each SWNT species. The diameter range of HiPco (~0.7 – 1.3 nm) is highlighted in orange and the horizontal lines signify the laser excitation wavelengths used during the Raman studies in this thesis.

The Raman spectrum of a SWNT dispersion (Figure 1.13) can be divided into four main regions: the radial breathing mode (RBM) between ~ 100 – 400 $cm^{-1}$, the D-band between ~1250 – 1450 $cm^{-1}$, the G-band between ~1550 – 1595 $cm^{-1}$, and the G'-band between ~2500 – 2900 $cm^{-1}$.[21] Among these regions, the RBM and D- and G-bands are the most used to characterize SWNT samples.

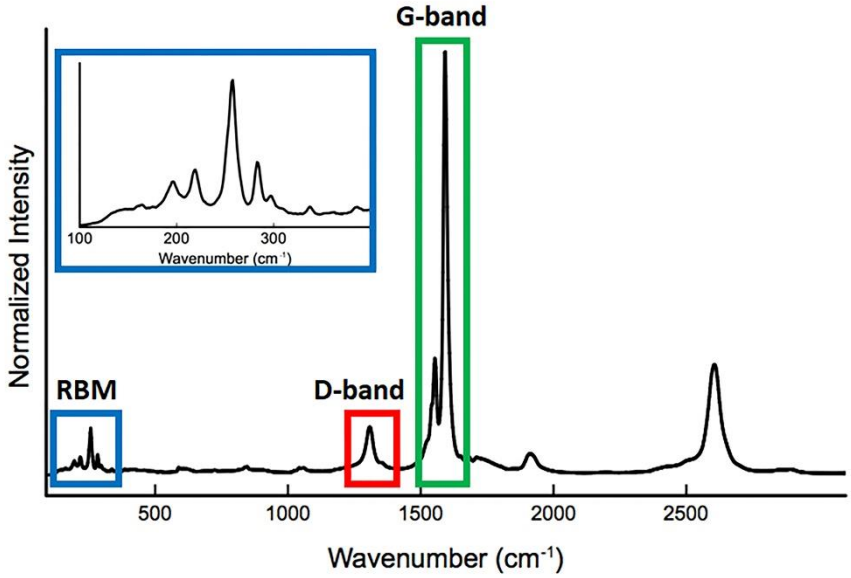


Figure 1.13. Example of a Raman spectrum for a sample of HiPco SWNTs showing the RBM (blue box), D-band (red box) and G-Band (blue box) regions. The inset shows the zoomed RBM region to provide more detail.

The RBM region arises from radial vibrations from the carbon network and depends on the diameter of the tubes. As described above, different laser excitation wavelengths can be used to examine both m- and sc-SWNTs present in a sample.[130] For HiPco SWNTs with a diameter range of ~ 0.7 – 1.2 nm, the 514 nm, 633 nm, and 785 nm laser excitation wavelengths can be used for complete characterization. The presence of sc- and m-SWNTs in a sample can also be evaluated using the G-band region of the Raman spectrum.

The G-band is specific to graphitic structures that contain $sp^2$ hybridized carbons. The G-band possesses two different modes: a low-frequency peak called $G^-$ and a high-frequency peak referred to as $G^+$.[131] The $G^-$feature is observed between 1550 – 1585 $cm^{-1}$, and results from circumferential vibrations of the SWNTs. The $G^+$ is at ~1590 $cm^{-1}$ and arises from the axial vibrations of

the tube. Qualitative observations of the G-band can be used to distinguish m-SWNTs and sc-SWNTs due to a change in the G⁻shape. With sc-SWNTs, both the $G^+$ and the $G^-$ bands exhibit Lorentzian lineshapes (Figure 1.14a). In contrast, with m-SWNTs species, only the $G^+$ exhibits the Lorentzian lineshape and the G⁻exhibits a broad, asymmetric feature (Breit-Wigner-Fano, or BWF lineshape) (Figure 1.14b). It should be noted that, despite their metallic character, the BWF lineshape is not observed for armchair nanotubes (n=m).[132]

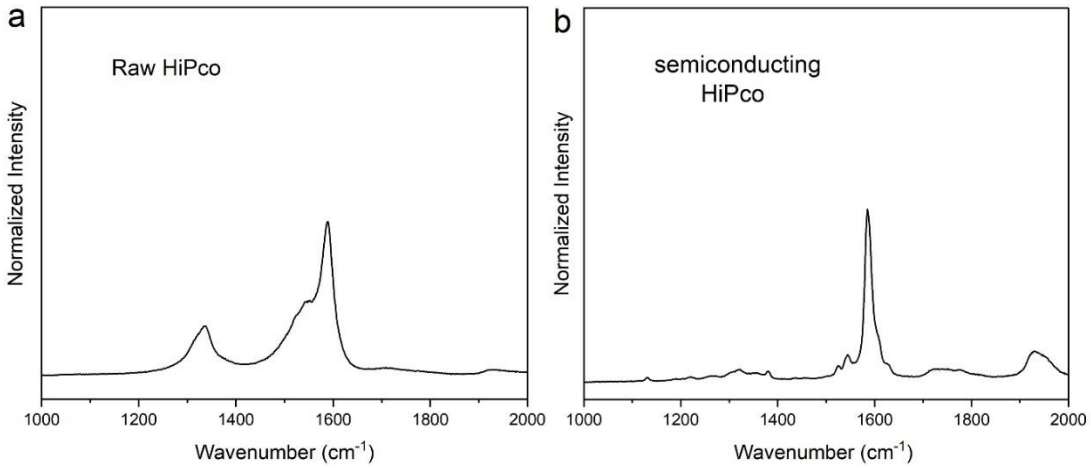


Figure 1.14. Raman spectra showing the G-band of a) a raw HiPco SWNT sample and b) a purified semiconducting HiPco SWNT sample, both observed using the 514 nm laser excitation wavelength.

Finally, the D-band is often referred to as the disorder mode. The presence of the D-band results in the electrons being scattered elastically by structural defects such as impurities or $sp^3$-hybridized carbons.[133,134] Therefore, examining the intensity of the D-band centred at ~1290 $cm^{-1}$ relative to the G-

band at ~1590 $cm^{-1}$ can indicate the presence of $sp^3$-hybridized carbons on the nanotube structure, which correspond to defect sites.

## 1.5 Printed carbon nanotube electronics

### 1.5.1 The Internet of Things and Printed Electronics

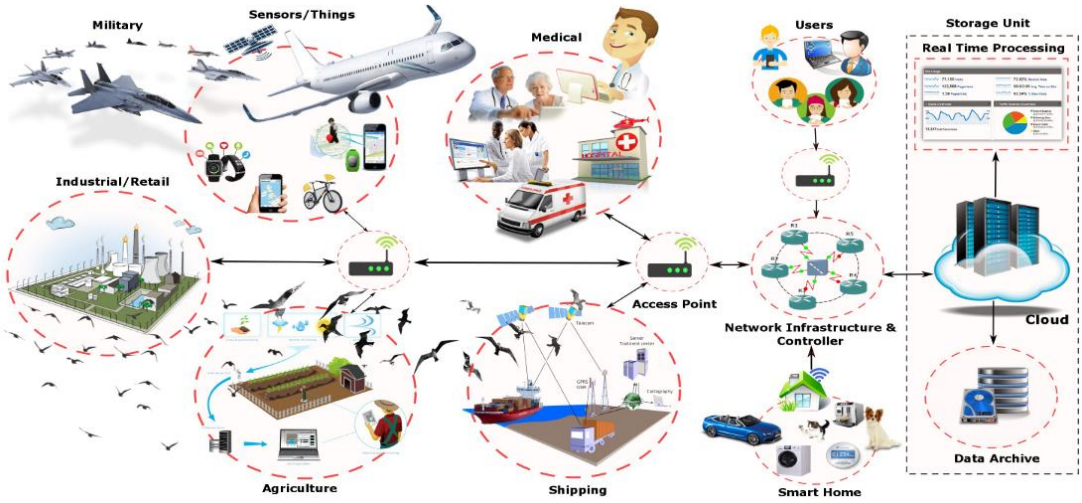


Figure 1.15. Internet of Things (IoT) architecture. Reproduced with permission.[135] Copyright 2011, IEEE.

The Internet of Things (IoT) is a term coined by Kevin Ashton in 1999 and represents the symbiosis of various technologies.[136,137] The IoT can be defined as an ecosystem where smart devices and sensors work together to collect and exchange data.[138] These internet-based devices aim to facilitate our life and are used in various domains such as cities, homes, universities, agriculture, health care and others (Figure 1.15).[135,137–139]

To promote and follow the demand for these smart devices, new technologies such as Printed Electronics (PEs) have received great interest.

Although conventional technologies produce performant devices, large-area production is limited. Indeed, these technologies referred to as subtractive technologies require a multi-step fabrication process that uses harsh conditions such as chemical vapor deposition, metal etching, lithography and high-temperature processing that can significantly increase the production cost and result in toxic waste.[140,141]

In comparison, PE is an addictive technology that combines conventional printing methods with the incorporation of conducting materials. This reduces the number of fabrication steps (Figure 1.16) and allows the fabrication of low-cost, large-area, lightweight, and more environmentally-friendly electronic devices.[140,142,143] Moreover printing techniques are compatible with a variety of substrates that can be flexible, stretchable, recyclable and/or biodegradable. This includes natural or synthetic recyclable substrates such as polyimide (PI),[144,145] polyethylene terephthalate (PET),[146] and polyethylene naphthalate (PEN),[147] paper,[148–150] nanocellulose,[151] silk,[152] shellac,[153] polydimethylsiloxane (PDMS),[154,155] polyvinyl alcohol (PVA)[156] and others[149,157–159]. These substrates are great alternatives to replace traditional substrates such as silicon (Si), silicon dioxide ($SiO_2$), Indium Tin Oxide (ITO), germanium (Ga), germanium arsenide (GaAs), and indium phosphide (InP).[158]

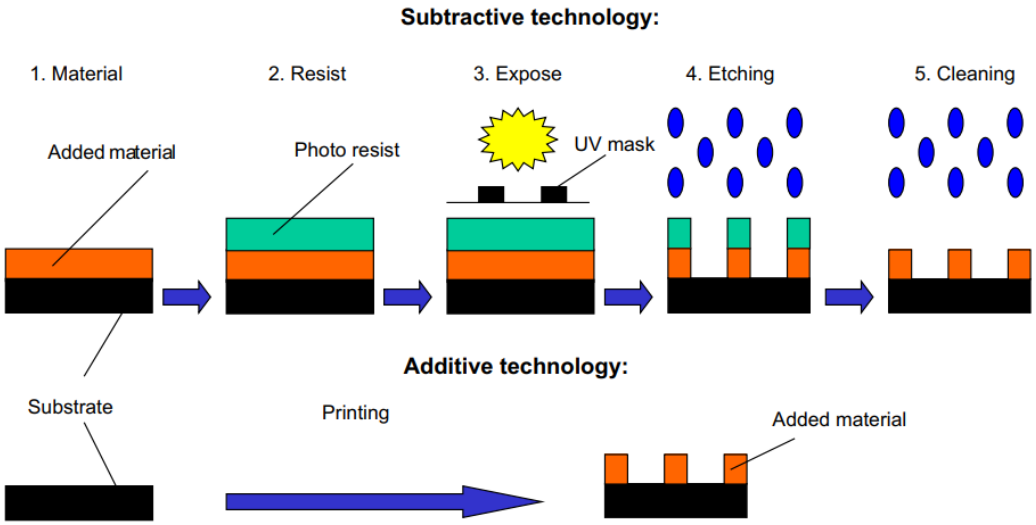


Figure 1.16. Differences between the fabrication process of traditional electronic devices (subtractive technology) and printed electronics (additive technology). Reproduced with permission.[143] Copyright 2008, Elsevier.

### 1.5.2 Materials for Printed Electronics

Different materials can be used as active layers for the fabrication of PEs. This includes metallic nanoparticles such a silver,[160,161] copper[162,163] and others,[164] metal-oxide,[165,166] organic semiconductors such as small molecules and conjugated polymers,[167–169] graphene,[170–172] and carbon nanotubes.[173–175].

Metallic nanoparticle inks can be dispersed in organic or aqueous solvents. Although they can be produced in large quantities, nanoparticle inks are not suitable for stretchable devices and tend to aggregate.[164] To prevent agglomeration, dispersants and stabilizers can be used.[160] However, this has an impact on the resulting conductivity and needs to be removed via a thermal, chemical, electric, or laser sintering process.[176,177] This results in extra cost

and time and can damage the substrate.[160,178] Moreover, nanoparticles such as copper tend to oxidize, which reduces the lifetime of the ink.[179]

As an alternative, metal oxide inks such as copper oxide (CuO), iron oxide (FeO), indium tin oxide (ITO), and zinc oxide (ZnO) nanoparticle inks[164] are less expensive than pure nanoparticle ink and can be used without fear of oxidation.[164] However, these inks still require a sintering process to be functional, which again increases the cost and time and limits the use of some substrates. A lower temperature sintering process (< 200°C) can be achieved by Atomic Layer Deposition (ALD).[180] However, the cost of this chemical vapor deposition technique can prevent the potential application of metal oxide inks for large-area PEs.

Organic semiconductors such as small molecules and conjugated polymers can also be used for the fabrication of PEs. This includes pentacene,[181] anthradithiophene,[182] benzothiophene,[183] poly(3-hexylthiophene) (P3HT),[184] poly(3,4-ethylenedioxythiophene) polystyrene sulfonate (PEDOT:PSS),[185] and others.[186,187] They offer low-cost and low-temperature processing, flexibility, and stretchability and are solution-processable in aqueous or organic solvents.[188] However, organic semiconductors suffer from a lower conductivity than other materials[189] and their reactivity with oxygen and moisture can limit their application under ambient atmosphere.[187]

Graphene is also a material compatible with PEs due to its flexibility, high surface-to-volume ratio and high carrier mobility.[190] Despite these advantages, graphene is considered a zero-bandgap semiconductor, and this can impact

devices' performance. For example, the lack of bandgap results in a low on/off ratio in transistors.[191] One solution is to oxidize graphene into graphene oxide (GO) using chemical exfoliation such as the Hummers 'method.[192] This process not only opens an energy bandgap but also introduces hydrophilic groups that can provide GO dispersion in water or can be further functionalized to obtain GO dispersion in organic solvents.[191] However, in some cases, GO needs to be further reduced to obtain reduced GO (rGO).[190,191]

In comparison to the materials mentioned above, SWNTs are an interesting alternative. Indeed, SWNTs have favourable properties due to their electrical[7] and mechanical[6] properties, their high aspect ratio and their ability to offer air stability, flexibility, stretchability, large-area production, low processing temperature, and low-cost devices.[173] They can also be easily tunable without using harsh chemical conditions.[175]

### 1.5.3 SWNT-based inks and printing processes

Covalently and non-covalently functionalized SWNTs as well as pristine SWNTs have been used to produce SWNT-based inks. Covalently functionalized SWNTs with carboxylic acids (-COOH),[193] amides (-$CONH_2$) or poly(ethylene glycol) (-PEG)[194] and surfactant-dispersed SWNTs with a surfactant such as sodium dodecyl sulfate (SDS),[195] are typically used to obtain SWNT inks in water. In contrast, pristine SWNTs[196,197] and polymer-wrapped SWNTs[198,199] are used to produce SWNT inks in organic solvents such as toluene,[118] tetralin,[118] N,N-dimethylformamide (DMF)[200,201] and N-methyl-2-pyrrolidone (NMP).[202] The use of water as a solvent for SWNT-based inks often

requires the addition of wetting agents to lower the surface tension.[203,204] In contrast, SWNT inks in organic solvents do not require additional surfactants,[204] however their toxicity makes them unsuitable for environmentally-mindful applications. At the time of this thesis, no SWNT inks using “green” solvents have been completely developed and used for the fabrication of electronic devices.

Different printing processes can be used to deposit the SWNT-based ink and can be classified into two main categories: template roll-to-roll (R2R) printing and direct-write printing.[174] One main R2R printing method used for the printing of SWNTs is gravure printing (Figure 1.17a).[205–207] This technique is a continuous printing process where an engraved cylinder is used as a template. The cylinder first rotates into an ink reservoir where a blade is used to remove the excess ink and only leaves ink in the engraved cells. The cylinder then transfers the ink onto the substrate. Although this process is suitable for large-scale production, some limitations should be noted. The use of a template prevents flexibility in terms of design and applications. Moreover, typical ink viscosities for these methods range from 40 – 2000 centipoise (cP) which require the use of binders such as a polymer matrix to achieve the desired viscosity.[174] The presence of binders can decrease the device's performance.[175]

As an alternative, the direct-write printing method such as inkjet printing does not require the use of a template.[174] Indeed, the ink is pushed out a nozzle at targeted positions on the substrate allowing the design of various patterns,

as well as the pattern thickness as the size of the ink droplet, can be controlled. The ink is ejected either in a continuous or drop-on-demand (DOD) way (Figure 1.17).[186] For the continuous mode (Figure 1.17b), the ink droplets are first selectively charged in the nozzle before passing through a deflection system where they are either printed on the substrate or deflected to the recycling system. The main advantage of this type of deposition is the printing speed. However, it requires the installation of a droplet charge device, a deflection system, and the recycling system which can increase the cost. In contrast, with the drop-on-demand mode (Figure 1.17c), the ink is pushed out the nozzle by applying an electrical pulse signal generated by a piezoelectric transducer. Therefore, the ink consumption is significantly reduced in comparison to the continuous mode. Typical viscosities for inkjet printing range from 1 to 20 cP.[174] However, with low-viscosity solvent, a coffee-ring effect where the solvent dries faster on the edges of the droplet can be observed.[175] Therefore, solvent properties such as boiling point, surface tension and viscosity must be carefully chosen.[175]

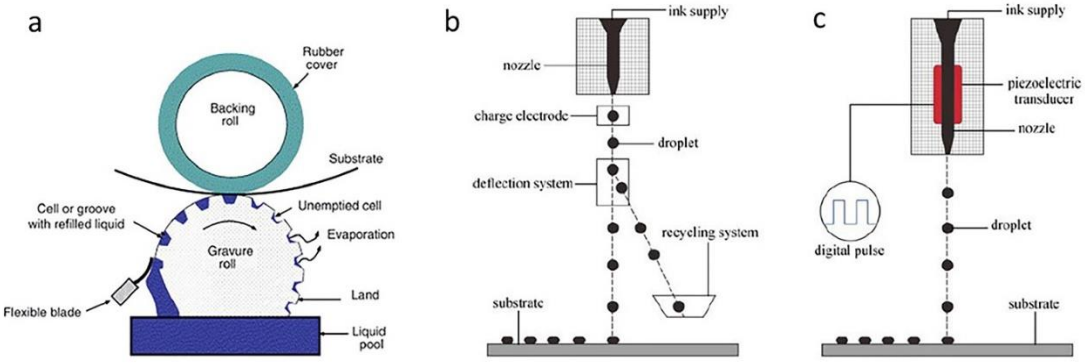


Figure 1.17. Schematic printing process for a) gravure printing. Reproduced with permission.[208] Copyright 2005 Elsevier Ltd. b) continuous mode of inkjet

printing and c) DOD mode of inkjet printing. Reproduced with permission.[209] Copyright © 2017, Higher Education Press and Springer-Verlag GmbH Germany.

### 1.5.4 Printed-SWNT devices: applications and challenges

As previously mentioned, SWNTs are great candidates to produce low-cost, large-area, lightweight, flexible and stretchable PEs. One of the main applications of printed SWNTs is SWNT-based thin film transistors (TFTs).[175,202,210] As any TFTs, SWNT-based TFTs are composed of three electrodes (source, drain and gate), a dielectric layer and a SWNT semiconducting layer. The SWNT layer is printed between the source (S) and the drain (D) metal electrodes with a channel length usually ranging from tens to hundreds of micrometres.[173] In terms of performance, printed SWNT-TFTs have shown mobilities up to 100 $cm^2 V^{-1} s^{-1}$, with on/off ratios of up to $10^6$.[173] Based on their performance, SWNT-TFTs can be tuned to develop different applications. Among these applications, radiofrequency (RF) devices[196,211] and sensors and biosensors[190,212–214], flexible displays,[211,215,216] and others[173–175,217] have been reported.

As mentioned in the section above, SWNT inks can be prepared with pristine SWNTs, covalently functionalized SWNTs, or non-covalently functionalized SWNTs. Among those three options, non-covalently functionalized SWNTs with molecules such as conjugated polymers are one of the best ways to purify and disperse pristine SWNTs without damaging the nanotube surface. However, in terms of applications, conjugated polymers

could also have an impact on the device's performance. Indeed, to achieve good solubility, conjugated polymers are often functionalized with large and non-conductive side-chains that can decrease the conductivity by preventing good contact between the nanotubes. The conjugated polymer backbone itself could also have an impact on the performance by hindering the surface of the nanotubes and therefore decreasing the sensing performance or hindering the charge transport.[218–220] Ideally, to maximize the device performances, non-conductive side-chains or insulating polymer backbones should be removed from the nanotube surface post-printing to fully benefit from the electronic properties of SWNTs.

### 1.6 Removal of conjugated polymer from carbon nanotubes

Some research groups have developed polymers with cleavable backbones. Among those backbones, polyimines[221,222] (Figure 1.18a) and polytetrazines[220] (Figure 1.18b) have shown successful cleavage and removal from the nanotube surface. Polyimines can be cleaved by the addition of a catalytic amount of acid such as trifluoroacetic acid (TFA) to protonate the imine bond (C=N).[223] Thermal decomposition and removal of polytetrazine at 250 °C have shown interesting results in terms of device performance with a detection limit of ammonia four times higher after removal of the polymer.[220] Cleavable copolymers have also been developed and used for the release of SWNTs. Chan-Park and coworkers have synthesized a polyfluorene containing disilane units in the backbone (Figure 1.18c) where the treatment with hydrofluoric acid (HF) solution breaks the disilane bond resulting in the decomposition of the

polymer.[224] Mayor and co-workers have also developed a photocleavable copolymer that contains a fluorene and an *o*-nitrobenzylether unit (Figure 1.18d).[225] The irradiation of the polymer degrades the polymer backbone resulting in the precipitation and release of the nanotubes. A poly(carbazole-co-terephthalate) polymer (Figure 1.18e) has also been developed by our group and was shown effective for the dispersion and release of sc-SWNTs upon irradiation for 72 hours.[226]

Alternative approaches for the release of the nanotubes post-dispersion include the use of polymers that can switch their conformation, as well as the utilization of supramolecular polymers. In 2014, our group synthesized a fluorene-based copolymer with a tetrathiafulvalene (TTFV) unit that undergoes a conformational change upon protonation with TFA resulting in the effective release of SWNTs (Figure 1.17f).[227] Toshimitsu and Nakashima have developed a metal-coordination polymer (CP-Ms) composed of fluorene-bridged bis(phenanthroline) ligands (Figure 1.17g) that can chelate different metal ions.[228] The CP-M polymer is then removed by the addition of a protic acid resulting in the depolymerization into monomers that can be reused after basic treatment. Following this work, Bao and co-workers synthesized a 2-ureido6[1H]-pyrimidinone (UPy)-based H-bonded supramolecular polymer[229] (Figure 1.18h) for the dispersion of sc-SWNTs. The hydrogen bonds can be disrupted by the addition of an acid resulting in depolymerization and isolation of dispersant-free sc-SWNTs.

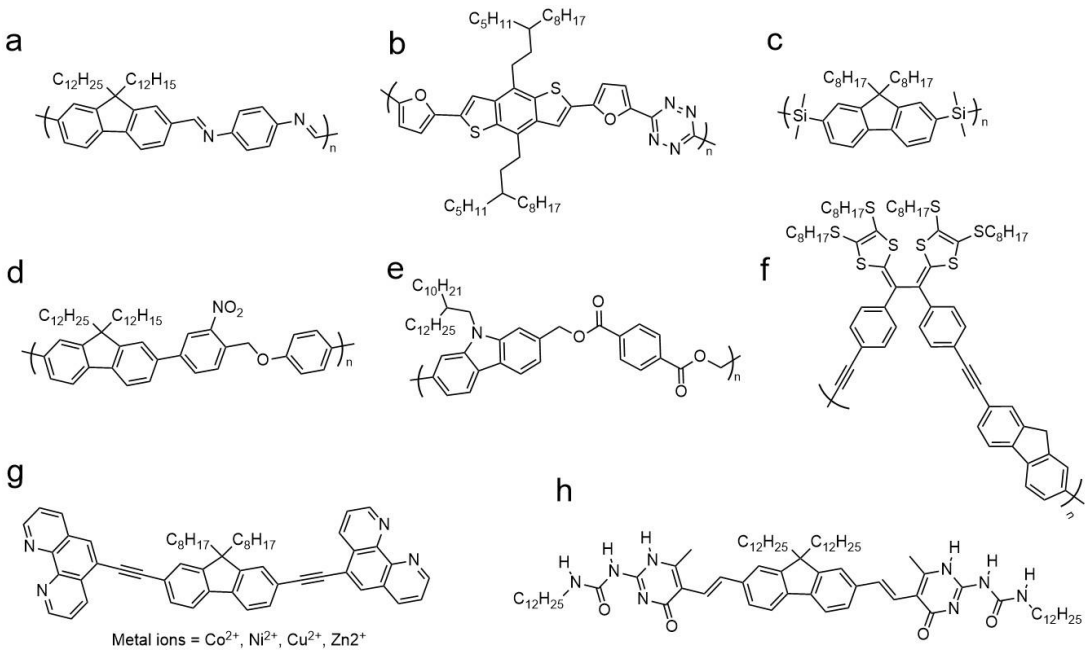


Figure 1.18. Conjugated polymers that have demonstrated removability from SWNT surfaces via a) imine hydrolysis,[221] b) thermal decomposition,[220] c) acid cleavage,[224] d) and e) photocleavage,[225,226] f) acid mediated conformation changes,[227] g) metal chelation mediated conformation changes[228] and h) hydrogen bond disruption.[229]

As an alternative to cleavable backbones, some studies focused on the cleavage of the insulating side-chains from the polymer. In 2019, Kawamoto and coworkers prepared SWNT thin films dispersed by polythiophene functionalized with carbonate linkers in their side-chains. When heating at 350 °C, the carbonate linkers are cleaved by decarboxylation resulting in higher conductivity.[230]

## 1.7 Objectives of this thesis

SWNTs possess great electronic, mechanical, and optical properties that make them promising materials for various applications. Currently, all SWNT production techniques generate a heterogeneous mixture of semiconducting and metallic species as well as non-SWNT impurities. Some purification techniques such as DGU or column chromatography have been used to purify SWNTs, however, they are expensive and difficult for large-scale purification. As an alternative, conjugated polymer sorting has proven to be a scalable method for the purification of SWNTs. They can easily be turned to disperse specific SWNT species and obtain solubility in target solvents. Overall, conjugated polymers are multifunctional and allow the purification, processability and extraction of specific SWNTs at the same time. Therefore, they are suitable as purification methods for the fabrication of SWNT-based devices, particularly in the area of printed electronics. However, the non-conductive side-chains and the polymer backbone could have an impact on the performance of the SWNT device by preventing good contact between the nanotubes. Some studies have shown that conjugated polymer backbones or side-chains can be cleaved and removed from the polymer-SWNT complex post-dispersion.

One major goal of this thesis focuses on the development of cleavable polymer-SWNT complexes to maximize the potential performance of printed devices post-precessing. In Chapter 2, I explore the impact on the conductivity of polymer-SWNT thin films upon the removal of non-conductive side-chains. This chapter is based on the functionalization of polymer with thermally

cleavable side-chains that contain a carbonate linker. When heating, the carbonate linker cleaves by decarboxylation. The study showed that the conductivity was an order of magnitude higher for the cleavable sample in comparison to the control sample after the removal of the side-chains. Additionally, I also investigated the dispersion of SWNTs using “greener solvents”. I, therefore, functionalized the polyfluorene with larger and cleavable side-chains that provided solubility in two new solvents: trimethylethylene glycol monomethyl ether and tetraethylene glycol dimethyl ether, both deemed “green” solvents and suitable for printing processes such as inkjet printing. In chapter 3, I functionalized the polyfluorene with a different type of side-chain to also examine the impact on the conductivity after side-chain removal. I used photocleavable side-chains that contain an ortho-nitrobenzyl ether linker that can be cleaved by irradiation with a 365 nm light. The overnight irradiation of the polyfluorene-SWNT complex resulted in the precipitation of the nanotubes and a broad absorption peak of the nanotubes indicating that the loss of side-chains eliminates steric stabilization of the nanotube dispersion. Although effective cleavage was observed, conductivity measurements could not be performed. For both studies, it was found that the surface of the nanotubes was not damaged upon the heating or irradiation process. These results represent proof-of-concept studies that could further be used for the fabrication of SWNT devices where the removal of the side-chains will improve the device performance.

To go further, I focused my attention on the synthesis of degradable and water-soluble conjugated polymers. In chapter 4, I synthesized a functionalized

and photocleavable polymer that contains a fluorene and an ortho-nitrobenzyl ether unit. Similarly to the work with the photocleavable side-chains, the backbone of the polymer degrades when exposed to a 365 nm UV light and can therefore release SWNTs. Characterization post-irradiation showed a decrease of 56% in polymer fraction from the surface of the nanotube. The polymer-SWNT complex was initially dispersed in an organic solvent such as THF, but after functionalization with hydrophilic groups such as polyethylene glycol side-chains, I was able to obtain a functionalized polymer-SWNT complex in water.

Finally, chapter 5 summarized my attempts at synthesizing a water-soluble and degradable zwitterionic functionalized conjugated polymer. The target polymer was a fluorene-based-conjugated polymer containing an imine linkage that can be easily cleavable via addition of an acid. Moreover, the target polymer was functionalized with amine groups at the end of the side-chain that can then react with 1,3-propanesultone to obtain a water-soluble degradable conjugated polymer. The non-cleavable analog polymer was also investigated. Unfortunately, it was not possible to prepare the target polymers, causing us to abandon this approach to disperse and release of SWNTs.

## 1.8 References

[1] B. Bhushan, *Springer Handbook of Nanotechnology*, **2007**.

[2] J. Hone, M. Whitney, A. Zettl, *Synth. Met.* **1999**, *103*, 2498–2499.

[3] Z. Han, A. Fina, *Prog. Polym. Sci.* **2011**, *36*, 914–944.

[4] B. Kumanek, D. Janas, *J. Mater. Sci.* **2019**, *54*, 7397–7427.

[5] M. Yu, B. S. Files, S. Arepalli, R. S. Ruoff, *Phys. Rev. Lett.* **2000**, *84*, 1–4.

[6] J. N. Coleman, U. Khan, W. J. Blau, Y. K. Gun'ko, *Carbon* **2006**, *44*, 1624–1652.

[7] P. G. Collins, P. Avouris, *Sci. Am.* **2000**, *283*, 62–69.

[8] P. Avouris, *Acc. Chem. Res.* **2002**, *35*, 1026–1034.

[9] S. M. Bachilo, M. S. Strano, C. Kittrell, R. H. Hauge, R. E. Smalley, R. B. Weisman, *Science* **2002**, *298*, 2361–2366.

[10] H. Kataura, Y. Kumazawa, Y. Maniwa, I. Umezu, S. Suzuki, Y. Ohtsuka, Y. Achiba, *Synth. Met.* **1999**, *103*, 2555−2558.

[11] H. Kataura, Y. Kumazawa, Y. Maniwa, I. Umezu, S. Suzuki, Y. Ohtsuka, Y. Achiba, *Synth. Met.* **1999**, *103*, 2555–2558.

[12] M. F. L. De Volder, S. H. Tawfick, R. H. Baughman, A. J. Hart, *Science* **2013**, *339*, 535–539.

[13] S. Park, M. Vosguerichian, Z. Bao, *Nanoscale* **2013**, *5*, 1727–1752.

[14] D. M. Sun, C. Liu, W. C. Ren, H. M. Cheng, *Small* **2013**, *9*, 1188–1205.

[15] P. Jarosz, C. Schauerman, J. Alvarenga, B. Moses, T. Mastrangelo, R. Raffaelle, R. Ridgley, B. Landi, *Nanoscale* **2011**, *3*, 4542–4553.

[16] M. W. Rowell, M. A. Topinka, M. D. McGehee, H. J. Prall, G. Dennler, N. S. Sariciftci, L. Hu, G. Gruner, *Appl. Phys. Lett.* **2006**, *88*, 6–9.

[17] P. Qi, O. Vermesh, M. Grecu, A. Javey, Q. Wang, H. Dai, S. Peng, K. J.

Cho, *Nano Lett.* **2003**, *3*, 347–351.

[18] G. A. Rivas, M. D. Rubianes, M. C. Rodríguez, N. F. Ferreyra, G. L. Luque, M. L. Pedano, S. A. Miscoria, C. Parrado, *Talanta* **2007**, *74*, 291–307.

[19] P. M. Ajayan, *Chem. Rev.* **1999**, *99*, 1787–1799.

[20] J. A. Fürst, J. G. Pedersen, C. Flindt, N. A. Mortensen, M. Brandbyge, T. G. Pedersen, A. P. Jauho, *New J. Phys.* **2009**, *11*.

[21] M. S. Dresselhaus, G. Dresselhaus, R. Saito, A. Jorio, *Phys. Rep.* **2005**, *409*, 47–99.

[22] S. Nanot, E. H. Hároz, J. H. Kim, R. H. Hauge, J. Kono, *Adv. Mater.* **2012**, *24*, 4977–4994.

[23] W. Gomulya, J. Gaoa, M. A. Loib, *Eur. Phys. J. B* **2013**, *86*, 1–13.

[24] C. L. Kane, E. J. Mele, *Phys. Rev. Lett.* **1997**, *78*, 1932–1935.

[25] M. J. O'Connell, S. M. Bachilo, C. B. Huffman, V. C. Moore, M. S. Strano, E. H. Haroz, K. L. Rialon, P. J. Boul, W. H. Noon, C. Kittrell, et al., *Science* **2002**, *297*, 593–596.

[26] S. Iijima, *Nature* **1991**, *354*, 56.

[27] S. Lljima, T. Lchihashi, *Nature* **1993**, *363*, 603–604.

[28] C. Journet, W. K. Maser, P. Bernier, A. Loiseau, M. Lamy de la Chapelle, S. Lefrant, P. Deniard, R. Lee, J. E. Fischer, *Nature* **1997**, *388*, 756–758.

[29] T. Guo, P. Nikolaev, A. Thess, D. T. Colbert, R. E. Smalley, *Chem. Phys.*

*Lett.* **1995**, *243*, 49–54.

[30] J. Kong, A. M. Cassell, *Chem. Phys. Lett.* **1998**, *292*, 567–574.

[31] P. Nikolaev, M. J. Bronikowski, R. K. Bradley, F. Rohmund, D. T. Colbert, K. A. Smith, R. E. Smalley, *Chem. Phys. Lett.* **1999**, *313*, 91–97.

[32] M. M. A. Rafique, J. Iqbal, *J. Encapsulation Adsorpt. Sci.* **2011**, *102*, 503–519.

[33] K. S. Kim, G. Cota-Sanchez, C. T. Kingston, M. Imris, B. Simard, G. Soucy, *J. Phys. D. Appl. Phys.* **2007**, *40*, 2375–2387.

[34] C. D. Scott, S. Arepalli, P. Nikolaev, R. E. Smalley, *Appl. Phys. A Mater. Sci. Process.* **2001**, *72*, 573–580.

[35] W. Z. Li, S. S. Xie, L. X. Qian, B. H. Chang, B. S. Zou, W. Y. Zhou, R. A. Zhao, G. Wang, *Science* **1996**, *274*, 1701–1703.

[36] C. Liu, H. M. Cheng, *Mater. Today* **2013**, *16*, 19–28.

[37] I. W. Chiang, B. E. Brinson, A. Y. Huang, P. A. Willis, M. J. Bronikowski, J. L. Margrave, R. E. Smalley, R. H. Hauge, *J. Phys. Chem. B* **2001**, *105*, 8297–8301.

[38] D. E. Resasco, W. E. Alvarez, F. Pompeo, L. Balzano, J. E. Herrera, B. Kitiyanan, A. Borgna, **2002**, 131–136.

[39] O. Smiljanic, B. L. Stansfield, J. P. Dodelet, A. Serventi, S. Désilets, *Chem. Phys. Lett.* **2002**, *356*, 189–193.

[40] T. W. Ebbesen, H. J. Lezec, H. Hiura, J. W. Bennett, H. F. Ghaemi, T.

Thio, *Nature* **1996**, *382*, 54–56.

[41] T. Dürkop, S. A. Getty, E. Cobas, M. S. Fuhrer, *Nano Lett.* **2004**, *4*, 35–39.

[42] K. A. Mirica, J. G. Weis, J. M. Schnorr, B. Esser, T. M. Swager, *Angew. Chem., Int. Ed.* **2012**, *51*, 10740–10745.

[43] M. Dionisio, J. M. Schnorr, V. K. Michaelis, R. G. Griffin, T. M. Swager, E. Dalcanale, *J. Am. Chem. Soc.* **2012**, *134*, 6540–6543.

[44] D. J. Bindl, N. S. Safron, M. S. Arnold, *ACS Nano* **2010**, *4*, 5657–5664.

[45] K. Y. Chun, Y. Oh, J. Rho, J. H. Ahn, Y. J. Kim, H. R. Choi, S. Baik, *Nat. Nanotechnol.* **2010**, *5*, 853–857.

[46] K. Kordás, T. Mustonen, G. Tóth, H. Jantunen, M. Lajunen, C. Soldano, S. Talapatra, S. Kar, R. Vajtai, P. M. Ajayan, *Small* **2006**, *2*, 1021–1025.

[47] D. S. Hecht, D. Thomas, L. Hu, C. Ladous, T. Lam, Y. Park, G. Irvin, P. Drzaic, *J. Soc. Inf. Disp.* **2009**, *17*, 941.

[48] D. Jariwala, V. K. Sangwan, L. J. Lauhon, T. J. Marks, M. C. Hersam, *Chem. Soc. Rev.* **2013**, *42*, 2824–2860.

[49] M. M. A. Rafique, J. Iqbal, *J. Encapsulation Adsorpt. Sci.* **2011**, *1*, 29–34.

[50] D. Tasis, N. Tagmatarchis, A. Bianco, M. Prato, *Chem. Rev.* **2006**, *106*, 1105–1136.

[51] A. Hirsch, *Angew. Chem., Int. Ed.* **2002**, *41*, 1853–1859.

[52] S. Campidelli, C. Klumpp, A. Bianco, D. M. Guldi, M. Prato, *J. Phys. Org.*

*Chem.* **2006**, *19*, 531–539.

[53] B. Parekh, T. Debies, P. Knight, K. S. V. Santhanam, G. A. Takacs, *Mater. Res. Soc. Symp. Proc.* **2006**, *887*, 9–14.

[54] J. Liu, A. G. Rinzler, H. Dai, J. H. Hafner, R. Kelley Bradley, P. J. Boul, A. Lu, T. Iverson, K. Shelimov, C. B. Huffman, et al., *Science* **1998**, *280*, 1253–1256.

[55] M. C. Hersam, *Nanosci. Technol. A Collect. Rev. from Nat. Journals* **2009**, *3*, 387–394.

[56] H. Wang, *Curr. Opin. Colloid Interface Sci.* **2009**, *14*, 364–371.

[57] M. F. Islam, E. Rojas, D. M. Bergey, A. T. Johnson, A. G. Yodh, *Nano Lett.* **2003**, *3*, 269–273.

[58] L. Vaisman, H. D. Wagner, G. Marom, *Adv. Colloid Interface Sci.* **2006**, *128–130*, 37–46.

[59] A. J. Blanch, C. E. Lenehan, J. S. Quinton, *J. Phys. Chem. B* **2010**, *114*, 9805–9811.

[60] V. C. Moore, M. S. Strano, E. H. Haroz, R. H. Hauge, R. E. Smalley, J. Schmidt, Y. Talmon, *Nano Lett.* **2003**, *3*, 1379–1382.

[61] M. S. Arnold, A. A. Green, J. F. Hulvat, S. I. Stupp, M. C. Hersam, *Nat. Nanotechnol.* **2006**, *1*.

[62] S. Ghosh, S. M. Bachilo, R. B. Weisman, *Nat. Nanotechnol.* **2010**, *5*, 443–450.

[63] H. Liu, Y. Feng, T. Tanaka, Y. Urabe, H. Kataura, *J. Phys. Chem.* **2010**, *114*, 9270–9276.

[64] T. Tanaka, H. Jin, Y. Miyata, H. Kataura, *Appl. Phys. Express* **2008**, *1*, 1140011–1140013.

[65] T. Tanaka, H. Jin, Y. Miyata, S. Fujii, H. Suga, Y. Naitoh, T. Minari, T. Miyadera, K. Tsukagoshi, H. Kataura, *Nano Lett.* **2009**, *9*, 1497–1500.

[66] B. S. Flavel, M. M. Kappes, R. Krupke, F. Hennrich, *ACS Nano* **2013**, *7*, 3557–3564.

[67] B. S. Flavel, K. E. Moore, M. Pfohl, M. M. Kappes, F. Hennrich, *ACS Nano* **2014**, *8*, 9687.

[68] S. Liang, H. Li, B. S. Flavel, A. Adronov, *Chem. Eur. J.* **2018**, *24*, 9799–9806.

[69] C. Y. Khripin, J. A. Fagan, M. Zheng, *J. Am. Chem. Soc.* **2013**, *135*, 6822–6825.

[70] J. A. Fagan, C. Y. Khripin, C. A. Silvera Batista, J. R. Simpson, E. H. Hároz, A. R. Hight Walker, M. Zheng, *Adv. Mater.* **2014**, *26*, 2800–2804.

[71] X. Tu, S. Manohar, A. Jagota, M. Zheng, *Nature* **2009**, *460*, 250–253.

[72] M. Zheng, A. Jagota, E. D. Semke, B. A. Diner, R. S. McLean, S. R. Lustig, R. E. Richardson, N. G. Tassi, *Nat. Mater.* **2003**, *2*, 338–42.

[73] S. Jung, J. Kim, J. Kim, S. H. Yang, S. K. Kim, *Biosens. Bioelectron.* **2017**, *94*, 256–262.

[74] M. Zheng, A. Jagota, M. S. Strano, A. P. Santos, P. Barone, S. G. Chou, B. A. Diner, M. S. Dresselhaus, R. S. McLean, G. B. Onoa, et al., *Science* **2003**, *302*, 1545–1548.

[75] M. S. Arnold, S. I. Stupp, M. C. Hersam, *Nano Lett.* **2005**, *5*, 713–718.

[76] G. Ao, C. Y. Khripin, M. Zheng, *J. Am. Chem. Soc.* **2014**, *136*, 10383–10392.

[77] S. N. Kim, Z. Kuang, J. G. Grote, B. L. Farmer, R. R. Naik, *Nano Lett.* **2008**, *8*, 4415–4420.

[78] P. Bilalis, D. Katsigiannopoulos, A. Avgeropoulos, G. Sakellariou, *RSC Adv.* **2014**, *4*, 2911–2934.

[79] S. K. Samanta, M. Fritsch, U. Scherf, W. Gomulya, S. Z. Bisri, M. A. Loi, *Acc. Chem. Res.* **2014**, *47*, 2446–2456.

[80] F. Chen, B. Wang, Y. Chen, L. J. Li, *Nano Lett.* **2007**, *7*, 3013–3017.

[81] J. Y. Hwang, A. Nish, J. Doig, S. Douven, C. W. Chen, L. C. Chen, R. J. Nicholas, *J. Am. Chem. Soc.* **2008**, *130*, 3543–3553.

[82] A. Nish, J. Hwang, J. Doig, R. J. Nicholas, *Nat. Nanotechnol.* **2007**, *2*.

[83] J. Gao, M. Kwak, J. Wildeman, A. Herrmann, M. A. Loi, *Carbon* **2011**, *49*, 333–338.

[84] G. J. Brady, Y. Joo, M. Y. Wu, M. J. Shea, P. Gopalan, M. S. Arnold, *ACS Nano* **2014**, *8*, 11614–11621.

[85] S. D. Stranks, A. M. R. Baker, J. A. Alexander-Webber, B. Dirks, R. J.

Nicholas, *Small* **2013**, *9*, 2245–2249.

[86] T. Schuettfort, A. Nish, R. J. Nicholas, *Nano Lett.* **2009**, *9*, 3871–3876.

[87] A. Ikeda, K. Nobusawa, T. Hamano, J. I. Kikuchi, *Org. Lett.* **2006**, *8*, 5489–5492.

[88] T. Schuettfort, H. J. Snaith, A. Nish, R. J. Nicholas, *Nanotechnology* **2010**, *21*, 1–9.

[89] H. W. Lee, Y. Yoon, S. Park, J. H. Oh, S. Hong, L. S. Liyanage, H. Wang, S. Morishita, N. Patil, Y. J. Park, et al., *Nat. Commun.* **2011**, *2*, 541–548.

[90] N. A. Rice, A. V Subrahmanyam, S. E. Laengert, A. Adronov, *Polym. Chem.* **2015**, *53*, 2510–2516.

[91] F. A. Lemasson, T. Strunk, P. Gerstel, F. Hennrich, S. Lebedkin, C. Barner-Kowollik, W. Wenzel, M. M. Kappes, M. Mayor, *J. Am. Chem. Soc.* **2011**, *133*, 652–655.

[92] N. A. Rice, A. Adronov, *J. Polym. Sci.* **2014**, *52*, 2738–2747.

[93] N. A. Rice, A. Adronov, *Macromolecules* **2013**, *46*, 3850–3860.

[94] P. Gerstel, S. Klumpp, F. Hennrich, O. Altintas, T. R. Eaton, M. Mayor, C. Barner-Kowollik, M. M. Kappes, *Polym. Chem.* **2012**, *3*, 1966–1970.

[95] T. Lei, Y. C. Lai, G. Hong, H. Wang, P. Hayoz, R. T. Weitz, C. Chen, H. Dai, Z. Bao, *Small* **2015**, *11*, 2946–2954.

[96] S. M. Keogh, T. G. Hedderman, E. Gregan, G. Farrell, G. Chambers, H. J. Byrne, *J. Phys. Chem. B* **2004**, *108*, 6233–6241.

[97] N. A. Rice, K. Soper, N. Zhou, E. Merschrod, Y. Zhao, *Chem. Commun.* **2006**, *4*, 4937–4939.

[98] K. Mulla, S. Liang, H. Shaik, E. A. Younes, A. Adronov, Y. Zhao, *Chem. Commun.* **2014**, *51*, 149–152.

[99] P. Imin, F. Cheng, A. Adronov, *Polym. Chem.* **2011**, *2*, 1404–1408.

[100] N. Berton, F. Lemasson, F. Hennrich, M. M. Kappes, M. Mayor, *Chem. Commun.* **2012**, *48*, 2516–2518.

[101] W. Gomulya, G. D. Costanzo, E. J. F. De Carvalho, S. Z. Bisri, V. Derenskyi, M. Fritsch, N. Fröhlich, S. Allard, P. Gordiichuk, A. Herrmann, et al., *Adv. Mater.* **2013**, *25*, 2948–2956.

[102] J. Ding, Z. Li, J. Lefebvre, F. Cheng, G. Dubey, S. Zou, P. Finnie, A. Hrdina, L. Scoles, G. P. Lopinski, et al., *Nanoscale* **2014**, *6*, 2328–2339.

[103] P. Imin, M. Imit, A. Adronov, *Macromolecules* **2011**, *44*, 9138–9145.

[104] L. Zhang, H. Wang, M. Chen, J. Ma, W. Wang, *Macromol. Res.* **2013**, *21*, 1083–1090.

[105] M. Y. Wu, J. Zhao, F. Xu, T. H. Chang, R. M. Jacobberger, Z. Ma, M. S. Arnold, *Appl. Phys. Lett.* **2015**, *107*.

[106] D. Sun, C. Liu, W. Ren, H. Cheng, *Small* **2013**, *9*, 1188–1205.

[107] B. Aksakal, A. R. Boccaccini, *J.R.Soc.Interface* **2010**, *7*, S581–S613.

[108] K. Wu, P. Imin, Y. Sun, X. Pang, A. Adronov, I. Zhitomirsky, *Mater. Lett.* **2012**, *67*, 248–251.

[109] E. Kymakis, E. Koudoumas, I. Franghiadakis, G. A. J. Amaratunga, *J. Phys. D. Appl. Phys.* **2006**, *39*, 1058–1062.

[110] C. Bounioux, E. A. Katz, R. Yerushalmi - Rozen, *Polym. Adv. Technol.* **2012**, *23*, 1129–1140.

[111] D. Fong, A. Adronov, *Chem. Sci.* **2017**, *8*, 7292–7305.

[112] S. N. Barman, M. C. Lemieux, J. Baek, R. Rivera, Z. Bao, *ACS Appl. Mater. Interfaces* **2010**, *2*, 2672–2678.

[113] W. Gomulya, J. M. S. Rios, V. Derenskyi, S. Z. Bisri, S. Jung, M. Fritsch, S. Allard, U. Scherf, M. C. Dos Santos, M. A. Loi, *Carbon* **2015**, *84*, 66–73.

[114] Z. Sun, I. O'Connor, S. D. Bergin, J. N. Coleman, *J. Phys. Chem. C* **2009**, *113*, 1260–1266.

[115] H. Wang, B. Hsieh, G. Jiménez-Osés, P. Liu, C. J. Tassone, Y. Diao, T. Lei, K. N. Houk, Z. Bao, *Small* **2015**, *11*, 126–133.

[116] F. Jakubka, S. P. Schießl, S. Martin, J. M. Englert, F. Hauke, A. Hirsch, J. Zaumseil, *ACS Macro Lett.* **2012**, *1*, 815–819.

[117] L. Qian, W. Xu, X. Fan, C. Wang, J. Zhang, J. Zhao, Z. Cui, *J. Phys. Chem. C* **2013**, *117*, 18243–18250.

[118] H. Wang, B. Hsieh, P. L. Gonzalo Jiménez-Osés, Y. D. Christopher J. Tassone, T. Lei, K. N. Houk, Zhenan Bao, *Small* **2015**, *11*, 126–133.

[119] D. Mann, Y. K. Kato, A. Kinkhabwala, E. Pop, J. Cao, X. Wang, L. Zhang,

Q. Wang, J. Guo, H. Dai, *Nat. Nanotechnol.* **2006**, *2*, 33–38.

[120] R. B. Weisman, *Appl. Phys. Carbon Nanotub. Fundam. Theory, Opt. Transp. Devices* **2005**, 183–202.

[121] A. V. Naumov, S. Ghosh, D. A. Tsyboulski, S. M. Bachilo, R. B. Weisman, *ACS Nano* **2011**, *5*, 1639–1648.

[122] R. B. Weisman, S. M. Bachilo, D. Tsyboulski, *Appl. Phys. A Mater. Sci. Process.* **2004**, *78*, 1111–1116.

[123] R. B. Weisman, S. M. Bachilo, *Nano Lett.* **2003**, *3*, 1235–1238.

[124] R. D. Mehlenbacher, M. Wu, M. Grechko, J. E. Laaser, M. S. Arnold, M. T. Zanni, *Nano Lett.* **2013**, *13*, 1495–1501.

[125] B. R. A. Graff, J. P. Swanson, P. W. Barone, S. Baik, D. A. Heller, M. S. Strano, *Adv. Mater.* **2005**, *17*, 980–984.

[126] N. A. Rice, A. V Subrahmanyam, B. R. Coleman, A. Adronov, *Macromolecules* **2015**, *48*, 5155–5161.

[127] D. Fong, W. J. Bodnaryk, N. A. Rice, S. Saem, J. M. Moran-Mirabal, A. Adronov, *Chem. Eur. J.* **2016**, *22*, 14560–14566.

[128] A. Jorio, M. A. Pimenta, A. G. Souza Filho, R. Saito, G. Dresselhaus, M. S. Dresselhaus, *New J. Phys.* **2033**, *5*, 139.1-139.17.

[129] S. Lefrant, M. Baibarac, I. Baltog, *J. Mater. Chem.* **2009**, *19*, 5690–5704.

[130] S. K. Doorn, *J. Nanosci. Nanotechnol.* **2005**, *5*, 1023–1034.

[131] S. D. M. Brown, A. Jorio, P. Corio, *Phys. Rev. Lett.* **2001**, *63*, 1–8.

[132] M. A. Pimenta, A. Marucci, *Phys. Rev. B* **1998**, *58*, 16–19.

[133] T. Park, S. Banerjee, T. Hemraj-benny, S. S. Wong, T. Park, *J. Mater. Chem.* **2006**, *16*, 141–154.

[134] M. Garrett, I. N. Ivanov, D. Geohegan, B. Hu, *Carbon* **2013**, *64*, 1–5.

[135] L. Farhan, R. Kharel, O. Kaiwartya, M. Quiroz-Castellanos, A. Alissa, *11th Int. Symp. Commun. Syst. Networks, Digit. Signal Process.* **2018**.

[136] M. N. Bhuiyan, M. Rahman, M. Billah, D. Saha, *IEEE Internet Things J.* **2021**, *8*, 10474–10498.

[137] T. Kramp, R. Van Kranenburg, S. Lange, *Enabling Things to Talk. Springer, Berlin, Heidelb.* **2013**.

[138] P. Asghari, A. Masoud, H. Haj, S. Javadi, *Comput. Networks* **2019**, *148*, 241–261.

[139] S. Kumar, P. Tiwari, M. Zymbler, *J. Big Data* **2019**, *6*, 1–21.

[140] S. Chandrasekaran, A. Jayakumar, R. Velu, *Nanomaterials* **2022**, *12*, 1–23.

[141] C. W. Shen, P. P. Tran, P. T. M. Ly, *Sustainability* **2018**, *10*, 1–14.

[142] C. S. Buga, J. C. Viana, *Flex. Print. Electron.* **2022**, *7*, 043001.

[143] E. Kunnari, J. Valkama, M. Keskinen, P. Mansikkama, *J. Clean. Prod.* **2009**, *17*, 791–799.

[144] P. Lall, G. Kartik, J. Narangaparambil, *2020 IEEE 70th Electron. Components Technol. Conf.* **2020**, 1070–1080.

[145] B. A. Kuzubasoglu, E. Sayar, S. K. Bahadir, *IEEE Sens. J.* **2021**, *21*, 13090–13097.

[146] A. Rivadeneyra, M. Bobinger, A. Albrecht, M. Becherer, P. Lugli, A. Falco, J. F. Salmer, *Polym. Eng. Sci.* **2019**, *11*, 1–11.

[147] L. D. Capabilities, *Sensors* **2017**, *17*, 1–12.

[148] S. Kim, *Electronics* **2020**, *9*, 1–22.

[149] L. Yang, S. Member, A. Rida, S. Member, R. Vyas, M. M. Tentzeris, S. Member, *IEEE Trans. Microw. Theory Tech.* **2007**, *55*, 2894–2901.

[150] L. Hu, J. Wook, Y. Yang, S. Jeong, F. La, L. Cui, Y. Cui, *PNAS* **2009**, *106*, 21490–21494.

[151] F. Hoeng, J. Bras, *Nanomaterials* **2016**, *8*, 13131–13154.

[152] C. Wang, K. Xia, Y. Zhang, D. L. Kaplan, *Acc. Chem. Res.* **2019**, *52*, 2916–2927.

[153] R. N. Hussein, K. Schlingman, C. Noade, R. S. Carmichael, *Flex. Print. Electron.* **2022**, *7*, 045007.

[154] J. Suikkola, T. Björninen, M. Mosallaei, T. Kankkunen, P. Iso-ketola, L. Ukkonen, J. Vanhala, M. Mäntysalo, *Sci. Rep.* **2016**, 1–8.

[155] A. Larmagnac, S. Eggenberger, H. Janossy, J. Vo, *Sci. Am.* **2014**, *4*, 1–7.

[156] A. You, M. Be, I. In, *Appl. Phys. Lett.* **2014**, *105*, 013506.

[157] V. R. Feig, H. Tran, Z. Bao, *ACS Cent. Sci.* **2018**, *4*, 337–348.

[158] M. J. Tan, C. Owh, P. L. Chee, A. Ko, K. Kyaw, D. Kai, X. J. Loh, *J. Mater. Chem. C* **2016**, *4*, 5531–5558.

[159] W. Li, Q. Liu, Y. Zhang, C. Li, Z. He, W. C. H. Choy, P. J. Low, P. Sonar, A. Ko, K. Kyaw, *Adv. Mater.* **2020**, *32*, 1–40.

[160] I. J. Fernandes, A. F. Aroche, A. Schuck, P. Lamberty, *Sci. Rep.* **2020**, *10*, 8878.

[161] A. Mahajan, C. D. Frisbie, L. F. Francis, *Appl. Mater. Interfaces* **2013**, *5*, 4856–4864.

[162] V. A. K, K. Rao, P. S. Karthik, S. Prakash, *RSC Adv.* **2015**, *5*, 63985–64030.

[163] J. Sung, K. Hak, S. Kim, J. Ryu, *J. Mater. Sci Mater Electron* **2010**, *21*, 1213–1220.

[164] H. W. Tan, J. An, C. K. Chua, T. Tran, *Adv. Electron. Mater.* **2019**, *5*, 1800831.

[165] C. G. Núñez, L. Manjakkal, F. Liu, R. Dahiya, *IEEE sensors* **2018**, *1*, 1–4.

[166] K. Liang, D. Li, H. Ren, M. Zhao, H. Wang, M. Ding, G. Xu, X. Zhao, S. Long, S. Zhu, et al., *Nano-Micro Lett.* **2021**, *13*, 1–11.

[167] M. Berggren, D. Nilsson, N. D. Robinson, O. Electronics, L. Universitet, S.- Norrköping, S.- Norrköping, *Nat. Mater.* **2007**, *6*, 3–5.

[168] W. Clemens, W. Fix, J. Ficker, A. Knobloch, A. Ullmann, *J.Mater.Res.*

**2004**, *19*, 1963–1973.

[169] K. Baeg, D. Khim, J. Kim, D. Kim, S. Sung, *IEEE Electron Device Lett.* **2013**, *34*, 126–128.

[170] F. Torrisi, T. Hasan, W. Wu, Z. Sun, A. Lombardo, T. S. Kulmala, G. Hsieh, S. Jung, F. Bonaccorso, P. J. Paul, et al., *acs n* **2012**, *6*, 2992–3006.

[171] P. He, J. Cao, H. Ding, C. Liu, J. Neilson, Z. Li, I. A. Kinloch, B. Derby, *Appl. Mater. Interfaces* **2019**, *11*, 32225–322234.

[172] Y. Z. N. Htwe, M. Mariatti, *J. Sci. Adv. Mater. Devices* **2022**, *7*, 100435.

[173] K. Schnittker, M. Tursunniyaz, J. B. Andrews, *J. Inf. Disp.* **2021**, *22*, 193–209.

[174] K. Chen, W. Gao, S. Emaminejad, D. Kiriya, H. Ota, H. Yin, Y. Nyein, K. Takei, A. Javey, *Adv. Mater.* **2016**, *28*, 4397–4414.

[175] S. Lu, A. D. Franklin, S. Lu, A. D. Franklin, *Nanoscale* **2020**, *12*, 23371–23390.

[176] R. Zhang, H. Nilsson, *PLoS One* **2011**, *6*, 1–6.

[177] J. Perelaer, P. J. Smith, D. Mager, D. Soltman, S. K. Volkman, V. Subramanian, G. Korvink, U. S. Schubert, *J. Mater. Chem.* **2010**, *20*, 8446–8453.

[178] J. Lee, J. Kim, J. Park, C. Lee, *Flex. Print. Electron.* **2018**, *3*, 025001.

[179] G. Cummins, P. Marc, Y. Desmulliez, *Circuit Wolrd* **2012**, *38*, 193–213.

[180] J. Sheng, H. Lee, S. Oh, J. Park, *Appl. Mater. Interfaces* **2016**, *8*, 33821–33828.

[181] M. M. Payne, S. R. Parkin, J. E. Anthony, C. Kuo, T. N. Jackson, *J. Am. Chem. Soc* **2005**, *127*, 4986–4987.

[182] Y. Mei, M. A. Loth, M. Payne, W. Zhang, J. Smith, C. S. Day, S. R. Parkin, M. Heeney, I. Mcculloch, T. D. Anthopoulos, et al., *Adv. Mater.* **2013**, *25*, 4352–4357.

[183] H. Minemawari, T. Yamada, H. Matsui, J. Tsutsumi, S. Haas, R. Chiba, R. Kumai, T. Hasegawa, *Nature* **2011**, *475*, 5–8.

[184] B. M. M. Voigt, A. Guite, D. Chung, R. U. A. Khan, A. J. Campbell, D. D. C. Bradley, F. Meng, J. H. G. Steinke, S. Tierney, I. Mcculloch, et al., *Adv. Funct. Mater.* **2010**, *20*, 239–246.

[185] L. Lo, J. Zhao, H. Wan, Y. Wang, S. Chakrabartty, C. Wang, *Appl. Mater. Interfaces* **2021**, *2021*, 21693–21702.

[186] S. Chung, K. Cho, T. Lee, *Adv. Sci.* **2019**, 6, *1801445*.

[187] Y. Woo, H. Klauk, *Chem. Soc. Rev.* **2010**, *39*, 2643–2666.

[188] J. Wiklund, A. Karakoç, T. Palko, H. Yi, K. Ruttik, R. Jäntti, J. Paltakari, *J. Manuf. Mater. Process.* **2021**, *5*, 1–36.

[189] B. S. Gamerith, A. Klug, H. Scheiber, U. Scherf, E. Moderegger, E. J. W. List, *Adv. Funct. Mater.* **2007**, *17*, 31111–3718.

[190] T. Pandhi, A. Chandnani, H. Subbaraman, D. Estrada, *Sensors* **2020**, *20*,

1–20.

[191] S. K. Garlapati, M. Divya, B. Breitung, R. Kruk, H. Hahn, *Adv. Mater.* **2018**, *1707600*, 1–55.

[192] E. Llobet, *Sensors Actuators B. Chem.* **2012**, *179*, 32–45.

[193] C. K. Najeeb, J. H. Lee, J. Chang, J. H. Kim, *Nanotechnology* **2010**, *21*.

[194] E. Gracia-espino, G. Sala, F. Pino, N. Halonen, J. Luomahaara, J. Ma, H. Jantunen, M. Terrones, P. Helisto, H. Seppa, et al., *ACS Nano* **2010**, *4*, 3318–3324.

[195] Y. Zhou, L. Hu, G. Grüner, *Appl. Phys. Lett.* **2006**, *88*, 1–4.

[196] L. Yang, S. Member, R. Zhang, S. Member, D. Staiculescu, *IEEE Antennas Wirel. Propag. Lett.* **2009**, *8*, 653–656.

[197] S. Matsuzaki, Y. Nobusa, R. Shimizu, K. Yanagi, H. Kataura, T. T. Ã, *Jpn. J. Appl. Phys.* **2012**, *51*, 1–3.

[198] J. Chen, S. Mishra, D. Vaca, N. Kumar, *Nanotechnology* **2020**, 235301.

[199] P. D. Angelo, R. R. Farnood, *J. Adhes. Sci. Technol.* **2010**, *24*, 643–659.

[200] H. Okimoto, T. Takenobu, K. Yanagi, Y. Miyata, H. Shimotani, H. Kataura, Y. Iwasa, *Adv. Mater.* **2010**, *22*, 3981–3986.

[201] Y. Nobusa, Y. Takagi, S. Gocho, S. Matsuzaki, K. Yanagi, T. Takenobu, *Jpn. J. Appl. Phys.* **2012**, *51*, 2–4.

[202] P. Beecher, P. Servati, A. Rozhin, A. Colli, V. Scardaci, S. Pisana, T. Hasan, A. J. Flewitt, J. Robertson, G. W. Hsieh, et al., *J. Appl. Phys.* **2007**,

*102*, 043710.

[203] A. R. Hopkins, D. C. Straw, K. C. Spurrell, *Thin Solid Films* **2011**, *520*, 1541–1545.

[204] R. Tortorich, J.-W. Choi, *Nanomaterials* **2013**, *3*, 453–468.

[205] C. Yeom, K. Chen, D. Kiriya, Z. Yu, G. Cho, A. Javey, *Adv. Mater.* **2015**, *27*, 1561–1566.

[206] U. S. C. Tfts, J. Noh, M. Jung, K. Jung, G. Lee, J. Kim, S. Lim, D. Kim, Y. Choi, Y. Kim, et al., *IEEE Antennas Wirel. Propag. Lett.* **2011**, *32*, 638–640.

[207] J. Noh, S. Kim, K. Jung, J. Kim, S. Cho, G. Cho, *IEEE Electron Device Lett.* **2011**, *32*, 1555–1557.

[208] X. Yin, S. Kumar, *Chem. Eng. Sci.* **2006**, *61*, 1146–1156.

[209] L. Lan, J. Zou, C. Jiang, B. Liu, L. Wang, J. Peng, *Front. Optoelectron.* **2017**, *10*, 329–352.

[210] B. Kim, M. L. Geier, M. C. Hersam, A. Dodabalapur, *Sci. Rep.* **2017**, *6*, 1–8.

[211] C. Wang, J. Chien, K. Takei, T. Takahashi, J. Nah, *Nano Lett.* **2012**, *12*, 1527–1533.

[212] X. Wang, M. Wei, X. Li, S. Shao, Y. Ren, W. Xu, M. Li, W. Liu, X. Liu, J. Zhao, *Appl. Mater. Interfaces* **2020**, *12*, 51797–51807.

[213] Y. Ren, M. Li, X. Li, Y. Geng, X. Wang, J. Zhao, *J. Mater. Chem. C* **2021**,

*9*, 2133–2144.

[214] T. Takahashi, K. Takei, A. G. Gillies, R. S. Fearing, A. Javey, *Nano Lett.* **2011**, *11*, 5408–5413.

[215] T. Sekitani, H. Nakajima, H. Maeda, T. Fukushima, T. Aida, K. Hata, T. Someya, *Nat. Mater.* **2009**, *8*, 4–6.

[216] T. Kim, H. Song, J. Ha, S. Kim, D. Kim, S. Chung, J. Lee, Y. Hong, *Appl. Phys. Lett.* **2014**, *104*, 113103.

[217] J. Zaumseil, *Semicond. Sci. Technol.* **2015**, *30*, 74001.

[218] S. Lu, A. D. Franklin, S. Lu, A. D. Franklin, *Nanoscale* **2020**, *12*, 23371–23390.

[219] B. Norton-baker, R. Ihly, I. E. Gould, A. D. Avery, Z. R. Owczarczyk, A. J. Ferguson, L. Blackburn, *ACS Energy Lett.* **2016**, *1*, 1212–1220.

[220] Z. Li, J. Ding, C. Guo, J. Lefebvre, P. R. L. Malenfant, *Adv. Funct. Mater.* **2018**, *28*, 1705568.

[221] T. Lei, X. Chen, G. Pitner, H. S. P. Wong, Z. Bao, *J. Am. Chem. Soc.* **2016**, *138*, 802–805.

[222] L. Xu, M. Valášek, F. Hennrich, R. Fischer, M. M. Kappes, M. Mayor, *Macromolecules* **2021**, *54*, 4363–4374.

[223] M. E. Belowich, J. F. Stoddart, *Chem. Soc. Rev.* **2012**, *41*, 2003–2024.

[224] W. Z. Wang, W. F. Li, X. Y. Pan, C. M. Li, L. Li, Y. G. Mu, J. A. Rogers, M. B. Chan-park, *Adv. Funct. Mater.* **2011**, *21*, 1643–1651.

[225] F. Lemasson, J. Tittmann, F. Hennrich, N. Stu, M. M. Kappes, M. Mayor, *Chem.Comm.* **2011**, *47*, 7428–7430.

[226] W. J. Bodnaryk, K. Li, A. Adronov, *J. Polym. Sci.* **2020**, *58*, 1965–1972.

[227] S. Liang, Y. Zhao, A. Adronov, *J. Am. Chem. Soc.* **2014**, *136*, 970–977.

[228] F. Toshimitsu, N. Nakashima, *Nat. Commun.* **2014**, *5*, 1–9.

[229] I. Pochorovski, H. Wang, J. I. Feldblyum, X. Zhang, A. L. Antaris, *J. Am. Chem. Soc.* **2015**, *137*, 4328–4331.

[230] P. He, S. Shimano, K. Salikolimi, T. Isoshima, Y. Kakefuda, T. Mori, Y. Taguchi, Y. Ito, M. Kawamoto, *ACS Appl. Mater. Interfaces* **2018**, *11*, 4211–4218.

# Chapter 2

# Functionalization of polyfluorene-wrapped carbon nanotubes using thermally cleavable side-chains

This chapter has been reprinted with permission from Journal of Polymer Science: Ritaine, D.; Adronov, A. Functionalization of polyfluorene-wrapped carbon nanotubes using thermally cleavable side-chains. *J. Polym. Sci.* (2022) doi:10.1002/pol.20220362.

**Abstract**

The length and nature of side-chains in conjugated polymer-wrapped carbon nanotubes can impact their conductivity. We investigate the functionalization of polyfluorene-SWNTs using cleavable side-chains that are removable post-processing. The triethylene glycol side-chains contain a thermally cleavable carbonate linker. Upon heating the films to 170 °C, the conductivity increased, reaching a plateau of $(2.0 \pm 0.1) \times 10^{-2}$ S/m after 16 hours, compared to $(1.0 \pm 0.2) \times 10^{-3}$ S/m for the control sample. UV-Vis-NIR and Raman spectroscopy show well-dispersed SWNT samples and confirm that the heating treatment did not damage the nanotubes. Functionalization using longer polyethylene glycol side-chains was also investigated. After heating, cleavage of the longer chains resulted in conductivity of $(8.2 \pm 1.6) \times 10^{-4}$ S/m compared to $(8.1 \pm 1.4) \times 10^{-5}$ S/m for the control. UV-Vis-NIR and Raman spectroscopy showed well-dispersed SWNT samples and confirmed that the nanotubes were not damaged. Finally, we investigate dispersions in triethylene glycol monomethyl ether and tetraethylene glycol dimethyl ether, generally deemed “green” solvents. Polymer-SWNT complexes functionalized with shorter side-chains did not form stable dispersions, resulting in precipitation of the nanotubes upon standing for a few minutes after the removal of THF, while complexes functionalized with longer side-chains formed stable dispersions.

## 2.1 Introduction

Since their discovery, single-walled carbon nanotubes (SWNTs)[1] have received extensive interest in materials science due to their mechanical,[2,3] optical,[4,5] and electronic properties.[6,7] Many applications of SWNTs have been reported, such as sensors,[8,9] thin film transistors,[10,11] organic photovoltaics,[12,13] flexible electronics,[14,15] conductive inks,[16,17] and numerous other devices.[18,19] However, all commercial methods for SWNT production[20,21] result in a complex mixture of amorphous carbon, leftover catalyst particles, as well as a heterogeneous mixture of semiconducting and metallic species (sc- and m-SWNTs, respectively) that significantly diminish their performance within many applications.[22] Moreover, the inter-tube π–π interactions result in an aggregation of SWNTs into bundles that are insoluble in common organic solvents.[23] As a result, various functionalization techniques have been developed to improve their solubility and purity, and these techniques are broadly classified as either covalent or non-covalent strategies. Covalent functionalization requires strongly oxidizing conditions that damage the SWNT surface and therefore impact SWNT properties.[24,25] In contrast, non-covalent functionalization uses sonication in the presence of a dispersant to form a dispersant-SWNT supramolecular complex that provides solubility in organic solvents and prevents the reaggregation of SWNTs into bundles.[26–28] Various dispersants such as small aromatic compounds,[29–31] surfactants,[32–34] biomolecules,[35–37] and conjugated polymers[38–41] have been used. Among these dispersants, conjugated polymers have received significant attention due to their facile structural modification, such as the molecular weight, polymer

backbone structure, and side-chain structure, to achieve desirable properties.[42–46] This has allowed conjugated polymer structures to achieve selective dispersion of either sc- or m-SWNTs,[47–50] reversible assembly on the nanotube surface,[51–55] or depolymerization in response to a stimulus to release SWNTs.[56–58]

Recently, attention has also been given to conjugated polymers that can react post-supramolecular functionalization. To this end, our group prepared polyfluorene derivatives containing azide groups in the side-chains and used them to noncovalently functionalize SWNTs.[59–61] The resulting polyfluorene-SWNT complexes, dispersed in organic or aqueous solvents were then functionalized using either copper-catalyzed azide–alkyne cycloaddition (CuAAC) or strain-promoted azide–alkyne cycloaddition (SPAAC) without damaging SWNT optoelectronic properties.[59–61] To achieve aqueous solubility, polyfluorene-SWNT complexes were functionalized using a series of polyethylene glycol (PEG) derivatives. However, these large side-chains are non-conductive and remain at the nanotube surface, resulting in a dramatic decrease in conductivity of the polymer-SWNT complex by preventing good contact between adjacent nanotubes. A potential approach to solve this problem is the use of cleavable side-chains that can be removed after the device's fabrication. Some studies have shown an increase in performance after removing the side-chain, such as improved power conversion efficiency for organic photovoltaic cells,[62–66] improvement in semiconducting properties,[67,68] or an increase in conductivity of polymer-SWNT thin films.[69,70]

In this report, we describe the functionalization of a polyfluorene-SWNT complex with a thermally cleavable side-chain containing a carbonate linker. Side-chains containing carbonate linkers can be cleaved by decarboxylation without leaving fragments on the polymer at temperatures from 140 to 350 °C.[69,71,72] The moderate processing temperature required to cleave the side-chains allows the fabrication of devices on different substrates and generally results in a more robust and performant device.[71] Here, we are interested in comparing the conductivity of our polyfluorene-SWNT complex functionalized with either cleavable or non-cleavable side-chains. We first prepared SWNT complexes containing triethylene glycol side-chains that provide solubility in organic solvents. Then, we were interested in using larger side-chains that could provide solubility in "greener" solvents, allowing their potential application in "green" organic electronics.

## 2.2 Results and Discussion

**Polymer synthesis and characterization.** To begin our investigation, we prepared an azide-containing polyfluorene (**PF-$N_3$**) according to literature procedures.[61] Commercial fluorene was brominated using *N*-bromosuccinimide (NBS) to produce precursor **1** (Supporting Information, Scheme 2.3) followed by phase-transfer alkylation with 1,6-dibromohexane to obtain compound **2**. Compound **2** was then borylated using Miyaura conditions to afford diboronate **3**. Monomers **2** and **3** were then copolymerized using Suzuki polycondensation to obtain the homopolymer **PF-Br** (Scheme 2.1). Gel permeation chromatography (GPC) revealed an $M_n$ of 33 kDa and a dispersity

(Đ) of 2.2. **PF-$N_3$** was then obtained via a reaction between **PF-Br** and $^{n}Bu_4N(N_3)$ (generated in situ). The homopolymers were characterized by $^{1}$H-NMR spectroscopy to confirm the presence of alkyl azides (3.15 ppm) in **PF-$N_3$** and the disappearance of the signal corresponding to the alkyl bromides (3.31 ppm) in **PF-Br** (Supporting Information, Figure 2.14).

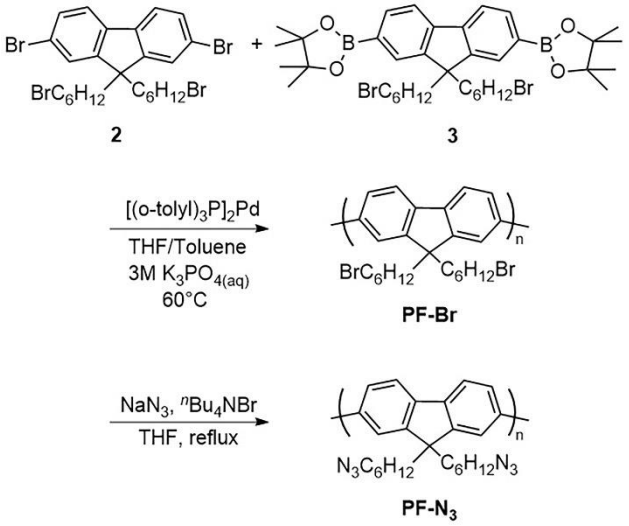


Scheme 2. 1. Synthesis of **PF-Br** and **PF-$N_3$**.

To introduce thermally cleavable side-chains, we prepared a TEG-carbonate-alkyne via activation of propargyl alcohol with N,N-carbonyldiimidazole (CDI) followed by treatment with triethylene glycol monomethyl ether and 4-dimethylaminopyridine (Supporting Information, Scheme 2.6). The non-thermally cleavable analog was obtained via nucleophilic substitution of propargyl bromide with triethylene glycol monomethyl ether (TEG-OH) to obtain the TEG-alkyne (Supporting Information, Scheme 2.7). **PF-$N_3$** was then functionalized with either TEG-alkyne (**P1**) or TEG-carbonate-alkyne (**P2**) using copper-catalyzed azide-alkyne cycloaddition (CuAAC) (see Supporting Information for details). The reaction was monitored by infrared (IR)

spectroscopy via the disappearance of the polymer azide stretch at ~2090 $cm^{-1}$ (Supporting Information, Figure 2.15). The resulting polymers were also characterized by $^{1}$H-NMR spectroscopy to confirm the disappearance of the alkyl azides (3.15 ppm), the appearance of the aromatic proton in the triazole ring (7.51 ppm), as well as the appearance of alkyl protons from the side-chain between 3 and 5 ppm (Supporting Information, Figure 2.16).

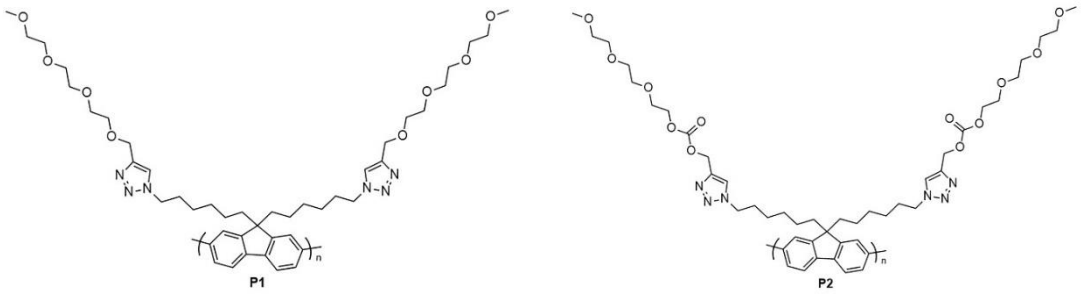


Figure 2.1. Chemical structure of **P1** and **P2**.

**Thermal cleavage of the side-chains.** The thermal cleavage of the side-chains was investigated by thermogravimetric analysis combined with mass spectrometry (TGA-MS) (Figure 2.2). The TGA-MS profile of **P2** exhibited ~15% weight loss between 150 °C and 200 °C, corresponding to the loss of $CO_2$ (m/z = 44). In contrast, no mass loss was detected for **P1** at the same temperature due to the absence of a cleavable linker. At higher temperatures, the decomposition of the side-chains is observed for both polymers. The major fragments detected by mass spectrometry correspond to the ether-based fragments from α-cleavage of the triethylene glycol chains as well as fragments corresponding to the triazole and fragmented alkyl chains of the polymer at m/z values of 31, 44, 59, 69, and 84 (see the Supporting Information, Figure 2.17).

This indicates that programmed cleavage of the carbonate linkage occurs at approximately 170 - 200 °C, followed by the decomposition of the rest of the side-chain.

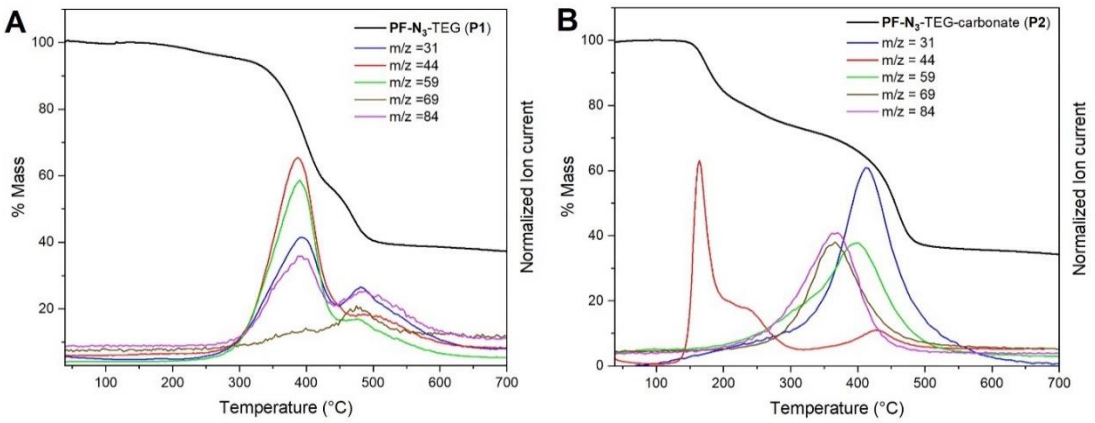


Figure 2.2. TGA-MS profiles under argon of A) **P1**, and B) **P2**. Heating rate: 10 °C/min.

We next investigated the length of time required to cleave the side-chains. Polymers were held at 200 °C under argon for 1 hour. As shown in Figure 2.3, the % mass of **P2** sharply decreased during the first 10 minutes from 100 % to ~ 80 %. In contrast, the mass loss for **P1** was significantly less pronounced, with a % mass decrease from 100 to 95% over the same time period. After 30 min of heating, the mass loss for both polymers slows significantly. This suggests that 30 minutes is sufficient to cleave the thermally cleavable side-chains.

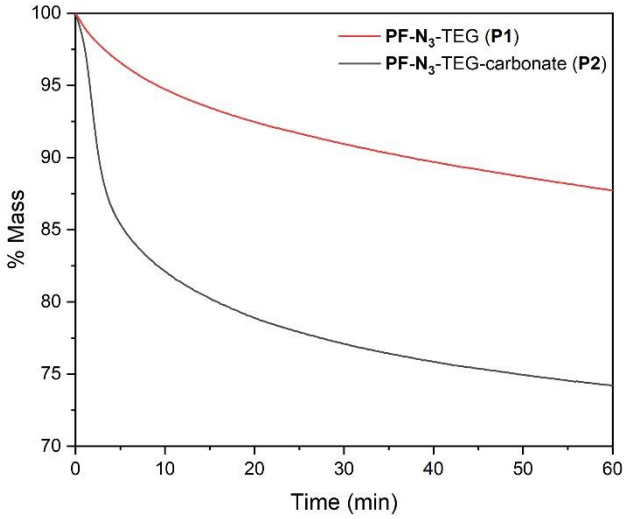


Figure 2.3. TGA thermograms for **P1** (red) and **P2** (black) at 200 °C under argon for 1 hour.

**Polymer-SWNT dispersions.** With the cleavage temperature and heating time identified, we next prepared our polymer-SWNT complexes. Complexes between either **P1** or **P2** and raw HiPco SWNTs (average tube diameter 0.8 – 1.2 nm) were prepared following literature procedures.[59] Briefly, a mixture of 7.5 mg of **P1** or **P2** and 5 mg of SWNTs in 10 mL of tetrahydrofuran (THF) was sonicated using a probe sonicator for 1 hour. The resulting black suspension was centrifuged at 8,346 *g* for 30 minutes, and the supernatant was carefully removed to isolate the **P1**-SWNT and **P2**-SWNT dispersions. Unfortunately, the resulting samples were not well dispersed and not concentrated enough to continue our study (see Supporting Information, Figure 2.18). This could be due to the presence of the TEG side-chains that may wrap around the polyfluorene backbone and therefore disrupt the π–π interaction between the backbone and the SWNTs. We then decided to functionalize **PF-N$_3$** post-dispersion. Briefly, a mixture of 7.5 mg of **PF-N$_3$** and 5 mg of SWNTs in 10 mL of tetrahydrofuran

(THF) was sonicated using a probe sonicator for 1 hour. The resulting black suspension was centrifuged at 8,346 *g* for 30 minutes, and the supernatant was carefully removed to isolate the **PF-$N_3$**-SWNT dispersion. Following literature procedures, the side-chains were introduced *in situ* via CuAAC (Scheme 2.2).[59] The reactions were monitored by IR spectroscopy via the disappearance of the polymer azide stretch at ~2090 $cm^{-1}$ (Supporting Information, Figure 2.19), filtered through a Teflon membrane with 0.2 µm pore diameter and thoroughly rinsed with THF to remove all free polymer in solution. The resulting thin films were then redispersed in 10 mL of THF using a probe sonicator for 30 minutes to obtain **PF-$N_3$**-TEG-SWNT and **PF-$N_3$**-TEG-carbonate-SWNT.

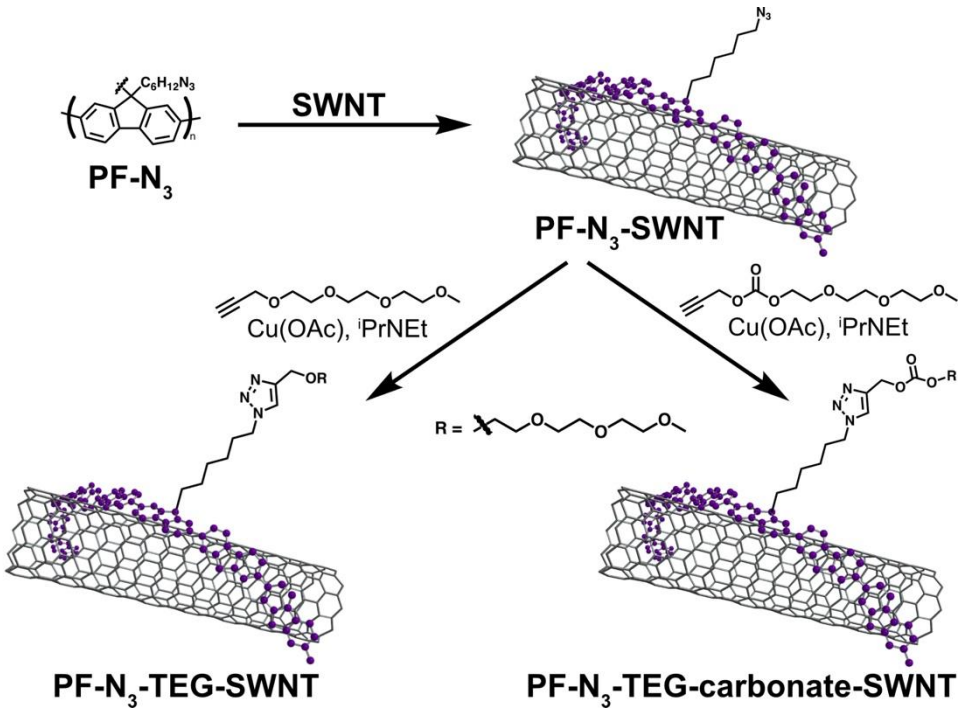


Scheme 2.2. Schematic representation of a CuAAC functionalization of **PF-$N_3$** using **TEG-alkyne** and **TEG-carbonate-alkyne.**

To characterize our polymer-SWNT complexes, we first used UV−Vis Near-Infrared (NIR) absorption spectroscopy (Figure 2.4). Each SWNT species present within the polymer-SWNT sample exhibits its own absorption signals. For HiPco SWNTs, three main regions are observed: two semiconducting regions, $S_{11}$ (830−1600 nm) and $S_{22}$ (600−800 nm), and one metallic region, $M_{11}$ (440−645 nm).[5] The absorption spectra were normalized to the maximum absorption of the peak at 1140 nm to compare the different SWNT species. **PF-$N_3$**-SWNT and the post-click dispersions (**PF-$N_3$**-TEG-SWNT and **PF-$N_3$**-TEG-carbonate-SWNT) show similar absorption features, suggesting a successful post-functionalization redispersion. As shown in Figure 2.4, both m- and sc-SWNT species are present within the polymer-SWNT complexes, suggesting a lack of any selectivity for specific SWNT types under the dispersion conditions used.

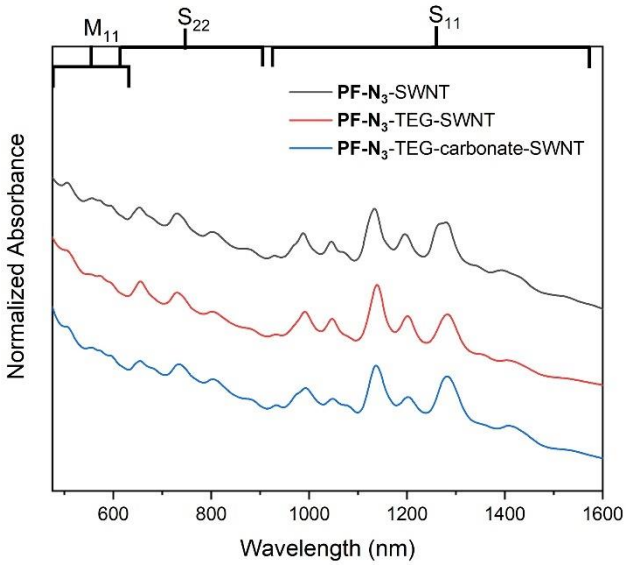


Figure 2.4. UV-Vis-NIR absorption spectra for **PF-$N_3$**-SWNT (top), **PF-$N_3$**-TEG-SWNT (middle) and **PF-$N_3$**-TEG carbonate-SWNT (bottom). Spectra were normalized to the signal at 1140 nm and offset for clarity.

To further characterize our polymer-SWNT complexes, Raman spectroscopy was performed. This technique utilizes laser excitation wavelengths that overlap with the van Hove singularities present in the density of states for a specific SWNT species.[73] Therefore, this technique allows the examination of both m- and sc-SWNT species present in the polymer-SWNT sample.[74] Since electronic transitions depend on SWNT diameter and type, multiple excitation wavelengths are needed for a broad range of SWNTs.[74] The polymer-SWNT samples for Raman spectroscopy were prepared by drop-casting the dispersion onto a silicon wafer, followed by evaporation at RT. A reference sample was prepared by sonicating raw SWNTs in chloroform followed by the same drop-casting method. For HiPco SWNTs, two excitation wavelengths were used: 633 and 785 nm. Using these wavelengths, both m- and sc-SWNTs are separately probed.[75] Figure 2.5 shows the radial breathing mode (RBM) for **PF-N$_3$**-SWNT, **PF-N$_3$**-TEG-SWNT and **PF-N$_3$**-TEG-carbonate-SWNT dispersions. The spectra were normalized to the G-band (~ 1590 cm$^{-1}$) for comparative analysis (full spectra are provided in the Supporting Information, Figure 2.20). Using the 633 nm excitation wavelength, both m- (175−230 cm$^{-1}$) and sc-SWNTs (240−300 cm$^{-1}$) are in resonance and signals corresponding to both nanotube types are observed (Figure 2.5A).[76] We then used the 785 nm excitation wavelength to characterize our samples. sc-SWNTs are primarily in resonance (175-280 cm$^{-1}$) when using this wavelength. When raw HiPco SWNTs are excited at 785 nm, a peak at 265 cm$^{-1}$ corresponding to bundled (10,2) SWNTs is observed.[77] As shown on the spectra (Figure 2.5B), the intensity of this peak in the polymer-SWNT samples is significantly lower

compared to the reference sample. This indicates that our samples are relatively well dispersed.

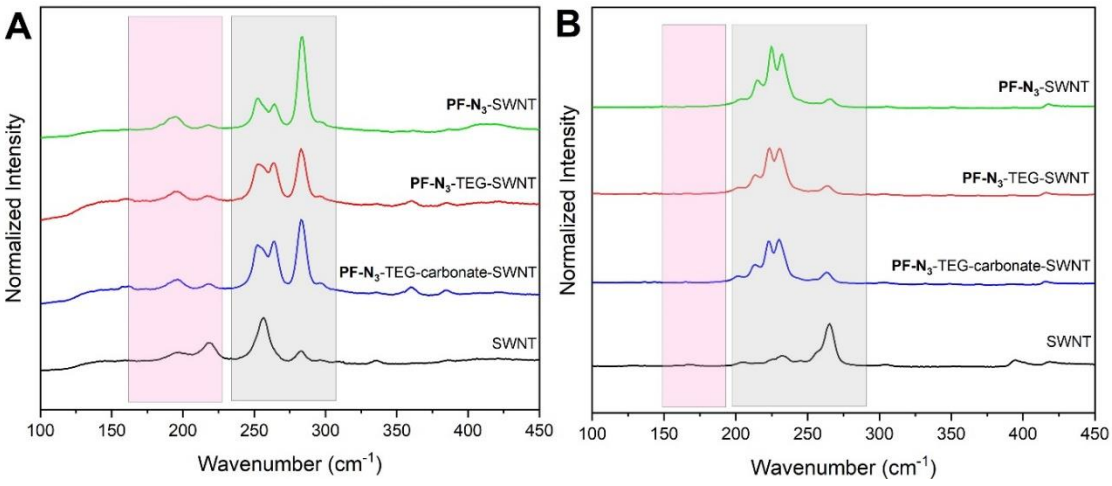


Figure 2.5. Raman Spectra of HiPco polymer-SWNT samples showing the RBM regions at A) $\lambda_{ex}$ = 633 nm, B) $\lambda_{ex}$ = 785 nm. Gray boxes represent signals arising for sc-SWNTs, whereas pink boxes represent m-SWNTs. All the spectra were normalized to the G-band at ~ 1590 $cm^{-1}$.

**Thermal cleavage of the side-chains on polymer-SWNT thin films.** As noted above, the temperature and heating time to cleave the side-chains on the polymer were determined to be 170 - 200 °C and 30 minutes of heating. To confirm that the polymer has the same behaviour within the polymer-SWNT complex, **PF-N$_3$**-TEG-SWNT and **PF-N$_3$**-TEG-carbonate-SWNT were heated at both 200 and 170 °C for 1 hour under argon in the TGA instrument. As shown in Figure 2.6, the behaviour of both samples is similar to that of the polymers alone. At both temperatures, the cleavable sample exhibits a pronounced mass loss due to thermal decomposition of side-chains, and the rate of mass loss is higher at the higher temperature, as expected. The non-cleavable sample

exhibits a small initial mass loss, likely due to the evaporation of residual strongly hydrogen-bonded water, but then the mass plateaus and remains constant. We also attempted heating at lower temperatures (130 and 150 °C) and found similar behaviour, where the amount of mass loss for the cleavable sample after 60 minutes decreased as the temperature was lowered (data not shown). From this data, it is clear that the cleavable samples undergo the expected side-chain cleavage at temperatures above 150 °C.

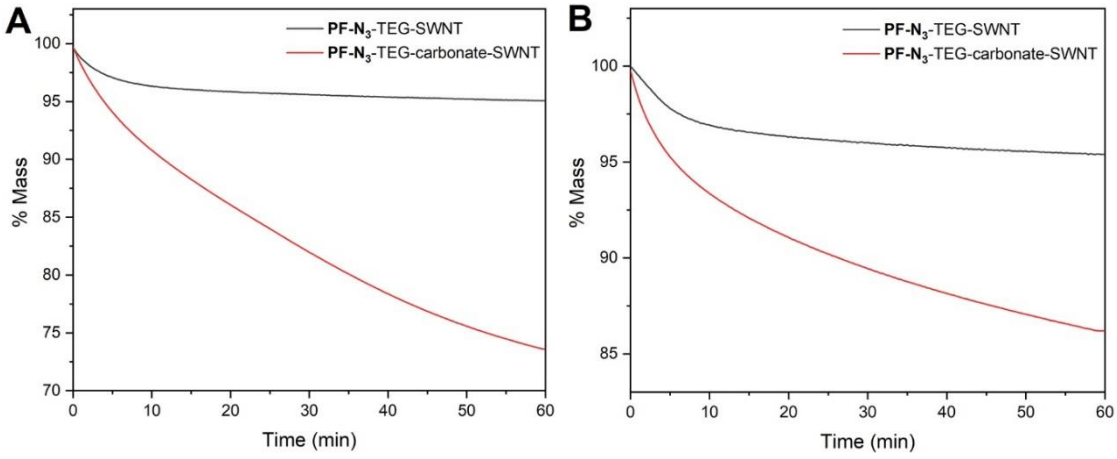


Figure 2.6. TGA thermographs of **PF-N$_3$**-TEG-SWNT and **PF-N$_3$**-TEG-carbonate-SWNT at A) 200 °C and B) 170 °C under argon for 1 hour.

**Conductivity measurements.** We next performed conductivity measurements using a four-point probe method (see Supporting Information for details). Thin films were prepared by filtration of **PF-N$_3$**-TEG-SWNT and **PF-N$_3$**-TEG-carbonate-SWNT through a Teflon membrane with 0.2 µm pore diameter followed by overnight drying at 75 °C in a vacuum oven. Measurements were performed in triplicate on each **PF-N$_3$**-TEG-SWNT and **PF-N$_3$**-TEG-carbonate-SWNT film. Before the heating treatment, no conductivity could be detected for either of the samples. The films were then heated at 170 °C for 30 minutes and,

surprisingly, no measurable conductivity was again observed. However, after a heating time of 1 hour, conductivity could be measured in both samples, where the conductivity of **PF-$N_3$**-TEG-SWNT was (8.7 ± 0.3) × $10^{-5}$ S/m and the conductivity of **PF-$N_3$**-TEG-carbonate-SWNT was (1.5 ± 0.1) × $10^{-4}$ S/m. Since the % weight loss observed in the TGA profiles did not plateau after 1 hour, we decided to monitor the changes in conductivity over a longer heating time (Figure 2.7). After 16 hours of heating, the conductivity of **PF-$N_3$**-TEG-SWNT and **PF-$N_3$**-TEG-carbonate-SWNT reached plateau values of (1.0 ± 0.2) × $10^{-3}$ S/m and (2.0 ± 0.1) × $10^{-2}$ S/m, respectively. Therefore, the conductivity of the cleavable sample was about 133 times higher after 16 hours of heating treatment compared to only 12 times higher for the control sample. This indicates that cleavable side-chains led to an order of magnitude higher conductivity upon extended annealing relative to the non-cleavable side-chain sample. The prolonged annealing time required to achieve the conductivity increase could be the result of the slow evaporation of TEG fragments from the film, followed by a gradual reorganization of the nanotubes such that closer inter-nanotube contacts are formed, leading to higher conductivity. No significant changes in thickness were observed before and after the heating treatment. However, a change in the physical characteristics of the films was noticed, where **PF-$N_3$**-TEG-carbonate-SWNT became more brittle than the sample with non-cleavable side-chains under identical conditions. This experiment was repeated a second time, and similar results were obtained (Supporting Information, Figure 2.21). We also attempted to perform the same heating treatment at 200 °C to determine if the conductivity of the cleavable

sample would increase at a faster rate, however, the films heated to this temperature became too brittle for the 4-point probe measurement (films cracked upon contact), and the experiment had to be abandoned.

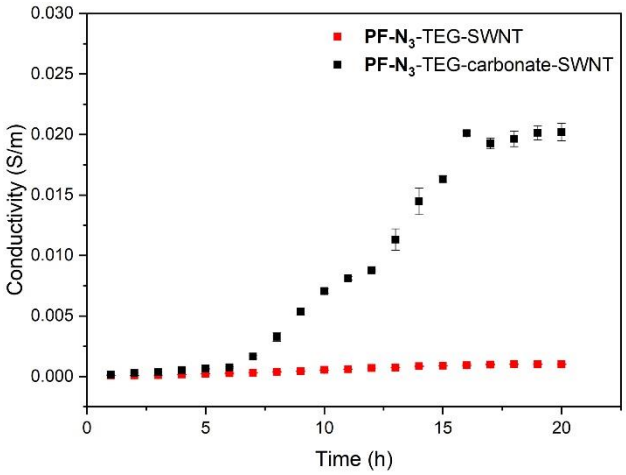


Figure 2.7. Conductivity of **PF-N$_3$**-TEG-SWNT (red) and **PF-N$_3$**-TEG-carbonate-SWNT (black) over time. Measurements were performed at 25°C using a four-point probe.

**Post-heating characterization.** Raman spectroscopy was used to determine if defects were introduced on the nanotube surface as a result of the heat treatment. Examining the intensity of the D-band centred at ~1290 cm$^{-1}$ relative to the G-band at ~1590 cm$^{-1}$ indicates the presence of sp$^3$ carbon atoms in the nanotube structure, which correspond to defect sites.[78] As shown in Figure 2.8, there is no significant difference between pre- and post-heated samples when observing the G and D-bands. This suggests that no nanotube defects were generated by the heating treatment.

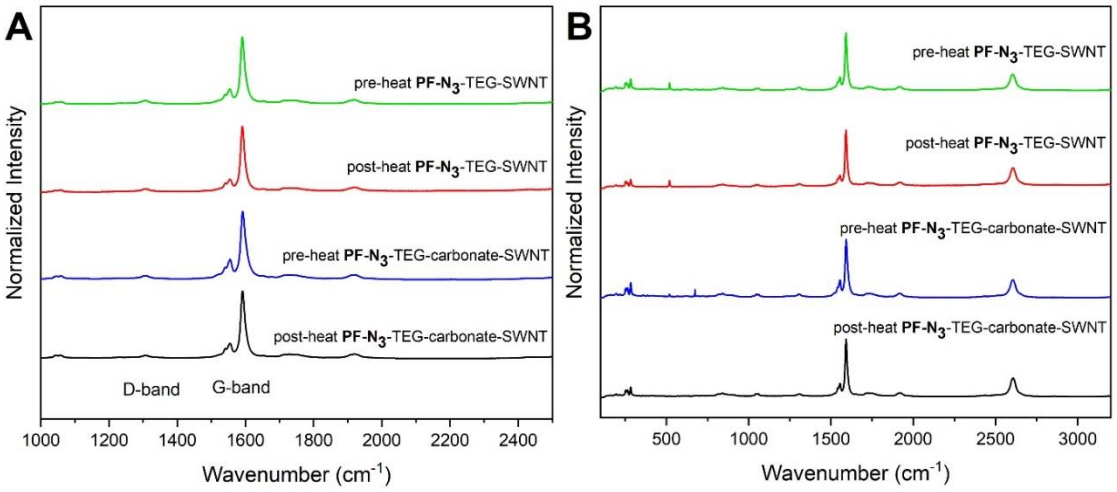


Figure 2.8. Raman Spectra for **PF-N$_3$**-TEG-SWNT and **PF-N$_3$**-TEG-carbonate-SWNT at $\lambda_{ex}$ = 633 nm showing A) the G- and D-band and B) the full spectrum pre-and post-heating treatment. All the spectra were normalized to the G-band at ~ 1590 cm$^{-1}$.

We then used contact angle measurements to evaluate the morphological changes before and after heating treatment. The samples were prepared by drop-casting **PF-N$_3$**-TEG-SWNT and **PF-N$_3$**-TEG-carbonate-SWNT onto a silicon wafer with dimensions of 1 x 1 cm followed by evaporation at RT. To characterize the surface properties, 2 µL of Milli-Q water (18.2 MΩ cm$^{-1}$) was deposited onto the surface. Contact angle measurements were performed in triplicate, with the water droplet being placed at a different location on the sample. As shown in Figure 2.9, **PF-N$_3$**-TEG-SWNT and **PF-N$_3$**-TEG-carbonate-SWNT had a contact angle of 98 ± 3° and 85 ± 4° respectively before the heating treatment. After heating the samples at 170 °C for 17 hours, **PF-N$_3$**-TEG-SWNT and **PF-N$_3$**-TEG-carbonate-SWNT had a contact angle of 99 ± 2° and 106 ± 2°, respectively. As expected, the contact angle of **PF-N$_3$**-TEG-carbonate-SWNT after the heating treatment is higher due to the removal of the

hydrophilic triethylene glycol side-chains, which is consistent with previous reports.[69]

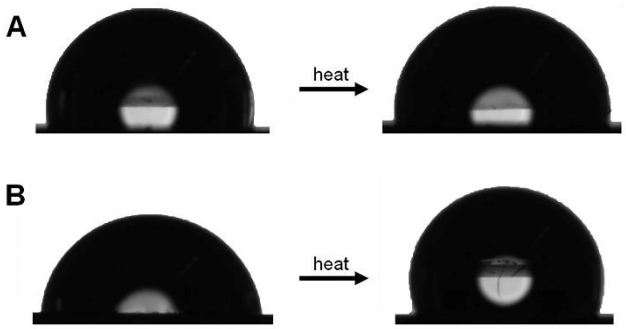


Figure 2.9. Photograph of a droplet of water on the polymer-SWNT deposited onto silicon wafer for A) **PF-$N_3$**-TEG-SWNT before and after the heating treatment. Contact angles are 98 ± 3° and 99 ± 2°, respectively and B) **PF-$N_3$**-TEG-carbonate-SWNT before and after the heating treatment. Contact angles are 85 ± 4° and 106 ± 2° respectively.

**Polymer-SWNT dispersions with longer side-chains.** We next functionalized **PF-$N_3$**-SWNT with a larger polyethylene glycol that can provide solubility in "greener" solvents, such as water or ethylene glycol derivatives. We used a mPEG polymer having $M_n$ of 2.0 kDa to prepare our thermally cleavable and non-cleavable side-chains as this chain length is expected to be effective for dispersion in polar solvents.[59] Preparation of the target side-chains with thermally cleavable and non-cleavable linkers was performed using the same synthetic protocols as with the TEG analogs above (Supporting Information, Schemes 2.10 and 2.11). Again, the **PF-$N_3$**-SWNT complex was first prepared and the side-chains were introduced *in situ* via CuAAC.[59] The reactions were monitored by IR spectroscopy via the disappearance of the polymer azide

stretch at ~2090 $cm^{-1}$ (Supporting Information, Figure 2.23), filtered through a Teflon membrane with 0.2 µm pore diameter, and thoroughly rinsed with THF to remove all free polymer. The resulting thin films were then redispersed in 10 mL of THF using a bath sonicator for 1 hour to obtain dispersions of **PF-$N_3$**-mPEG$_{2000}$-SWNT and **PF-$N_3$**-mPEG$_{2000}$-carbonate-SWNT.

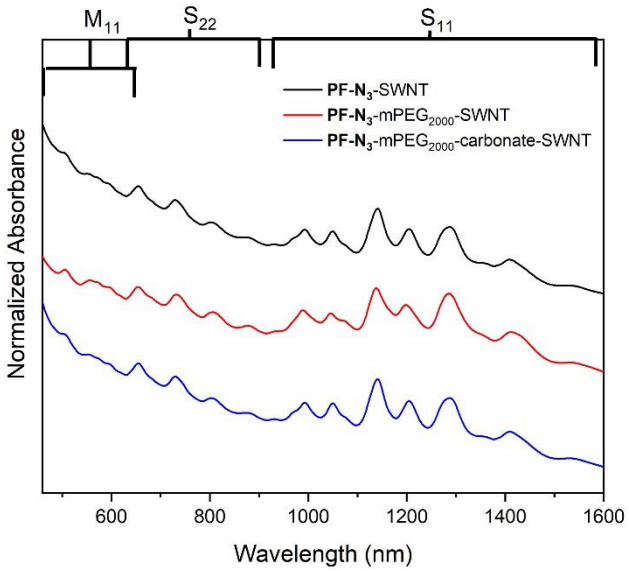


Figure 2.10. UV-Vis-NIR absorption spectra for **PF-$N_3$**-SWNT (top), **PF-$N_3$**-mPEG$_{2000}$-SWNT (middle) and **PF-$N_3$**-mPEG$_{2000}$-carbonate-SWNT (bottom) in THF. Spectra were normalized to the signal at 1140 nm and offset for clarity.

UV−vis−NIR absorption spectroscopy was used to characterize **PF-$N_3$**-mPEG$_{2000}$-SWNT and **PF-$N_3$**-mPEG$_{2000}$-carbonate-SWNT. The absorption spectra were normalized to the maximum absorption of the peak at 1140 nm to compare the different SWNT species (full spectra are provided in the Supporting Information, Figure 2.24). As shown in Figure 2.10, both m- and sc-SWNT species are present within the polymer-SWNT complexes, consistent with the lack of selectivity for specific SWNT types we observed with the shorter side-

chains (see above). Raman spectroscopy of drop-cast samples using both 633 nm and 785 nm excitation wavelengths again indicated that both m- and sc-SWNTs were present in the samples (Figure 2.11A).[76]

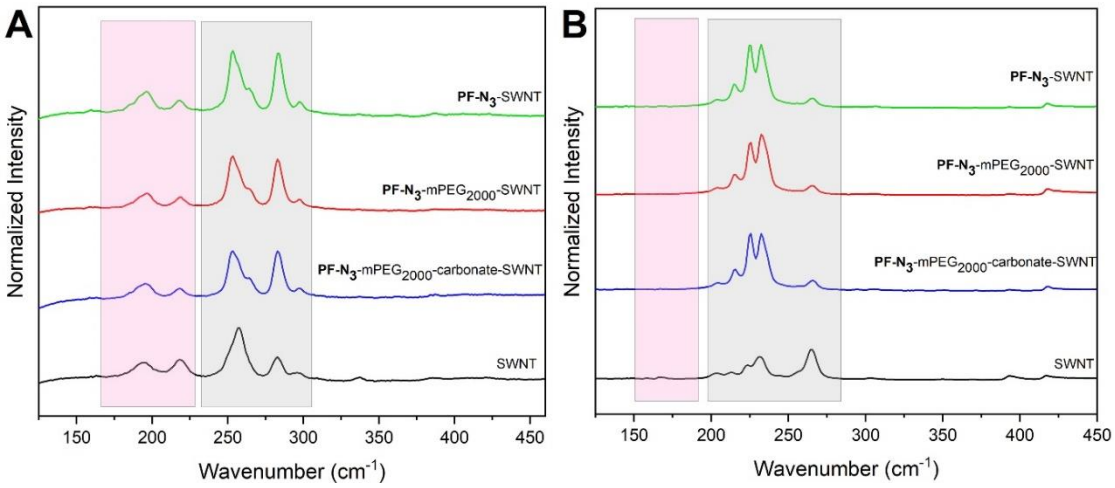


Figure 2.11. Raman Spectra for HiPco polymer-SWNT samples showing the RBM regions at A) $\lambda_{ex}$ = 633 nm, B) $\lambda_{ex}$ = 785 nm. Gray boxes represent signals arising for sc-SWNTs, whereas pink boxes represent m-SWNTs. All the spectra were normalized to the G-band at ~ 1590 $cm^{-1}$.

**Conductivity measurements. PF-$N_3$**-$mPEG_{2000}$-SWNT and **PF-$N_3$**-$mPEG_{2000}$-carbonate-SWNT thin films were prepared identically to the TEG analogs (see above). Again, no conductivity could be detected for either of the samples before the heating treatment. The films were then heated at 170 °C for 17 hours. Since polyethylene glycol polymer is not volatile at this temperature, the thin films were washed with hot water to remove the cleaved side-chains and dried at 70 °C for 1 hour in a vacuum oven. Conductivity measurements were then performed in triplicate on each **PF-$N_3$**-$mPEG_{2000}$-SWNT and **PF-$N_3$**-$PEG_{2000}$-carbonate-SWNT film. After the heating treatment, the conductivity of **PF-$N_3$**-

mPEG$_{2000}$-SWNT and **PF-N$_3$**-mPEG$_{2000}$-carbonate-SWNT was (7.4 ± 0.4) × 10$^{-5}$ S/m and (7.4 ± 0.6) × 10$^{-4}$ S/m, respectively. Similar to the results with TEG side-chains, the longer cleavable side-chains led to an order of magnitude higher conductivity upon extended annealing relative to the non-cleavable side-chain sample. No significant changes in thickness were observed before and after the heating treatment. However, as observed with the shorter side-chains, **PF-N$_3$**-mPEG$_{2000}$-carbonate-SWNT became more brittle than the sample with non-cleavable side-chains under identical conditions. This experiment was repeated a second time, and similar results were obtained with a conductivity of (8.1 ± 1.4) × 10$^{-5}$ S/m and (8.2 ± 1.6) × 10$^{-4}$ S/m for **PF-N$_3$**-mPEG$_{2000}$-SWNT and **PF-N$_3$**-mPEG$_{2000}$-carbonate-SWNT, respectively. As with the TEG analogs above, post-heating Raman analysis confirmed that the nanotubes were not affected by the heating treatment (Supporting Information, Figure 2.25). Additionally, contact angle measurements were performed on the samples pre- and post-heating. As shown in Figure 2.12, **PF-N$_3$**-mPEG$_{2000}$-SWNT and **PF-N$_3$**-mPEG$_{2000}$-carbonate-SWNT had a contact angle of 70 ± 3° and 66 ± 2° respectively before the heating treatment. After heating at 170 °C for 17 hours, **PF-N$_3$**-mPEG$_{2000}$-SWNT and **PF-N$_3$**-mPEG$_{2000}$-carbonate-SWNT had a contact angle of 79 ± 2° and 98 ± 3°, respectively. As expected, the contact angle of **PF-N$_3$**-mPEG$_{2000}$-carbonate-SWNT after the heating treatment exhibited a much larger increase than the control sample due to the removal of the hydrophilic polyethylene glycol side-chains.

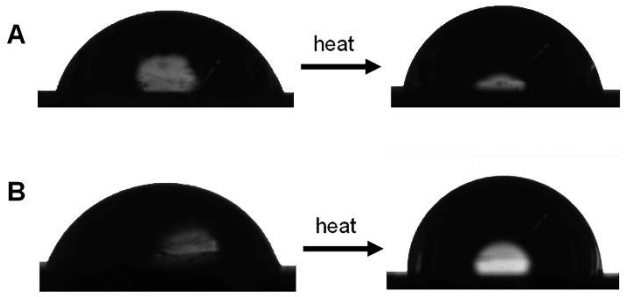


Figure 2.12. Photograph of a droplet of water on the polymer-SWNT deposited onto silicon wafer for A) **PF-$N_3$**-m$PEG_{2000}$-SWNT before and after the heating treatment. Contact angles are 70 ± 3° and 79 ± 2° respectively, and B) **PF-$N_3$**-m$PEG_{2000}$-carbonate-SWNT before and after the heating treatment. Contact angles are 66 ± 2° and 98 ± 3°, respectively.

**Dispersion in green solvents.** We next investigated the dispersion in more eco-friendly solvents that can be suitable for inkjet printing applications.[79–85] Common solvents used for SWNT inkjet printing include water,[85–87] N,N-dimethylformamide (DMF),[81,82,88,89] and N-methyl-2-pyrrolidone (NMP).[90] However, the use of water as an inkjet-printing solvent often requires the addition of wetting agents to lower the surface tension.[79] While DMF and NMP do not require additional surfactants, their toxicity makes them unsuitable for sustainable and environmentally-mindful applications. As an alternative, we decided to use ethylene glycol oligomers such as triethylene glycol monomethyl ether (TEGME) and tetraethylene glycol dimethyl ether (Tetraglyme) for our SWNT dispersions. Their viscosity, 7.8 and 4.05 cP, respectively and boiling point of 249 °C and 275 °C are suitable for potential inkjet printing applications.[91–93]

Using the preparation procedures described above, a THF dispersion of **PF-$N_3$**-m$PEG_{2000}$-carbonate was prepared (10 mL). To this was added an equivalent volume of either triethylene glycol monomethyl ether or tetraethylene glycol dimethyl ether and the THF was removed by rotary evaporation *in vacuo*. As shown in Figure 2.13D, the dispersions were stable in both green solvents after the removal of THF. We then characterized the dispersions using UV−vis−NIR absorption spectroscopy. The absorption spectra were normalized to the maximum absorption of the peak at 1140 nm to compare the different SWNT species. As shown in Figure 2.13A, the **PF-$N_3$**-m$PEG_{2000}$-carbonate-SWNT sample in THF and the dispersions in greener solvents show similar absorption features, suggesting that the nanotubes remain well dispersed after the solvent exchange process. Raman analysis also indicated that there were no appreciable differences in the nanotubes dispersed in the green solvents relative to the dispersion in THF (Figures 2.13B and 2.13C). The solvent exchange was also performed on **PF-$N_3$**-m$PEG_{2000}$-SWNT and gave similar results (Supporting Information, Figures 2.27 and 2.28). It should be noted that when the solvent exchange process was performed with **PF-$N_3$**-TEG-SWNT and **PF-$N_3$**-TEG-carbonate-SWNT dispersions, complete precipitation of the nanotube complexes was observed upon standing, confirming the requirement for the longer PEG chains to achieve solubility in the green solvent (Supporting Information, Figure 2.29).

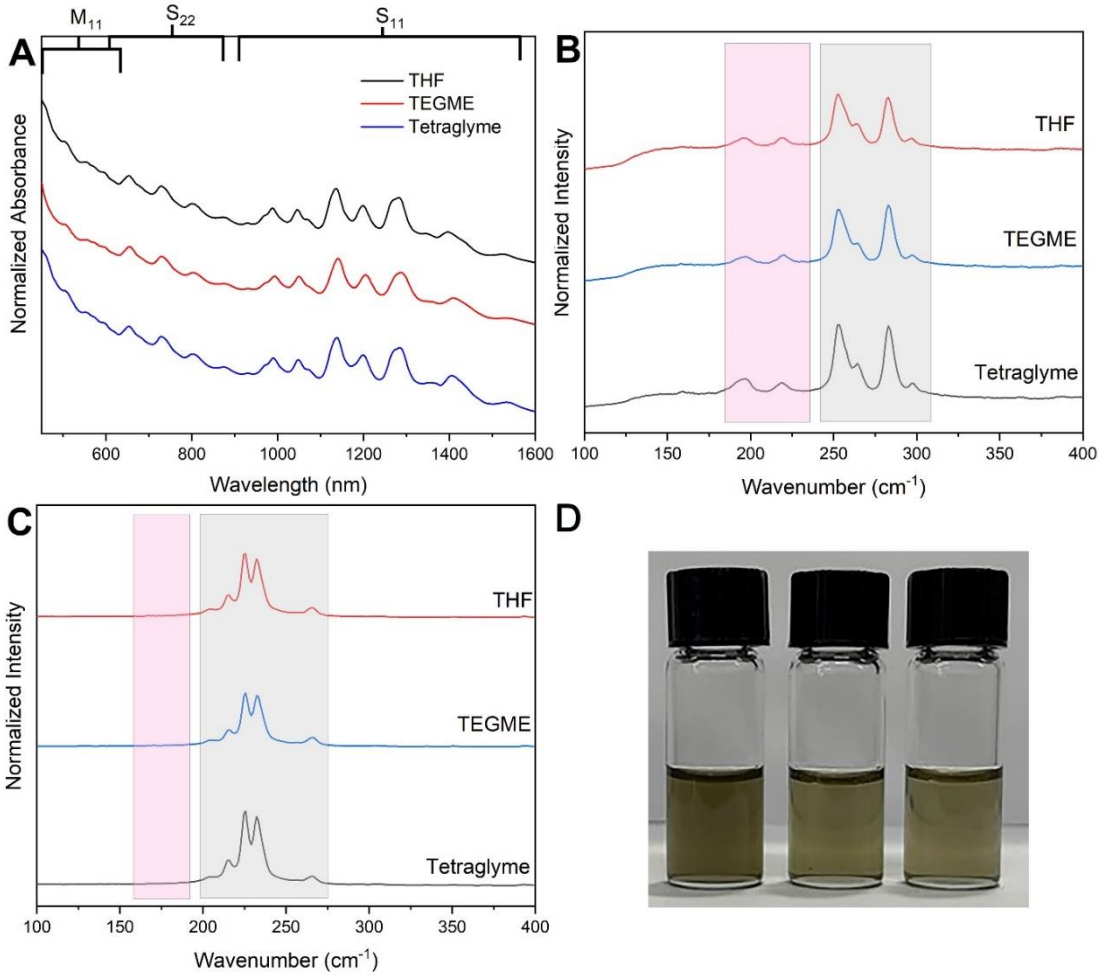


Figure 2.13. A) UV-Vis-NIR absorption spectra for **PF-N$_3$**- mPEG$_{2000}$-carbonate-SWNT before and after solvent exchange. Spectra were normalized to the signal at 1140 cm$^{-1}$ and offset for clarity. B) Raman Spectra for HiPco polymer-SWNT samples showing the RBM regions at $\lambda_{ex}$ = 633 nm, C) Raman Spectra for HiPco polymer-SWNT samples showing the RBM regions at $\lambda_{ex}$ = 785 nm. Gray boxes represent signals arising for sc-SWNTs, whereas pink boxes represent m-SWNTs. All the spectra were normalized to the G-band at ~ 1590 cm$^{-1}$. D) photograph of **PF-N$_3$**-mPEG$_{2000}$-carbonate-SWNT in THF (left), triethylene glycol monomethyl ether (middle) and tetraethylene glycol dimethyl ether (right).

## 2.3 Conclusion

Polyfluorene-SWNT complexes were functionalized with either thermally cleavable or non-cleavable TEG side-chains. Characterization using UV-Vis-NIR and Raman spectroscopy showed that the nanotubes were well dispersed by these polymers. The thermal cleavage of the side-chains was first investigated by TGA-MS on the polymer and indicated that the decarboxylation occurs between 150 and 200 °C. Thin film samples of the polymer-wrapped SWNTs were prepared, and the heating temperature of the films was set to 170 °C. The conductivity was monitored as a function of heating time and reached a plateau of $(2.0 \pm 0.1) \times 10^{-2}$ S/m for the cleavable sample, which is 20 times higher than the non-cleavable sample. Characterization after the heating treatment showed no damage to the nanotube surface. Functionalization using longer PEG side-chains was also investigated. After the heating treatment at 170 °C followed by a wash with water, the conductivity of the cleavable sample was $(8.2 \pm 1.6) \times 10^{-4}$ S/m, which is 10 times higher than the non-cleavable sample. No defects on the nanotubes were observed post-heating treatment. Lastly, the stability of the dispersions in greener solvents was investigated through a solvent exchange process. Polymer-SWNT complexes functionalized with polyethylene glycol side-chains remained stable and well-dispersed in both triethylene glycol monomethyl ether and tetraethylene glycol dimethyl ether after the solvent-exchange process. This was confirmed by UV-Vis-NIR absorption spectroscopy and Raman spectroscopy. The increase of conductivity after the removal of the side-chains and the stability of these

nanotube dispersions in greener solvents warrant further investigation and development of these SWNT materials as green inks for inkjet printing.

## 2.4 Supporting information

### 2.4.1 General

Raw HiPco SWNTs were purchased from NanoIntegris (batch #HR30-166 and #HR37-033) and used without further purification. All reagents were purchased from commercial chemical suppliers and used as received. Flash chromatography was performed using an Intelliflash280 by AnaLogix. Unless otherwise noted, compounds were monitored using a variable wavelength detector at 254 nm. Solvent amounts used for gradient or isocratic elution were reported in column volumes (CV). Columns were prepared in Biotage® SNAP KP-Sil cartridges using 40 – 63 µm silica or 25 – 40 µm silica purchased from Silicycle. $^{1}$H-NMR and $^{13}$C-NMR spectra were recorded on Bruker Avance 600 MHz and shift-referenced to the residual solvent resonance. Polymer molecular weights and dispersities were analyzed (relative to polystyrene standards) via GPC using a Waters 2695 Separations Module equipped with a Waters 2414 refractive index detector and a Jordi Fluorinated DVB mixed bed column in series with a Jordi Fluorinated DVB 105 Å pore size column. THF with 2% acetonitrile was used as the eluent at a flow rate of 2.0 mL/min. Sonication was performed using a QSonica Q700 Sonicator equipped with a 13 mm probe. The amplitude of the probe was 60 µm and the sonication power was 30 Watts. Centrifugation of the polymer-SWNT samples was performed using a Beckman Coulter Allegra X-22 centrifuge. UV-Vis-NIR absorption spectra were recorded

on a Cary 5000 spectrometer in dual beam mode, using matched 10 mm quartz cuvettes. Raman spectra were collected with a Renishaw InVia Laser Raman spectrometer, using two different lasers: a 500 mW HeNe Renishaw laser (633 nm, 1800 L/mm grating); and a 300 mW Renishaw laser (785 nm, 1200 L/mm grating). Raman samples were drop-cast onto freshly cleaned silicon wafers and allowed to air-dry at room temperature. Thermogravimetric analysis was performed on a Mettler Toledo TGA/DSC 3+, equipped with a Pfeiffer ThermoStar GSD 320 mass spectrometer, and all measurements were conducted under an argon atmosphere. The TGA plots in Figure 2.6 were obtained by heating the sample to 100 °C for 45 minutes to drive off water, followed by heating to 170 or 200 °C (20 °C per min), followed by a hold for 1 hour. Data was collected during the hold period at 170 or 200 °C. Conductivity measurements were recorded using an Ossila four-point probe system. Contact angle measurements were obtained using an Optical Contact Angle (OCA35) instrument from the DataPhysics instrument and the software used was SCA20.

## 2.4.2 Synthesis

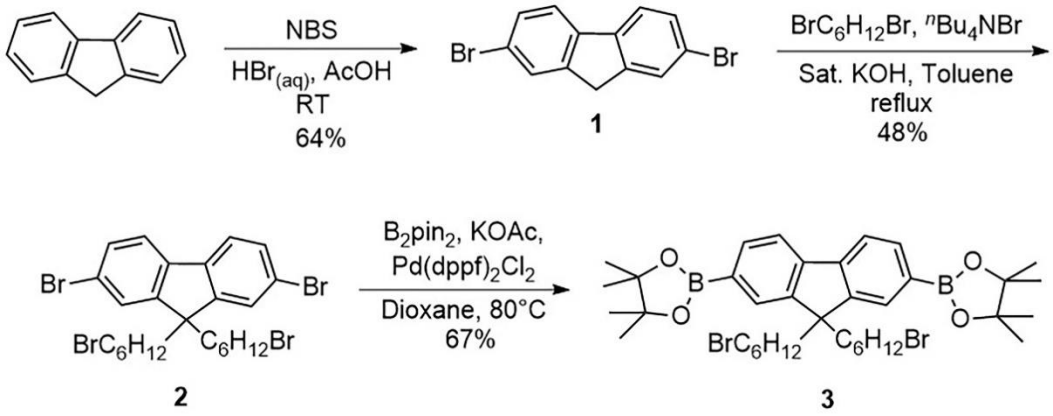


Scheme 2.3. Synthesis of monomers **2** and **3**.

Compounds **1, 2** and **3** were prepared according to literature procedures.[61]

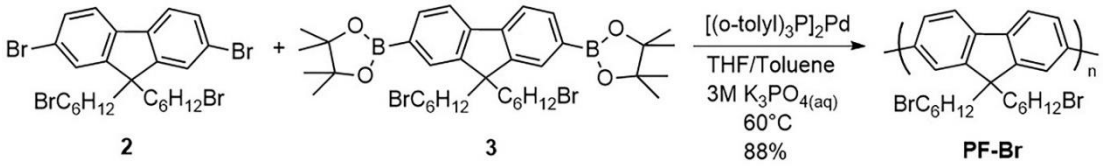


Scheme 2.4. Synthesis of **PF-Br**.

**Poly(bis(6-bromohexyl)fluorene) (PF-Br)**[61]

A Schlenk tube equipped with a stir bar was charged with **2** (0.87 g, 1.34 mmol), **3** (1.00 g, 1.34 mmol), THF (6.7 mL), toluene (6.7 mL), and 3M $K_3PO_{4(aq)}$ (13.4 mL). The reaction mixture was degassed by three freeze-pump-thaw cycles. The biphasic mixture was frozen under liquid nitrogen, then $[(o\text{-tol})_3P]_2Pd$ (14 mg, 20.2 µmol) was added under a positive pressure of nitrogen. The Schlenk tube was evacuated and backfilled three times, and the reaction was vigorously stirred at 60 °C for 2 h 30 min. The phases were allowed to separate, and the

organic layer was filtered through a plug of celite and neutral alumina (1:1 composition). The plug was washed with THF, and the filtrate was concentrated *in vacuo*. The crude polymer was precipitated in MeOH (~ 200 mL) and filtered to afford **PF-Br** as a yellow solid (1.16 g, 88%). $^1$H-NMR (600 MHz; $CDCl_3$): δ 7.86 (m, 2H), 7.73-7.67 (m, 4H), 3.31-3.28 (m, 4H), 2.15 (m, 4H), 1.71-1.69 (m, 4H), 1.28-1.25 (m, 4H), 1.18 (m,4H), 0.88 (m, 4H).

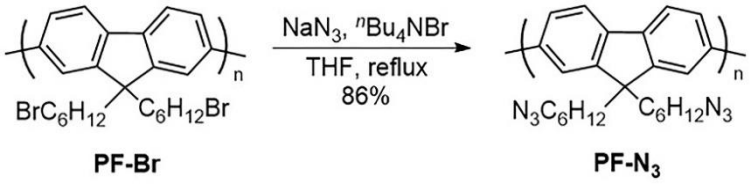


Scheme 2.5. Synthesis of **PF-$N_3$**.

**Poly(bis(6-azidohexyl)fluorene) (PF-$N_3$)**[61]

A round bottom flask equipped with a stir bar was charged with **PF-Br** (1.00 g, 2.04 mmol), $NaN_3$ (1.33 g, 20.3 mmol), $^n$Bu$_4$NBr (1.33 g, 4.1 mmol) and THF (200 mL). The reaction mixture was heated to reflux for 24 h. The reaction mixture was filtered through a neutral alumina plug, washed with THF and precipitated in MeOH (~ 200 mL) to afford **PF-$N_3$** (0.73 g, 86%).$^1$H-NMR (600 MHz; $CDCl_3$): δ 7.87-7.85 (m, 2H), 7.72-7.68 (m, 4H), 3.16-3.14 (m, 4H), 2.15 (m, 4H), 1.46, 1.40 (m, 4H), 1.25-1.20 (m, 8H), 0.88-0.83 (m, 4H).

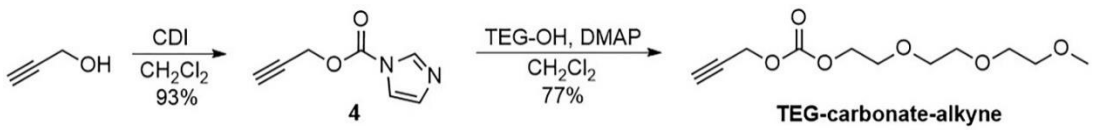


Scheme 2.6. Synthesis of **TEG-carbonate-alkyne**.

**1*H*-Imidazole-1-carboxylic acid, 2-propyn-1-yl-ester (4)**[94]

A round bottom flask equipped with a stir bar was charged with N,N-carbonyldiimidazole (3.47 g, 21.4 mmol) in 180 mL of dichloromethane. Propargyl alcohol (1.00 g, 17.8 mmol) was added, and the solution was stirred for 2 h. The organic layer was washed with water (3 x 90 mL), dried with $MgSO_4$ and concentrated to give a brown solid (2.49 g, 93%). $^1$H-NMR (600 MHz, $CDCl_3$): δ 8.16 (s, 1H), 7.44 (s, 1H), 7.08 (s, 1H), 4.99 (d, J=2.49 Hz, 2H), 2.62 (t, J=2.49 Hz, 1H).

**2-(2-(2-methoxyethoxy)ethoxy)ethyl prop-2-yn-1-yl carbonate (TEG-carbonate-alkyne)**

A 100 mL round bottom flask equipped with a stir bar was charged with **4** (2.0 g, 13.3 mmol), triethylene glycol monomethyl ether (2.6 g, 15.9 mmol) in 27 mL of dichloromethane. 4-dimethylaminopyridine (0.3 g, 2.66 mmol) was added, and the solution was stirred for 2 h. The organic layer was washed with water (3 x 10 mL), dried with $MgSO_4$ and concentrated to give a colourless oil (2.52 g, 77%). $^1$H-NMR (600 MHz, $CDCl_3$): δ 4.73 (d, *J* = 2.5 Hz, 2H), 4.33-4.31 (m, 2H), 3.74-3.73 (m, 2H), 3.66-3.64 (m, 6H), 3.56-3.54 (m, 2H), 3.38 (s, 3H), 2.52 (t, *J* = 2.5 Hz, 1H). $^{13}$C NMR (151 MHz, $CDCl_3$): δ 154.7, 77.1, 75.8, 72.1, 70.86, 70.78, 70.75, 69.0, 67.7, 59.2. ESI-MS m/z calculated for $C_{11}H_{18}O$ $[M]^+$: 246.11 found $[M+Na]^+$:269.0

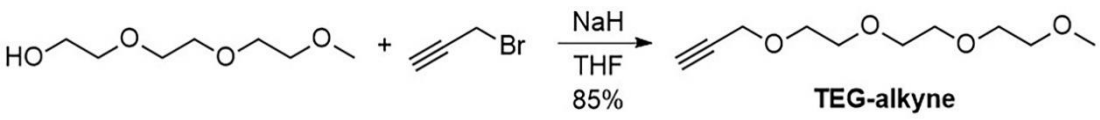


Scheme 2.7. Synthesis of **TEG-alkyne**.

**Triethylene glycol methyl propargyl ether (TEG-alkyne)**[95]

A round bottom flask equipped with a stir bar was charged with triethylene glycol monomethyl ether (1.00 g, 6.09 mmol) in 60 mL of dry THF at 0 °C. NaH (0.28 g, 6.69 mmol) was added to the solution, and the reaction mixture was stirred at 0 °C. After 1 h, propargyl bromide (80% in toluene, 1.43 g, 7.91 mmol) was added dropwise. The reaction mixture was stirred at RT overnight, quenched with water (30 mL) and extracted with DCM (3 x 30 mL). The organic layers were combined, washed with brine (3 x 25mL), dried with $MgSO_4$ and concentrated *in vacuo* to afford **TEG-alkyne** as an orange oil (1.05 g, 85%). $^1$H-NMR (600 MHz; $CDCl_3$): δ 4.20 (d, *J* = 2.4 Hz, 2H), 3.71-3.63 (m, 10H), 3.55-3.54 (m, 2H), 3.37 (s, 3H), 2.42 (t, *J* = 2.4 Hz, 1H).

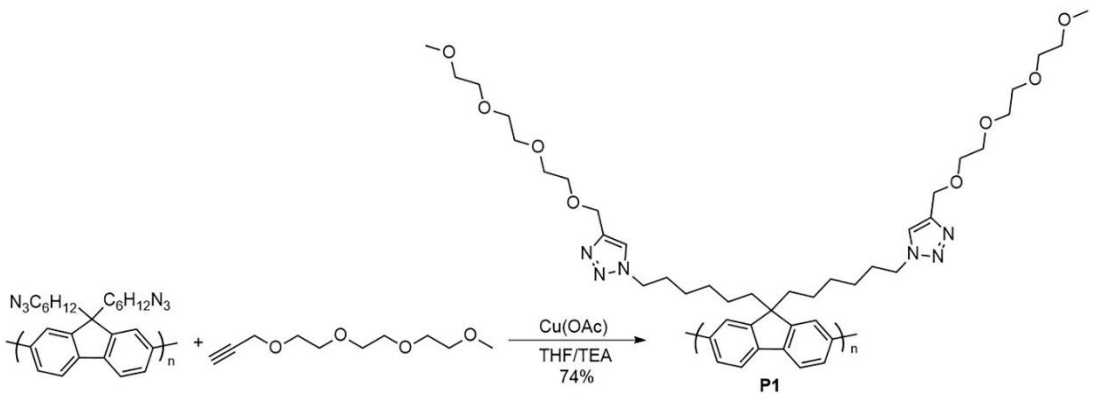


Scheme 2.8. Synthesis of **PF-$N_3$-TEG (P1)**.

**CuAAC procedure for PF-$N_3$ and TEG-alkyne (P1)**

A round bottom flask equipped with a stir bar was charged with **PF-$N_3$** (0.1 g, 0.24 mmol), TEG -alkyne (0.11 g, 0.53 mmol) in 16 mL of 1:1 THF/TEA. To the reaction mixture, Cu(OAc) (1 mg, 0.01 µmol). The reaction mixture was stirred

at 30 °C under $N_2$. The reaction progress was monitored by IR spectroscopy for the disappearance of the azide stretch ~2090 $cm^{-1}$. After overnight stirring, the polymer precipitated and was filtered to obtain **P1** (0.14 mg, 74 %). $^1$H-NMR (600 MHz; $CDCl_3$): δ 7.90-7.85 (m, 2H), 7.77-7.67 (m, 4H), 7.53-7.48 (m, 2H), 4.69-4.63 (m, 4H), 4.27-4.19 (m, 4H), 3.69-3.64 (m, 18H), 3.58-3.52 (m, 4H), 3.39-3.37 (m, 6H), 2.20-2.09 (m, 4H), 1.79-1.71 (m, 4H), 1.23-1.11 (m, 10H), 0.88-0.77 (m, 4H).

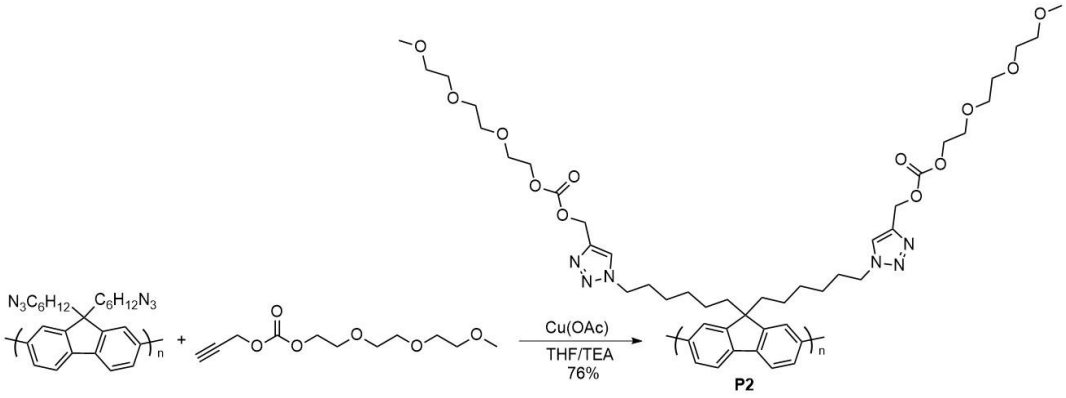


Scheme 2.9. Synthesis of **PF-$N_3$-TEG-carbonate (P2)**.

**CuAAC procedure for PF-$N_3$ and TEG-carbonate-alkyne (P2)**

A round bottom flask equipped with a stir bar was charged with **PF-$N_3$** (0.1 g, 0.24 mmol), TEG-carbonate-alkyne (0.13 g, 0.53 mmol) in 16 mL of 1:1 THF/TEA. To the reaction mixture, Cu(OAc) (1 mg, 0.01 µmol). The reaction mixture was stirred at 30 °C under $N_2$. The reaction progress was monitored by IR spectroscopy for the disappearance of the azide stretch ~2090 $cm^{-1}$. After overnight stirring, the polymer precipitated and was filtered to obtain **P2** (0.16 mg, 76 %). $^1$H-NMR (600 MHz; $CDCl_3$): δ 7.90-7.85 (m, 2H), 7.76-7.67 (m, 4H), 7.62-7.57 (m, 2H), 5.27-5.22 (m, 4H), 4.31-4.29 (m, 4H), 4.26-4.22 (m, 4H),

3.74-3.71 (m, 4H), 3.66-3.65 (m, 10H), 3.56-3.54 (m, 4H), 3.39-3.36 (m, 6H), 2.20-2.10 (m, 4H), 1.81-1.71 (m, 6H), 1.25-1.11 (m, 10H), 0.88-0.76 (m, 4H).

**General CuAAC procedure for PF-$N_3$-SWNT and the side-chains**

A glass vial equipped with a stir bar was charged with 10 mL of **PF-$N_3$**-SWNT and 2.05 equivalents of the side-chains. Equivalents were calculated using the mass of the polymer present (based on the SWNT dispersion protocol) and then using the molecular weight of the repeat unit. To the mixture, 1 mg of Cu(OAc) and 10 equivalents of Hünig's base with respect to Cu(OAc) (10 mg, 86 µmol) were added. The reaction mixture was stirred at RT, and reaction progress was monitored by IR spectroscopy for the disappearance of the azide stretch ~ 2090 $cm^{-1}$. Isolated polymer-SWNT complexes were found to be easily dispersible in THF and other organic solvents, with concentrations approaching 3 mg/mL.

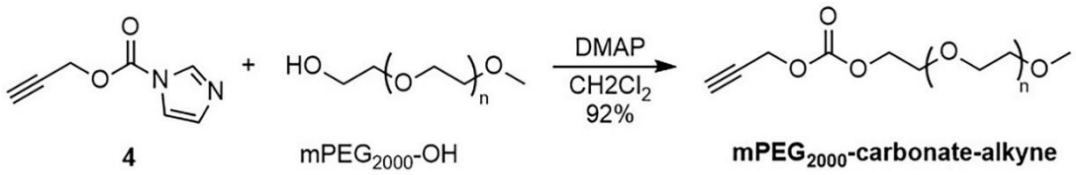


Scheme 2.10. Synthesis of **mPEG$_{2000}$-carbonate-alkyne**.

**mPEG$_{2000}$-carbonate-alkyne**

A 20 mL vial equipped with a stir bar was charged with compound **4** (50 mg, 0.33 mmol) in 3 mL of dichloromethane. mPEG$_{2000}$-OH (0.73 g, 0.36 mmol) and 4-dimethylaminopyridine ( 10 mg, 66 µmol) were added. The solution was stirred overnight at RT. The reaction mixture was precipitated into 1:1 Hexanes/ $Et_2O$ (~ 200 mL). The precipitate was collected in a Hirsch funnel and then

washed with $Et_2O$ (3 x 20 mL), followed by drying *in vacuo* to afford **mPEG$_{2000}$-carbonate-alkyne** as a white powder (0.64 g, 92%). $^1$H-NMR (600 MHz; $CDCl_3$): δ 4.73 (d, *J* = 2.5 Hz, 2H), 4.32-4.31 (m, 2H), 3.74-3.72 (m, 7H), 3.67-3.63 (m, 186H), 3.55-3.54 (m, 4H), 3.38 (s, 3H), 2.54 (t, *J* = 2.4 Hz, 1H).$^{13}$C NMR (151 MHz; CDCl3): δ 75.7, 71.9, 70.71, 70.65, 70.62, 70.58, 70.53, 68.8, 67.5, 59.0, 55.3

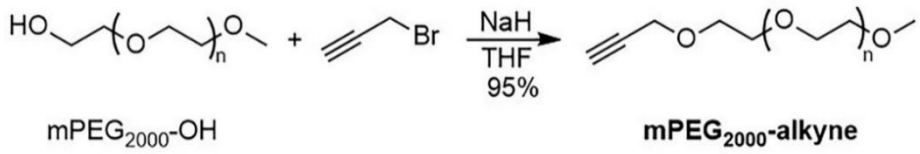


mPEG$_{2000}$-OH **mPEG$_{2000}$-alkyne**

Scheme 2.11. Synthesis of **mPEG$_{2000}$-alkyne**.

**mPEG$_{2000}$-alkyne**

A 20 mL vial equipped with a stir bar was charged with mPEG$_{2000}$-OH (0.5 g, 0.25 mmol) in 2.5 mL of dry THF. The solution was cooled at 0°C and NaH was added (12 mg, 0.32 mmol). The solution was stirred at 0°C for 30 minutes and propargyl bromide (69 mg, 0.32 mmol) was added dropwise. The solution was stirred overnight at RT. The reaction mixture was precipitated into 1:1 Hexanes/ $Et_2O$. The precipitate was collected in a Hirsch funnel, then washed with $Et_2O$ (3 x 20 mL) followed by drying in vacuo to afford **mPEG$_{2000}$-alkyne** as a white powder (0.46 g, 95%).$^1$H-NMR (600 MHz; $CDCl_3$): δ 4.20 (d, *J* = 2.4 Hz, 2H), 3.76-3.73 (m, 2H), 3.71-3.60 (m, 186H), 3.56-3.51 (m, 4H), 3.37-3.36 (m, 3H), 2.43 (t, *J* = 2.4 Hz, 1H).$^{13}$C NMR (151 MHz; CDCl3): δ 79.6, 74.6, 71.9, 70.54, 70.49, 70.46, 70.37, 69.1, 59.0, 58.4

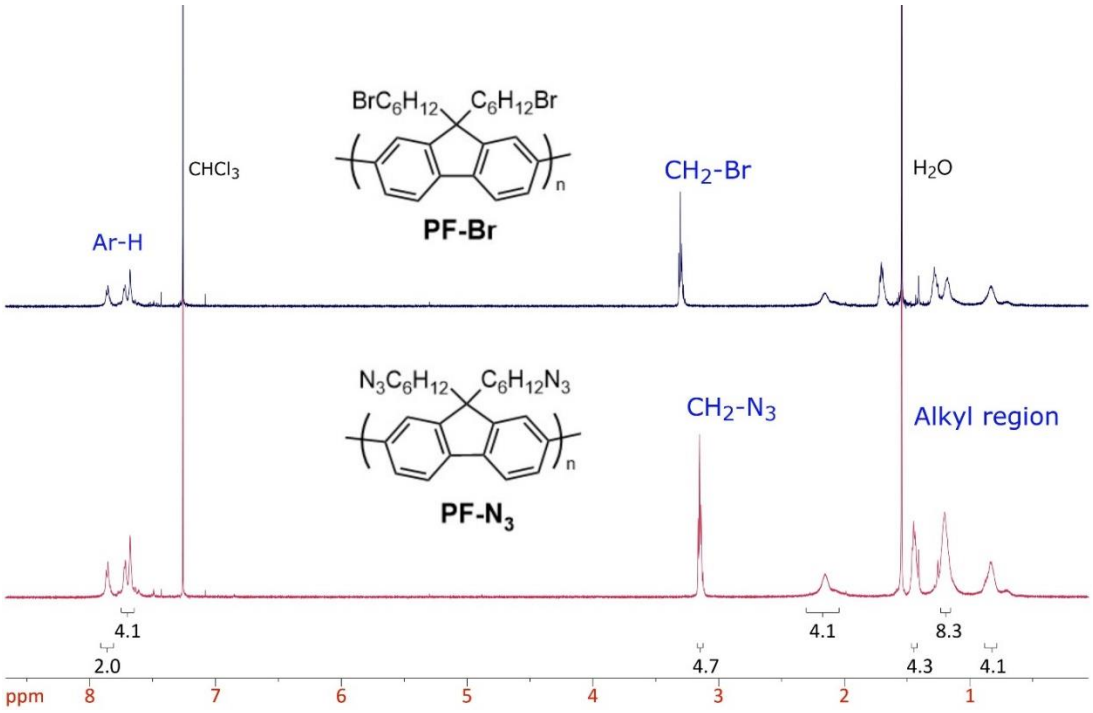


Figure 2.14. $^{1}$H NMR overlay of **PF-Br** (blue) and **PF-N$_3$** (red).

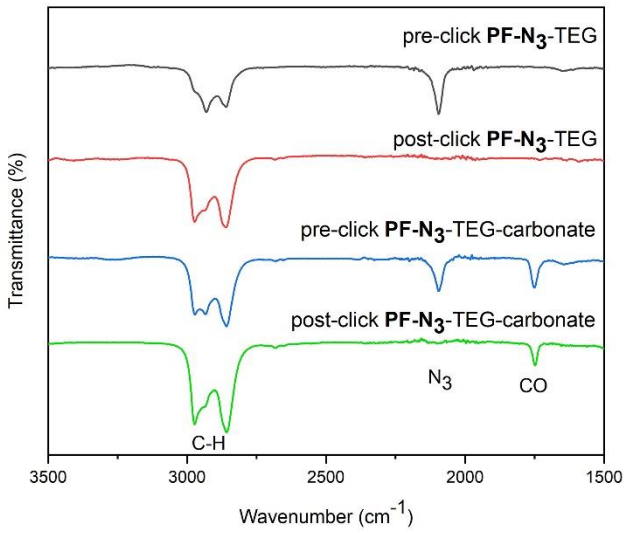


Figure 2.15. FT-IR overlay of the click reaction between **PF-N$_3$**, TEG-alkyne and TEG-carbonate alkyne.

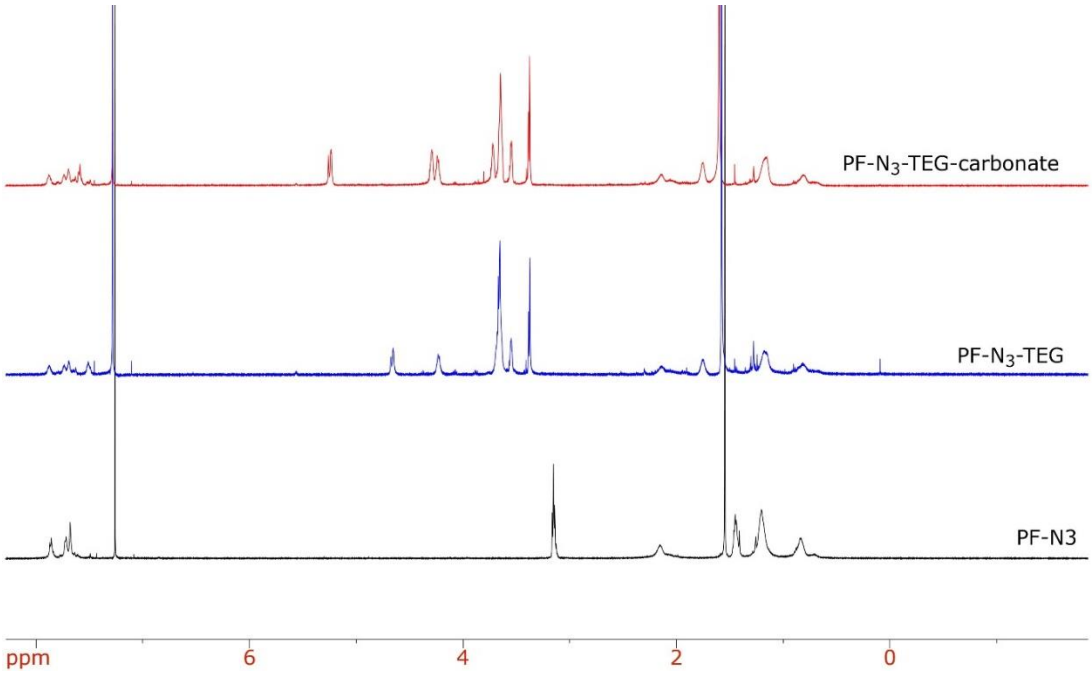


Figure 2.16. $^{1}$H NMR overlay of **PF-N$_3$** (bottom), **PF-N$_3$**-TEG (middle) and **PF-N$_3$**-TEG-carbonate (top).

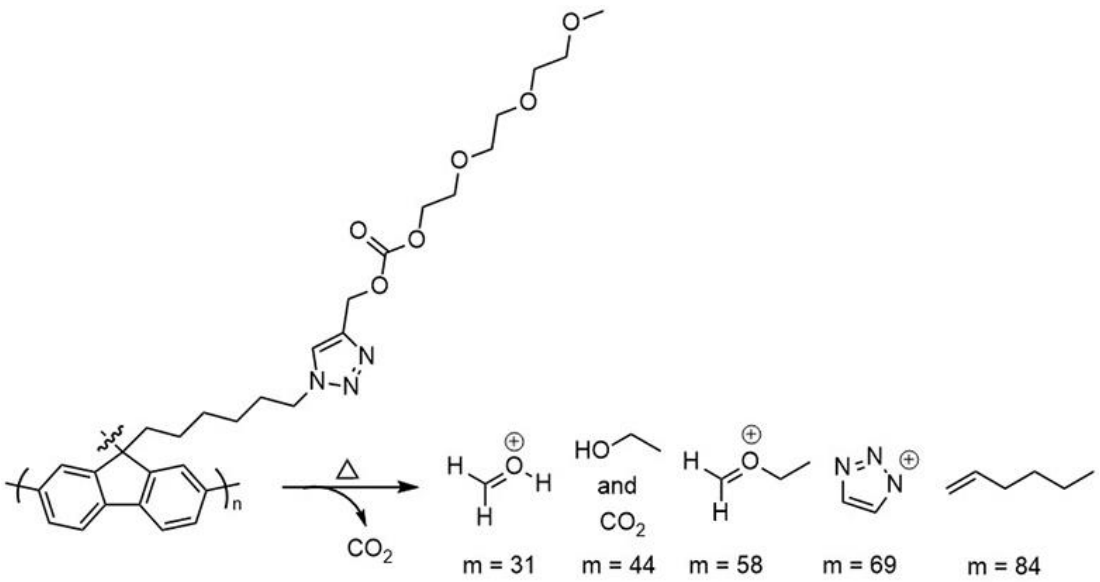


Figure 2.17. Possible cleavage mechanism and fragmented side-chains with masses (m) listed.

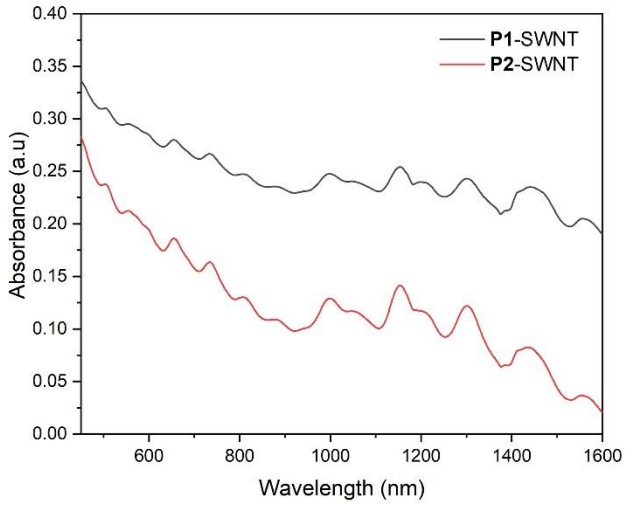


Figure 2.18. UV-Vis-NIR absorption spectra for **P1**-SWNT (red) and **P2**-TEG-SWNT (black).

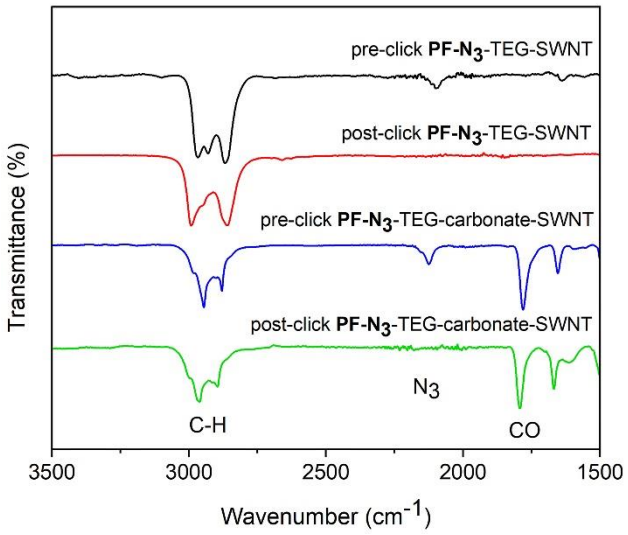


Figure 2.19. FT-IR overlay of the click reaction between the **PF-$N_3$**-SWNT complex, TEG alkyne and TEG-carbonate-alkyne.

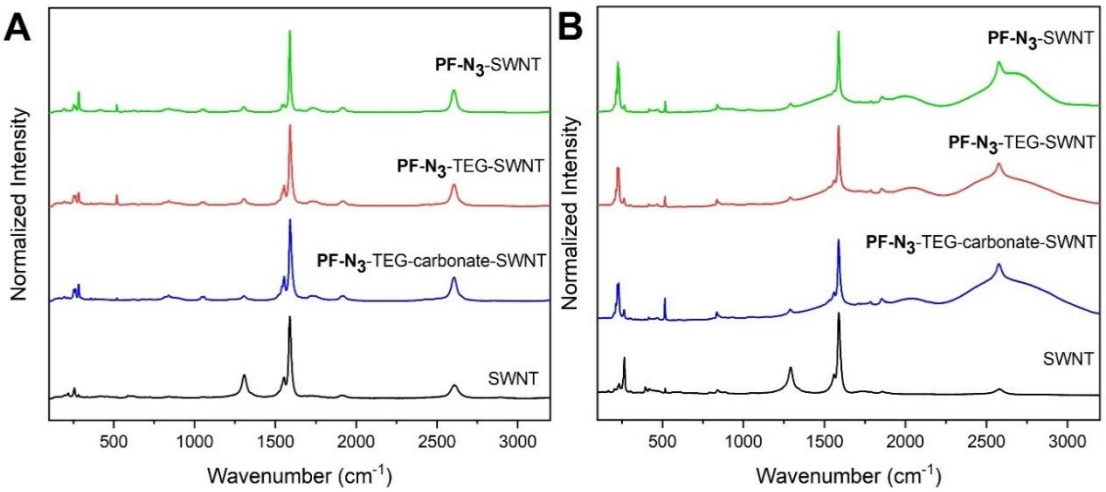


Figure 2.20. Full Raman spectra for HiPco polymer-SWNT samples at A) $\lambda_{ex}$ = 633 nm, B) $\lambda_{ex}$ = 785 nm. All the spectra were normalized at ~ 1590 $cm^{-1}$.

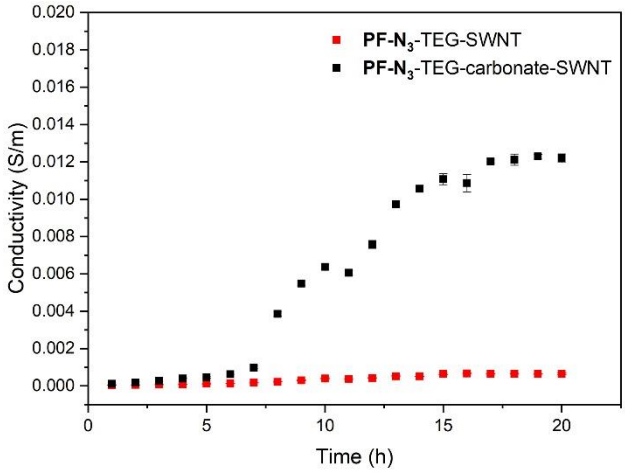


Figure 2.21. Conductivity of **PF-$N_3$**-TEG-SWNT (red) and **PF-$N_3$**-TE-carbonate-SWNT (black) of the repeated experiment. Measurements were performed at 25°C using a four-point probe.

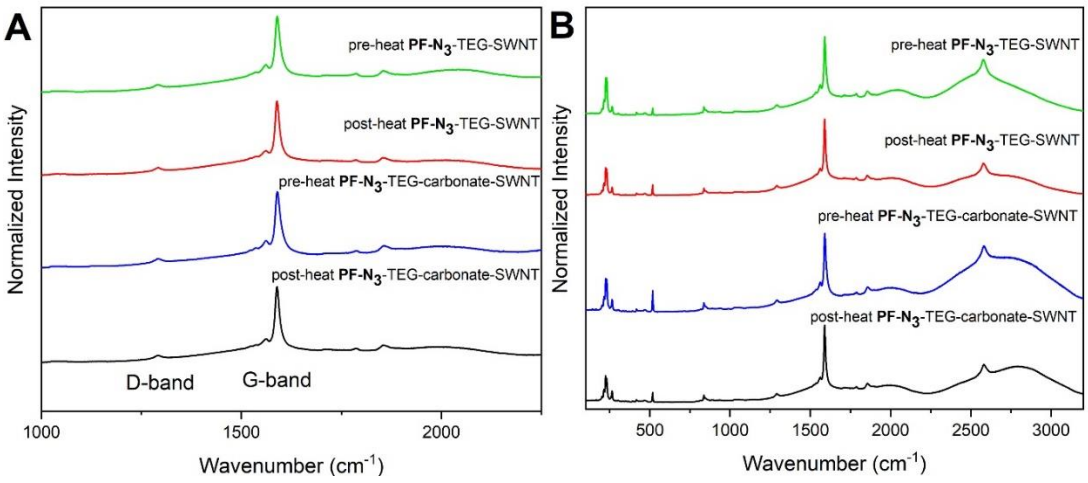


Figure 2.22. Raman spectra for **PF-N$_3$**-TEG-SWNT and **PF-N$_3$**-TEG-carbonate-SWNT at $\lambda_{ex}$= 785nm showing A) the G- and D-band and B) the full spectrum pre-and post-heating treatment. All the spectra were normalized to the G-band at ~1590 cm$^{-1}$.

.

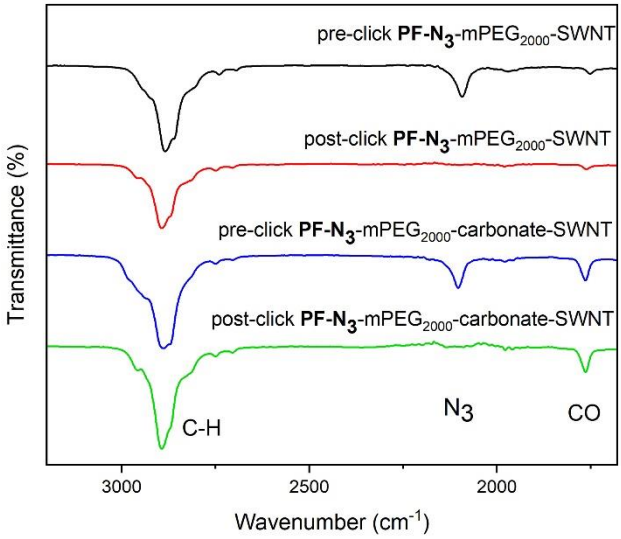


Figure 2.23. FT-IR overlay of the click reaction between the **PF-N$_3$**-SWNT complex, mPEG$_{2000}$-alkyne and mPEG$_{2000}$-carbonate-alkyne.

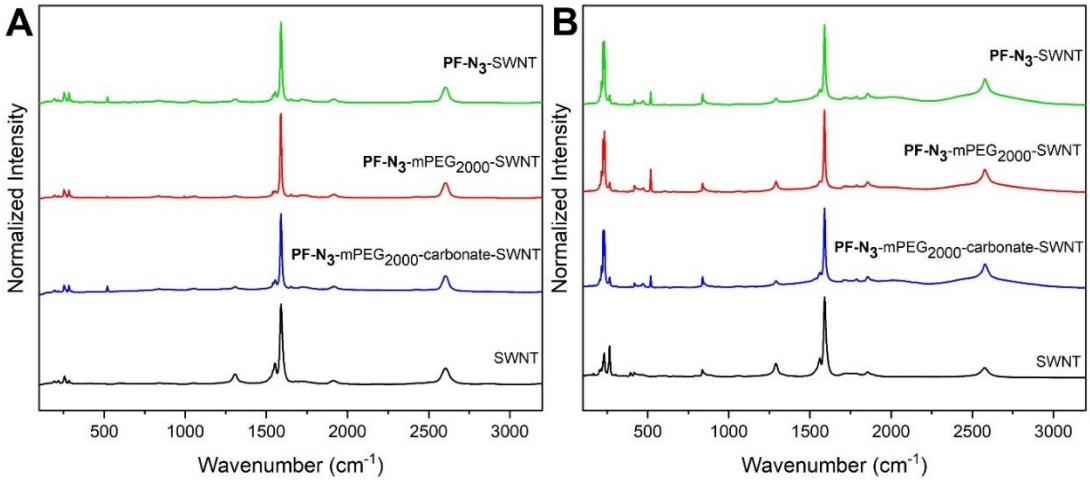


Figure 2.24. Full Raman spectra for HiPco polymer-SWNT samples at A) $\lambda_{ex}$ = 633 nm, B) $\lambda_{ex}$ =785 nm. All the spectra were normalized at ~ 1590 $cm^{-1}$.

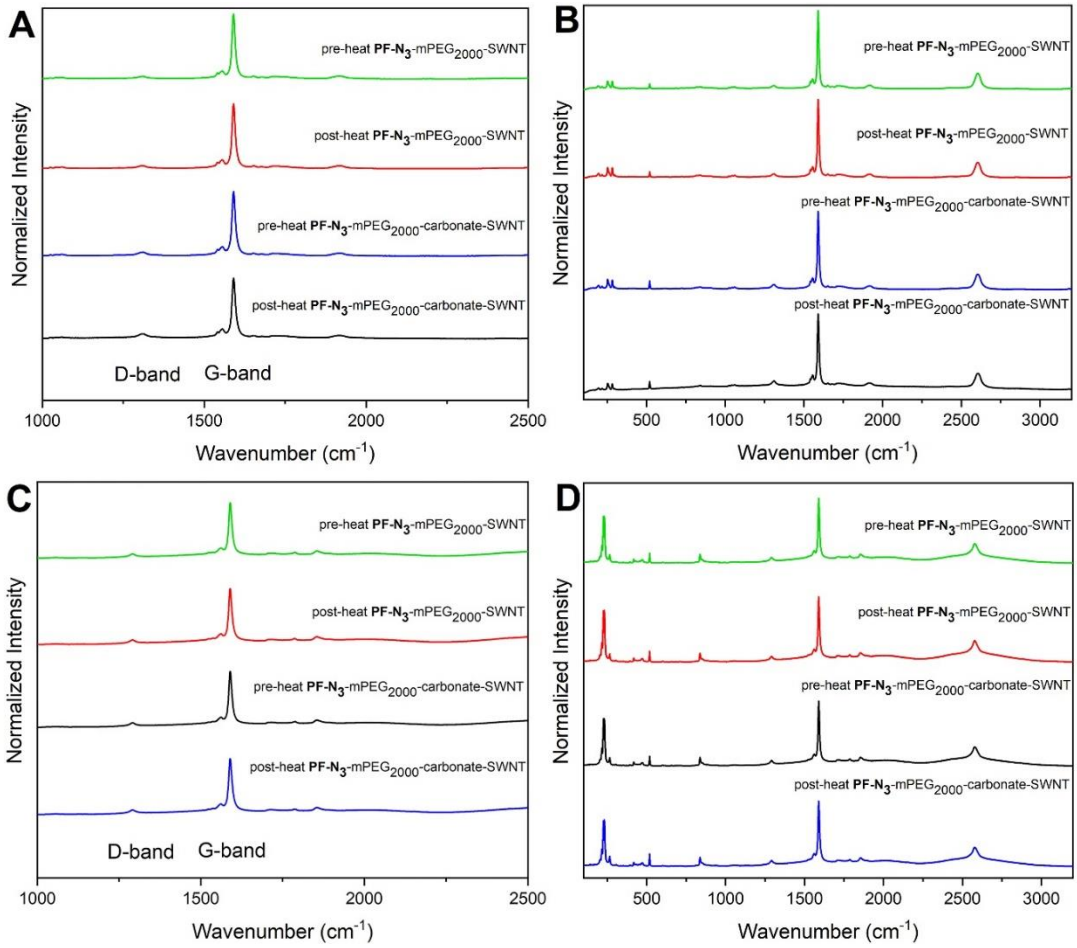


Figure 2.25. Raman Spectra for **PF-N$_3$**-mPEG$_{2000}$-SWNT and **PF-N$_3$**-mPEG$_{2000}$-carbonate-SWNT pre- and post-heating treatment at $\lambda_{ex}$ = 633 nm showing A) the G- and D-band and B) the full spectrum and at $\lambda_{ex}$ = 785 nm showing C) the G- and D-band and D) the full spectrum. All the spectra were normalized to the G-band at ~ 1590 cm$^{-1}$.

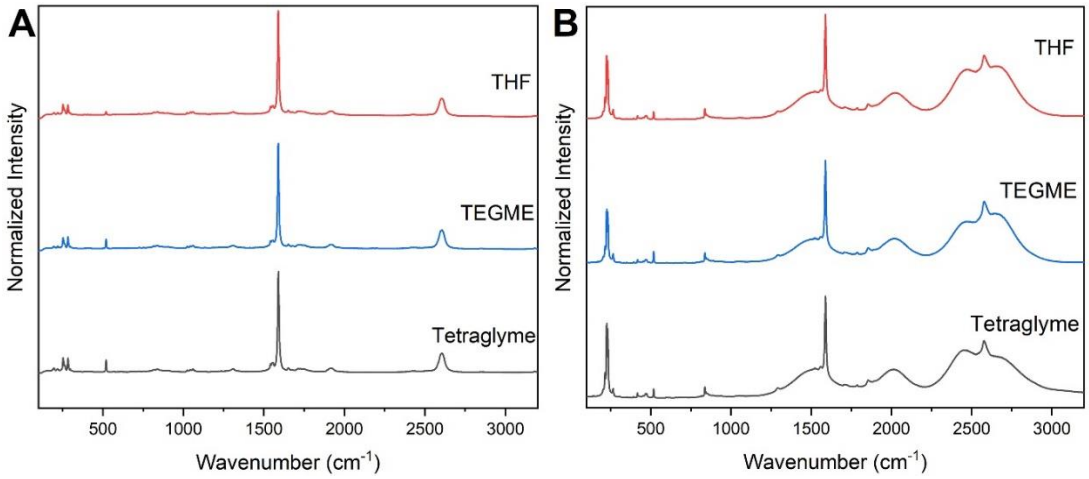


Figure 2.26. Full Raman spectra for **PF-$N_3$**- $mPEG_{2000}$-carbonate-SWNT before and after solvent exchange at A) $\lambda_{ex}$ = 633 nm, B) A) $\lambda_{ex}$ = 785 nm. All the spectra were normalized at ~1590 $cm^{-1}$.

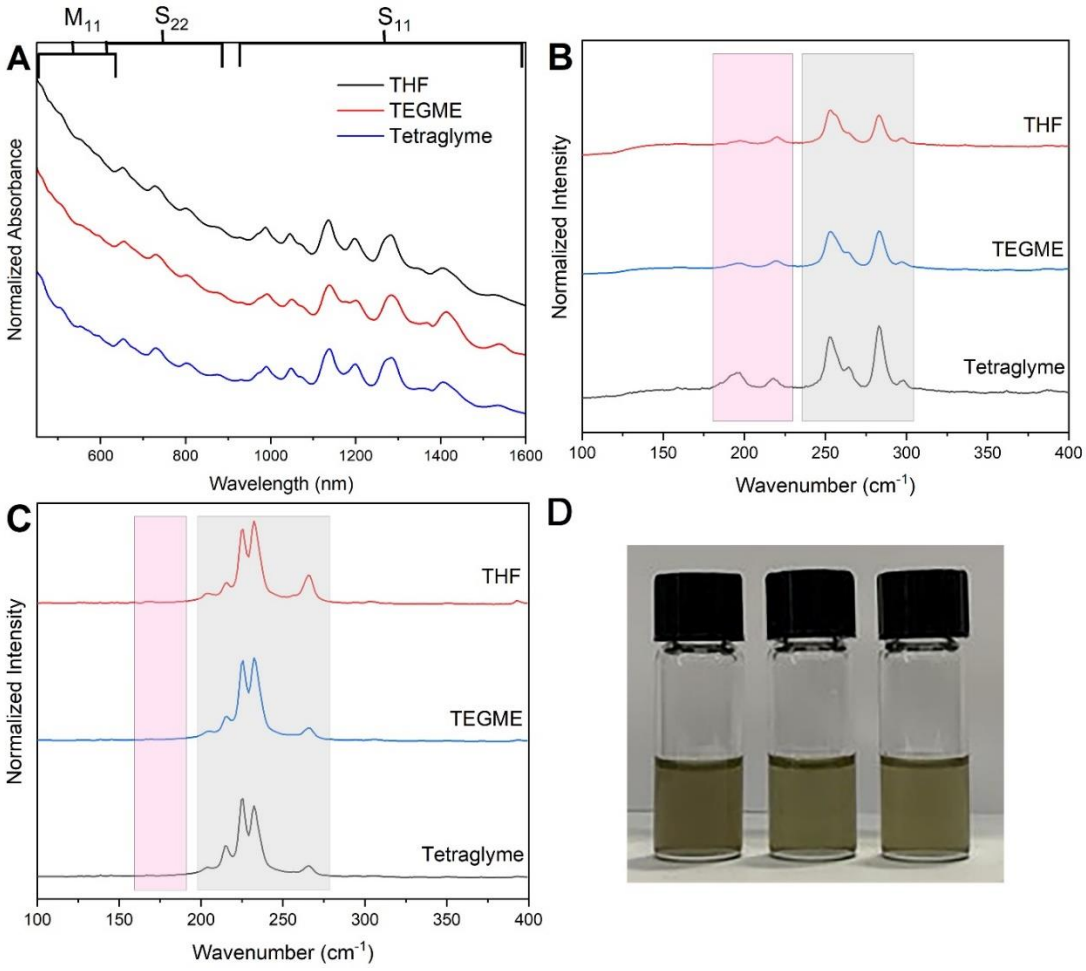


Figure 2.27. A) UV-Vis-NIR absorption spectra for **PF-N$_3$**-mPEG$_{2000}$-SWNT before and after solvent exchange. Spectra were normalized to the signal at 1140 cm$^{-1}$ and offset for clarity. B) Raman Spectra for HiPco polymer-SWNT samples showing the RBM regions at $\lambda_{ex}$ = 633 nm, C) $\lambda_{ex}$ = 785 nm. Gray boxes represent signals arising for sc-SWNTs, whereas pink boxes represent m-SWNTs. All the spectra were normalized to the G-band at ~ 1590 cm$^{-1}$ and D) photograph of **PF-N$_3$**-mPEG$_{2000}$-SWNT in THF (right), triethylene glycol monomethyl ether (middle) and tetraethylene glycol dimethyl ether (right).

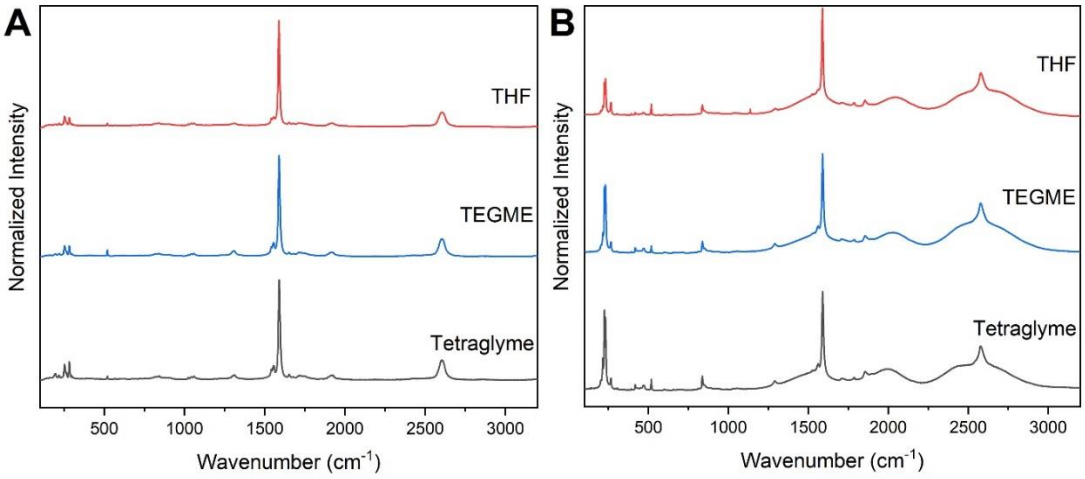


Figure 2.28. Full Raman spectra for **PF-$N_3$**- $mPEG_{2000}$-SWNT before and after solvent-exchange at A) $\lambda_{ex}$ = 633 nm, B) $\lambda_{ex}$ 785 nm. All the spectra were normalized at ~ 1590 $cm^{-1}$.

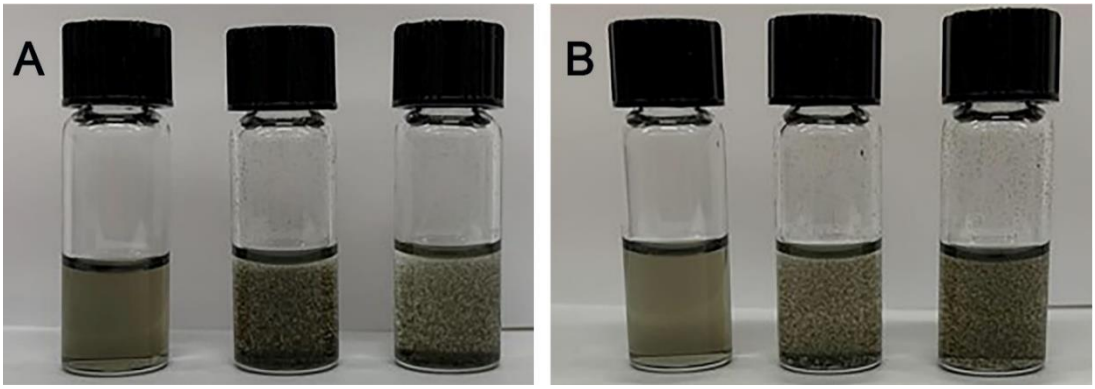


Figure 2.29. Photograph of the polymer-SWNT complex before and after the green solvent exchange A) **PF-$N_3$**-TEG-SWNT in THF (left), triethylene glycol monomethyl ether (middle) and tetraethylene glycol dimethyl ether (right), B) **PF-$N_3$**-TEG-carbonate-SWNT in THF (left), triethylene glycol monomethyl ether (middle) and tetraethylene glycol dimethyl ether (right).

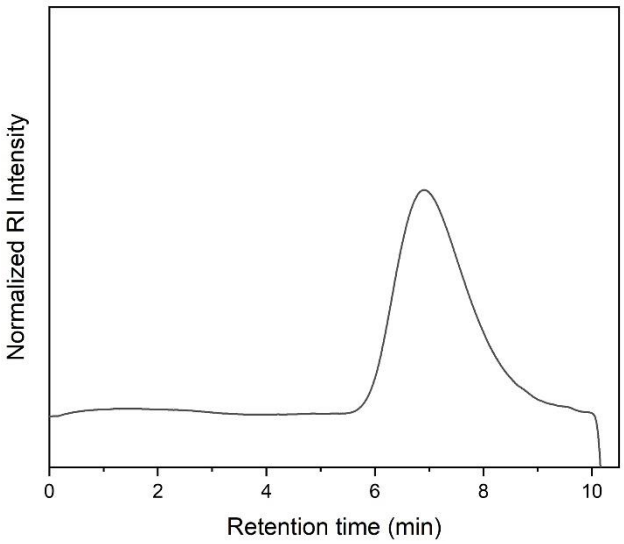


Figure 2.30. GPC trace of **PF-Br**.

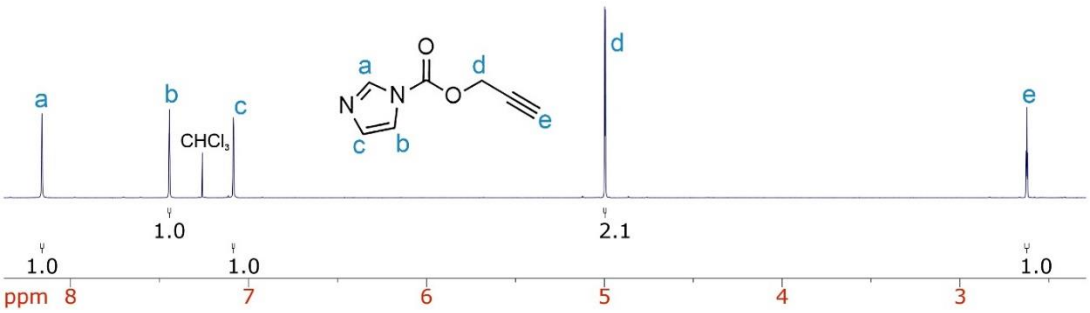


Figure 2.31. $^{1}$H-NMR spectrum of compound **4**.

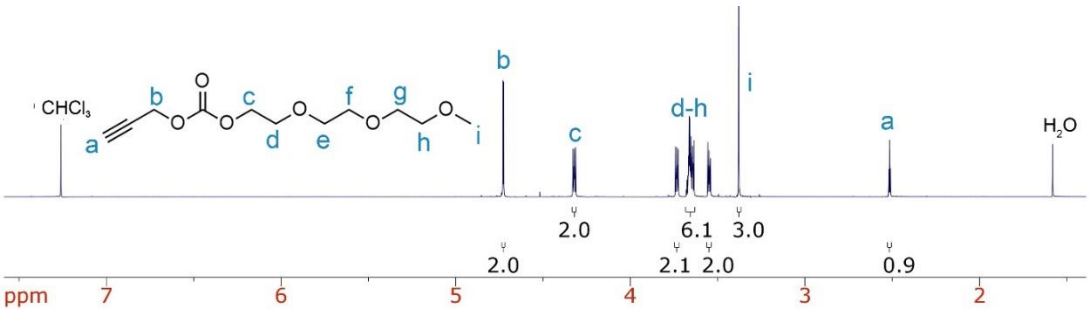


Figure 2.32. $^{1}$H-NMR spectrum of **TEG-carbonate-alkyne**.

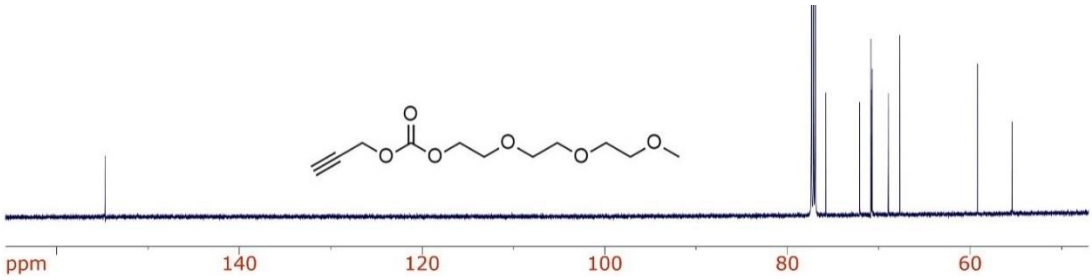


Figure 2.33. $^{13}$C-NMR spectrum of **TEG-carbonate-alkyne** in $CDCl_3$.

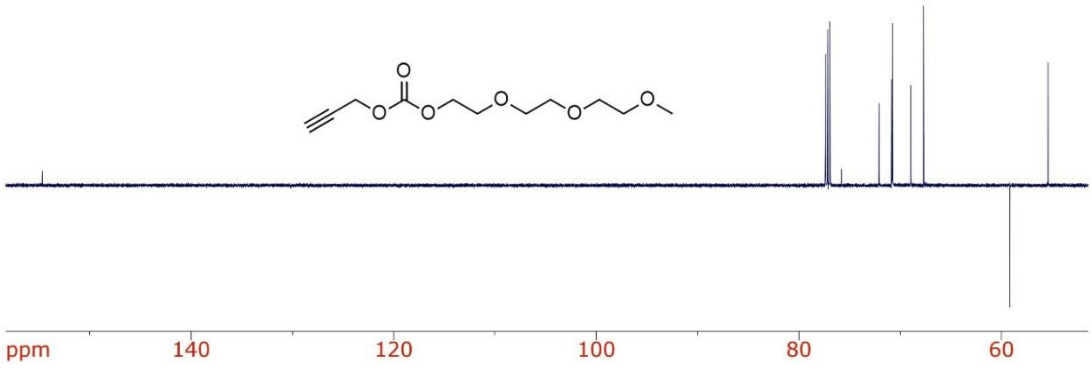


Figure 2.34. DEPTq spectrum of **TEG-carbonate-alkyne** in $CDCl_3$.

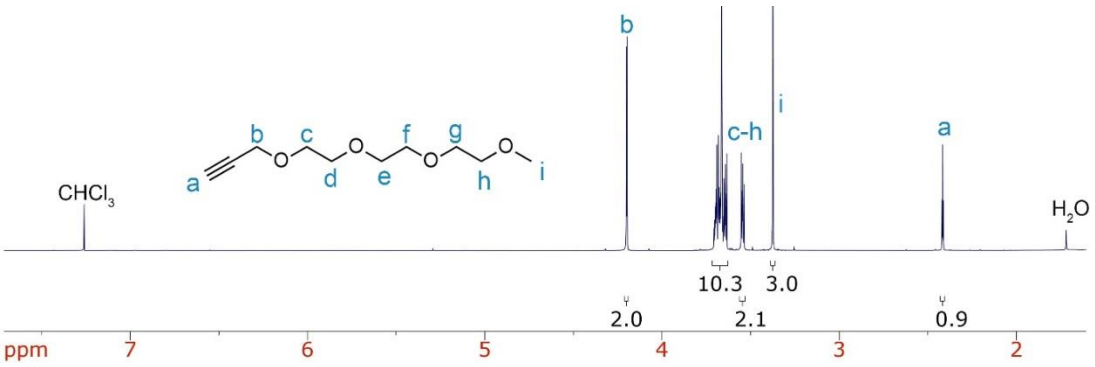


Figure 2.35. $^{1}$H-NMR spectrum of **TEG-alkyne** in $CDCl_3$.

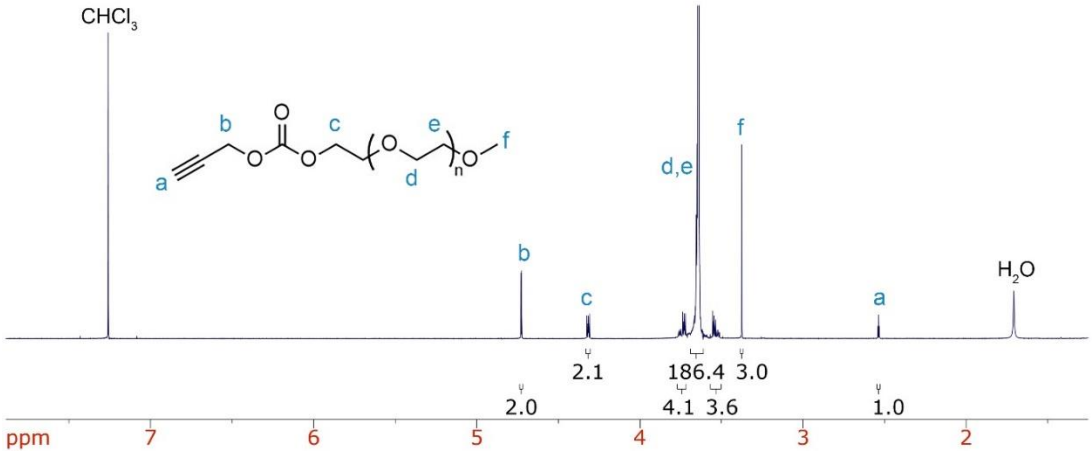


Figure 2.36. $^{1}$H-NMR spectrum of **mPEG$_{2000}$-carbonate-alkyne**.

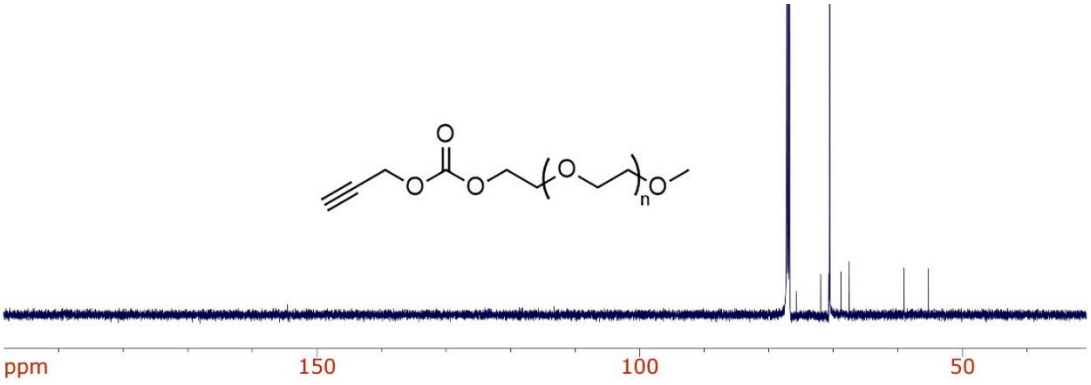


Figure 2.37. $^{13}$C-NMR spectrum of **mPEG$_{2000}$-carbonate-alkyne** in $CDCl_3$.

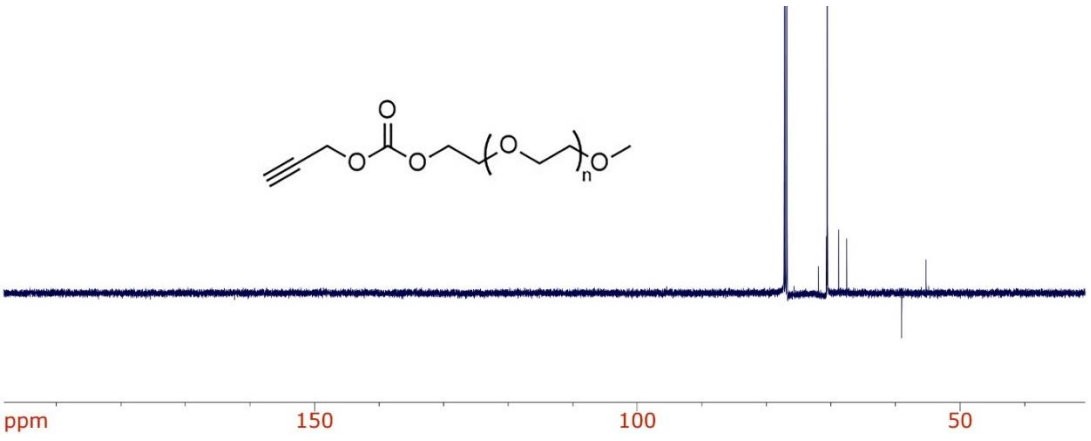


Figure 2.38. $^{13}$C-NMR spectrum of **mPEG$_{2000}$-carbonate-alkyne** in $CDCl_3$.

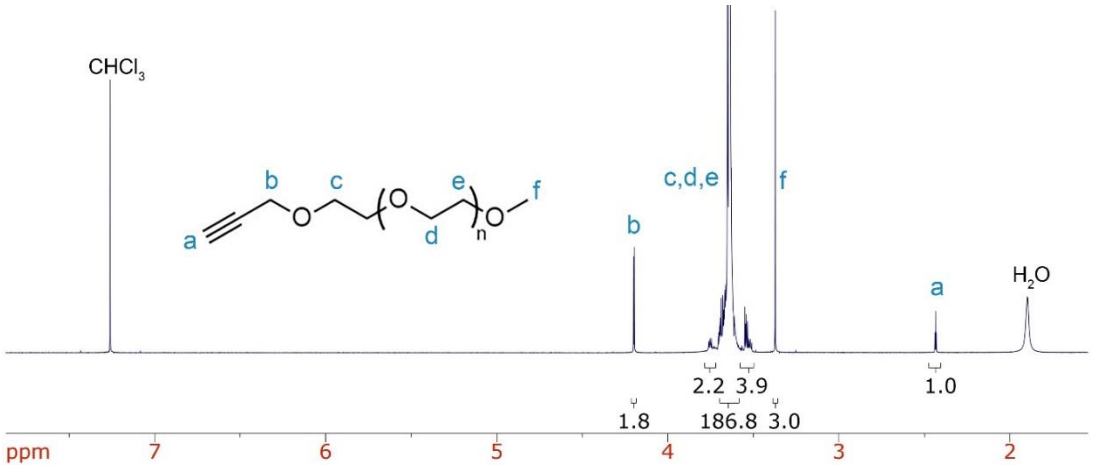


Figure 2.39. $^{1}$H-NMR spectrum of **mPEG$_{2000}$-alkyne** in $CDCl_3$.

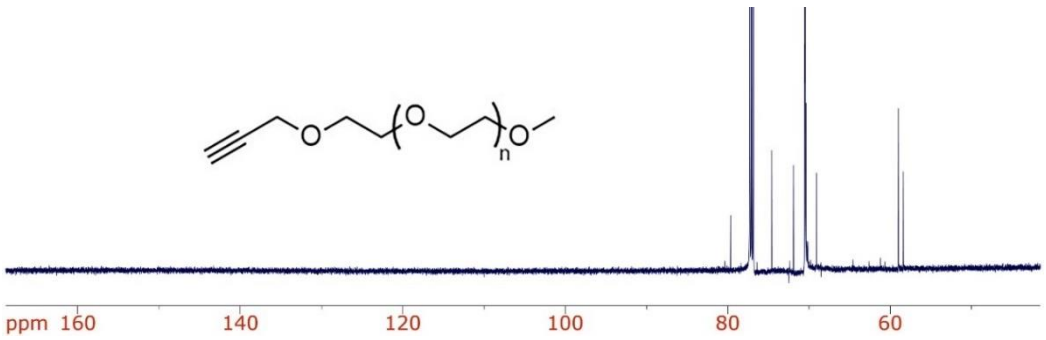


Figure 2.40. $^{13}$C-NMR spectrum of **mPEG$_{2000}$-alkyne** in $CDCl_3$.

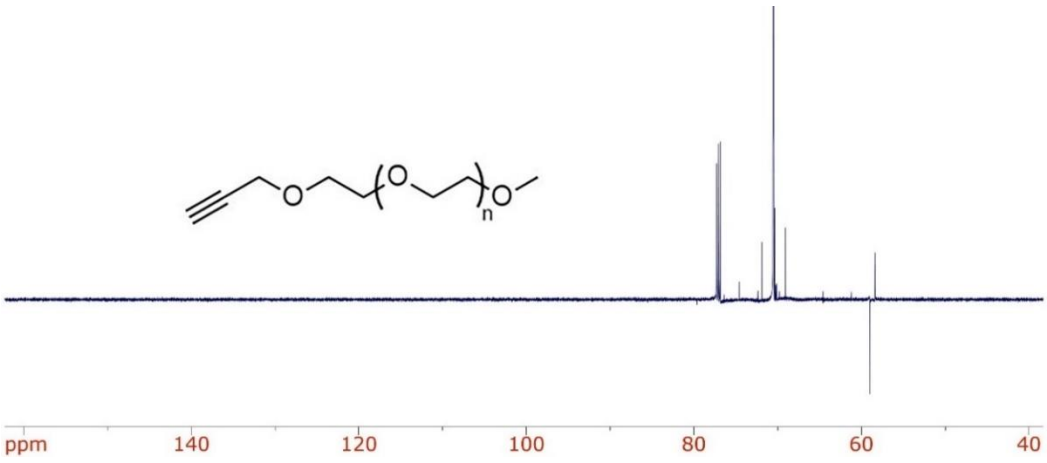


Figure 2.41. Deptq NMR spectrum of **mPEG$_{2000}$-alkyne** in $CDCl_3$.

## 2.5 References

[1] S. Iijima, *Nature* **1991**, *354*, 56.

[2] M. Yu, B. S. Files, S. Arepalli, R. S. Ruoff, *Phys. Rev. Lett.* **2000**, *84*, 1–4.

[3] J. N. Coleman, U. Khan, W. J. Blau, Y. K. Gun'ko, *Carbon* **2006**, *44*, 1624–1652.

[4] H. Kataura, Y. Kumazawa, Y. Maniwa, I. Umezu, S. Suzuki, Y. Ohtsuka, Y. Achiba, *Synth. Met.* **1999**, *103*, 2555−2558.

[5] S. M. Bachilo, M. S. Strano, C. Kittrell, R. H. Hauge, R. E. Smalley, R. B. Weisman, *Science* **2002**, *298*, 2361–2366.

[6] P. G. Collins, P. Avouris, *Sci. Am.* **2000**, *283*, 62–69.

[7] P. Avouris, *Acc. Chem. Res.* **2002**, *35*, 1026–1034.

[8] P. Qi, O. Vermesh, M. Grecu, A. Javey, Q. Wang, H. Dai, S. Peng, K. J. Cho, *Nano Lett.* **2003**, *3*, 347–351.

[9] M. Dionisio, J. M. Schnorr, V. K. Michaelis, R. G. Griffin, T. M. Swager, E. Dalcanale, *J. Am. Chem. Soc.* **2012**, *134*, 6540–6543.

[10] T. Dürkop, S. A. Getty, E. Cobas, M. S. Fuhrer, *Nano Lett.* **2004**, *4*, 35–39.

[11] D. M. Sun, C. Liu, W. C. Ren, H. M. Cheng, *Small* **2013**, *9*, 1188–1205.

[12] M. W. Rowell, M. A. Topinka, M. D. McGehee, H. J. Prall, G. Dennler, N. S. Sariciftci, L. Hu, G. Gruner, *Appl. Phys. Lett.* **2006**, *88*, 6–9.

[13] D. J. Bindl, N. S. Safron, M. S. Arnold, *ACS Nano* **2010**, *4*, 5657–5664.

[14] S. Park, M. Vosguerichian, Z. Bao, *Nanoscale* **2013**, *5*, 1727–1752.

[15] S. Park, M. Vosguerichian, Z. Bao, *Proc. Natl. Acad. Sci.* **2014**, *111*, 4776–4781.

[16] K. Kordás, T. Mustonen, G. Tóth, H. Jantunen, M. Lajunen, C. Soldano, S. Talapatra, S. Kar, R. Vajtai, P. M. Ajayan, *Small* **2006**, *2*, 1021–1025.

[17] K. Y. Chun, Y. Oh, J. Rho, J. H. Ahn, Y. J. Kim, H. R. Choi, S. Baik, *Nat. Nanotechnol.* **2010**, *5*, 853–857.

[18] D. Jariwala, V. K. Sangwan, L. J. Lauhon, T. J. Marks, M. C. Hersam, *Chem. Soc. Rev.* **2013**, *42*, 2824–2860.

[19] W. Gomulya, J. Gaoa, M. A. Loib, *Eur. Phys. J. B* **2013**, *86*, 1–13.

[20] P. Nikolaev, M. J. Bronikowski, R. K. Bradley, F. Rohmund, D. T. Colbert, K. A. Smith, R. E. Smalley, *Chem. Phys. Lett.* **1999**, *313*, 91–97.

[21] K. S. Kim, G. Cota-Sanchez, C. T. Kingston, M. Imris, B. Simard, G. Soucy, *J. Phys. D. Appl. Phys.* **2007**, *40*, 2375–2387.

[22] M. M. A. Rafique, J. Iqbal, *J. Encapsulation Adsorpt. Sci.* **2011**, *102*, 503–519.

[23] D. Tasis, N. Tagmatarchis, A. Bianco, M. Prato, *Chem. Rev.* **2006**, *106*, 1105–1136.

[24] S. Campidelli, C. Klumpp, A. Bianco, D. M. Guldi, M. Prato, *J. Phys. Org. Chem.* **2006**, *19*, 531–539.

[25] A. Hirsch, *Angew. Chem., Int. Ed.* **2002**, *41*, 1853–1859.

[26] Y.-L. Zhao, J. F. Stoddart, *Chem. Nanocarbons* **2010**, *42*, 1162–1171.

[27] A. Star, Y. Liu, K. Grant, L. Ridvan, J. F. Stoddart, D. W. Steuerman, M. R. Diehl, A. Boukai, J. R. Heath, *Macromolecules* **2003**, *36*, 553–560.

[28] A. Star, D. W. Steuerman, J. R. Heath, J. F. Stoddart, *Angew. Chem., Int. Ed.* **2002**, *41*, 2508–2512.

[29] Y. Tomonari, H. Murakami, N. Nakashima, *Chem. Eur. J.* **2006**, *12*, 4027–4034.

[30] K. Yang, L. Zhu, B. Xing, *Environ. Sci. Technol.* **2006**, *40*, 1855–1861.

[31] R. J. Chen, Y. Zhang, D. Wang, H. Dai, *J. Am. Chem. Soc.* **2001**, *123*, 3838–3839.

[32] V. C. Moore, M. S. Strano, E. H. Haroz, R. H. Hauge, R. E. Smalley, J. Schmidt, Y. Talmon, *Nano Lett.* **2003**, *3*, 1379–1382.

[33] M. F. Islam, E. Rojas, D. M. Bergey, A. T. Johnson, A. G. Yodh, *Nano Lett.* **2003**, *3*, 269–273.

[34] M. J. O'Connell, S. M. Bachilo, C. B. Huffman, V. C. Moore, M. S. Strano, E. H. Haroz, K. L. Rialon, P. J. Boul, W. H. Noon, C. Kittrell, et al., *Science* **2002**, *297*, 593–596.

[35] Z. Guo, P. J. Sadler, S. C. Tsang, *Adv. Mater.* **1998**, *10*, 701–703.

[36] K. Bradley, M. Briman, A. Star, G. Gruner, *Nano Lett.* **2004**, *4*, 253–256.

[37] M. Zheng, A. Jagota, E. D. Semke, B. A. Diner, R. S. McLean, S. R.

Lustig, R. E. Richardson, N. G. Tassi, *Nat. Mater.* **2003**, *2*, 338–42.

[38] J. Chen, H. Liu, W. A. Weimer, M. D. Halls, D. H. Waldeck, G. C. Walker, *J. Am. Chem. Soc.* **2002**, *124*, 9034–9035.

[39] J. Y. Hwang, A. Nish, J. Doig, S. Douven, C. W. Chen, L. C. Chen, R. J. Nicholas, *J. Am. Chem. Soc.* **2008**, *130*, 3543–3553.

[40] F. Chen, B. Wang, Y. Chen, L. J. Li, *Nano Lett.* **2007**, *7*, 3013–3017.

[41] A. Star, J. F. Stoddart, D. Steuerman, M. Diehl, A. Boukai, E. W. Wong, X. Yang, S. Chung, H. Choi, J. R. Heath, *Angew. Chem.* **2001**, *40*, 1721–1725.

[42] D. Fong, A. Adronov, *Chem. Sci.* **2017**, *8*, 7292–7305.

[43] S. K. Samanta, M. Fritsch, U. Scherf, W. Gomulya, S. Z. Bisri, M. A. Loi, *Acc. Chem. Res.* **2014**, *47*, 2446–2456.

[44] P. Imin, F. Cheng, A. Adronov, *Polym. Chem.* **2011**, *2*, 1404–1408.

[45] D. Fong, W. J. Bodnaryk, N. A. Rice, S. Saem, J. M. Moran-Mirabal, A. Adronov, *Chem. Eur. J.* **2016**, *22*, 14560–14566.

[46] J. Ding, Z. Li, J. Lefebvre, F. Cheng, G. Dubey, S. Zou, P. Finnie, A. Hrdina, L. Scoles, G. P. Lopinski, et al., *Nanoscale* **2014**, *6*, 2328–2339.

[47] F. A. Lemasson, T. Strunk, P. Gerstel, F. Hennrich, S. Lebedkin, C. Barner-Kowollik, W. Wenzel, M. M. Kappes, M. Mayor, *J. Am. Chem. Soc.* **2011**, *133*, 652–655.

[48] P. Gerstel, S. Klumpp, F. Hennrich, A. Poschlad, V. Meded, E. Blasco,

W. Wenzel, M. M. Kappes, C. Barner-kowollik, *ACS Macro Lett.* **2014**, *3*, 2–7.

[49] N. A. Rice, A. V Subrahmanyam, B. R. Coleman, A. Adronov, *Macromolecules* **2015**, *48*, 5155–5161.

[50] W. J. Bodnaryk, D. Fong, A. Adronov, *ACS Omega* **2018**, *3*, 16238–16245.

[51] T. Lei, I. Pochorovski, Z. Bao, *Acc. Chem. Res.* **2017**, *50*, 1096–1104.

[52] T. Lei, X. Chen, G. Pitner, H. S. P. Wong, Z. Bao, *J. Am. Chem. Soc.* **2016**, *138*, 802–805.

[53] I. Pochorovski, H. Wang, J. I. Feldblyum, X. Zhang, A. L. Antaris, Z. Bao, *J. Am. Chem. Soc.* **2015**, *137*, 4328–4331.

[54] F. Toshimitsu, N. Nakashima, *Nat. Commun.* **2014**, *5*, 1–9.

[55] S. Liang, Y. Zhao, A. Adronov, *J. Am. Chem. Soc.* **2014**, *136*, 970–977.

[56] L. Xu, M. Valášek, F. Hennrich, R. Fischer, M. M. Kappes, M. Mayor, *Macromolecules* **2021**, *54*, 4363–4374.

[57] W. J. Bodnaryk, K. Li, A. Adronov, *J. Polym. Sci.* **2020**, *58*, 1965–1972.

[58] F. Lemasson, J. Tittmann, F. Hennrich, N. Stürzl, S. Malik, M. M. Kappes, M. Mayor, *Chem. Commun.* **2011**, *47*, 7428–7430.

[59] D. Fong, G. M. Andrews, A. Adronov, *Polym. Chem.* **2018**, *9*, 2873–2879.

[60] D. Fong, G. M. Andrews, S. A. McNelles, A. Adronov, *Polym. Chem.* **2018**, *9*, 4460–4467.

[61] D. Fong, J. Yeung, E. Meichsner, A. Adronov, *ACS Appl. Polym. Mater.* **2019**, *1*, 797–803.

[62] M. Helgesen, M. V. Madsen, B. Andreasen, T. Tromholt, J. W. Andreasen, F. C. Krebs, *Polym. Chem.* **2011**, *2*, 2536–2542.

[63] J. L. Brusso, M. R. Lilliedal, S. Holdcroft, *Polym. Chem.* **2011**, *2*, 175–180.

[64] M. Helgesen, S. A. Gevorgyan, F. C. Krebs, R. A. J. Janssen, *Chem. Mater.* **2009**, *21*, 4669–4675.

[65] M. H. Petersen, S. A. Gevorgyan, F. C. Krebs, *Macromolecules* **2008**, *41*, 8986–8994.

[66] J. Liu, E. N. Kadnikova, Y. Liu, M. D. McGehee, J. M. J. Fréchet, *J. Am. Chem. Soc.* **2004**, *126*, 9486–9487.

[67] B. Sun, W. Hong, H. Aziz, Y. Li, *J. Mater. Chem.* **2012**, *22*, 18950–18955.

[68] L. Yang, Y. Yu, Y. Gong, J. Li, F. Ge, L. Jiang, F. Gao, Y. Dan, *Polym. Chem.* **2015**, *6*, 7005–7014.

[69] P. He, S. Shimano, K. Salikolimi, T. Isoshima, Y. Kakefuda, T. Mori, Y. Taguchi, Y. Ito, M. Kawamoto, *ACS Appl. Mater. Interfaces* **2018**, *11*, 4211–4218.

[70] J. F. Ponder, S. A. Gregory, A. Atassi, A. K. Menon, A. W. Lang, L. R. Savagian, J. R. Reynolds, S. K. Yee, *J. Am. Chem. Soc.* **2022**, *144*, 1351–1360.

[71] M. Kuhn, J. Ludwig, T. Marszalek, T. Adermann, W. Pisula, K. Müllen, A. Colsmann, M. Hamburger, *Chem. Mater.* **2015**, *27*, 2678–2686.

[72] W. Zhu, C. Li, D. Zhang, G. Guan, Y. Xiao, L. Zheng, *Polym. Degrad. Stab.* **2012**, *97*, 1589–1595.

[73] M. S. Dresselhaus, G. Dresselhaus, R. Saito, A. Jorio, *Phys. Rep.* **2005**, *409*, 47–99.

[74] S. K. Doorn, *J. Nanosci. Nanotechnol.* **2005**, *5*, 1023–1034.

[75] S. K. Doorn, D. A. Heller, P. W. Barone, M. L. Usrey, M. S. Strano, *Appl. Phys. A* **2004**, *78*, 1147–1155.

[76] M. S. Strano, S. K. Doorn, E. H. Haroz, C. Kittrell, R. H. Hauge, R. E. Smalley, *Nano Lett.* **2003**, *3*, 1091–1096.

[77] D. A. Heller, P. W. Barone, J. P. Swanson, R. M. Mayrhofer, M. S. Strano, *J. Phys. Chem. B* **2004**, *108*, 6905–6909.

[78] S. D. M. Brown, A. Jorio, M. S. Dresselhaus, G. Dresselhaus, *Phys. Rev. B* **2001**, *64*, 3–6.

[79] R. Tortorich, J.-W. Choi, *Nanomaterials* **2013**, *3*, 453–468.

[80] T. Pandhi, A. Chandnani, H. Subbaraman, D. Estrada, *Sensors* **2020**, *20*, 1–20.

[81] S. Matsuzaki, Y. Nobusa, R. Shimizu, K. Yanagi, H. Kataura, T. Takenobu, *Jpn. J. Appl. Phys.* **2012**, *51*, 1–3.

[82] J. Yun, H. Chang-soo, J. Kim, J. Song, D. Shin, Y. Park, *3rd IEEE Int.*

*Conf. Nano/Micro Eng. Mol. Syst.* **2008**, 506–509.

[83] H. Okimoto, T. Takenobu, K. Yanagi, Y. Miyata, H. Shimotani, H. Kataura, Y. Iwasa, *Adv. Mater.* **2010**, *22*, 3981–3986.

[84] O. S. Kwon, H. Kim, H. Ko, J. Lee, B. Lee, C. H. Jung, J. H. Choi, K. Shin, *Carbon* **2013**, *58*, 116–127.

[85] T. Kim, H. Song, J. Ha, S. Kim, D. Kim, S. Chung, J. Lee, Y. Hong, *Appl. Phys. Lett.* **2014**, *104*, 113103.

[86] P. D. Angelo, R. R. Farnood, *J. Adhes. Sci. Technol.* **2010**, *24*, 643–659.

[87] D. H. Kim, H. Shin, H. S. Lee, J. Lee, B. Lee, W. H. Lee, J. Lee, K. Cho, W. Kim, S. Y. Lee, et al., *ACS Nano* **2012**, *6*, 662–670.

[88] J. W. Song, J. Kim, Y. H. Yoon, B. S. Choi, J. H. Kim, C. S. Han, *Nanotechnology* **2008**, *19*, 0–6.

[89] Y. Nobusa, Y. Takagi, S. Gocho, S. Matsuzaki, K. Yanagi, T. Takenobu, *Jpn. J. Appl. Phys.* **2012**, *51*, 2–4.

[90] P. Beecher, P. Servati, A. Rozhin, A. Colli, V. Scardaci, S. Pisana, T. Hasan, A. J. Flewitt, J. Robertson, G. W. Hsieh, et al., *J. Appl. Phys.* **2007**, *102*.

[91] I. Hoogmartens (Agfa Graphics NV), US7699923B2, **2010.**

[92] K. B. Gundlach, R. L. Colt (Xerox Corp.), EP1103585A1, **2001**.

[93] A. Abbas, I. Bajwa, Protoc. Rep. **2017**, 1,1.

[94] J. Zhang, C. Li, Y. Wang, R.-X. Zhuo, X.-Z. Zhang, *ChemComm* **2011**,

*47*, 4457–4459.

[95] P. Chandra, A. M. Jonas, A. E. Fernandes, *J. Am. Chem. Soc.* **2018**, *140*, 5179–5184.

# Chapter 3

# Decoration of Polyfluorene-Wrapped Carbon Nanotubes with Photocleavable Side-Chains

This chapter has been reprinted with permission from MDPI: Ritaine, D.; Adronov, A. Decoration of Polyfluorene-Wrapped Carbon Nanotubes with Photocleavable Side-Chains. Molecules 2023, 28, 1471. https://doi.org/10.3390/molecules28031471

## Abstract

Functionalizing polyfluorene-wrapped carbon nanotubes without damaging their properties is effective via Copper-Catalyzed Azide–Alkyne Cycloaddition. However, the length and nature of polymer side-chains can impact the conductivity of polyfluorene-SWNT films by preventing close contact between the nanotubes. Here, we investigate the functionalization of a polyfluorene-SWNT complex using photocleavable side-chains that can be removed post-processing. The cleavage of the side-chains containing an ortho-nitrobenzyl ether derivative is efficient when exposed to a UV lamp at 365 nm. The photoisomerization of the *o*-nitrobenzyl ether linker into the corresponding *o*-nitrosobenzaldehyde was first monitored via UV-Vis absorption spectroscopy and $^{1}$H-NMR spectroscopy on the polymer, which showed efficient cleavage after 2 h. We next investigated the cleavage on the polyfluorene-SWNT complex via UV-Vis-NIR absorption spectroscopy. The precipitation of the nanotube dispersion and the broad absorption peaks after overnight irradiation also indicated effective cleavage. In addition, Raman spectroscopy post-irradiation showed that the nanotubes were not damaged upon irradiation. This paper reports a proof of concept that may find applications for SWNT-based materials in which side-chain removal could lead to higher device performance.

## 3.1 Introduction

Since the discovery of single-walled carbon nanotubes in 1991[1], significant effort has been made to take advantage of their mechanical[2,3], optical[4,5], and electronic properties[6,7]. Numerous applications of SWNTs such as sensors[8,9], thin film transistors[10,11], organic photovoltaics[12,13], flexible electronics[14,15], and conductive inks[16,17] have been developed[18,19]. However, due to inter-tube π–π interactions, SWNTs tend to aggregate into insoluble bundles in organic solvents[20]. Moreover, all commercial techniques to produce SWNTs[21,22] result in a complex mixture of amorphous carbon, leftover catalyst particles, and a mixture of semiconducting and metallic species (sc- and m-SWNTs, respectively) that impede their performance within several applications[23]. To address this issue, covalent or non-covalent functionalization of SWNTs has been developed to improve their solubility and purity. Covalent functionalization requires strongly oxidizing conditions that damage SWNTs' properties by destroying the $sp^2$ hybridized surface and therefore impact on SWNTs' properties[24,25]. In contrast, non-covalent functionalization uses sonication in the presence of a dispersant to form a dispersant-SWNTs supramolecular complex that provides solubility in organic solvents and prevents SWNTs reaggregation into bundles[26–28]. To this end, dispersants such as small aromatic compounds[29–31], surfactants[32–34], biomolecules[35–37], and conjugated polymers[38–41] have been used. Due to their facile synthesis and structural modification[42–46], conjugated polymers can be used to achieve different properties such as selective dispersion of either sc- or

m-SWNTs[47–50], reversible assembly on the nanotube surface[51–56], or depolymerization in response to a stimulus to release SWNTs.[57–59]

Attention has also been given to conjugated polymers that exhibit reactive functionality post-supramolecular assembly with SWNTs. Specifically, polyfluorene derivatives containing azide groups in the side-chains have been prepared and used to noncovalently functionalize SWNTs[60–62]. The resulting polyfluorene-SWNTs complexes, dispersed in organic or aqueous solvents, were then functionalized using either Copper-Catalyzed Azide–Alkyne Cycloaddition (CuAAC) or Strain-Promoted Azide–Alkyne Cycloaddition (SPAAC) without damaging SWNTs' optoelectronic properties[60–62]. However, the introduction of large side-chains that are non-conductive results in a dramatic decrease in conductivity of the polymer-SWNTs complex by preventing good contact between adjacent nanotubes. A potential approach to solve this problem is the use of cleavable side-chains that can be removed after the device's fabrication. In 2019, Kawamoto and coworkers prepared SWNTs thin films dispersed using polythiophene functionalized with carbonate linkers in their side-chains. When heated at 350 °C, the carbonate linkers were cleaved by decarboxylation resulting in higher conductivity[63]. More recently, our group prepared a polyfluorene-SWNTs complex functionalized with thermally cleavable side-chains that also contain a carbonate linker. The conductivity increased over time upon heating the films at 170 °C and reached a plateau of $(2.0 \pm 0.1) \times 10^{-2}$ S/m after 17 h of heating, which was 20 times higher than the non-cleavable sample. This demonstrates the effect of removing the side-chains post-processing[64].

Here, we report a different type of cleavable side-chain that contains an ortho-nitrobenzyl (*o*NB) ether linker. This linker is cleaved when exposed to a 300–365 nm UV light[65,66]. The cleavage time varies from minutes to a few hours, depending on the intensity of the light, which usually ranges from 1 to 60 $mW.cm^{-2}$[65]. *o*NB linkers have been widely used as cross-linkers for photodegradable polymers[67], side-chain functionalization[68–72], solid-phase synthesis[73–75], photolithography[76,77], self-immolative polymers[78,79], and other applications[65,66,80,81]. In this work, we prepared a polyfluorene-SWNTs complex functionalized with either photocleavable or non-cleavable side-chains. The cleavage study was first performed on the polymers using UV-Vis absorption and $^{1}H$ NMR spectroscopy. We next studied the polyfluorene-SWNTs complexes using UV-Vis-NIR absorption spectroscopy. Characterization post-irradiation was also performed using Raman spectroscopy to verify that the irradiation did not damage the nanotubes.

### 3.2 Results and Discussion

**Polymer Synthesis and Characterization.** To begin our study, we first synthesized an azide-containing polyfluorene (**PF-$N_3$**) according to procedures in the literature[62]. Bromination of fluorene using *N*-bromosuccinimide (NBS) was performed to obtain precursor **1** ( Scheme 3.3 (Supplementary Materials)), which was then alkylated with 1,6-dibromohexane to afford monomer **2**. Borylation of this monomer using Miyaura conditions afforded the diboronic ester **3.** Monomers **2** and **3** were then copolymerized using a Suzuki polycondensation to obtain the homopolymer (**PF-Br**) (Scheme 3.1). Gel

permeation chromatography (GPC) revealed an $M_n$ of 33 kDa and a dispersity (Đ) of 2.2. **PF-$N_3$** was then prepared via a reaction between **PF-Br** and $NaN_3$ in the presence of $^nBu_4NBr$. The homopolymers were characterized by $^1H$ NMR spectroscopy to confirm the presence of alkyl azides (3.15 ppm) in **PF-$N_3$** and the disappearance of the signal of the alkyl bromides (3.31 ppm) in **PF-Br** (Supporting Information, Figure 3.8).

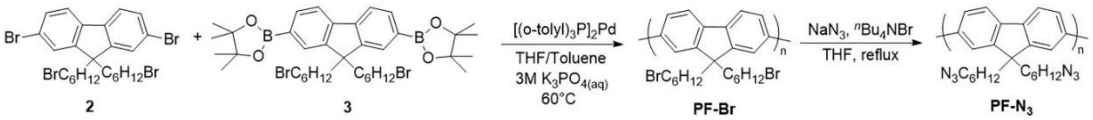


Scheme 3.1. Synthesis of **PF-Br** and **PF-$N_3$**.

To introduce our photocleavable side-chains, we first prepared an *o*NB-TEG-alkyne via activation of triethyelene glycol monomethyl ether with tosyl chloride (Supporting Information, Scheme 3.6), followed by alkylation with 5-Hydroxy-2-nitrobenzaldehyde to obtain compound **5**. Compound **5** was then reduced using sodium borohydride to afford the corresponding alcohol **6**. Nucleophilic substitution of this alcohol with propargyl bromide was finally performed to obtain *o*NB-TEG-alkyne. The non-cleavable analog was prepared via nucleophilic substitution of triethylene glycol monomethyl ether (TEG-OH) with propargyl bromide to give TEG-alkyne (Supporting Information, Scheme 3.7). PF-$N_3$ was then functionalized with either TEG-alkyne (**P1**) or *o*NB-TEG-alkyne (**P2**) (Figure 3.1) using copper-catalyzed azide-alkyne cycloaddition (CuAAC) (see Supplementary Materials for details). The reaction was monitored by infrared (IR) spectroscopy via the disappearance of the polymer azide stretch at ~2090 $cm^{-1}$ (Supporting Information, Figure 3.9). The resulting

polymers were also characterized by $^{1}$H–NMR spectroscopy to confirm the disappearance of the alkyl azides (3.15 ppm), the appearance of the aromatic proton in the triazole ring (7.51 ppm), as well as the appearance of alkyl protons from the side-chain between 3 and 5 ppm (Supporting Information, Figure 3.10).

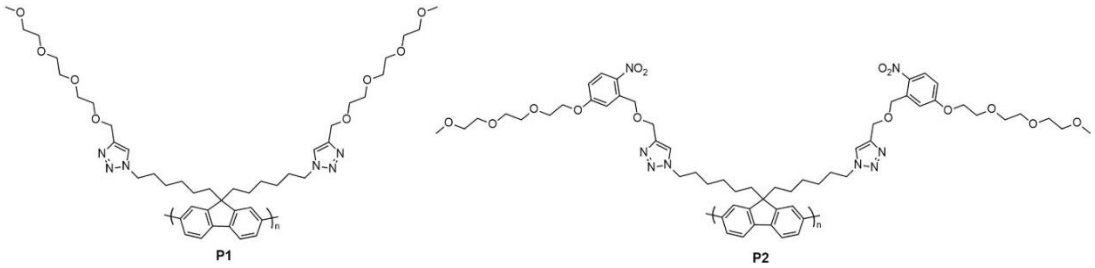


Figure 3.1 Chemical structure of **PF-TEG** (**P1**) and **PF-*o*NB-TEG** (**P2**).

**Photocleavage Study of The Polymers.** With **PF-TEG** (**P1**) and **PF-oNB-TEG** (**P2**) in hand, we studied the cleavage of the side-chain using UV-Vis absorption spectroscopy. To confirm that the polyfluorene does not degrade upon irradiation, **PF-N$_3$** was also studied. Polymers were dissolved in tetrahydrofuran (THF), transferred into quartz cuvettes, and irradiated at 365 nm in a UV reactor. The UV-Vis spectrum of each sample was measured every 15 min for a total duration of 2 h when no further changes in absorbance were observed (Figure 2). Not surprisingly, **PF-N$_3$** and **PF-TEG** do not show any degradation during the irradiation process (Figure 2A, B). As shown in Figure 3.2C, when **P2** was subjected to the irradiation process, a decrease in the absorbance is observed at 300 nm, corresponding to the cleavage of the *o*-nitrobenzyl linker. Meanwhile, as the peak at 300 nm decreases, a new peak at 350 nm arises. This new peak corresponds to the *o*-nitrosobenzaldehyde compound produced during the cleavage (see Supporting Information, Figure 3.11)[65]. As shown in the

spectrum, this new peak overlaps with the absorption of the polyfluorene. Therefore, the cleavage was also monitored on the ***o*NB-TEG-alkyne** side-chain (Figure 3.2D) and provided similar observations. This suggests that the cleavage is effective, and 2 h is sufficient to cleave the side-chain.

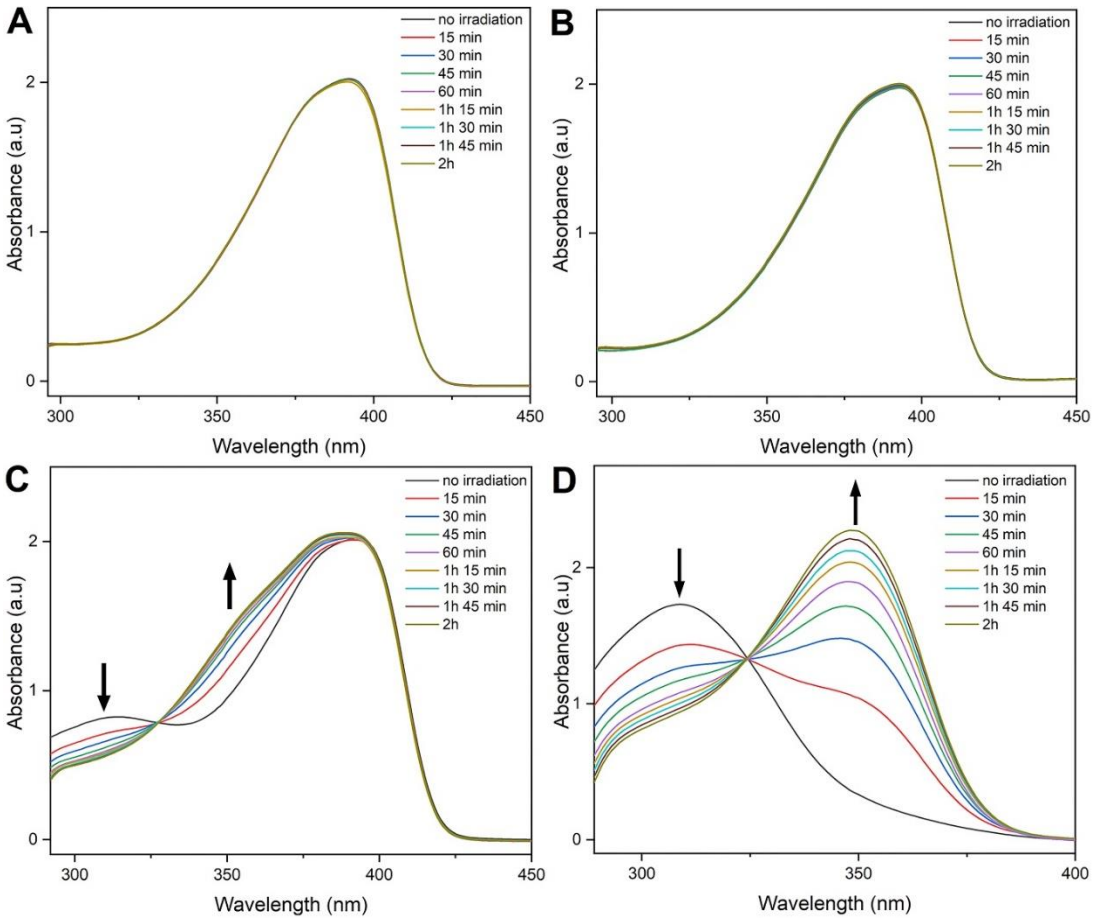


Figure 3.2. UV-Vis absorbance spectra overlays of (**A**) **PF-N$_3$**, (**B**) **PF-TEG**, (**C**) **PF-*o*NB-TEG**, and (**D**) ***o*-NB-TEG-alkyne** side-chain only upon irradiation for 2 h at 365 nm in THF (0.1 mg/mL).

To further characterize the cleavage, we used $^1$H–NMR spectroscopy (Figure 3.3). Polymers were dissolved in $CDCl_3$ and irradiated for 2 h. Despite the appearance of new signals at 11 ppm and in the aromatic region (6.5–8

ppm) corresponding to the aldehyde and the nitrosobenzaldehyde derivative, respectively, the cleavage of the side-chain was incomplete after 2 h. Therefore, the irradiation was resumed for one more hour. Surprisingly, the degradation was still incomplete as observed by the presence of the aromatic signals corresponding to the *o*NB linker (Figure 3.3). The sample was then irradiated overnight and, as shown in Figure 3.3, the complete disappearance of aromatic signals corresponding to the *o*NB linker was observed. The control sample **PF-TEG** was also irradiated overnight, and no changes were observed (see Supporting Information, Figure 3.12). The difference in the irradiation time evaluated by UV-Vis absorption spectroscopy and $^{1}$H NMR spectroscopy can be explained by the significant difference in concentration of the samples between the two techniques (~ 0.1 mg/mL for the UV-Vis absorbance spectroscopy sample compared to ~ 5 mg/mL for the $^{1}$H-NMR spectroscopy sample).

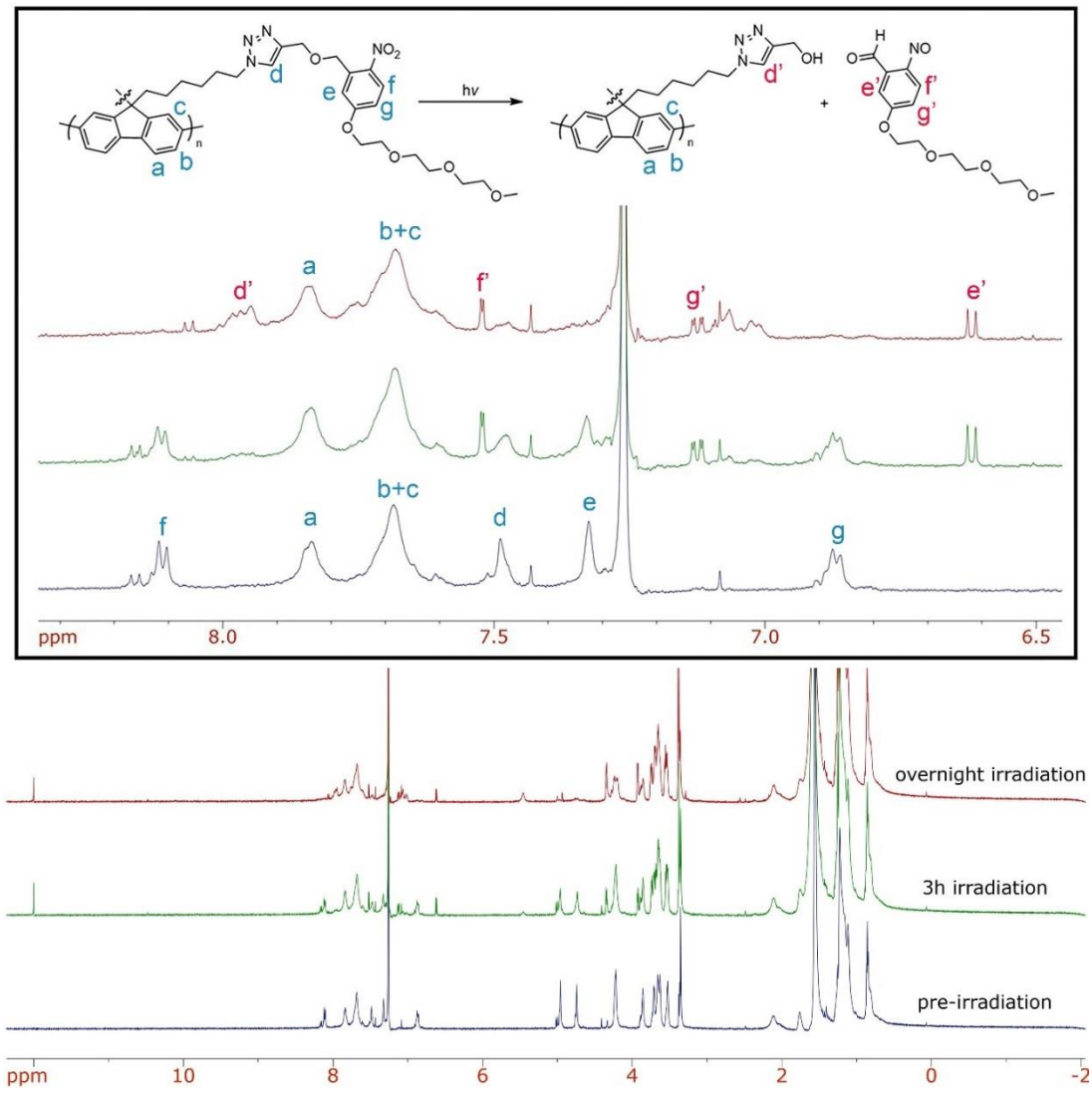


Figure 3.3. $^{1}$H–NMR overlay of **PF-*o*NB-TEG** before irradiation (bottom), after 3 h of irradiation (middle) and after overnight irradiation (top) in $CDCl_3$. The top shows the aromatic region from 6.5 to 9 ppm.

**Polymer-SWNTs Dispersions and Characterization.** Having shown that cleavage of the side-chains is effective on the polymer in solution, we next investigated polymer-SWNTs complexes. Based on our previous work[64], direct dispersion of SWNTs using functionalized polyfluorene led to poorly dispersed samples. Therefore, **PF-$N_3$** was functionalized post-dispersion. **PF-$N_3$** and raw

HiPco SWNTs (average tube diameter 0.8–1.2 nm) complexes were prepared following the procedures in the literature[60], Briefly, a mixture of 7.5 mg of **PF-$N_3$** and 5 mg of SWNTs in 10 mL of THF was sonicated using a probe sonicator for 1 h. The resulting black suspension was centrifuged at 8346× *g* for 30 min, and the supernatant was carefully removed to isolate the **PF-$N_3$-SWNTs** dispersion. The side-chains were then introduced in situ by CuAAC following the procedures in the literature (Scheme 2)[60]. The reactions were monitored by IR spectroscopy via the disappearance of the polymer azide stretch at ~2090 $cm^{-1}$ (Supporting Information, Figure 3.13). Once the complete disappearance of the azide stretch was observed, the sample was filtered through a Teflon membrane with 0.2 µm pore diameter and thoroughly rinsed with THF until the filtrate did not fluoresce when excited with a hand-held UV lamp at 365 nm. The resulting thin films were then redispersed in 10 mL of THF.

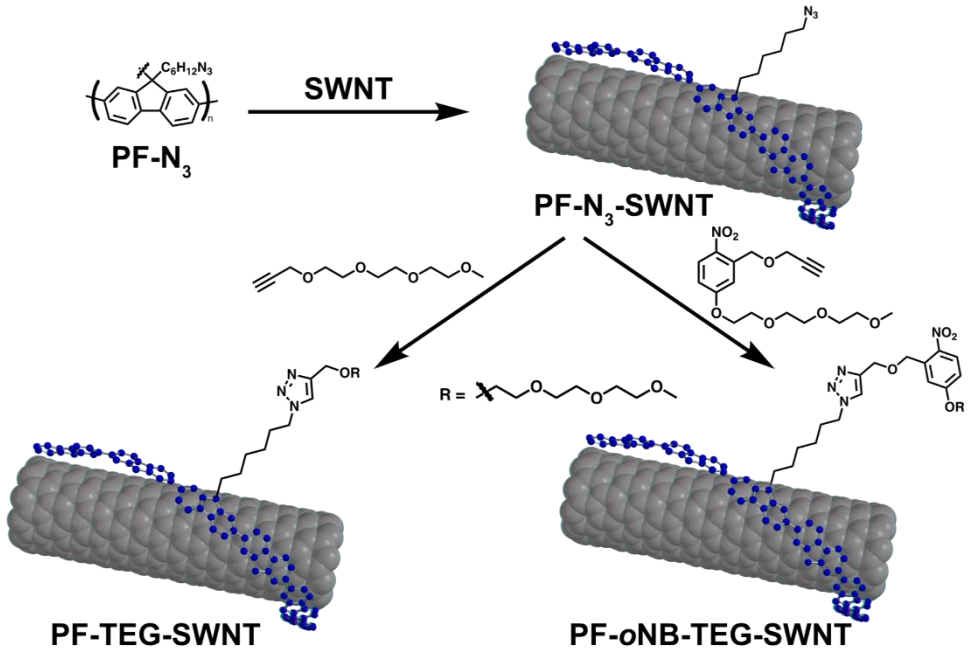


Scheme 3.2. Schematic representation of a CuAAC functionalization of **PF-$N_3$-SWNTs** using **TEG-alkyne** and ***o*NB-TEG-alkyne.**

Characterization using UV−Vis−Near-Infrared (NIR) absorption spectroscopy was next performed (Figure 3.4). Each SWNTs species present within the polymer-SWNT sample exhibits its own absorption signals. Three main regions are observed for HiPco SWNTs: two semiconducting regions, $S_{11}$ (830−1600 nm) and $S_{22}$ (600−800 nm), and one metallic region, $M_{11}$ (440−645 nm)[5]. The absorption spectra were normalized to the maximum absorption of the peak at 1140 nm to compare the different SWNTs' species. **PF-$N_3$**-SWNTs and the post-click dispersions (**PF-TEG-SWNTs** and **PF-*o*NB-TEG-SWNTs**) show similar absorption features, suggesting a successful post-functionalization redispersion. As shown in Figure 3.4, both m- and sc-SWNTs' species are present within the polymer-SWNTs complexes, suggesting a lack of selectivity for specific SWNTs' species under the dispersion conditions used.

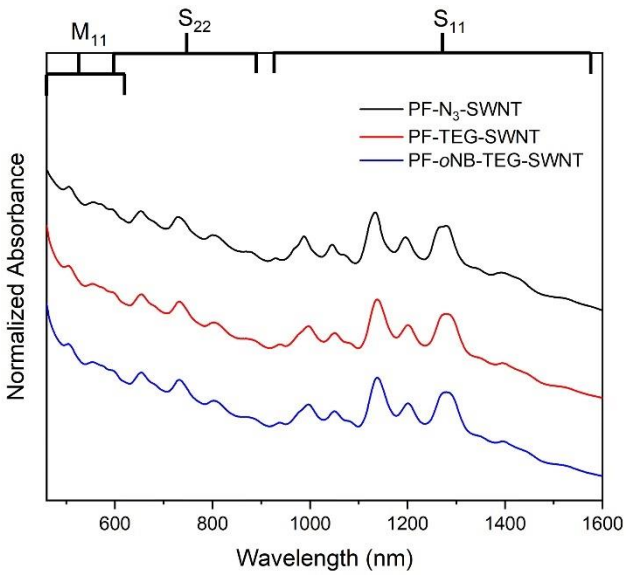


Figure 3.4. UV-Vis-NIR absorption spectra for **PF-SWNTs** (top), **PF-TEG-SWNTs** (middle) and **PF-oNB-TEG-SWNTs** (bottom). Spectra were normalized to the signal at 1140 nm and offset for clarity.

To further characterize our polymer-SWNTs complexes, Raman spectroscopy was performed. In this technique, laser excitation wavelengths overlap with the Van Hove singularities present in the density of states for specific SWNTs species[82]. Therefore, this technique allows the examination of both m- and sc-SWNTs species present in the polymer-SWNTs sample[83]. Since electronic transitions depend on SWNTs' diameter and type, multiple excitation wavelengths are needed to achieve full characterization[83]. The polymer-SWNT samples for Raman spectroscopy were prepared by drop-casting the dispersion onto a silicon wafer, followed by evaporation at RT. A reference sample was prepared by sonicating raw SWNTs in chloroform and depositing it on silicon using the same drop-casting method. For HiPco SWNTs, two excitation wavelengths were used: 633 and 785 nm. Using these

wavelengths, both m- and sc-SWNTs are separately probed[84]. Figure 3.5 shows the radial breathing mode (RBM) for **PF-N$_3$**-SWNT, **PF-TEG**-SWNT, and **PF-oNB-TEG**-SWNT dispersions. The spectra were normalized to the G-band (~1590 cm$^{-1}$) for comparative analysis. Using the 633 nm excitation wavelength, both m- (175−230 cm$^{-1}$) and sc-SWNTs (240−300 cm$^{-1}$) are in resonance and signals corresponding to both nanotube types are observed (Figure 3.5A)[85]. We then used the 785 nm excitation wavelength to characterize our samples. sc-SWNTs are primarily in resonance (175–280 cm$^{-1}$) when using this wavelength. When raw HiPco SWNTs are excited at 785 nm, a peak at 265 cm$^{-1}$ corresponding to bundled (10,2) SWNTs is observed[86]. As shown in the spectra (Figure 3.5B), the intensity of this peak is significantly lower compared to the reference sample of unfunctionalized SWNTs. This indicates that our samples are relatively well dispersed.

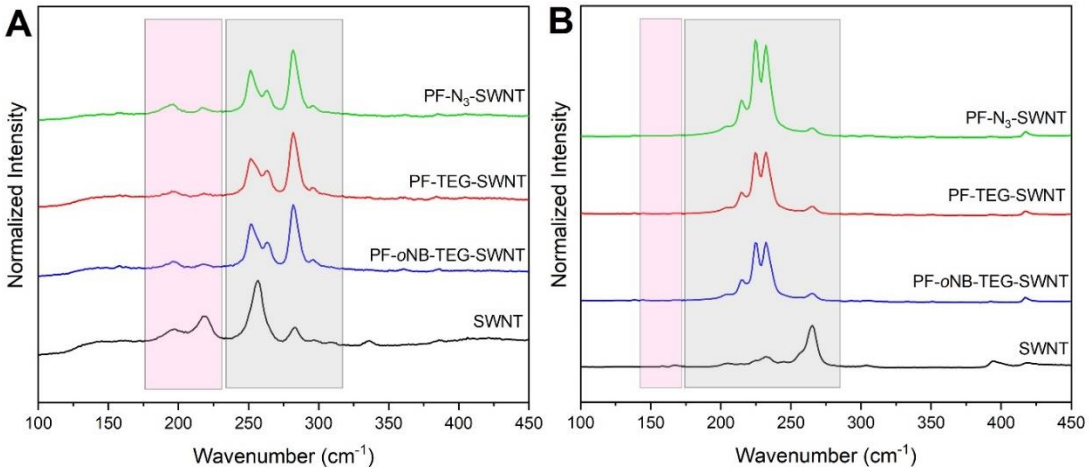


Figure 3.5. Raman Spectra for HiPco polymer-SWNTs samples showing the RBM regions at (**A**) $\lambda_{ex}$ = 633 nm and (**B**) $\lambda_{ex}$ = 785 nm. Gray boxes represent signals arising for sc-SWNTs, whereas pink boxes represent m-SWNTs. All the spectra were normalized to the G-band at ~1590 cm$^{-1}$.

**Photocleavage Study of the PF-SWNTs Complexes. PF-TEG-SWNTs** and **PF-*o*NB-TEG-SWNTs** dispersed in THF were transferred into quartz cuvettes and irradiated at 365 nm. The UV-Vis-NIR data were collected every 15 min for the first 2 h, and the final data were collected after overnight irradiation. As shown in Figure 3.6A, no changes were observed for the control sample. Figure 3.6B shows that the absorbance of the different SWNTs' species in the photocleavable sample decreased upon cleavage of the side-chains. As shown in Figure 3.6B, overnight irradiation caused the dispersion to precipitate, resulting in broad absorption peaks for the nanotubes. This indicates that the loss of side-chains eliminates the steric stabilization of the nanotubes' dispersion.

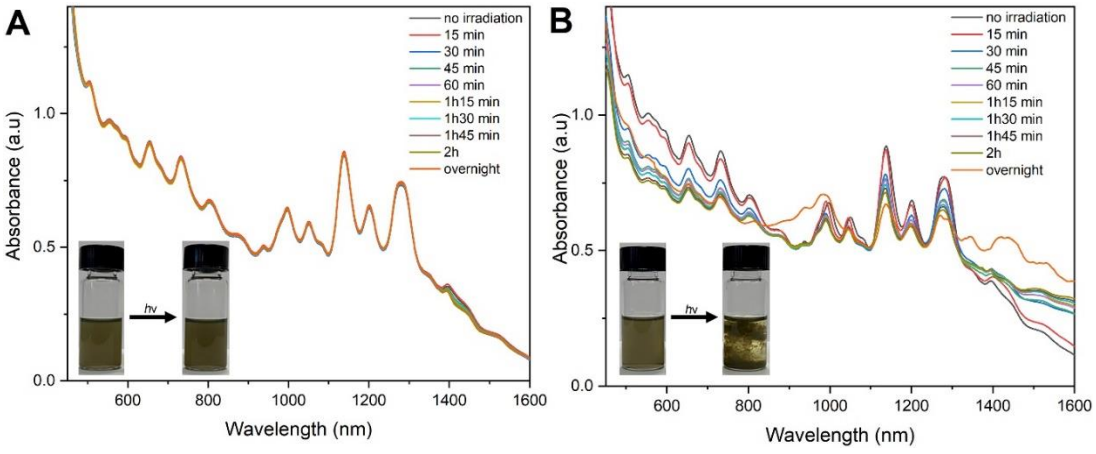


Figure 3.6. UV−Vis−NIR absorption spectra and photographs of (**A**) **PF-TEG-SWNTs** and (**B**) **PF-*o*NB-TEG-SWNTs** upon irradiation at 365 nm.

**Conductivity Measurements.** Using UV-Vis-NIR absorption spectroscopy, we observed that the side-chain cleavage is effective and complete after overnight irradiation. We next performed conductivity measurements. **PF-TEG-**SWNT and **PF-*o*NB-TEG**-SWNT thin films were prepared by filtering the dispersions

through a Teflon membrane with a 0.2 µm pore diameter followed by overnight drying at 75 °C in a vacuum oven. Before irradiation, no conductivity could be detected for either of the samples. The films were then placed into the UV reactor and irradiated at 365 nm overnight. The samples were then washed with hot methanol to eliminate the *o*-nitrosobenzaldehyde derivative produced from the cleavage and placed under vacuum at 75 °C for 1 h (in a vacuum oven). However, no conductivity was detected for either of the samples, probably as a result of the limited light penetration through the black polymer-SWNTs thin films (see Supplementary Materials for details), thus resulting in limited side-chain cleavage in the solid state.

**Characterization of the Polymer-SWNTs Dispersions Post-Irradiation.** To verify that the irradiation did not damage the surface of the nanotubes, Raman spectroscopy with an excitation wavelength of 633 nm was performed. Comparing the intensity of the D-band centred at ~1290 $cm^{-1}$ relative to the G-band at ~1590 $cm^{-1}$ indicates the presence of $sp^3$ carbon defects[87]. As shown in Figure 7, there is no significant difference between pre-and-post-irradiated samples when observing the G and D-band. This suggests that no nanotube defects have been generated during the irradiation process.

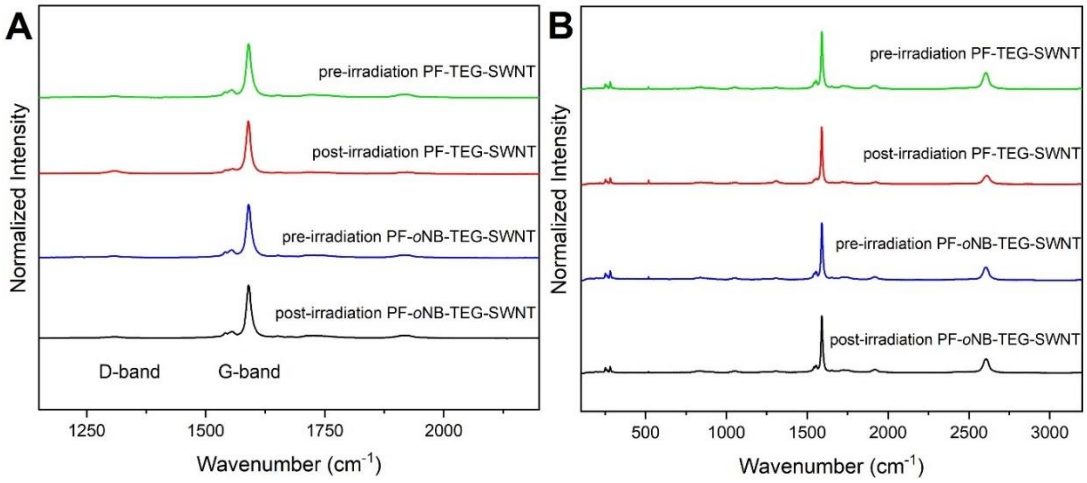


Figure 3.7. Raman Spectra for **PF-TEG-SWNTs** and **PF-*o*NB-TEG-SWNTs** at $\lambda_{ex}$ = 633 nm showing (**A**) the G- and D-band and (**B**) the full spectrum pre- and post-irradiation. All the spectra were normalized to the G-band at ~1590 $cm^{-1}$.

### 3.3 Conclusion

Polyfluorene-SWNT complexes were functionalized with either photocleavable or non-cleavable TEG side-chains. The photocleavage of the side-chains was first studied on the polymer using UV-Vis absorption spectroscopy. As the irradiation time increased, a decrease in the absorbance was observed at 300 nm, while a new peak at 350 nm arose for the cleavable sample. This corresponds to the photoisomerization of the *o*NB linker into the corresponding *o*-nitrosobenzaldehyde. Functionalized polyfluorene-wrapped SWNTs were then prepared, and the photocleavage was studied using UV-Vis-NIR absorption spectroscopy. After overnight irradiation, the cleavage of the side-chains led to the precipitation of the dispersion, resulting in broad absorption peaks. Finally, thin film samples of the polymer-wrapped SWNTs were prepared and irradiated overnight. Unfortunately, due to the limited ability

of the light to penetrate through the thin films, no conductivity could be detected pre-and post-irradiation. However, these results demonstrate the ability to efficiently cleave the side-chains using light without damaging the structure of the nanotubes.

## 3.4 Supporting Information

### 3.4.1 General

Raw HiPco SWNTs were purchased from NanoIntegris (batch #HR30-166 and #HR37-033) and used without further purification. All reagents were purchased from commercial chemical suppliers and used as received. Flash chromatography was performed using an Intelliflash280 by AnaLogix. Unless otherwise noted, compounds were monitored using a variable wavelength detector at 254 nm. Solvent amounts used for gradient or isocratic elution were reported in column volumes (CV). Columns were prepared in Biotage® SNAP KP-Sil cartridges using 40–63 µm silica or 25–40 µm silica purchased from Silicycle. $^{1}$H–NMR and $^{13}$C-NMR spectra were recorded on Bruker Avance 600 MHz and shift-referenced to the residual solvent resonance. Electrospray MS was performed using a Micromass Quattro triple quadrupole instrument in positive mode. Polymer molecular weights and dispersities were analyzed (relative to polystyrene standards) via GPC using a Waters 2695 Separations Module equipped with a Waters 2414 refractive index detector and a Jordi Fluorinated DVB mixed bed column in series with a Jordi Fluorinated DVB 105 Å pore size column. THF with 2% acetonitrile was used as the eluent at a flow rate of 2.0 mL/min. Sonication was performed using a QSonica Q700 Sonicator

equipped with a 13 mm probe at an amplitude of 60 µm and a sonication power of 30 Watts. Centrifugation of the polymer-SWNT samples was performed using a Beckman Coulter Allegra X-22 centrifuge. UV-Vis-NIR absorption spectra were recorded on a Cary 5000 spectrometer in dual beam mode, using matched 10 mm quartz cuvettes. Raman spectra were collected with a Renishaw InVia Laser Raman spectrometer, using two different lasers: a 500 mW HeNe Renishaw laser (633 nm, 1800 L/mm grating); and a 300 mW Renishaw laser (785 nm, 1200 L/mm grating). Photoirradiation of the samples was performed in a home-built UV reactor equipped with one 25W lamp exhibiting emission at 365 nm.

### 3.4.2. Synthesis

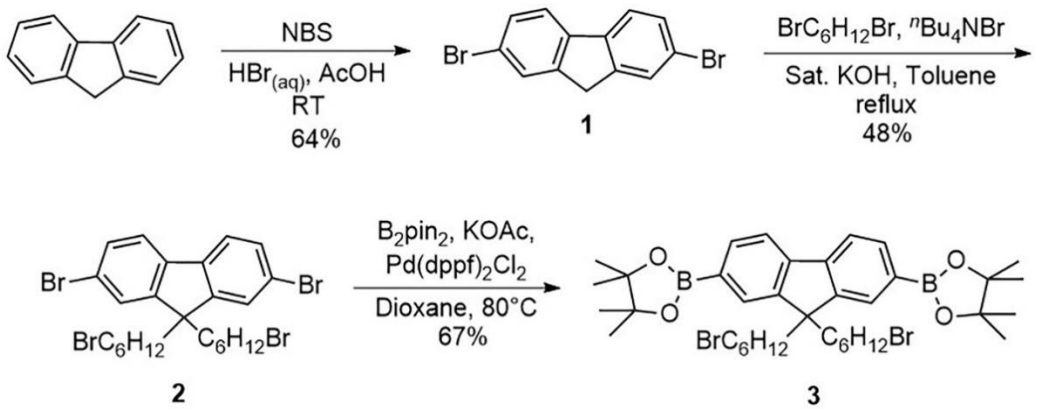


Scheme 3.3. Synthesis of monomers **2** and **3**.

Compounds **1**, **2**, and **3** were prepared according to the procedures in the literature[62].

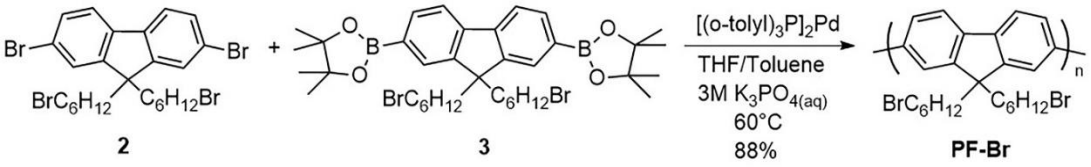


Scheme 3.4. Synthesis of **PF-Br**.

**Poly(bis(6-bromohexyl)fluorene) (PF-Br)**[62]

A Schlenk tube equipped with a stir bar was charged with 2 (0.87 g, 1.34 mmol), 3 (1.00 g, 1.34 mmol), THF (6.7 mL), toluene (6.7 mL), and 3M $K_3PO_{4(aq)}$ (13.4 mL). The reaction mixture was degassed by three freeze–pump–thaw cycles. The biphasic mixture was frozen under liquid nitrogen, then $[(o\text{-tol})_3P]_2Pd$ (14 mg, 20.2 µmol) was added under a positive pressure of nitrogen. The Schlenk tube was evacuated and backfilled three times, and the reaction was vigorously stirred at 60 °C for 2 h 30 min. The phases were allowed to separate, and the organic layer was filtered through a plug of celite and neutral alumina (1:1 composition). The plug was washed with THF, and the filtrate was concentrated *in vacuo*. The crude polymer was precipitated in MeOH (~ 200 mL) and filtered to afford PF-Br as a yellow solid (1.16 g, 88%). $^1$H–NMR (600 MHz; $CDCl_3$): δ 7.86 (m, 2H), 7.73**–**7.67 (m, 4H), 3.31**–**3.28 (m, 4H), 2.15 (m, 4H), 1.71**–**1.69 (m, 4H), 1.28**–**1.25 (m, 4H), 1.18 (m, 4H), 0.88 (m, 4H).

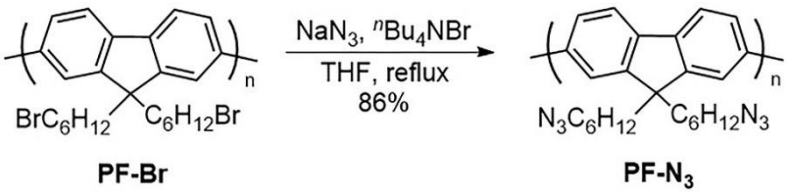


Scheme 3.5. Synthesis of **PF-$N_3$**.

**Poly(bis(6-azidohexyl)fluorene) (PF-$N_3$)**[62]

A round bottom flask equipped with a stir bar was charged with **PF-Br** (1.00 g, 2.03 mmol), $NaN_3$ (1.32 g, 20.3 mmol), $^nBu_4NBr$ (1.32 g, 4.1 mmol), and THF (200 mL). The reaction mixture was heated to reflux for 24 h. The reaction mixture was filtered through a neutral alumina plug, washed with THF, and precipitated in MeOH (~ 200 mL) to afford **PF-$N_3$** (0.73 g, 86%).$^1$H–NMR (600 MHz; $CDCl_3$): δ 7.87**–**7.85 (m, 2H), 7.72**–**7.68 (m, 4H), 3.16**–**3.14 (m, 4H), 2.15 (m, 4H), 1.46, 1.40 (m, 4H), 1.25**–**1.20 (m, 8H), 0.88**–**0.83 (m, 4H).

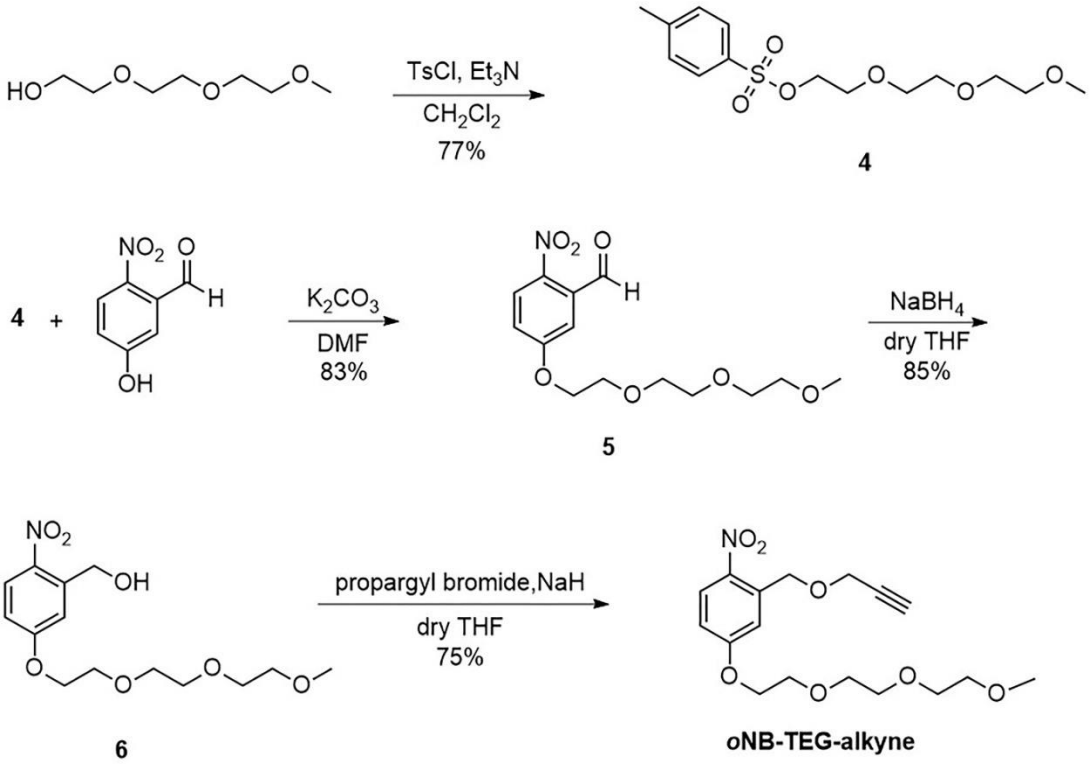


Scheme 3.6. Synthesis of ***o*NB-TEG-alkyne**.[88,89]

**2-(2-(2-methoxyethoxy)ethoxy)ethyl 4-methylbenzenesulfonate (4)**[88]

A 20 mL vial equipped with a stir bar was charged with triethylene glycol monomethyl ether (1 g, 6.09 mmol), Tosyl chloride (1.05 g, 5.53 mmol) in 6 mL of dichloromethane. Triethylamine (1.23 g, 12.2 mmol) was added dropwise. The solution was stirred for 4 h. The reaction was quenched with water (6 mL) and extracted with DCM (3 × 12 mL). The combined organic layers were washed with brine (3 × 12 mL), dried with $MgSO_4$, and concentrated *in vacuo*. The product was purified by flash chromatography Hex/EtOAc (0% to 75%) to give a colourless oil (1.5 g, 77%). $^1$H–NMR (600 MHz, $CDCl_3$): δ 7.82 (d, J = 8.2 Hz, 2H), 7.36 (d, J = 7.9 Hz, 2H), 4.15 (m, 2H), 3.68 (m, 2H), 3.60 (m, 6H), 3.53 (m, 2H), 3.36 (s, 3H), 2.44 (s, 3H).

**5-(2-(2-(2-methoxyethoxy)ethoxy)ethoxy)-2-nitrobenzaldehyde (5)**[89]

A 10 mL vial equipped with a stir bar was charged with 5-Hydroxy-2-nitrobenzaldehyde (0,5 g, 2.9 mmol), compound 4 (0.86 g, 2.7 mmol), and potassium carbonate (0.41 g, 2.9 mmol) in 6 mL of dimethylformamide. The solution was stirred at 50 °C overnight. The solution was quenched with water (6 mL), and the mixture was extracted with EtOAc (3 × 12 mL). The recombined organic layers were washed with water (3 × 12 mL) and brine (3 × 12 mL). The organic layer was dried with $MgSO_4$ and concentrated *in vacuo*. The compound was purified by flash chromatography Hex/EtOAc (0% to 50%) to give a colourless oil (0.78 g, 83%). $^1$H–NMR (600 MHz, $CDCl_3$): δ 10.47 (s, 1H), 8.1 (d, J = 9.04 Hz, 1H), 7.35 (d, J = 2.9 Hz, 1H), 7.19–7.17 (dd, J = 9.05, J= 2.9 Hz, 1H), 4.27 (m, 2H), 3.90 (m, 2H), 3.73 (m, 2H), 3.67 (m, 2H), 3.64 (s, 2H),

3.54 (s, 3H), 3.37 (s, 3H).

**(5-(2-(2-(2-.methoxyethoxy)ethoxy)ethoxy)-2-nitrophenyl) methanol (6)**[89]

A 20 mL vial equipped with a stir bar was charged with compound 5 (0.75 g, 2.24 mmol) in 6 mL of dry THF. Sodium borohydride (0.13 g, 3.35 mmol) was added, and the solution was stirred at 0 °C for 1 h. After completion, the mixture was diluted with EtOAc, filtered through a silica plug using EtOAc as eluent, and concentrated *in vacuo* to give a yellowish solid (0.64 g, 85%). $^{1}$H–NMR (600 MHz, $CDCl_3$): 8.17 (d, J = 9.04 Hz, 1H), 7.30 (d, J = 2.9 Hz, 1H), 6.90 (dd, J = 9.05, J= 2.9 Hz, 1H), 4.98 (s, 2H), 4.47 (m, 2H), 3.89 (m, 2H), 3.73 (m, 2H), 3.67 (m, 2H), 3.64 (m, 2H), 3.54 (m, 2H), 3.37 (s,3H).

**4-(2-(2-(2-methoxyethoxy)ethoxy)ethoxy)-1-nitro-2-((prop-2-yn-1-yloxy)methyl)benzene (oNB-TEG-alkyne)**

A 100 mL round bottom flask equipped with a stir bar was charged with compound 6 (0.6 mg, 1.90 mmol) and sodium hydride (54 mg, 2.28 mmol) in 20 mL of dry THF. The solution was stirred at 0 °C for 1 h, and propargyl bromide (0.34 g, 2.85 mmol) was added dropwise. The mixture was stirred overnight at RT, then quenched with water (10 mL), extracted with dichloromethane (3 × 20 mL), and washed with water (3 × 30 mL) and brine (3 × 30 mL). The organic layer was dried with $MgSO_4$, and concentrated *in vacuo*. The compound was purified by flash chromatography Hex/EtOAc (0% to 90%) to give a brown oil (0.5 g, 75%). $^{1}$H–NMR (600 MHz; $CDCl_3$): δ 8.16 (d, *J* = 9.1 Hz, 1H), 7.30 (d, *J* = 2.8 Hz, 1H), 6.91 (dd, *J* = 9.1, 2.8 Hz, 1H), 4.99 (d, *J* = 6.5 Hz, 2H), 4.27–4.25 (m, 2H), 3.90–3.88 (m, 2H), 3.74–3.63 (m, 6H), 3.55–3.54 (m, 2H), 3.37 (s, 3H),

2.71 (t, *J* = 6.6 Hz, 1H).$^{13}$C–NMR (151 MHz; CDCl3): δ 163.5, 140.49, 140.34, 127.9, 114.6, 113.9, 71.9, 70.89, 70.70, 70.55, 69.6, 68.2, 62.9, 59.0. ESI-MS: m/z calculated for $C_{17}H_{23}NO_7$ [$M^+$]: 353.15 found [M+Na]$^+$: 376.1

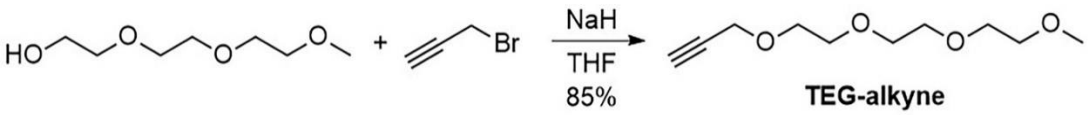


Scheme 3.7. Synthesis of **TEG-alkyne**.[90]

**Triethylene glycol methyl propargyl ether (TEG-alkyne)**[90]

A round bottom flask equipped with a stir bar was charged with triethylene glycol monomethyl ether (1.00 g, 6.09 mmol) in 60 mL of anhydrous THF at 0 °C. NaH (0.28 g, 6.69 mmol) was added to the solution, and the reaction mixture was stirred at 0 °C. After 1 h, propargyl bromide (80% in toluene, 1.43 g, 7.91 mmol) was added dropwise. The reaction mixture was stirred at RT overnight, quenched with water (30 mL) and extracted with DCM (3 × 30 mL). The organic layers were combined, washed with brine (3 × 25 mL), dried with $MgSO_4$ and concentrated in vacuo to afford TEG-alkyne as an orange oil (1.05 g, 85%). $^1$H–NMR (600 MHz; $CDCl_3$): δ 4.20 (d, *J* = 2.4 Hz, 2H), 3.71–3.63 (m, 10H), 3.55–3.54 (m, 2H), 3.37 (s, 3H), 2.42 (t, *J* = 2.4 Hz, 1H).

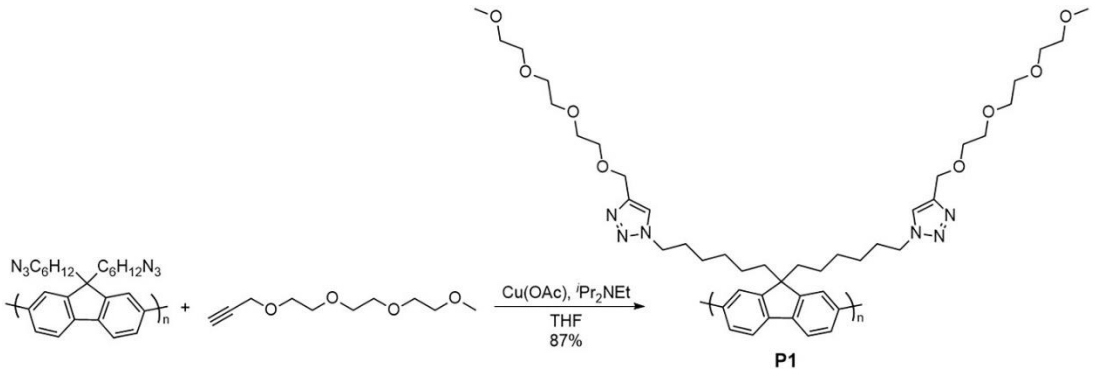


Scheme 3.8. Synthesis of **PF-TEG (P1)**.

**CuAAC procedure for PF-TEG (P1)**

A glass vial was charged with PF-$N_3$ (30 mg, 70 µmol) in 7 mL THF and 2.1 equivalents of TEG-alkyne (30 mg, 150 µmol). To the reaction mixture, 4 mg of Cu(OAc) and 10 equivalents of Hünig's base with respect to Cu(OAc) (40 mg, 0.36 mmol) were added. The reaction mixture was stirred at RT, and reaction progress was monitored by IR spectroscopy for the disappearance of the azide stretch at ~2090 $cm^{-1}$. The solution was filtered through an alumina plug, concentrated in vacuo and redissolved in a minimum of THF. The polymer was precipitated in ~50 mL of cold MeOH to give a yellow solid (51 mg, 87%). $^1$H–NMR (600 MHz; $CDCl_3$): δ 7.90–7.85 (m, 2H), 7.77–7.67 (m, 4H), 7.53–7.48 (m, 2H), 4.69–4.63 (m, 4H), 4.27–4.19 (m, 4H), 3.69–3.64 (m, 18H), 3.58–3.52 (m, 4H), 3.39–3.37 (m, 6H), 2.20–2.09 (m, 4H), 1.79–1.71 (m, 4H), 1.23–1.11 (m, 10H), 0.88–0.77 (m, 4H).

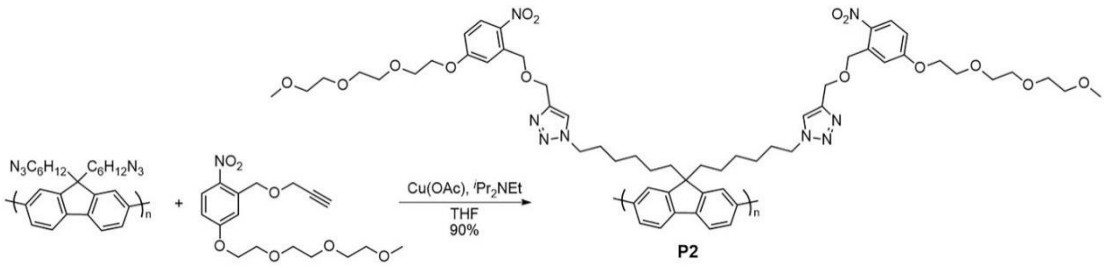


Scheme 3.9. Synthesis of **PF-*o*NB-TEG (P2)**.

**CuAAC procedure for PF-oNB-TEG (P2)**

A glass vial was charged with PF-$N_3$ (30 mg, 70 µmol) in 7 mL THF and 2.1 equivalents of *o*NB-TEG-alkyne (50 mg, 150 µmol). To the reaction mixture, 4 mg of Cu(OAc) and 10 equivalents of Hünig's base with respect to Cu(OAc) (40 mg, 0.36 mmol) were added. The reaction mixture was stirred at RT, and the reaction progress was monitored by IR spectroscopy for the disappearance of the azide stretch at ~2090 $cm^{-1}$. The solution was filtered through an alumina plug, concentrated in vacuo and redissolved in a minimum of THF. The polymer was precipitated in ~50 mL of cold MeOH to give a yellow solid (67 mg, 90%). $^1$H–NMR (600 MHz, $CDCl_3$): δ 8.11 (m, 2H), 7.83 (m, 2H), 7.68 (m, 4H), 7.48 (m, 2H), 7.32 (m, 2H), 4.95 (m, 4H),4.74 (m, 4H), 4.22(m, 6H), 3.92 (m, 4H), 3.73–3.65 (m, 12H), 3.52 (m, 4), 3.36 (m, 6H), 2.12 (m, 4H), 1.76 (m, 4H), 1.22 (m, 8H), 0.84 (m, 8H).

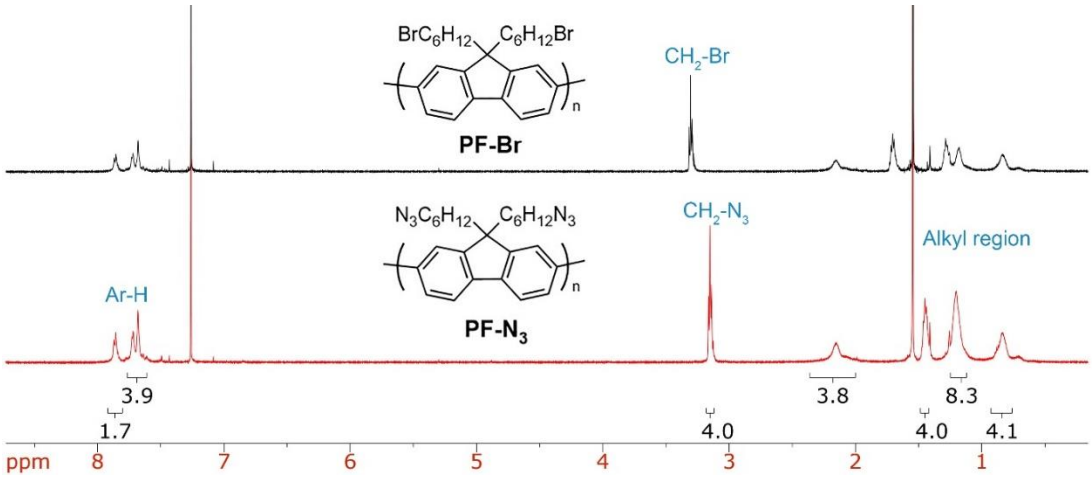


Figure 3.8. $^{1}$H-NMR overlay of **PF-Br** (top) and **PF-N$_3$** (bottom).

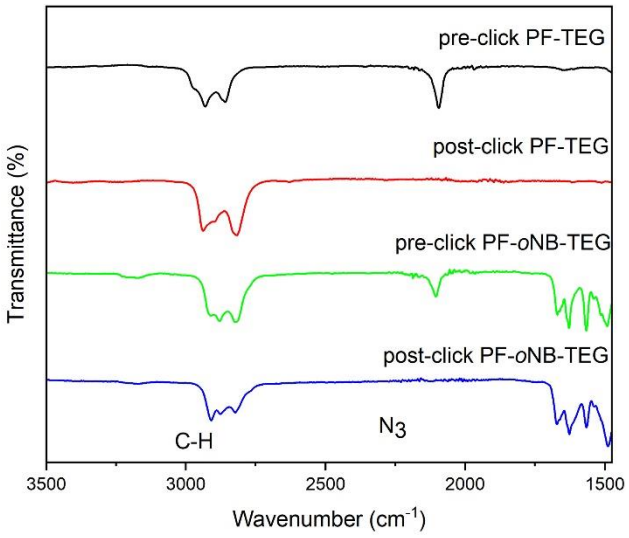


Figure 3.9. FT-IR overlay of the click reaction between **PF-N$_3$**, **TEG-alkyne** and ***o*NB-TEG-alkyne**.

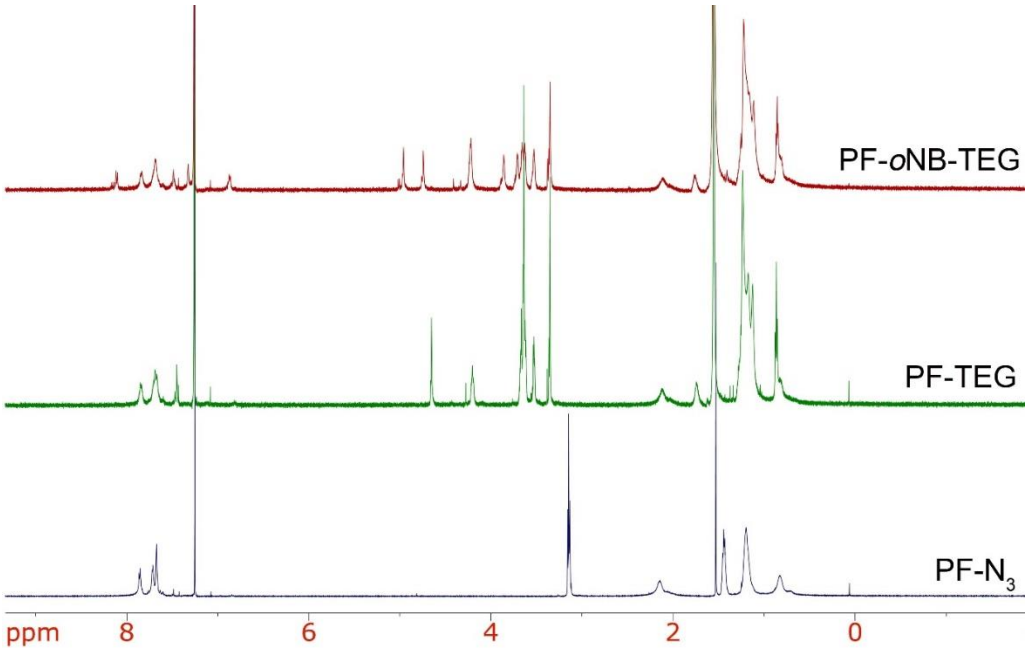


Figure 3.10. $^{1}$H NMR overlay of **PF-N$_3$** (bottom), **PF-TEG** (middle) and **PF-oNB-TEG** (top).

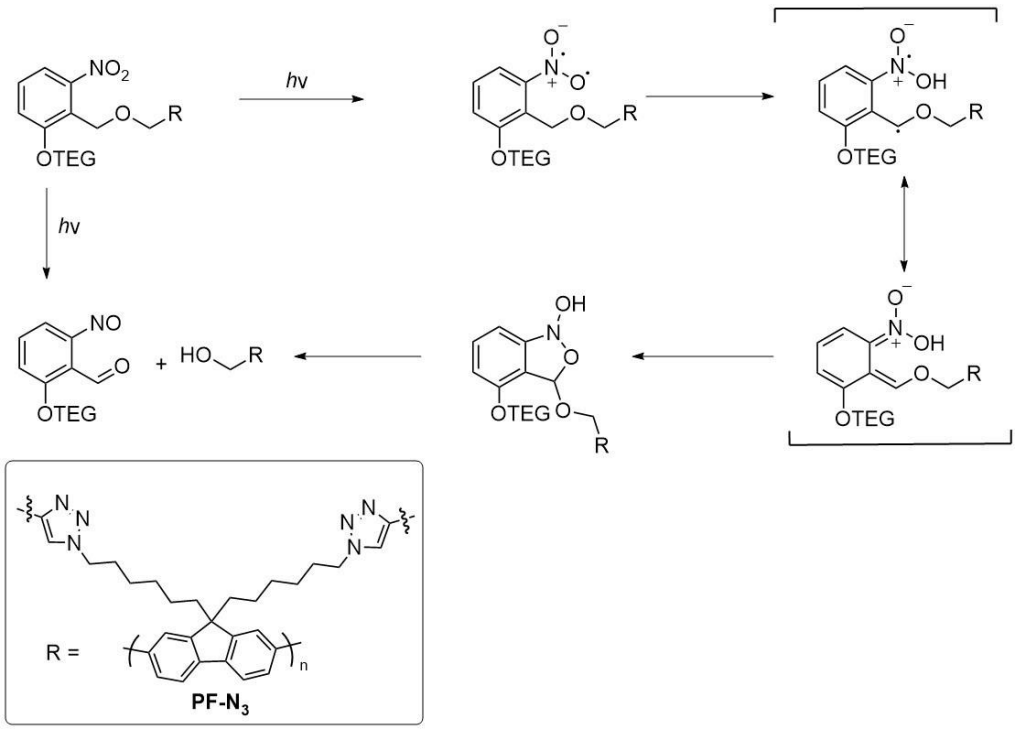


Figure 3.11. Photoisomerization mechanism of **PF**-*o*NB-TEG. Adapted from reference.[65]

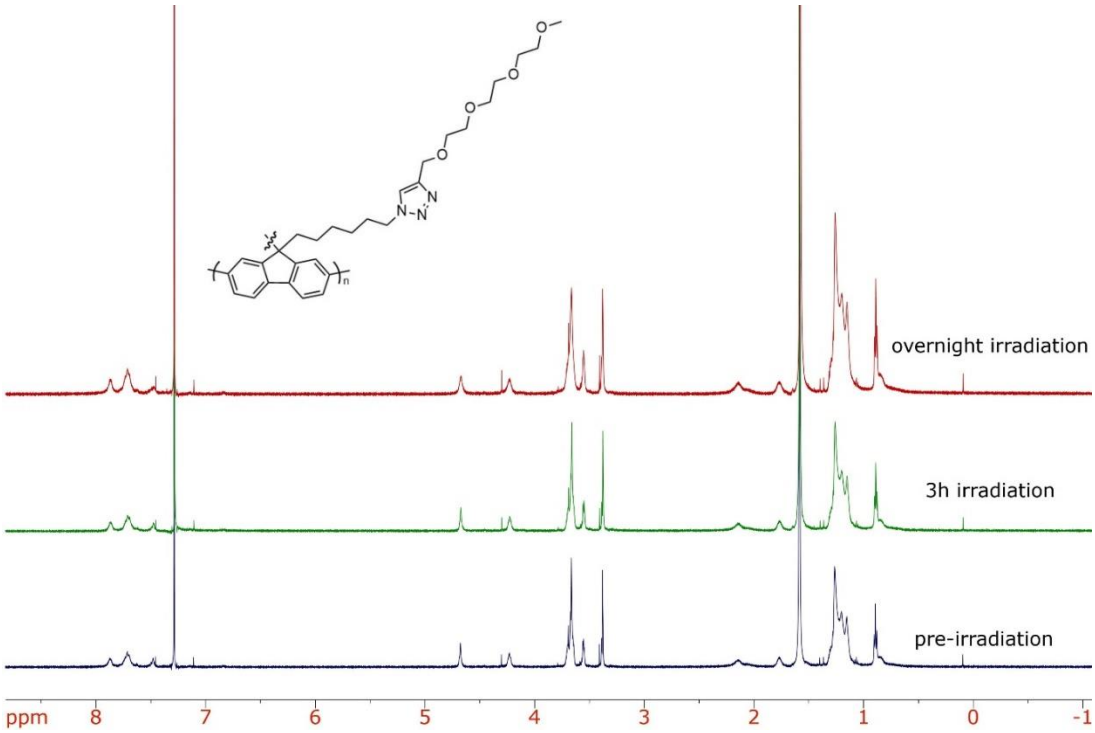


Figure 3.12. $^{1}$H-NMR overlay of **PF-TEG** before irradiation (bottom), after 3 hours of irradiation (middle) and after overnight irradiation (top).

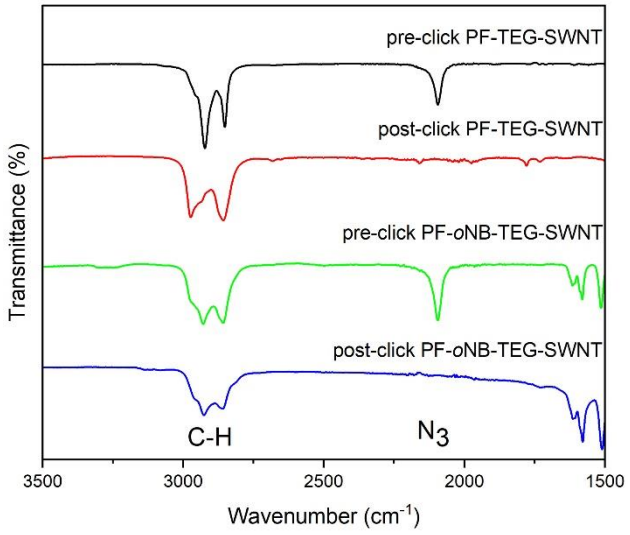


Figure 3.13. FT-IR overlay of the click reaction between the **PF-N$_3$**-SWNT complex, TEG-alkyne and *o*NB-TEG-alkyne.

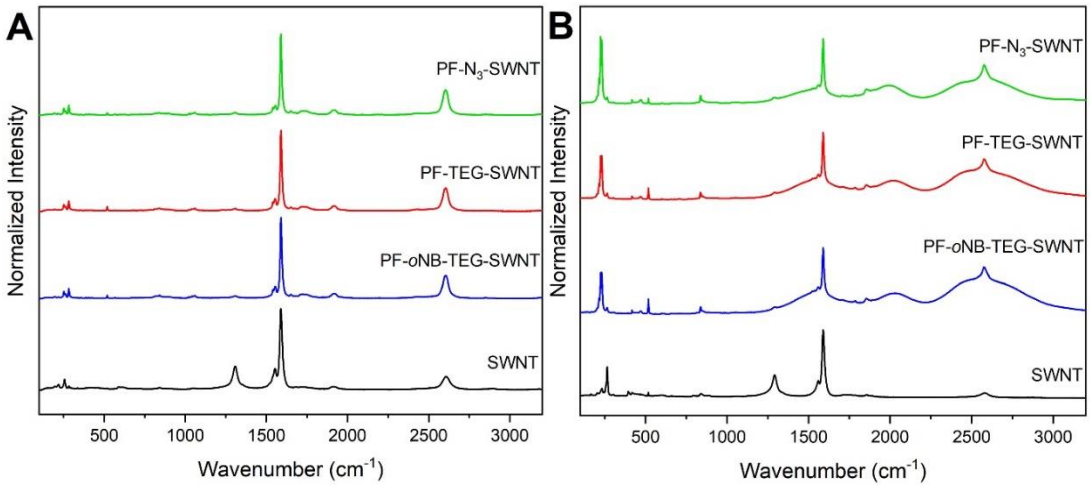


Figure 3.14. Full Raman spectra for HiPco polymer-SWNT samples at A) $\lambda_{ex}$ = 633 nm, B) $\lambda_{ex}$ = 785 nm. All the spectra were normalized at ~ 1590 $cm^{-1}$.

Figure 3.15. Photograph of a **PF**-SWNT thin film.

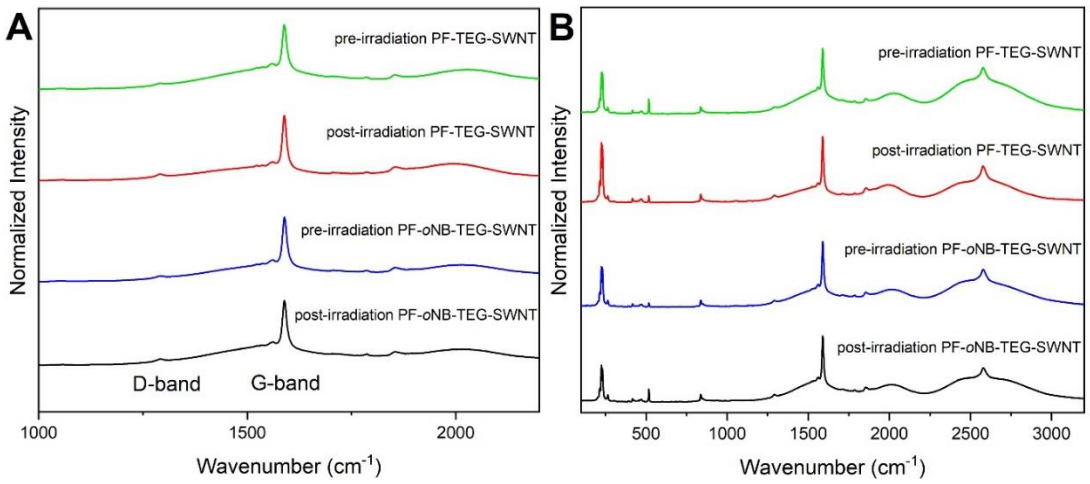


Figure 3.16. Full Raman spectra for **PF-TEG**-SWNT and **PF-*o*NB-TEG**-SWNT pre- and post-irradiation at A) $\lambda_{ex}$ = 785 nm. All the spectra were normalized at ~ 1590 $cm^{-1}$.

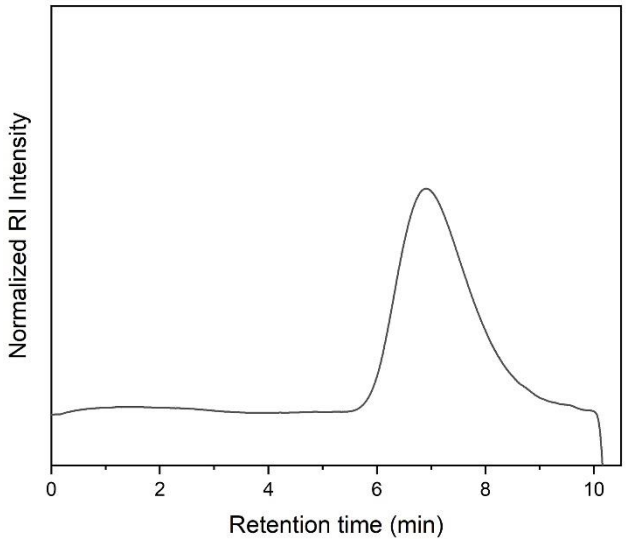


Figure 3.17. GPC trace of **PF-Br**.

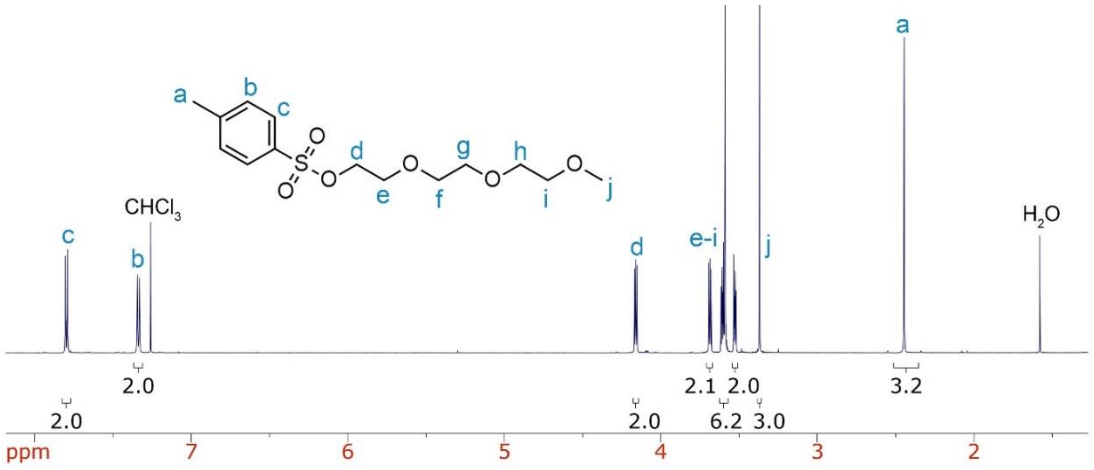


Figure 3.18. $^{1}$H-NMR spectrum of compound **4** in $CDCl_3$.

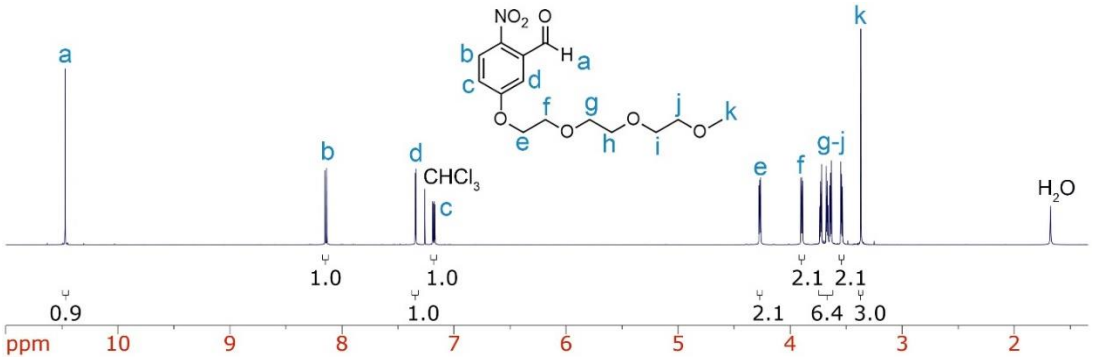


Figure 3.19. $^{1}$H-NMR spectrum of compound **5** in $CDCl_3$.

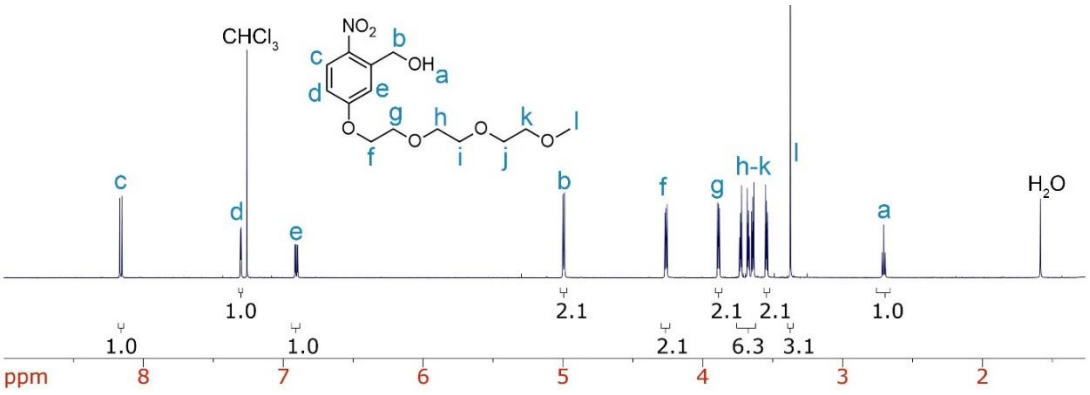


Figure 3.20. $^{1}$H-NMR of compound **6** in $CDCl_3$.

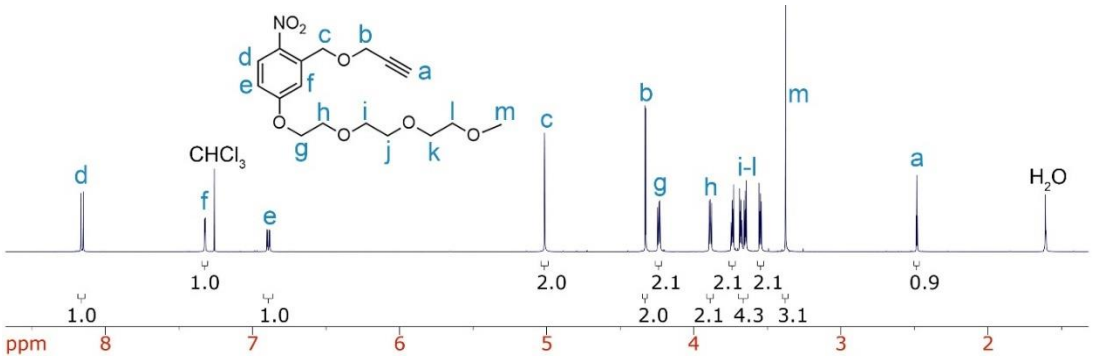


Figure 3.21. $^{1}$H-NMR spectrum of ***o*NB-TEG-alkyne** in $CDCl_3$.

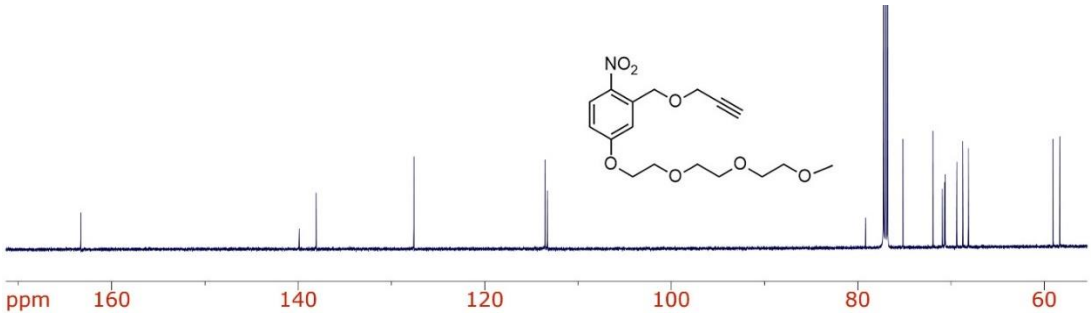


Figure 3.22. $^{13}$C-NMR spectrum of compound ***o*NB-TEG-alkyne** in $CDCl_3$.

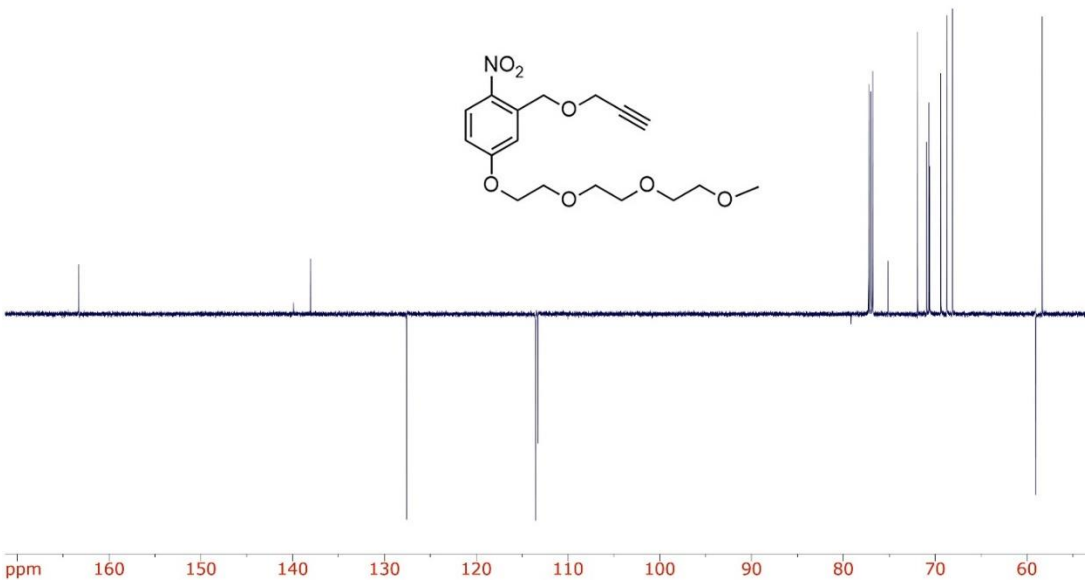


Figure 3.23. Deptq NMR of compound ***o*NB-TEG-alkyne** $CDCl_3$.

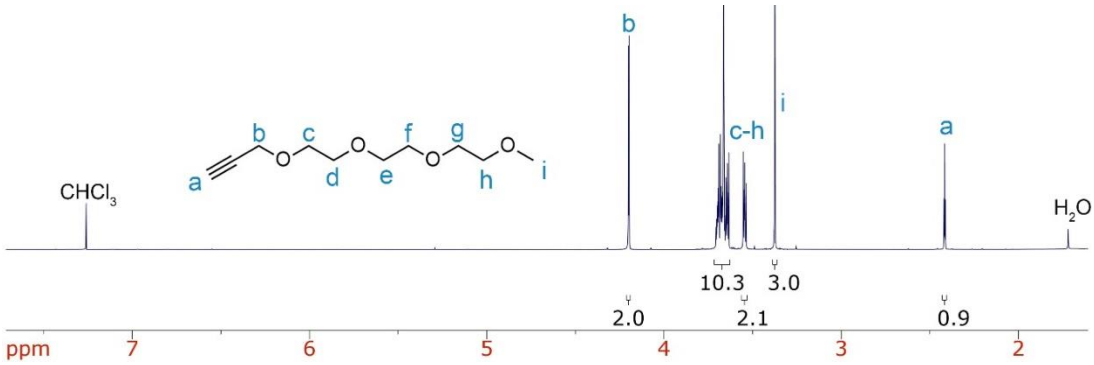


Figure 3.24. $^{1}$H-NMR spectrum of **TEG-alkyne** in $CDCl_3$.

## 3.5 References

[1] S. Iijima, *Nature* **1991**, *354*, 56.

[2] M. Yu, B. S. Files, S. Arepalli, R. S. Ruoff, *Phys. Rev. Lett.* **2000**, *84*, 1–4.

[3] J. N. Coleman, U. Khan, W. J. Blau, Y. K. Gun'ko, *Carbon* **2006**, *44*, 1624–1652.

[4] H. Kataura, Y. Kumazawa, Y. Maniwa, I. Umezu, S. Suzuki, Y. Ohtsuka, Y. Achiba, *Synth. Met.* **1999**, *103*, 2555−2558.

[5] S. M. Bachilo, M. S. Strano, C. Kittrell, R. H. Hauge, R. E. Smalley, R. B. Weisman, *Science* **2002**, *298*, 2361–2366.

[6] P. G. Collins, P. Avouris, *Sci. Am.* **2000**, *283*, 62–69.

[7] P. Avouris, *Acc. Chem. Res.* **2002**, *35*, 1026–1034.

[8] P. Qi, O. Vermesh, M. Grecu, A. Javey, Q. Wang, H. Dai, S. Peng, K. J. Cho, *Nano Lett.* **2003**, *3*, 347–351.

[9] M. Dionisio, J. M. Schnorr, V. K. Michaelis, R. G. Griffin, T. M. Swager, E.

Dalcanale, *J. Am. Chem. Soc.* **2012**, *134*, 6540–6543.

[10] T. Dürkop, S. A. Getty, E. Cobas, M. S. Fuhrer, *Nano Lett.* **2004**, *4*, 35–39.

[11] D. M. Sun, C. Liu, W. C. Ren, H. M. Cheng, *Small* **2013**, *9*, 1188–1205.

[12] M. W. Rowell, M. A. Topinka, M. D. McGehee, H. J. Prall, G. Dennler, N. S. Sariciftci, L. Hu, G. Gruner, *Appl. Phys. Lett.* **2006**, *88*, 6–9.

[13] D. J. Bindl, N. S. Safron, M. S. Arnold, *ACS Nano* **2010**, *4*, 5657–5664.

[14] S. Park, M. Vosguerichian, Z. Bao, *Nanoscale* **2013**, *5*, 1727–1752.

[15] S. Park, M. Vosguerichian, Z. Bao, *Proc. Natl. Acad. Sci.* **2014**, *111*, 4776–4781.

[16] K. Kordás, T. Mustonen, G. Tóth, H. Jantunen, M. Lajunen, C. Soldano, S. Talapatra, S. Kar, R. Vajtai, P. M. Ajayan, *Small* **2006**, *2*, 1021–1025.

[17] K. Y. Chun, Y. Oh, J. Rho, J. H. Ahn, Y. J. Kim, H. R. Choi, S. Baik, *Nat. Nanotechnol.* **2010**, *5*, 853–857.

[18] W. Gomulya, J. Gaoa, M. A. Loib, *Eur. Phys. J. B* **2013**, *86*, 1–13.

[19] D. Jariwala, V. K. Sangwan, L. J. Lauhon, T. J. Marks, M. C. Hersam, *Chem. Soc. Rev.* **2013**, *42*, 2824–2860.

[20] D. Tasis, N. Tagmatarchis, A. Bianco, M. Prato, *Chem. Rev.* **2006**, *106*, 1105–1136.

[21] P. Nikolaev, M. J. Bronikowski, R. K. Bradley, F. Rohmund, D. T. Colbert, K. A. Smith, R. E. Smalley, *Chem. Phys. Lett.* **1999**, *313*, 91–97.

[22] K. S. Kim, G. Cota-Sanchez, C. T. Kingston, M. Imris, B. Simard, G. Soucy, *J. Phys. D. Appl. Phys.* **2007**, *40*, 2375–2387.

[23] M. M. A. Rafique, J. Iqbal, *J. Encapsulation Adsorpt. Sci.* **2011**, *1*, 29–34.

[24] S. Campidelli, C. Klumpp, A. Bianco, D. M. Guldi, M. Prato, *J. Phys. Org. Chem.* **2006**, *19*, 531–539.

[25] A. Hirsch, *Angew. Chem., Int. Ed.* **2002**, *41*, 1853–1859.

[26] Y.-L. Zhao, J. F. Stoddart, *Chem. Nanocarbons* **2010**, *42*, 1162–1171.

[27] A. Star, Y. Liu, K. Grant, L. Ridvan, J. F. Stoddart, D. W. Steuerman, M. R. Diehl, A. Boukai, J. R. Heath, *Macromolecules* **2003**, *36*, 553–560.

[28] D. W. Steuerman, A. Star, R. Narizzano, H. Choi, R. S. Ries, C. Nicolini, J. F. Stoddart, J. R. Heath, *J. Phys. Chem. B* **2002**, *106*, 3124–3130.

[29] Y. Tomonari, H. Murakami, N. Nakashima, *Chem. Eur. J.* **2006**, *12*, 4027–4034.

[30] K. Yang, L. Zhu, B. Xing, *Environ. Sci. Technol.* **2006**, *40*, 1855–1861.

[31] R. J. Chen, Y. Zhang, D. Wang, H. Dai, *J. Am. Chem. Soc.* **2001**, *123*, 3838–3839.

[32] V. C. Moore, M. S. Strano, E. H. Haroz, R. H. Hauge, R. E. Smalley, J. Schmidt, Y. Talmon, *Nano Lett.* **2003**, *3*, 1379–1382.

[33] M. F. Islam, E. Rojas, D. M. Bergey, A. T. Johnson, A. G. Yodh, *Nano Lett.* **2003**, *3*, 269–273.

[34] M. J. O'Connell, S. M. Bachilo, C. B. Huffman, V. C. Moore, M. S. Strano,

E. H. Haroz, K. L. Rialon, P. J. Boul, W. H. Noon, C. Kittrell, et al., *Science* **2002**, *297*, 593–596.

[35] Z. Guo, P. J. Sadler, S. C. Tsang, *Adv. Mater.* **1998**, *10*, 701–703.

[36] K. Bradley, M. Briman, A. Star, G. Gruner, *Nano Lett.* **2004**, *4*, 253–256.

[37] M. Zheng, A. Jagota, E. D. Semke, B. A. Diner, R. S. McLean, S. R. Lustig, R. E. Richardson, N. G. Tassi, *Nat. Mater.* **2003**, *2*, 338–42.

[38] J. Chen, H. Liu, W. A. Weimer, M. D. Halls, D. H. Waldeck, G. C. Walker, *J. Am. Chem. Soc.* **2002**, *124*, 9034–9035.

[39] J. Y. Hwang, A. Nish, J. Doig, S. Douven, C. W. Chen, L. C. Chen, R. J. Nicholas, *J. Am. Chem. Soc.* **2008**, *130*, 3543–3553.

[40] F. Chen, B. Wang, Y. Chen, L. J. Li, *Nano Lett.* **2007**, *7*, 3013–3017.

[41] A. Star, J. F. Stoddart, D. Steuerman, M. Diehl, A. Boukai, E. W. Wong, X. Yang, S. Chung, H. Choi, J. R. Heath, *Angew. Chem.* **2001**, *113*, 1771–1775.

[42] D. Fong, A. Adronov, *Chem. Sci.* **2017**, *8*, 7292–7305.

[43] S. K. Samanta, M. Fritsch, U. Scherf, W. Gomulya, S. Z. Bisri, M. A. Loi, *Acc. Chem. Res.* **2014**, *47*, 2446–2456.

[44] P. Imin, F. Cheng, A. Adronov, *Polym. Chem.* **2011**, *2*, 1404–1408.

[45] D. Fong, W. J. Bodnaryk, N. A. Rice, S. Saem, J. M. Moran-Mirabal, A. Adronov, *Chem. Eur. J.* **2016**, *22*, 14560–14566.

[46] J. Ding, Z. Li, J. Lefebvre, F. Cheng, G. Dubey, S. Zou, P. Finnie, A.

Hrdina, L. Scoles, G. P. Lopinski, et al., *Nanoscale* **2014**, *6*, 2328–2339.

[47] F. A. Lemasson, T. Strunk, P. Gerstel, F. Hennrich, S. Lebedkin, C. Barner-Kowollik, W. Wenzel, M. M. Kappes, M. Mayor, *J. Am. Chem. Soc.* **2011**, *133*, 652–655.

[48] P. Gerstel, S. Klumpp, F. Hennrich, A. Poschlad, V. Meded, E. Blasco, W. Wenzel, M. M. Kappes, C. Barner-kowollik, *ACS Macro Lett.* **2014**, *3*, 2–7.

[49] N. A. Rice, A. V Subrahmanyam, S. E. Laengert, A. Adronov, *Polym. Chem.* **2015**, *53*, 2510–2516.

[50] W. J. Bodnaryk, D. Fong, A. Adronov, *ACS Omega* **2018**, *3*, 16238–16245.

[51] T. Lei, I. Pochorovski, Z. Bao, *Acc. Chem. Res.* **2017**, *50*, 1096–1104.

[52] T. Lei, X. Chen, G. Pitner, H. S. P. Wong, Z. Bao, *J. Am. Chem. Soc.* **2016**, *138*, 802–805.

[53] I. Pochorovski, H. Wang, J. I. Feldblyum, X. Zhang, A. L. Antaris, Z. Bao, *J. Am. Chem. Soc.* **2015**, *137*, 4328–4331.

[54] F. Toshimitsu, N. Nakashima, *Nat. Commun.* **2014**, *5*, 1–9.

[55] S. Liang, Y. Zhao, A. Adronov, *J. Am. Chem. Soc.* **2014**, *136*, 970–977.

[56] S. Liang, G. Chen, J. Peddle, Y. Zhao, *Chem. Commun.* **2012**, *48*, 3100–3102.

[57] L. Xu, M. Valášek, F. Hennrich, R. Fischer, M. M. Kappes, M. Mayor,

*Macromolecules* **2021**, *54*, 4363–4374.

[58] W. J. Bodnaryk, K. Li, A. Adronov, *J. Polym. Sci.* **2020**, *58*, 1965–1972.

[59] F. Lemasson, J. Tittmann, F. Hennrich, N. Stürzl, S. Malik, M. M. Kappes, M. Mayor, *Chem. Commun.* **2011**, *47*, 7428–7430.

[60] D. Fong, G. M. Andrews, A. Adronov, *Polym. Chem.* **2018**, *9*, 2873–2879.

[61] D. Fong, G. M. Andrews, S. A. McNelles, A. Adronov, *Polym. Chem.* **2018**, *9*, 4460–4467.

[62] D. Fong, J. Yeung, E. Meichsner, A. Adronov, *ACS Appl. Polym. Mater.* **2019**, *1*, 797–803.

[63] P. He, S. Shimano, K. Salikolimi, T. Isoshima, Y. Kakefuda, T. Mori, Y. Taguchi, Y. Ito, M. Kawamoto, *ACS Appl. Mater. Interfaces* **2018**, *11*, 4211–4218.

[64] D. Ritaine, A. Adronov, *J. Polym. Sci.* **2022**, *60*, 1–13.

[65] H. Zhao, E. S. Sterner, E. B. Coughlin, P. Theato, *Macromolecules* **2012**, *45*, 1723–1736.

[66] A. Romano, I. Roppolo, E. Rossegger, S. Schlögl, M. Sangermano, **2020**, *13*, 12–14.

[67] L. Peles-Strahl, R. Sasson, G. Slor, N. Edelstein-Pardo, A. Dahan, R. J. Amir, *Macromolecules* **2019**, *52*, 3268–3277.

[68] J. Sun, D. Jung, T. Schoppa, J. Anderski, M. Picker, Y. Ren, D. Mulac, N. Stein, K. Langer, D. Kuckling, *ACS Appl. Bio Mater.* **2019**, *2*, 3038–3051.

[69] B. Schmatz, Z. Yuan, A. W. Lang, J. L. Hernandez, E. Reichmanis, J. R. Reynolds, *ACS Cent. Sci.* **2017**, *3*, 961–967.

[70] Z. C. Smith, D. M. Meyer, M. G. Simon, C. Staii, D. Shukla, S. W. Thomas, *Macromolecules* **2015**, *48*, 959–966.

[71] S. W. Thomas, R. H. Pawle, Z. C. Smith, *J. Photochem. Photobiol. A Chem.* **2016**, *322–323*, 119–128.

[72] W. Zhu, L. Zhang, Y. Chen, K. Zhang, *Macromol. Rapid Commun.* **2017**, *38*, 1–6.

[73] R. Rodebaugh, B. Fraser-Reid, H. M. Geysen, *Tetrahedron Lett.* **1997**, *38*, 7653–7656.

[74] E. B. Åkerblom, *Mol. Divers.* **1998**, *4*, 53–69.

[75] Y. Kikuchi, J. Nakanishi, H. Nakayama, T. Shimizu, Y. Yoshino, K. Yamaguchi, Y. Yoshida, Y. Horiike, *Chem. Lett.* **2008**, *37*, 10–11.

[76] F. Huang, H. Xu, W. Tan, H. Liang, *ACS Nano* **2014**, *8*, 6849–6855.

[77] A. F. Hirschbiel, S. Geyer, B. Yameen, A. Welle, P. Nikolov, S. Giselbrecht, S. Scholpp, G. Delaittre, C. Barner-Kowollik, *Adv. Mater.* **2015**, *27*, 2621–2626.

[78] Y. Wu, L. Zhang, M. Zhang, Z. Liu, W. Zhu, K. Zhang, *Polym. Chem.* **2018**, *9*, 1799–1806.

[79] J. Anderski, L. Mahlert, J. Sun, W. Birnbaum, D. Mulac, S. Schreiber, F. Herrmann, D. Kuckling, K. Langer, *Int. J. Pharm.* **2019**, *557*, 182–191.

[80] J. Sun, W. Birnbaum, J. Anderski, M. T. Picker, D. Mulac, K. Langer, D. Kuckling, *Biomacromolecules* **2018**, *19*, 4677–4690.

[81] J. Lai, Y. Xu, X. Mu, X. Wu, C. Li, J. Zheng, C. Wu, J. Chen, Y. Zhao, *Chem. Commun.* **2011**, *47*, 3822–3824.

[82] M. S. Dresselhaus, G. Dresselhaus, R. Saito, A. Jorio, *Phys. Rep.* **2005**, *409*, 47–99.

[83] S. K. Doorn, *J. Nanosci. Nanotechnol.* **2005**, *5*, 1023–1034.

[84] S. K. Doorn, D. A. Heller, P. W. Barone, M. L. Usrey, M. S. Strano, *Appl. Phys. A,* **2004**, *78*, 1147–1155.

[85] M. S. Strano, C. A. Dyke, M. L. Usrey, P. W. Barone, M. J. Allen, H. Shan, C. Kittrell, R. H. Hauge, J. M. Tour, R. E. Smalley, *Science* **2003**, *301*, 1519–1522.

[86] D. A. Heller, P. W. Barone, J. P. Swanson, R. M. Mayrhofer, M. S. Strano, *J. Phys. Chem. B* **2004**, *108*, 6905–6909.

[87] S. D. M. Brown, A. Jorio, M. S. Dresselhaus, G. Dresselhaus, *Phys. Rev. B* **2001**, *64*, 3–6.

[88] E. W. C. Chan, P. Baek, S. M. Tan, S. J. Davidson, D. Barker, J. Travas-Sejdic, *Macromol. Rapid Commun.* **2019**, *40*, 1–6.

[89] Y. Suzuki, T. Sakamoto, M. Yoshio, T. Kato, *Eur. Polym. J.* **2020**, *134*, 109859.

[90] P. Chandra, A. M. Jonas, A. E. Fernandes, *J. Am. Chem. Soc.* **2018**, *140*, 5179–5184.

# Chapter 4

# Synthesis of a functionalized and photodegradable fluorene-based polymer for aqueous SWNT dispersion

This chapter has been submitted (August 2023) to *Polymer Chemistry.*

**Abstract**

Due to their tunability, conjugated polymers have received significant interest in the dispersion of single-walled carbon nanotubes. Indeed, interactions with conjugated polymers enable solubility, extraction, and purification of carbon nanotubes at the same time. However, due to the strong π-interactions between the carbon nanotubes and the polymer backbone, the polymer remains at the surface and can decrease the performance of a SWNT-based device. Therefore, the removal of the polymer backbone post-processing seems to be a promising alternative. Here, we report the synthesis of a functionalized and photodegradable fluorene-based polymer. The polymer contains an ortho-nitrobenzylether linker that can be cleaved by irradiation using UV light. The irradiation was first investigated on the monomer and polymer by UV-Vis and $^{1}$H-NMR spectroscopy and showed efficient degradation over time. Irradiation of the polymer-SWNT complex has also been investigated. Precipitation of the nanotubes upon irradiation was observed and confirmed the effective degradation of the polymer into smaller fragments. Characterization post-irradiation of the SWNT residues using thermogravimetric analysis was performed to quantify the proportion of polymer removed from the surface of the nanotubes.

In addition, the synthesized fluorene-based polymer has azide groups at the end of the side-chains. We therefore functionalized the polymer with hydrophilic side-chains to disperse and release SWNTs in water. The photodegradation of the polymer was observed via UV-Vis spectroscopy and

the polymer was efficient at dispersing SWNTs in the aqueous solvent. However, the irradiation of the polymer-SWNT complex did not result in the precipitation of the nanotubes. As a result, the characterization of the SWNT residues could not be performed.

### 4.1 Introduction

With their extraordinary mechanical,[1,2] optical,[3,4] and electronic properties,[5,6] single-walled carbon nanotubes (SWNTs) have received significant interest from researchers. SWNTs have been incorporated into many applications such as sensors,[7,8] thin-film transistors,[9–11] organic photovoltaics,[12,13] flexible electronics,[14–16] conductive inks,[17,18] and multiple other devices.[19–21] However, this task is limited by the impurity of SWNTs due to a complex mixture of amorphous carbon, leftover catalyst particles, as well as a heterogeneous mixture of semiconducting and metallic species (sc- and m-SWNTs, respectively) present in all SWNT samples produced using commercial methods.[22–24] Moreover, due to their strong inter-tube π–π interactions, SWNTs aggregate into bundles that are insoluble in common organic solvents.[25] As a result, functionalization techniques that can broadly be classified as either covalent or non-covalent strategies have been developed to improve the solubility and purity of SWNTs. Covalent functionalization involves strongly oxidizing conditions to introduce functional groups at the surface of the nanotubes. This disrupts the π-system and therefore impacts the SWNT properties.[26,27] In contrast, non-covalent functionalization involves the formation of a supramolecular complex between a dispersant and SWNTs. This

imparts solubility in organic solvents and prevents the reaggregation of SWNTs into bundles.[28–30] Numerous dispersants such as small aromatic compounds,[31–33] surfactants,[34–36] biomolecules,[36–38] and conjugated polymers[39–41] have been used. Among these dispersants, conjugated polymers have received significant attention due to their facile structural tuning, such as the molecular weight, polymer backbone structure, and side-chain structure, to achieve different properties.[42–47] This has allowed conjugated polymer structures to achieve selective dispersion of either sc- or m-SWNTs.[40,46,48–50] Recently, attention has been given to polymers that can be removed from the nanotube surface. To this end, different strategies have been employed to release SWNTs. Polymers that can change their conformation[51,52] or non-covalent polymers[53,54] have shown effective release of SWNTs upon the stimulus of an acid. Cleavable backbone polymers such as tetrazine-based[55], silane-based[56] or imine-based[57,58] polymers have also been studied. Although these processes are effective at releasing SWNTs, they either require harsh conditions such as high temperature[55] or the addition of additives like an acid.[52,53,57] These conditions can be incompatible with some substrates or can alter device performance. An alternative is the use of polymers that can be degraded using milder conditions. To this end, photocleavable polymers are promising. Mayer et al. designed a fluorene-based polymer containing an ortho-nitrobenzyl ether unit.[59] The release of SWNTs was observed due to the precipitation of the nanotubes upon irradiation. Recently, our group has also developed a new photodegradable poly(carbazole-co-terephthalate) (PCPT).[60] Thermogravimetric analysis was used to determine the amount of polymer left

on the nanotube surface after irradiation and indicated that a large proportion of the polymer is removed.

All of these studies have shown that it is possible to remove the polymer from the nanotube backbone. However, this concept has only been achieved in organic solvents such as toluene, THF or benzonitrile. Here, we report the study of a functionalized and photodegradable fluorene-based polymer to release SWNTs in water. The polymer contains an ortho-benzyl ether unit that can be cleaved by irradiation. It also has azide groups at the end of the side-chain that is functionalized post-polymerization with hydrophilic side-chains via strain-promoted azide-alkyne cycloaddition (SPACC). We first studied the non-functionalized polymer in THF. The photodegradation was monitored with the monomer, polymer and polymer-SWNT complex. Characterization post-irradiation of the polymer-SWNT complex allowed the quantification of the polymer removed from the surface of the nanotubes. On the other hand, we functionalized the polymer with poly(ethylene glycol) side-chains and investigated the release of SWNTs in water.

### 4.2 Results and Discussion

**Polymer synthesis.** To begin our investigation, we first prepared our fluorene-based polymer (**PF-*o*NB**). Monomer **3** was prepared according to literature procedures (Supporting Information, Scheme 4.2).[61] Briefly, commercial fluorene was brominated using N-bromosuccinimide to obtain compound **1** followed by phase-transfer alkylation with 1,6-dibromohexane under basic conditions to produce compound **2**. Compound 2 was then borylated using

Miyaura conditions to obtain diboronate **3**. Monomer **5** was also prepared following literature procedures.[59] Briefly, 4-bromo-2-nitrobenzaldehyde was first reduced using sodium borohydride to obtain the corresponding alcohol **4** followed by a Mitsonobu reaction with compound **4** and 4-bromophenol to produce monomer **5**. Monomers **3** and **5** were copolymerized using Suzuki polycondensation to obtain copolymer **6** (Scheme 4.1). Gel permeation chromatography (GPC) revealed an $M_n$ of 8 kDa and a dispersity (Đ) of 1.7. **PF-*o*NB** was then obtained via a reaction between copolymer **6** and $NaN_3$ in the presence of $^{n}Bu_4NBr$. The polymers were characterized by $^1$H-NMR spectroscopy to confirm the presence of the alkyl azides (3.11 pm) and the disappearance of the signal corresponding to the alkyl bromides (3.26 ppm) (Supporting information, Figure 4.8).

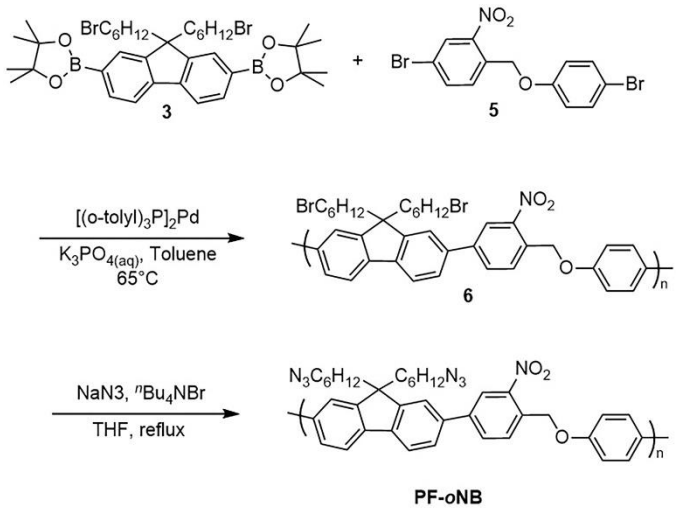


Scheme 4.1. Synthesis of copolymer **6** and **PF-oNB**.

**Photodegradation of the monomer and polymer**. The photodegradation was first studied on monomer **5** and characterized via $^1$H-NMR spectroscopy. Monomer **5** was dissolved in $CDCl_3$ and irradiated at 365 nm in a UV reactor.

As shown in Figure 4.9 (Supporting Information), three new significant signals at 6.7, 7.2 ppm and 10.3 ppm were observed. These new signals correspond to 4-bromophenol and 4-bromo-2-nitrosoaldehyde that arise from the degradation of the compound (Figure 4.10, Supporting Information). As the irradiation time increased, we observed the increase of these new signals and the decrease of the monomer signals until their complete disappearance after 24 hours of irradiation. We also observed that the signal at 10.3 ppm which corresponds to the aldehyde signal and the signal of the residual $H_20$ solvent disappeared as the irradiation time increased (Full spectra overlay is provided in Figure 4.9, Supporting Information). This suggests that some side reactions occurred, resulting in minor decomposition products. Other characterization techniques such as UV-Vis spectroscopy and high-performance liquid chromatography (HPLC) were used and showed the complete disappearance of the monomer signals. (Figure 4.11, Supporting Information).

We then investigated the photodegradation of the polymer. **PF-*o*NB** was dissolved in $CDCl_3$ and irradiated at 365 nm in the UV reactor. In comparison to the monomer, we could not observe a complete disappearance of the polymer backbone because the polymer is cleaved into lower molecular weight fragments and not into the two starting monomers. However, we still observed the appearance of the two NMR signals at ~ 6.9 and 7.6 ppm that correspond to the aromatic protons of the phenol end fragment. To further confirm the cleavage of the polymer backbone, UV-vis absorption spectroscopy and GPC were used. **PF-*o*NB** was dissolved in tetrahydrofuran (THF), transferred into a quartz cuvette and irradiated. As shown in Figure 4.1B, as the irradiation time

increased, we observed a decrease in the absorbance of the polymer confirming the effective degradation of the backbone. GPC also confirmed the photodegradation with the shift of the polymer signal to a lower molecular weight signal post-irradiation (Figure 4.13, supporting information).

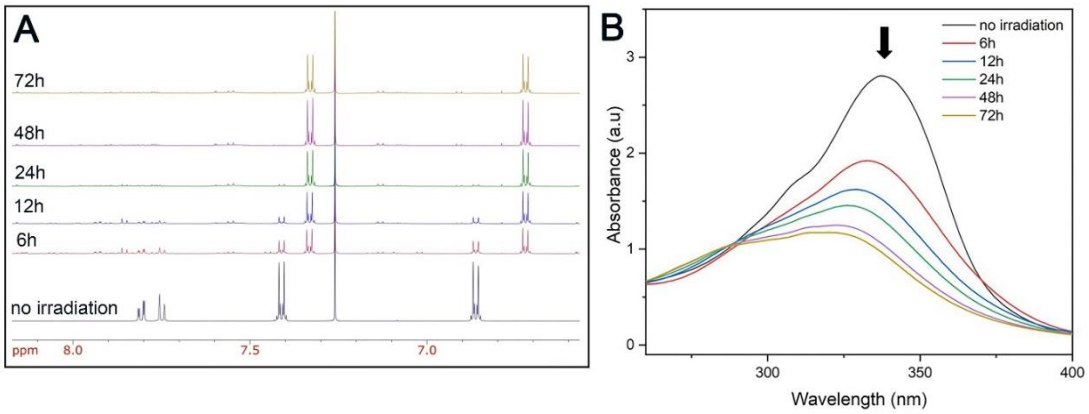


Figure 4.1. A) $^{1}$H-NMR spectral overlay upon irradiation of monomer **5** at 365 nm in $CDCl_3$ and B) UV-Vis absorption overlay upon irradiation of **PF-*o*NB** at 365 nm in THF (0.05 mg/mL).

**Polymer-SWNT dispersion**. Although the polymer backbone is not fully conjugated, previous studies have shown effective SWNT dispersions using polymers that have non-conjugated linkers.[60,62] A supramolecular complex of **PF-*o*NB** and raw HiPco SWNTs (average tube diameter 0.8 – 1.2 nm) was then prepared following literature procedures.[63] Briefly, a mixture of 7.5 mg of **PF-*o*NB** and 5 mg of raw HiPco SWNTs in 10 mL of THF were sonicated using a probe sonicator for 1 h. The resulting black suspension was then centrifuged at 8 346 g for 30 min. The supernatant was carefully removed, passed through a cotton plug, and filtered through a Teflon membrane (0.2 µm pore diameter). The residue was thoroughly rinsed with THF to remove the excess polymer,

redispersed in 10 mL of THF, sonicated for 1 h and centrifuged at 8 346 g for 30 min.

We then characterized our **PF-*o*NB**-SWNT complex. We first used UV-Vis-NIR absorption spectroscopy (Figure 4.2). Each SWNT species present within the polymer-SWNT dispersion exhibits its own absorption signals. For HiPco SWNTs, three main regions are observed: two semiconducting regions, $S_{11}$ (830−1600 nm) and $S_{22}$ (600−800 nm), and one metallic region, $M_{11}$ (440−645 nm).[4] As shown in Figure 4.1A, sharp and well-defined signals were observed, suggesting an effective dispersion of SWNTs using our **PF-*o*NB** polymer. However, both m- and sc-SWNT species are present within the polymer-SWNT complexes, suggesting a lack of any selectivity for specific SWNT types under the dispersion conditions used.

To further characterize our **PF-*o*NB**-SWNT dispersion, Raman spectroscopy was performed. This technique utilizes laser excitation wavelengths that overlap with the van Hove singularities present in the density of states for a specific SWNT species.[64] Therefore, both m- and sc-SWNT species present in the polymer-SWNT sample can be characterized.[65] Since electronic transitions depend on SWNT diameter and type, multiple excitation wavelengths are needed for complete characterization.[65] The **PF-*o*NB**-SWNT sample was prepared by drop-casting the dispersion onto a silicon wafer, followed by evaporation at RT. A reference sample was prepared by sonicating raw HiPco SWNTs in THF followed by the same drop-casting method. For HiPco SWNTs, two excitation wavelengths were used: 633 and 785 nm. Both

m- and sc-SWNTs are separately probed using these laser wavelengths.[66] Figures 4.2B and 4.2C show the radial breathing mode (RBM) of **PF-*o*NB**-SWNT and raw HiPco SWNT samples. The spectra were normalized to the G-band (~ 1590 $cm^{-1}$) for comparative analysis (full spectra are provided in Figure 4.4, Supporting Information). Using the 633 nm excitation wavelength, both m- (175−230 $cm^{-1}$) and sc-SWNTs (240−300 $cm^{-1}$) are in resonance and signals corresponding to both nanotube types are observed (Figure 4.2B).[67] We then used the 785 nm excitation wavelength to complete the characterization. sc-SWNTs are primarily in resonance (175-280 $cm^{-1}$) when using this wavelength. Moreover, when raw HiPco SWNTs are excited at 785 nm, a peak at 265 $cm^{-1}$ corresponding to bundled (10,2) SWNTs is observed.[68] As shown on the spectra (Figure 4.2C), the intensity of this peak in the **PF-oNB**-SWNT sample is significantly lower compared to the reference sample. This indicates that the sample is relatively well dispersed.

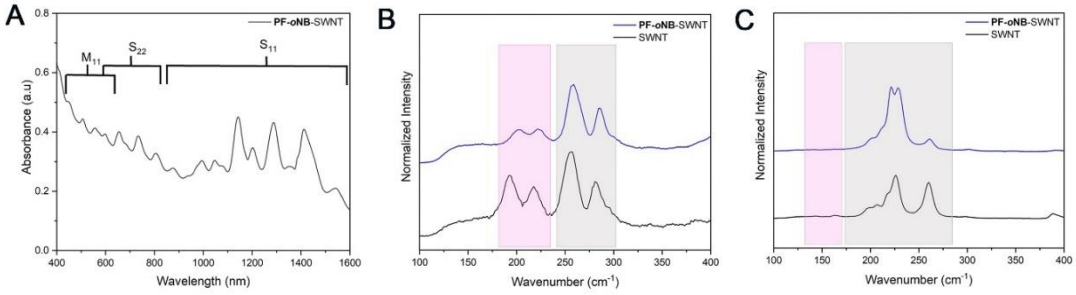


Figure 4.2. A) UV-Vis-NIR absorption spectrum of **PF-*o*NB**-SWNT in THF, Raman spectra overlay of **PF-*o*NB**-SWNT and raw HiPco -SWNT samples showing the RBM regions at B) $\lambda_{ex}$ = 633 nm, C) $\lambda_{ex}$ = 785 nm. Gray boxes represent signals arising for sc-SWNTs, whereas pink boxes represent m-SWNTs. All the spectra were normalized to the G-band at ~ 1590 $cm^{-1}$.

**Photodegradation of the PF-oNB-SWNT complex.** Next, we investigated the photodegradation of our **PF-*o*NB**-SWNT dispersion. Since the dispersion is black, we diluted it 20-fold to allow the light to penetrate the solution. The resulting dispersions were then transferred into glass vials equipped with stir bars. The solutions were stirred and placed in the UV reactor under 365 nm irradiation for 24, 48 and 72 h. As shown in Figure 4.3, after 24 h of irradiation, a precipitate was observed. This suggests the effective cleavage and desorption of the polymer from the surface of the nanotubes, followed by their aggregation and precipitation. Similar observations were made for the 48 and 72-h irradiated samples.

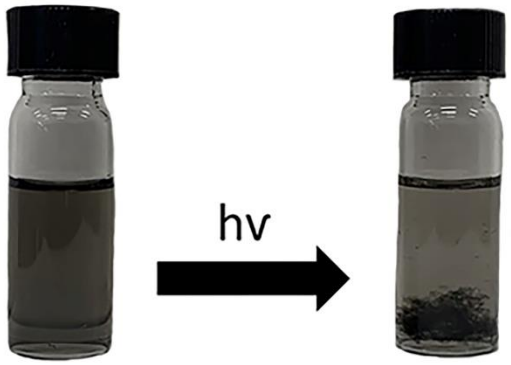


Figure 4.3. Photograph of **PF-*o*NB**-SWNT pre- and post-irradiation at 365 nm for 24 h.

Characterization of the post-irradiation samples was then performed. First, the samples were centrifuged at 8,346 g for 30 min and the supernatants and SWNT residues were analyzed. UV-Vis-NIR absorption spectroscopy was performed on the supernatants. As shown in Figure 4.4A, as the irradiation time increased, the absorption peaks associated with the nanotubes decreased. After 72 h of irradiation, broad absorption peaks were observed. This indicates

that the cleavage of the polymer backbone into smaller fragments eliminates the stabilization of the nanotube dispersion. Lastly, we analyzed the SWNT residues obtained after centrifugation. The residues were first filtered through a 0.2 µm pore diameter Teflon membrane. A previous study from our group has shown that washing the residues with hot solvent was more efficient at removing the cleaved fragments. We, therefore, rinsed our SWNT residues with boiling THF until no polymer absorption ( 300 - 380 nm) was detected. 40 mL of boiling THF was used for each sample during the washing step (Figure 4.15, Supporting Information).

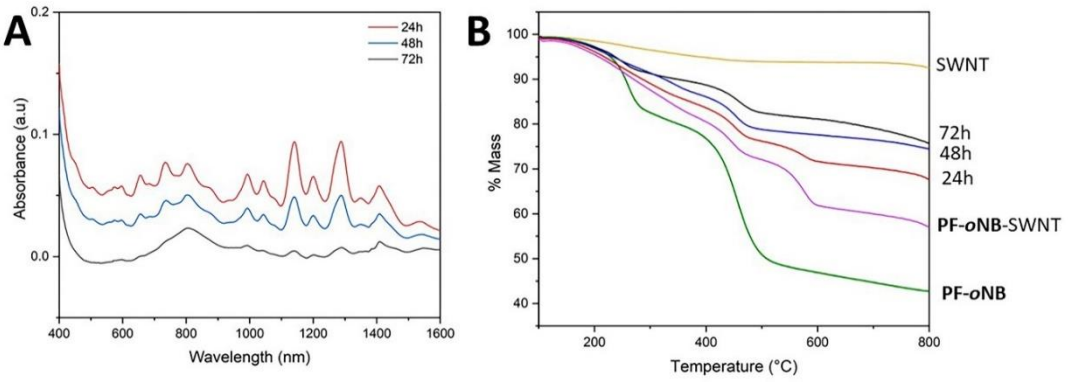


Figure 4.4. A) UV-Vis-NIR absorption spectra overlay of the supernatants after irradiation at 365 nm and B) TGA thermograms for raw HiPco SWNTs (yellow), **PF-*o*NB** (green) and **PF-*o*NB-**SWNT samples, before and after irradiation. Samples were measured under argon with a heating rate of 10 °C/min.

The residues were characterized using thermogravimetric analysis (TGA) to quantify the amount of polymer that remained on the surface of the SWNTs after irradiation (Figure 4.4B). For comparison, TGA was also performed on the polymer only. We observed a two-step mass loss for **PF-*o*NB**

which corresponds to the loss of the azide groups and the nitro groups followed by the loss of the alkyl side-chains. We also observed that the mass loss of the polymer did not stay constant above 600 °C. This is most likely because the polymer backbone is not fully conjugated, therefore the backbone can break into smaller fragments by slowly releasing phenyl units during continued heating. Overall, the polymer exhibits a mass loss of approximately 51%. For the **PF-*o*NB**-SWNT sample, we also observed two-step mass losses but these steps are less-defined as described in the literature.[69] The overall mass loss was 38%. Since the mass loss of SWNTs is negligible under the conditions used for TGA, the fraction of polymer can be calculated as:

$$f_{\mathbf{PF\text{-}oNB}} = \frac{\varphi_{\mathbf{PF-}o\mathbf{NB-SWNT}}}{\varphi_{\mathbf{PF-}o\mathbf{NB}}} \quad (4.1)$$

where $\varphi_{\mathbf{PF-}o\mathbf{NB}}$ is the mass loss of **PF-*o*NB** and $\varphi_{\mathbf{PF-}o\mathbf{NB-SWNT}}$ is the mass loss of the **PF-*o*NB**-SWNT complex. Thus, the $f_{\mathbf{PF\text{-}oNB}}$ is 0.75 and the $f_{SWNT}$ is 0.25 (given that $f_{\mathbf{PF\text{-}oNB}} + f_{SWNT} = 1$). After irradiation, we observed a decrease in the mass loss of the irradiated samples. This is due to the cleavage of the polymer backbone that leads to the desorption of the small polymer fragments from the surface of the nanotubes. After 72 h of irradiation, $f_{\mathbf{PF\text{-}oNB}}$ was 0.33. Since the initial $f_{\mathbf{PF\text{-}oNB}}$ is considered as the reference, the $f_{\mathbf{PF\text{-}oNB}}$ after 72 h of irradiation corresponds to a decrease of 56 % of the polymer from the surface of the nanotubes (Table 5.1). The remaining polymer mass on the SWNTs is most likely due to the strong interactions of the oligomers with the nanotubes.

Table 4.1. Tabulated TGA data.

| Sample | Mass loss (%) | $f_{polymer}$ | % decrease in $f_{polymer}$ (%) |
|---|---|---|---|
| PF-oNB | 51 | 1.00 | - |
| PF-oNB-SWNT | 38 | 0.75[a] | - |
| 24h | 28 | 0.60 | 20 |
| 48h | 21 | 0.41 | 45 |
| 72h | 17 | 0.33 | 56 |

Lastly, we used Raman spectroscopy with the 633 nm laser excitation wavelength to verify that the irradiation process did not damage the surface of the nanotubes. The comparison of the D-band centred at ~1290 $cm^{-1}$ relative to the G-band at ~1590 $cm^{-1}$ indicates the presence of $sp^3$ carbon which corresponds to defect sites.[70] As shown in Figure 4.5A, there is no significant difference between the pre-and post-irradiated sample when observing the G and D-bands. This suggests that no nanotube defects were generated by the irradiation process.

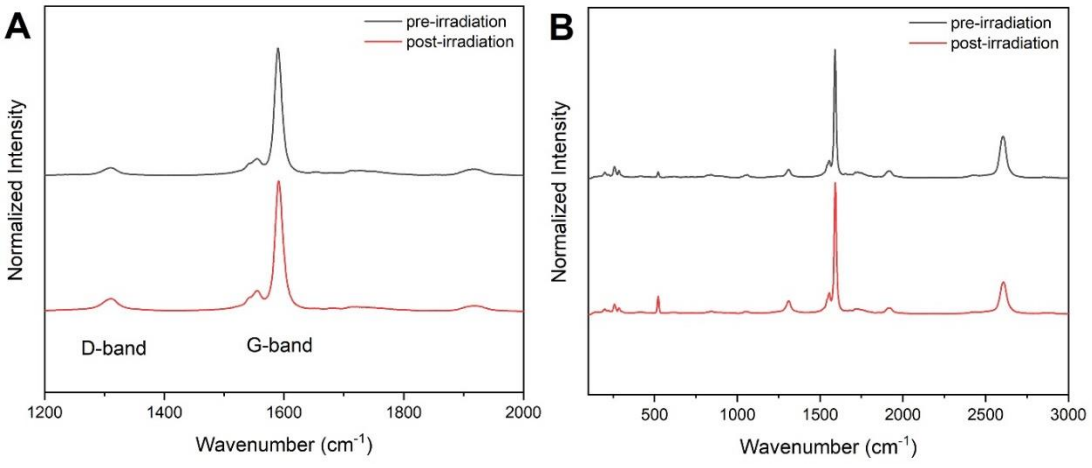


Figure 4.5. Raman Spectra for **PF-oNB**-SWNT at $\lambda_{ex}$ = 633 nm showing A) the G- and D-band and B) the full spectra pre-and post-irradiation at 365 nm for 72 h. All the spectra were normalized to the G-band at ~ 1590 $cm^{-1}$.

**Photodegradation of polymer-SWNT in water**. Our next investigation was the photodegradation of the polymer-SWNT complex in water. To introduce hydrophilic side-chains on the polymer, we prepared DIBAC-functionalized poly(ethylene glycol) (PEG) ($M_n$ of 2 kDa) via Steglish esterification of poly(ethylene glycol) monomethyl ether ($mPEG_{2000}$-OH) with DIBAC-COOH (Scheme 4.6 Supporting Information). **PF-*o*NB** was then functionalized with DIBAC-$mPEG_{2000}$ via SPAAC reaction to obtain **PF-*o*NB-mPEG$_{2000}$** (Figure 4.6A). The reaction was monitored by infrared spectroscopy (IR) via the disappearance of the azide stretch at ~ 2090 $cm^{-1}$ (Figure 4.17).

The photodegradation was then performed on **PF-*o*NB-mPEG$_{2000}$**. The polymer was dissolved in $H_2O$, transferred into a quartz cuvette and irradiated at 365 nm in the UV reactor. Similar to its organo-soluble analog, we observed a decrease in the absorbance of the polymer as the irradiation time increased (Figure 4.6B). This indicates the effective cleavage of the polymer backbone.

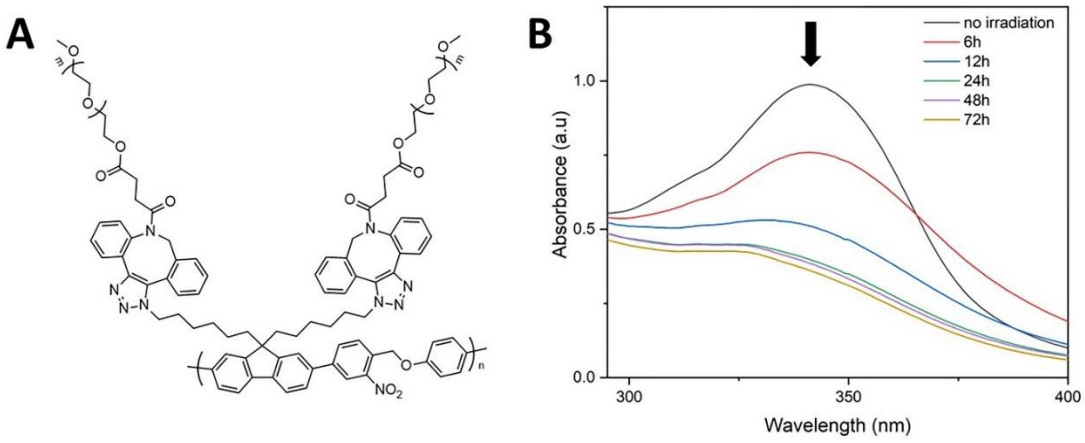


Figure 4.6. A) Chemical structure of **PF-*o*NB-mPEG$_{2000}$** and B) UV-Vis absorption spectra overlay of the irradiation of **PF-*o*NB-mPEG$_{2000}$** in $H_2O$ (0.1 mg/mL).

A supramolecular complex of **PF-*o*NB-mPEG$_{2000}$** and raw HiPco SWNTs was prepared with 7.5 mg of polymer, 5 mg of SWNTs in 10 mL of $H_2O$. The mixture was sonicated using a probe sonicator for 1 h and the black suspension was centrifuged at 8,346 g for 30 min. The supernatant was carefully removed, passed through a cotton plug and filtered through a 0.2 µm diameter hydrophilic Teflon membrane. The residue was then washed with water to remove the excess polymer, re-dispersed in 10 mL of water using the probe sonicator for 1 h and finally centrifuged at 8 346 g for 30 min to obtain **PF-*o*NB-mPEG$_{2000}$**-SWNT. The sample was characterized by UV-Vis-NIR-absorbance spectroscopy. Similar to **PF-oNB**-SWNT dispersion, both m-SWNT and sc-SWNT species are present in the sample (Figure 4.7A). In comparison to the sample in THF, the absorbance peaks of the nanotube are broader suggesting the presence of some bundles. To further investigate this, Raman spectroscopy was performed using the 785 nm excitation wavelength (Figure 4.7B). A

comparison of the peak at ~265 $cm^{-1}$ shows no significant increase of this peak suggesting that **PF-*o*NB-mPEG$_{2000}$**-SWNT is relatively well dispersed. Finally, the excitation using the 633 nm laser wavelength confirmed the presence of both m-SWNT and sc-SWNT species in the sample (Figure 4.7C).

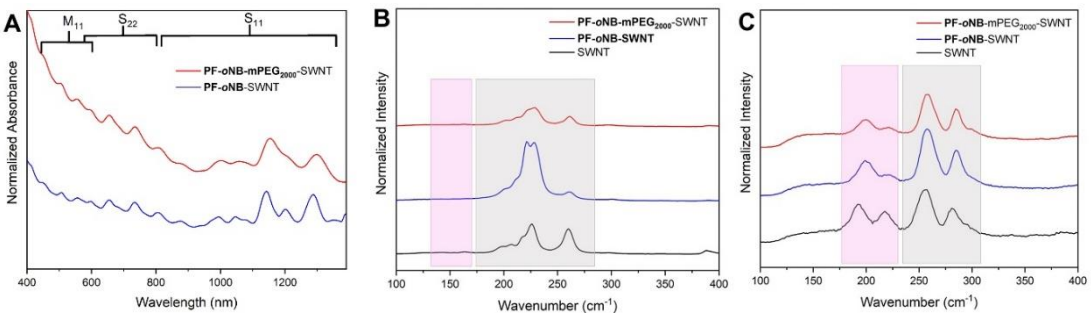


Figure 4.7. A) UV-Vis-NIR absorbance spectrum of **PF-*o*NB-mPEG$_{2000}$**-SWNT in THF. Spectra were normalized to the local minimum at 917 nm and offset for clarity. Raman spectra overlay of **PF-*o*NB-mPEG$_{2000}$**-SWNT and raw HiPco-SWNT samples showing the RBM regions with B) $\lambda_{ex}$ = 785 nm, C) $\lambda_{ex}$ = 633 nm. Gray boxes represent signals arising for sc-SWNTs, whereas pink boxes represent m-SWNTs. All the spectra were normalized to the G-band at ~ 1590 $cm^{-1}$.

The photodegradation was performed on **PF-*o*NB-mPEG$_{2000}$**-SWNT. The dispersions were first diluted to obtain a similar absorbance to the **PF-*o*NB**-SWNT samples. The dispersions were then transferred into glass vials and stirred under 365 nm light in the UV reactor. Surprisingly, no precipitate was observed for the samples after the different irradiation times. This suggests that the polymer fragments remain strongly bonded to the nanotubes. The samples were centrifuged at 8 346 g for 30 min to sediment any nanotube structures

from which the cleaved polymer had desorbed. Unfortunately, this resulted in a negligible amount of SWNT residues (< 1 mg). Increasing the centrifugation speed to 22 000 g for 30 min did not result in the sedimentation of a larger amount of SWNT residue. With the absence of SWNT residues, TGA analysis could not be performed. We therefore could not compare the release of SWNTs in aqueous solvent.

### 4.3 Conclusion

A functionalized and photodegradable fluorene-based polymer containing an ortho-nitrobenzylether linker has been synthesized. The photodegradation was first studied on the monomer and polymer by UV-Vis and $^{1}$H-NMR spectroscopy and showed efficient degradation over time. A supramolecular complex with the polymer and raw HiPco SWNTs was prepared. After irradiation of the complex at 365 nm for 24 h, precipitation of the nanotubes was observed and confirmed the effective degradation of the polymer into smaller fragments. Characterization post-irradiation of the samples has been performed. TGA thermograms of the SWNT residues showed a decrease in mass loss for the irradiated samples due to the removal of the polymer backbone from the surface of the nanotubes. After 72 h of irradiation, a decrease of 56% of the polymer was calculated. Finally, the functionalization of the polymer via SPAAC reaction with hydrophilic side-chains was performed to disperse and release SWNTs in water. Despite the relatively well-dispersed SWNT dispersion, irradiation of the complex in water did not lead to the

precipitation of the nanotubes mostly due to the strong interactions between the polymer fragments and the surface of the nanotubes.

## 4.4 Supporting Information

### 4.4.1 General

Raw HiPco SWNTs were purchased from NanoIntegris (batch #HR37-0878) and used without further purification. All reagents were purchased from commercial chemical suppliers and used as received. Flash chromatography was performed using a CombiflashRF200 by Teledyne ISCO. Unless otherwise noted, compounds were monitored using a variable wavelength detector at 254 nm. Solvent amounts used for gradient or isocratic elution were reported in column volumes (CV). Columns were prepared in Biotage® SNAP KP-Sil cartridges using 40 – 63 µm silica or 25 – 40 µm silica purchased from Silicycle. $^{1}$H-NMR and $^{13}$C-NMR spectra were recorded on Bruker Avance 600 MHz and shift-referenced to the residual solvent resonance. The polymer molecular weight and the dispersity were analyzed (relative to polystyrene standards) via GPC using a Waters 2695 Separations Module equipped with a Waters 2414 refractive index detector and a TSKgel SuperHZM-N with 3 µm particle diameter. THF with 2% acetonitrile was used as the eluent at a flow rate of 0.3 mL/min. Photoirradiation of the samples was performed in a home-built UV reactor equipped with a 25W lamp exhibiting emission at 365 nm. HPLC analysis was performed using a Waters Alliance 2695 separations module equipped with a 150 × 46 mm Phenomenex Kinetex column (2.6 µm particle size) at 35 °C and a Waters 2487 Dual wavelengths absorbance detector. 5%

of acetonitrile in water was used as the eluent at a flow rate of 1.23 mL/min. All Sonication was performed using a QSonica Q700 Sonicator equipped with a 13 mm probe. The amplitude of the probe was 60 µm and the sonication power was 30 Watts. Centrifugation of the polymer-SWNT samples was performed using a Beckman Coulter Allegra X-22 centrifuge. UV-Vis-NIR absorption spectra were recorded on a Cary 5000 spectrometer in dual beam mode, using matched 10 mm quartz cuvettes. Raman spectra were collected with a Renishaw InVia Laser Raman spectrometer, using two different excitation lasers: a 500 mW HeNe Renishaw laser (633 nm, 1800 L/mm grating); and a 300 mW Renishaw laser (785 nm, 1200 L/mm grating). Raman samples were drop-cast onto freshly cleaned silicon wafers and allowed to air-dry at room temperature. Thermogravimetric analysis was performed on a Mettler Toledo TGA/DSC 3+, and all measurements were conducted under an argon atmosphere. The TGA plots in Figure 4.4 were obtained by heating the sample to 100 °C for 5 minutes to drive off water, followed by heating to 800 °C (10 °C per min).

### 4.4.2 Synthesis

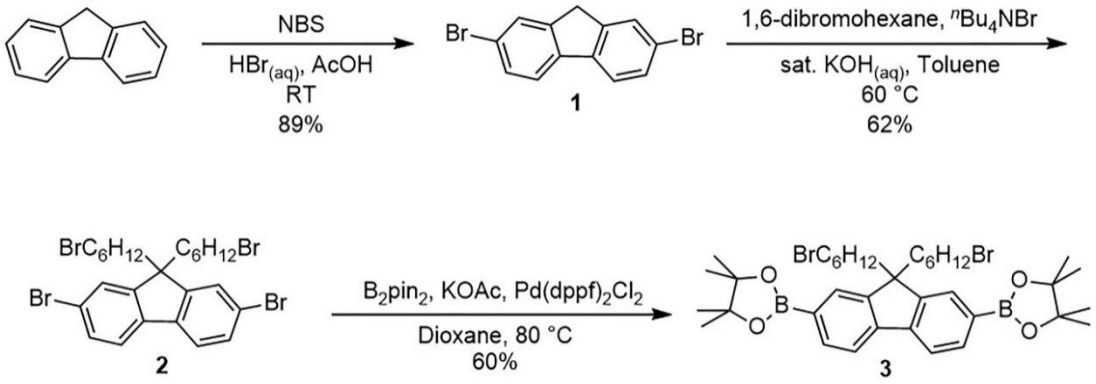


Scheme 4.2. Synthesis of monomer **3**.

Compounds **1**, **2** and **3** were synthesized following literature procedures.[61]

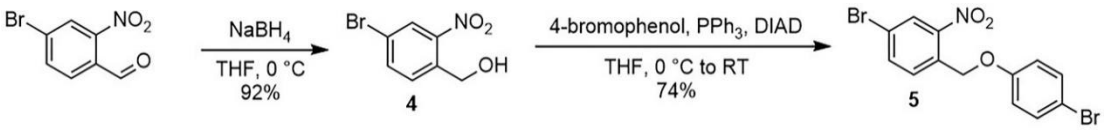


Scheme 4.3. Synthesis of monomer **5**.

**(4-bromo-2-nitrophenyl)methanol (5)**.[59] Adapted from ref. 59.

A 50 mL round bottom flask equipped with a stir bar was charged with 4-bromo-2nitrobenzaldehyde (0.75 g, 3.3 mmol) in 11 mL of dry THF. $NaBH_4$ (0.25 g, 6.5 mmol) was added by portion and the solution was stirred at 0 °C for 1h30 min, quenched with water (10 mL) and extracted with $Et_2O$ (3 x 20 mL). The organic phases were combined, dried over $MgSO_4$ and concentrated *in vacuo*. The crude product was purified by flash chromatography (Hex/EtOAc 0% to 50%) to afford compound **4** as a light yellow powder (0.7 g, 92%). $^1$H-NMR (600 MHz; $CDCl_3$): δ 8.25 (d, *J* = 2.0 Hz, 1H), 7.80 (dd, *J* = 8.3, 2.0 Hz, 1H), 7.67 (d, *J* = 8.3 Hz, 1H), 4.96 (d, *J* = 6.3 Hz, 2H), 2.36 (t, *J* = 6.4 Hz, 1H).

**4-bromo-1-((4-bromophenoxy)methyl)-2-nitrobenzene (5).**[59] Adapted from ref. 59.

The reaction was performed in the absence of light. A 50 mL round bottom flask equipped with a stir bar was charged with **4** (0.5 g, 2.2 mmol), 4-bromophenol (0.45 g, 2.6 mmol) and triphenylphosphine (0.68 g, 2.6 mmol) in 17 mL of dry THF. The solution was stirred at 0 °C and Diisopropyl azodicarboxylate (0.53 g, 2.6 mmol) was added dropwise within 10 min. The reaction was stirred overnight and concentrated *in vacuo*. The crude mixture was purified by flash chromatography (Hex/ DCM, 0% to 50%) to give compound **5** (0.62 g, 74%). $^1$H-NMR (600 MHz; $CDCl_3$): δ 8.32 (d, *J* = 2.0 Hz, 1H), 7.81 (dd, *J* = 8.4, 2.0 Hz, 1H), 7.75 (d, *J* = 8.4 Hz, 1H), 7.42-7.40 (m, 2H), 6.88-6.85 (m, 2H), 5.40 (s, 2H).

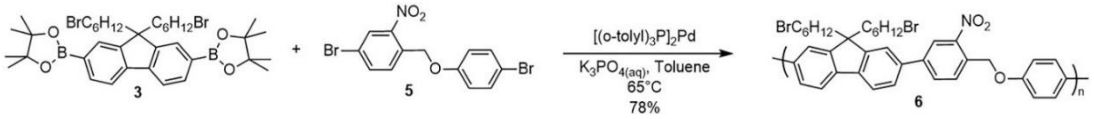


Scheme 4.4. Synthesis of copolymer **6**.

**Copolymer (6)**

A 100 mL Schlenk tube equipped with a magnetic stir bar was charged with **3** (0.38 g, 0.52mmol), **5** (0.20 g, 0.52 mmol), toluene (10.3 mL) and 3M $K_3PO_{4(aq)}$ (10.3 mL). The biphasic mixture was degassed by three freeze-pump-thaw cycles, then, while frozen under liquid nitrogen, $[(o\text{-tolyl})_3P]_2Pd$ (18 mg, 26 µmol) was added under a positive pressure of nitrogen. The Schlenk tube was evacuated and backfilled with nitrogen four times, and the reaction mixture was vigorously stirred at 65°C for 6h. The phases were allowed to separate, and the

organic layer was isolated and filtered through a single plug of celite and neutral alumina. The plug was thoroughly washed with THF and the filtrate was concentrated *in vacuo*. The crude polymer was precipitated into MeOH (~ 200 mL) and then filtered to afford **PF-oNB** as a yellow solid (0.3 g, 78%). $^{1}$H-NMR (600 MHz; $CDCl_3$): δ 8.51-8.44 (m, 1H), 8.06-7.97 (m, 2H), 7.89-7.49 (m, 8H), 7.18-7.07 (m, 2H), 5.69-5.55 (m, 2H), 3.35-3.20 (m, 4H), 2.16-1.98 (m, 4H), 1.74-1.60 (m, 4H), 1.29-1.03 (m, 8H), 0.79-0.59 (m, 4H).

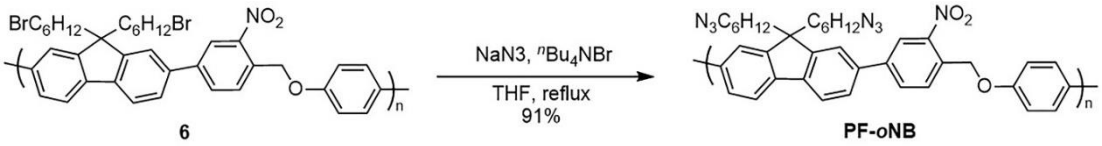


Scheme 4.5. Synthesis of **PF-*o*NB**.

**PF-*o*NB**

A 100 mL round bottom flask equipped with a magnetic stir bar and a reflux condenser was charged with **6** (0.29 g, 0.4 mmol), $NaN_3$ (0.26 g, 4.0 mmol), $^{n}Bu_4NBr$ (0.26 g, 4.0 mmol), and THF (40 mL). The reaction mixture was heated to reflux for 12 h. The reaction mixture was filtered through an alumina plug, concentrated *in vacuo*, precipitated into MeOH (~ 200 mL) and filtered to afford **PF-*o*NB** as a yellow solid (0.23 g, 91%).$^{1}$H-NMR (600 MHz; $CDCl_3$): δ 8.50-8.46 (m, 1H), 8.05-7.97 (m, 2H), 7.89-7.49 (m, 8H), 7.18-7.10 (m, 2H), 5.66-5.53 (m, 2H), 3.13-3.08 (m, 4H), 2.12-2.00 (m, 4H), 1.57-1.51 (m, 4H), 1.43-1.35 (m, 4H), 1.14-1.04 (m, 8H), 0.77-0.64 (m, 4H).


Scheme 4.6. Synthesis of **DIBAC-mPEG$_{2000}$**.

DIBAC-COOH was synthesized following literature procedures.[69]

**DIBAC-mPEG$_{2000}$**

A 20 mL glass vial equipped with a stir bar was charged with poly(ethylene glycol) monomethyl ether (mPEG$_{2000}$-OH) (100 mg, 50 µmol), DIBAC-COOH (46 mg, 200 µmol), 4-dimethylaminopyridine (3 mg, 25 µmol) in 1 mL of DCM. To the solution, N-(3- dimethylaminopropyl)-N'-ethylcarbodiimide hydrochloride (EDC·HCl) (34 mg, 175 µmol) was added and the reaction was stirred at RT for 12h. The reaction mixture was diluted with ~ 5 mL of DCM, precipitated into 100 mL of 1:1 Hexanes/$Et_2O$ and washed with cold $Et_2O$ (3 x 20 mL). $^1$H-NMR (600 MHz; DMSO-$d_6$): δ 7.68-7.65 (m,1H), 7.62-7.61 (m, 1H), 7.53-7.45 (m, 3H), 7.40-7.33 (m, 1H), 7.30 (dd, *J* = 7.4, 1.3 Hz, 1H), 5.05-5.02 (m, 1H), 4.03-3.91 (m, 2H), 3.64-3.60 (m, 4H), 3.49 (m, 160H), 3.42 (m, 3H), 3.24 (s, 3H), 2.66-2.61 (m, 2H), 2.44-2.35 (m, 2H), 2.34-2.25 (m, 2H), 1.89-1.77 (m, 2H), 1.78-1.73 (m, 2H). $^{13}$C-NMR (151 MHz; DMSO-$d_6$): δ 172.0, 170.5, 151.4, 148.3, 132.4, 129.6, 128.9, 128.2, 128.0, 127.7, 126.8, 125.1, 122.5, 121.5, 114.3, 108.0, 71.3, 69.6, 68.1, 63.2, 58.0, 54.9, 29.1, 28.8.

**PF-*o*NB-mPEG$_{2000}$**

A 100 mL round bottom flask equipped with a stir bar was charged with **PF-*o*NB** (14 mg, 21 µmol) and **DIBAC-mPEG$_{2000}$** (100 mg, 43 µmol) in 21 mL of THF. The solvent was evaporated using an $N_2$ stream. The polymer was then precipitated into a mixture of 1:1 Hex/$Et_2O$ (100 mL) to afford **PF-*o*NB-mPEG$_{2000}$** (100 mg, 90%). $^1$H-NMR (600 MHz; DMSO-$d_6$): δ 8.66-8.34 (m, 1H), 8.29-8.08 (m, 2H), 8.04-7.77 (m, 2H), 7.77-6.99 (m, 16H), 5.99-5.65 (m, 2H), 5.65-5.36 (m, 2H), 4.50-4.23 (m, 2H), 4.23-3.88 (m, 8H), 3.38-3.23 (m, 204H), 2.31-2.06 (m, 12H), 2.10-1.94 (m, 4H), 1.94-1.68 (m, 4H), 1.57-1.17 (m, 12H), 1.17-0.71 (m, 8H), 0.69-0.41 (m, 4H).

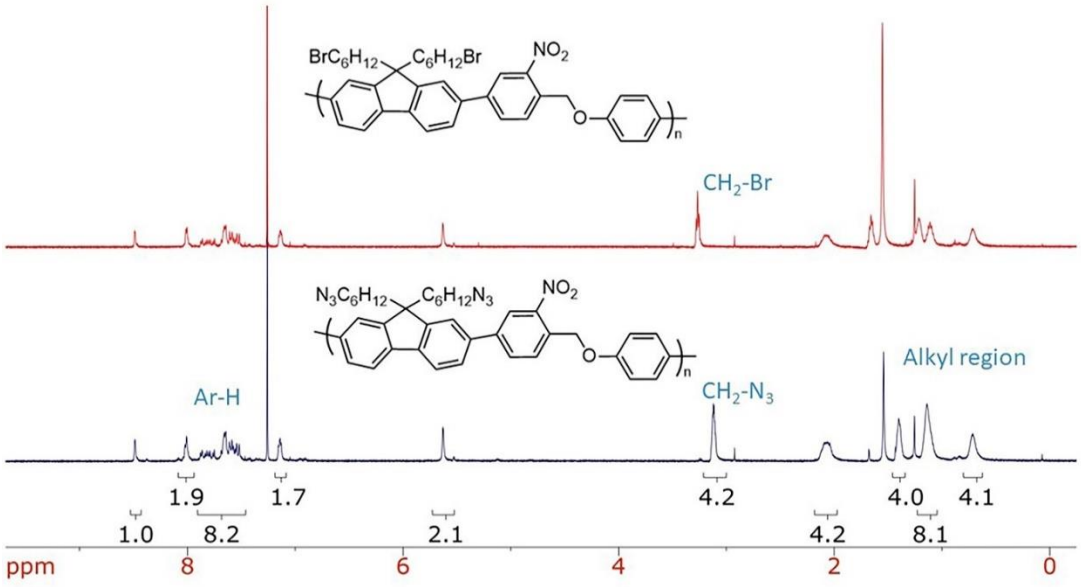


Figure 4.8. $^1$H-NMR overlay of copolymer **6** (red) and **PF-*o*NB** (blue).

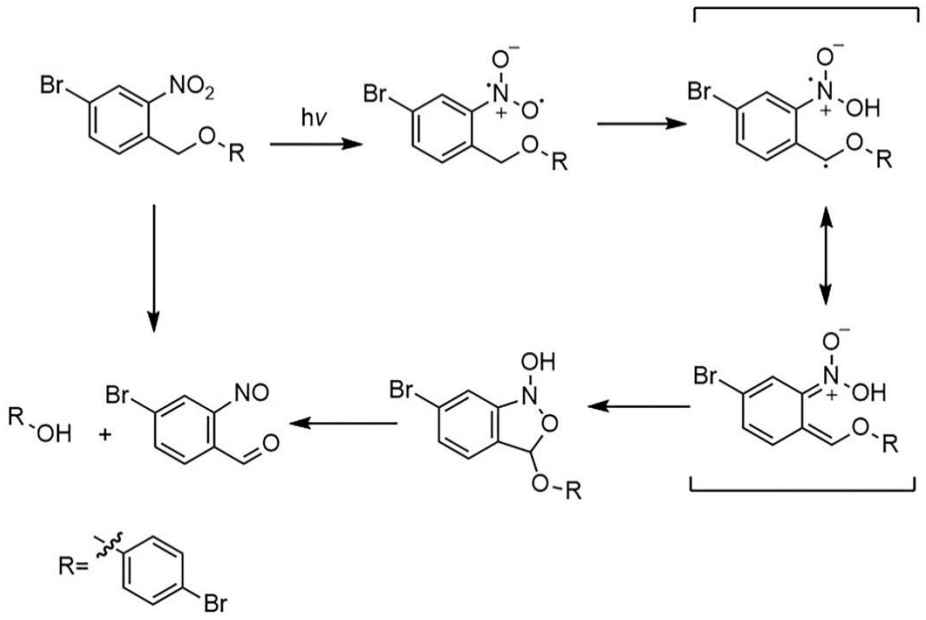


Figure 4.9. Photoisomerization mechanism of monomer **5**. Adapted from reference.[72]

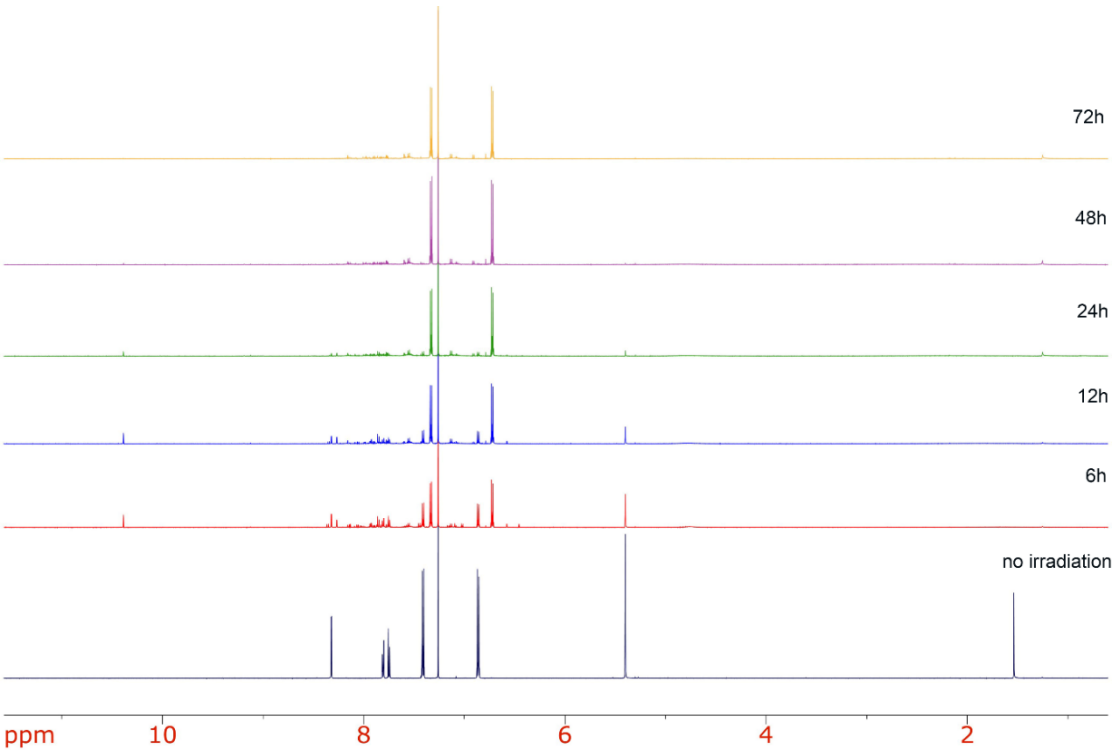


Figure 4.10. Full $^{1}$H-NMR spectra overlay of monomer **5** in $CDCl_3$ upon irradiation at 365 nm for 72 h.

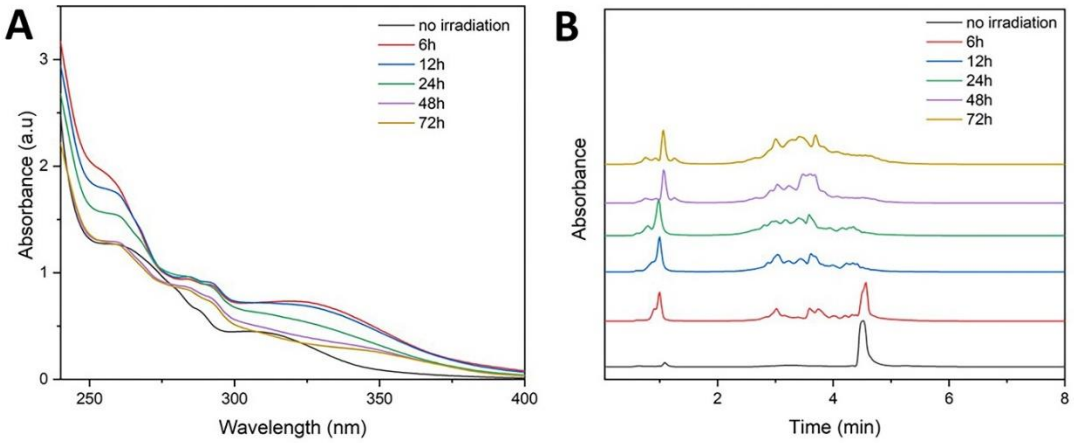


Figure 4.11. A) UV-Vis absorption spectra overlay of monomer **5** in THF (0.1 mg/mL) upon irradiation at 365 nm for 72 h and B) HPLC chromatogram overlay of monomer **5** upon irradiation at 365 nm for 72 h.

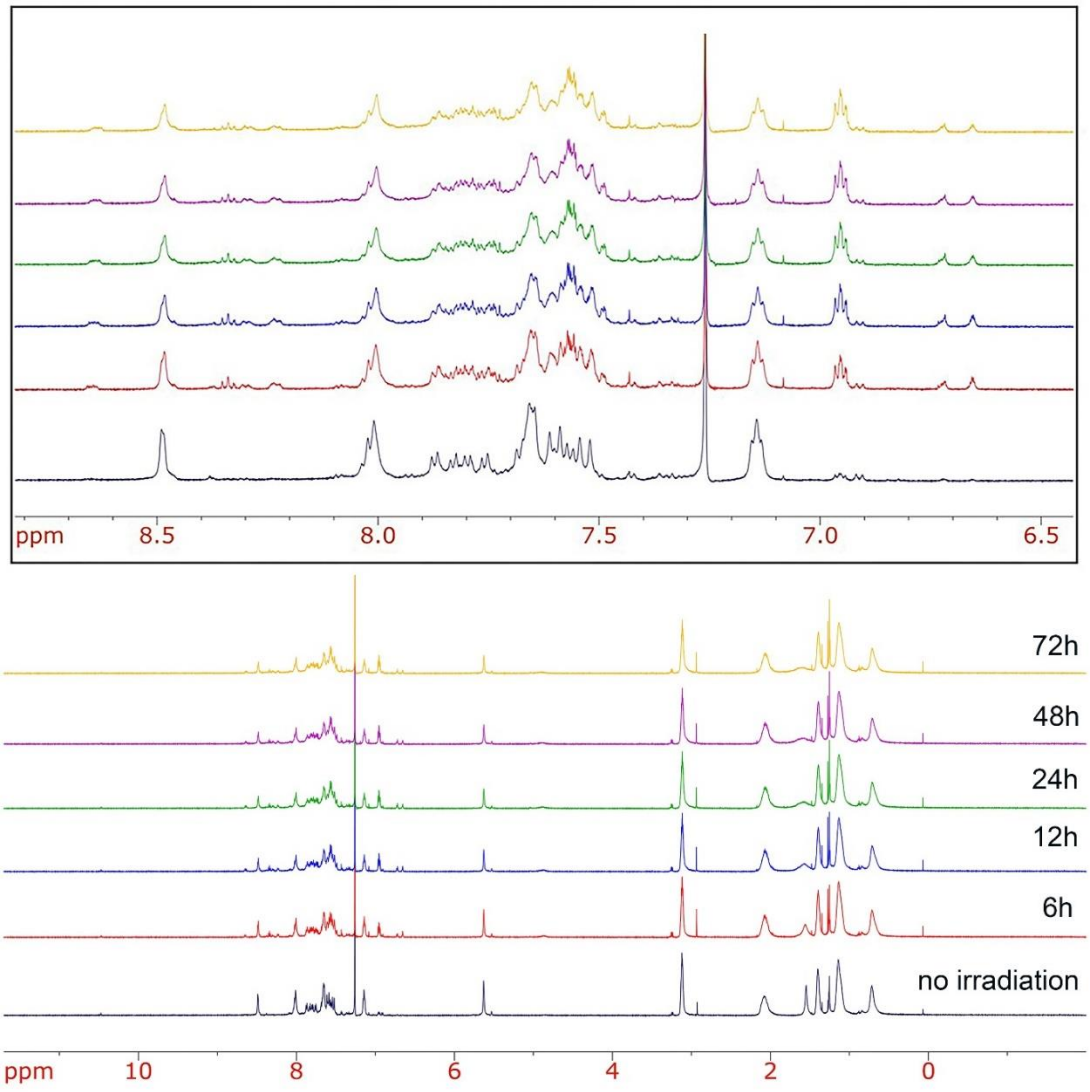


Figure 4.12. $^{1}$H-NMR spectra overlay of **PF-*o*NB** in $CDCl_3$ upon irradiation at 365 nm for 72 h. The top shows the aromatic region from 6.5 to 9 ppm.

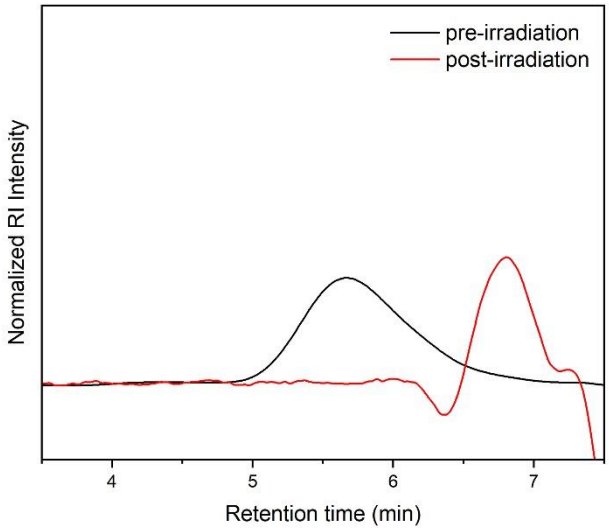


Figure 4.13. GPC trace of **PF-*o*NB** pre- (black) and post-irradiation (red) at 365 nm.

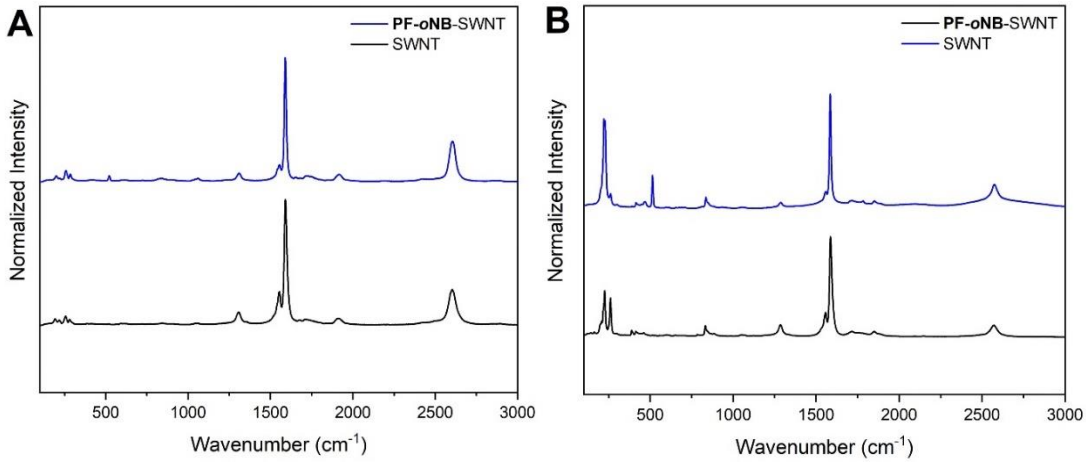


Figure 4.14. Full Raman spectra for HiPco **PF-*o*NB** -SWNT samples at A) $\lambda_{ex}$ = 633 nm, B) $\lambda_{ex}$ = 785 nm. All the spectra were normalized at ~ 1590 $cm^{-1}$.

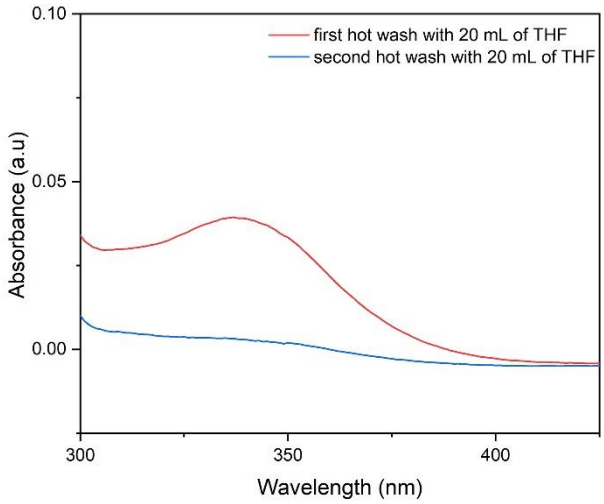


Figure 4.15. UV-Vis absorbance spectra overlay of washing step of the SWNT residues with boiling THF post-irradiation.

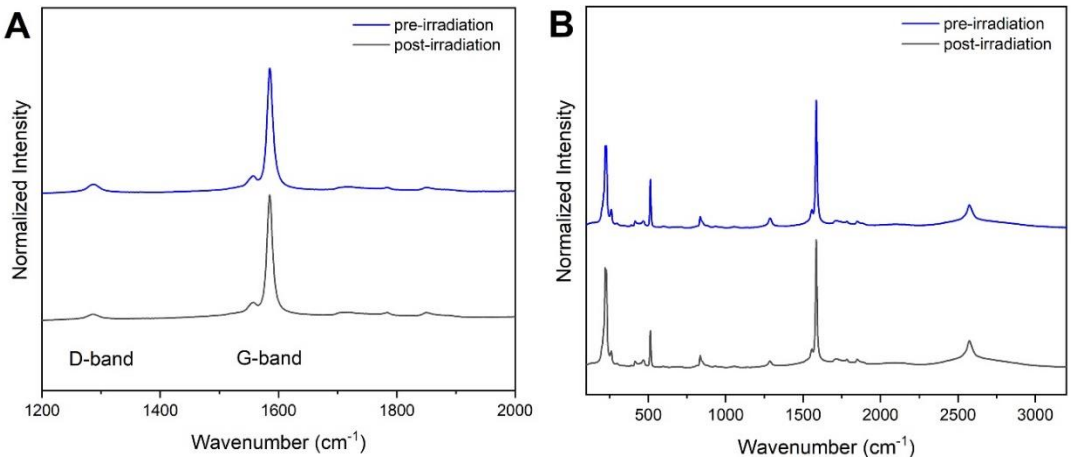


Figure 4.16. Full Raman spectra for HiPco **PF-*o*NB** -SWNT samples at $\lambda_{ex}$ = 785 nm pre- and post-irradiation showing A) the G- and D-band and B) the full spectrum. All the spectra were normalized at ~ 1590 $cm^{-1}$.

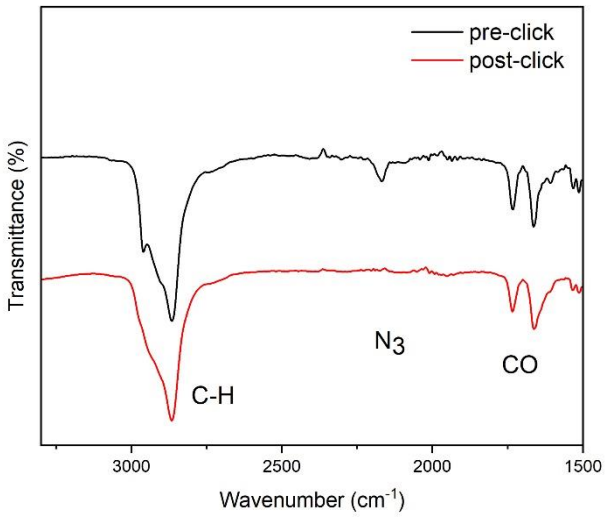


Figure 4.17. Overlay of FT-IR spectra of the SPACC reaction between **PF-*o*NB** and **DIBAC-mPEG$_{2000}$**.

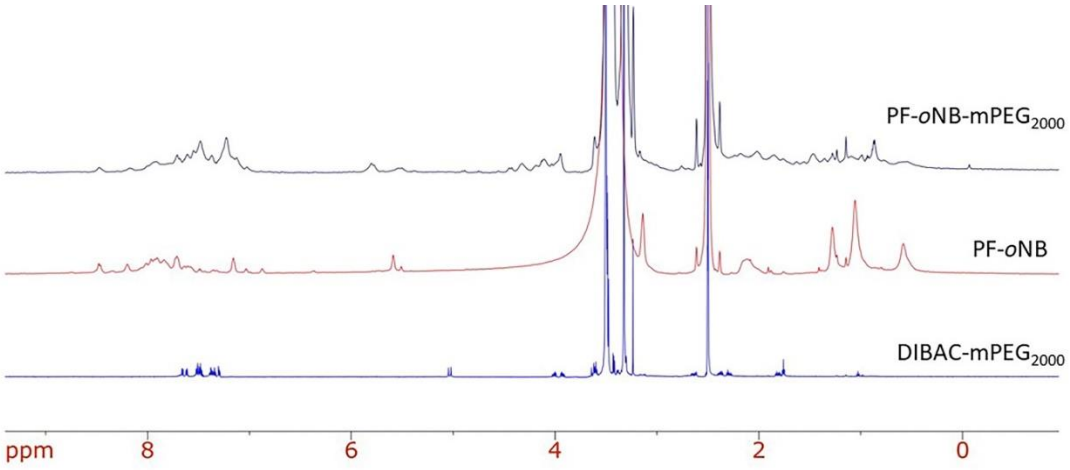


Figure 4.18. Overlay of $^{1}$H-NMR spectra of **PF-*o*NB, DIBAC-mPEG$_{2000}$** and **PF-*o*NB-mPEG$_{2000}$** in DMSO-d$_6$.

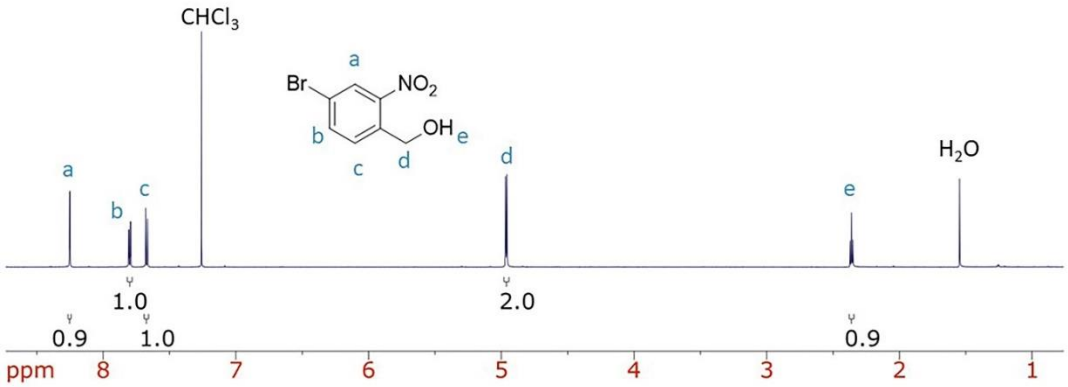


Figure 4.19. $^{1}$H-NMR spectrum of compound **4** in $CDCl_3$.

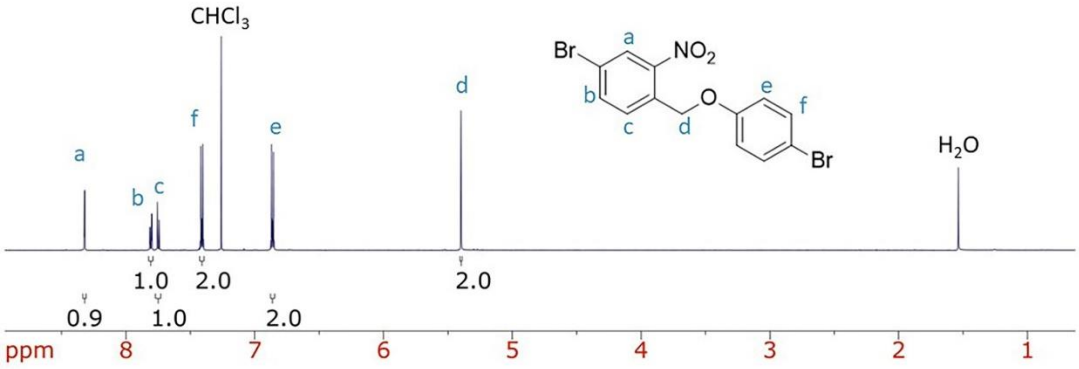


Figure 4.20. $^{1}$H-NMR spectrum of monomer **5** in $CDCl_3$.

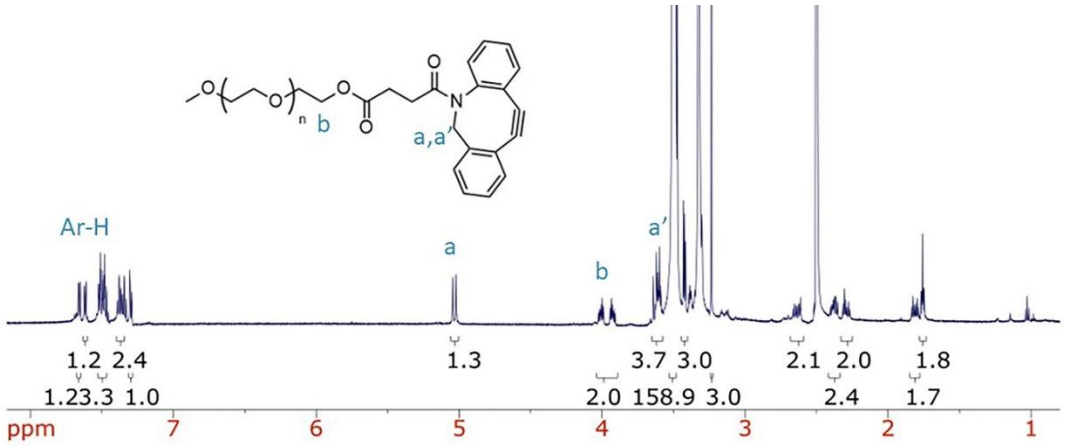


Figure 4.21. $^{1}$H-NMR spectrum of **DIBAC-mPEG$_{2000}$** in DMSO-$d_6$.

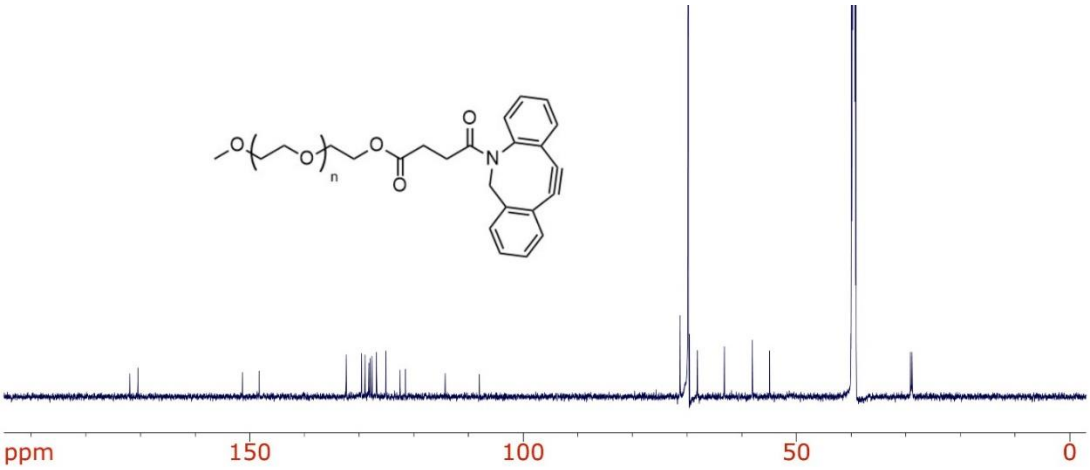


Figure 4.22. $^{13}$C-NMR spectrum of **DIBAC-mPEG$_{2000}$** in DMSO-d$_6$.

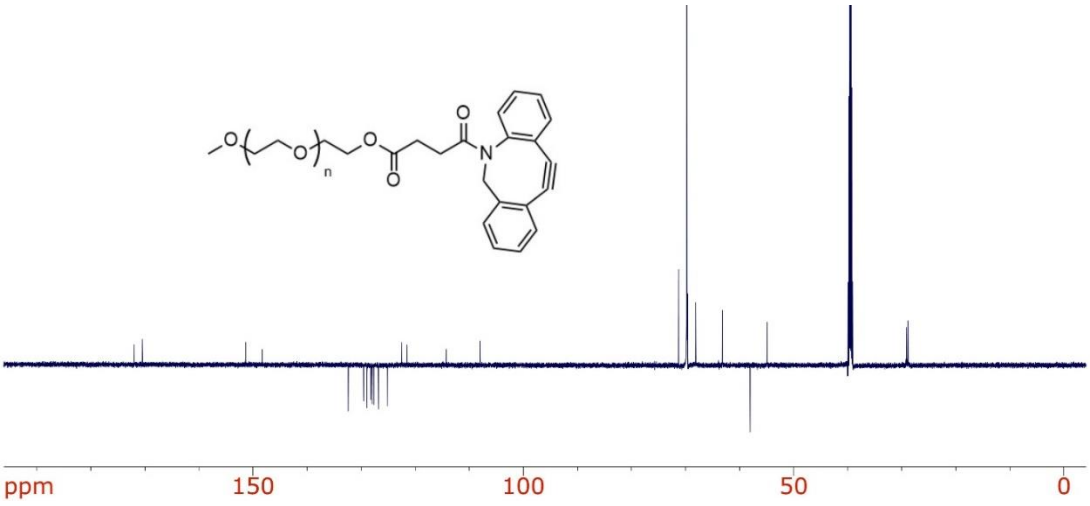


Figure 4.23. Deptq NMR spectrum of **DIBAC-mPEG$_{2000}$** in DMSO-d$_6$.

## 4.5 References

[1] M. Yu, B. S. Files, S. Arepalli, R. S. Ruoff, *Phys. Rev. Lett.* **2000**, *84*, 1–4.

[2] J. N. Coleman, U. Khan, W. J. Blau, Y. K. Gun'ko, *Carbon* **2006**, *44*, 1624–1652.

[3] H. Kataura, Y. Kumazawa, Y. Maniwa, I. Umezu, S. Suzuki, Y. Ohtsuka,

Y. Achiba, *Synth. Met.* **1999**, *103*, 2555−2558.

[4] S. M. Bachilo, M. S. Strano, C. Kittrell, R. H. Hauge, R. E. Smalley, R. B. Weisman, *Science* **2002**, *298*, 2361–2366.

[5] P. Avouris, *Acc. Chem. Res.* **2002**, *35*, 1026–1034.

[6] P. G. Collins, P. Avouris, *Sci. Am.* **2000**, *283*, 62–69.

[7] G. A. Rivas, M. D. Rubianes, M. C. Rodríguez, N. F. Ferreyra, G. L. Luque, M. L. Pedano, S. A. Miscoria, C. Parrado, *Talanta* **2007**, *74*, 291–307.

[8] P. Qi, O. Vermesh, M. Grecu, A. Javey, Q. Wang, H. Dai, S. Peng, K. J. Cho, *Nano Lett.* **2003**, *3*, 347–351.

[9] T. Dürkop, S. A. Getty, E. Cobas, M. S. Fuhrer, *Nano Lett.* **2004**, *4*, 35–39.

[10] L. Zhang, H. Wang, M. Chen, J. Ma, W. Wang, *Macromol. Res.* **2013**, *21*, 1083–1090.

[11] D. Sun, C. Liu, W. Ren, H. Cheng, *Small* **2013**, *9*, 1188–1205.

[12] M. W. Rowell, M. A. Topinka, M. D. McGehee, H. J. Prall, G. Dennler, N. S. Sariciftci, L. Hu, G. Gruner, *Appl. Phys. Lett.* **2006**, *88*, 6–9.

[13] C. Bounioux, E. A. Katz, R. Yerushalmi - Rozen, *Polym. Adv. Technol.* **2012**, *23*, 1129–1140.

[14] D. M. Sun, C. Liu, W. C. Ren, H. M. Cheng, *Small* **2013**, *9*, 1188–1205.

[15] S. Park, M. Vosguerichian, Z. Bao, *Nanoscale* **2013**, *5*, 1727–1752.

[16] S. Park, M. Vosguerichian, Z. Bao, *Proc. Natl. Acad. Sci.* **2014**, *111*, 4776–4781.

[17] K. Kordás, T. Mustonen, G. Tóth, H. Jantunen, M. Lajunen, C. Soldano, S. Talapatra, S. Kar, R. Vajtai, P. M. Ajayan, *Small* **2006**, *2*, 1021–1025.

[18] K. Y. Chun, Y. Oh, J. Rho, J. H. Ahn, Y. J. Kim, H. R. Choi, S. Baik, *Nat. Nanotechnol.* **2010**, *5*, 853–857.

[19] D. Jariwala, V. K. Sangwan, L. J. Lauhon, T. J. Marks, M. C. Hersam, *Chem. Soc. Rev.* **2013**, *42*, 2824–2860.

[20] D. S. Hecht, D. Thomas, L. Hu, C. Ladous, T. Lam, Y. Park, G. Irvin, P. Drzaic, *J. Soc. Inf. Disp.* **2009**, *17*, 941.

[21] P. Jarosz, C. Schauerman, J. Alvarenga, B. Moses, T. Mastrangelo, R. Raffaelle, R. Ridgley, B. Landi, *Nanoscale* **2011**, *3*, 4542–4553.

[22] P. Nikolaev, M. J. Bronikowski, R. K. Bradley, F. Rohmund, D. T. Colbert, K. A. Smith, R. E. Smalley, *Chem. Phys. Lett.* **1999**, *313*, 91–97.

[23] M. M. A. Rafique, J. Iqbal, *J. Encapsulation Adsorpt. Sci.* **2011**, *1*, 29–34.

[24] K. S. Kim, G. Cota-Sanchez, C. T. Kingston, M. Imris, B. Simard, G. Soucy, *J. Phys. D. Appl. Phys.* **2007**, *40*, 2375–2387.

[25] D. Tasis, N. Tagmatarchis, A. Bianco, M. Prato, *Chem. Rev.* **2006**, *106*, 1105–1136.

[26] A. Hirsch, *Angew. Chem., Int. Ed.* **2002**, *41*, 1853–1859.

[27] J. G. Wiltshire, A. N. Khlobystov, L. J. Li, S. G. Lyapin, G. A. D. Briggs,

R. J. Nicholas, *Chem. Phys. Lett.* **2004**, *386*, 239–243.

[28] Y.-L. Zhao, J. F. Stoddart, *Chem. Nanocarbons* **2010**, *42*, 1162–1171.

[29] A. Star, Y. Liu, K. Grant, L. Ridvan, J. F. Stoddart, D. W. Steuerman, M. R. Diehl, A. Boukai, J. R. Heath, *Macromolecules* **2003**, *36*, 553–560.

[30] V. C. Moore, M. S. Strano, E. H. Haroz, R. H. Hauge, R. E. Smalley, J. Schmidt, Y. Talmon, *Nano Lett.* **2003**, *3*, 1379–1382.

[31] R. J. Chen, Y. Zhang, D. Wang, H. Dai, *J. Am. Chem. Soc.* **2001**, *123*, 3838–3839.

[32] Y. Tomonari, H. Murakami, N. Nakashima, *Chem. Eur. J.* **2006**, *12*, 4027–4034.

[33] K. Yang, L. Zhu, B. Xing, *Environ. Sci. Technol.* **2006**, *40*, 1855–1861.

[34] L. Vaisman, H. D. Wagner, G. Marom, *Adv. Colloid Interface Sci.* **2006**, *128–130*, 37–46.

[35] H. Wang, *Curr. Opin. Colloid Interface Sci.* **2009**, *14*, 364–371.

[36] A. J. Blanch, C. E. Lenehan, J. S. Quinton, *J. Phys. Chem. B* **2010**, *114*, 9805–9811.

[37] Z. Guo, P. J. Sadler, S. C. Tsang, *Adv. Mater.* **1998**, *10*, 701–703.

[38] A. Star, D. W. Steuerman, J. R. Heath, J. F. Stoddart, *Angew. Chem., Int. Ed.* **2002**, *41*, 2508–2512.

[39] A. Star, J. F. Stoddart, D. Steuerman, M. Diehl, A. Boukai, E. W. Wong, X. Yang, S. Chung, H. Choi, J. R. Heath, *Angew. Chem.* **2001**, *113*, 1771–

1775.

[40] D. Fong, A. Adronov, *Chem. Sci.* **2017**, *8*, 7292–7305.

[41] S. K. Samanta, M. Fritsch, U. Scherf, W. Gomulya, S. Z. Bisri, M. A. Loi, *Acc. Chem. Res.* **2014**, *47*, 2446–2456.

[42] N. A. Rice, A. V Subrahmanyam, S. E. Laengert, A. Adronov, *Polym. Chem.* **2015**, *53*, 2510–2516.

[43] F. Jakubka, S. P. Schießl, S. Martin, J. M. Englert, F. Hauke, A. Hirsch, J. Zaumseil, *ACS Macro Lett.* **2012**, *1*, 815–819.

[44] N. Berton, F. Lemasson, F. Hennrich, M. M. Kappes, M. Mayor, *Chem. Commun.* **2012**, *48*, 2516–2518.

[45] P. Imin, F. Cheng, A. Adronov, *Polym. Chem.* **2011**, *2*, 1404–1408.

[46] N. A. Rice, A. V Subrahmanyam, B. R. Coleman, A. Adronov, *Macromolecules* **2015**, *48*, 5155–5161.

[47] D. Fong, G. M. Andrews, A. Adronov, *Polym. Chem.* **2018**, *9*, 2873–2879.

[48] J. Ding, Z. Li, J. Lefebvre, F. Cheng, G. Dubey, S. Zou, P. Finnie, A. Hrdina, L. Scoles, G. P. Lopinski, et al., *Nanoscale* **2014**, *6*, 2328–2339.

[49] W. Gomulya, G. D. Costanzo, E. J. F. De Carvalho, S. Z. Bisri, V. Derenskyi, M. Fritsch, N. Fröhlich, S. Allard, P. Gordiichuk, A. Herrmann, et al., *Adv. Mater.* **2013**, *25*, 2948–2956.

[50] W. J. Bodnaryk, D. Fong, A. Adronov, *ACS Omega* **2018**, *3*, 16238–16245.

[51] K. Mulla, S. Liang, H. Shaik, E. A. Younes, A. Adronov, Y. Zhao, *Chem. Commun.* **2014**, *51*, 149–152.

[52] S. Liang, Y. Zhao, A. Adronov, *J. Am. Chem. Soc.* **2014**, *136*, 970–977.

[53] I. Pochorovski, H. Wang, J. I. Feldblyum, X. Zhang, A. L. Antaris, *J. Am. Chem. Soc.* **2015**, *137*, 4328–4331.

[54] F. Toshimitsu, N. Nakashima, *Nat. Commun.* **2014**, *5*, 1–9.

[55] Z. Li, J. Ding, C. Guo, J. Lefebvre, P. R. L. Malenfant, *Adv. Funct. Mater.* **2018**, *28*, 1705568.

[56] W. Z. Wang, W. F. Li, X. Y. Pan, C. M. Li, L. Li, Y. G. Mu, J. A. Rogers, M. B. Chan-park, *Adv. Funct. Mater.* **2011**, *21*, 1643–1651.

[57] T. Lei, X. Chen, G. Pitner, H. S. P. Wong, Z. Bao, *J. Am. Chem. Soc.* **2016**, *138*, 802–805.

[58] L. Xu, M. Valášek, F. Hennrich, R. Fischer, M. M. Kappes, M. Mayor, *Macromolecules* **2021**, *54*, 4363–4374.

[59] F. Lemasson, J. Tittmann, F. Hennrich, N. Stürzl, S. Malik, M. M. Kappes, M. Mayor, *Chem. Commun.* **2011**, *47*, 7428–7430.

[60] W. J. Bodnaryk, K. Li, A. Adronov, *J. Polym. Sci.* **2020**, *58*, 1965–1972.

[61] D. Fong, J. Yeung, E. Meichsner, A. Adronov, *ACS Appl. Polym. Mater.* **2019**, *1*, 797–803.

[62] D. Fong, A. Adronov, *Macromolecules* **2017**, *50*, 8002–8009.

[63] D. Fong, A. Adronov, *Chem. Sci.* **2017**, *8*, 7292–7305.

[64] M. S. Dresselhaus, G. Dresselhaus, R. Saito, A. Jorio, *Phys. Rep.* **2005**, *409*, 47–99.

[65] S. K. Doorn, *J. Nanosci. Nanotechnol.* **2005**, *5*, 1023–1034.

[66] S. K. Doorn, D. A. Heller, P. W. Barone, M. L. Usrey, M. S. Strano, *Appl. Phys. A.* **2004**, *78*, 1147–1155.

[67] M. S. Strano, S. K. Doorn, E. H. Haroz, C. Kittrell, R. H. Hauge, R. E. Smalley, *Nano Lett.* **2003**, *3*, 1091–1096.

[68] D. A. Heller, P. W. Barone, J. P. Swanson, R. M. Mayrhofer, M. S. Strano, *J. Phys. Chem. B* **2004**, *108*, 6905–6909.

[69] D. Fong, G. M. Andrews, S. A. McNelles, A. Adronov, *Polym. Chem.* **2018**, *9*, 4460–4467.

[70] S. D. M. Brown, A. Jorio, M. S. Dresselhaus, G. Dresselhaus, *Phys. Rev. B* **2001**, *64*, 3–6.

[71] S. A. Mcnelles, J. L. Pantaleo, A. Adronov, *Org. Process Res. Dev.* **2019**, 2740–2745.

[72] H. Zhao, E. S. Sterner, E. B. Coughlin, P. Theato, *Macromolecules* **2012**, *45*, 1723–1736.

# Chapter 5

# Synthesis of a zwitterionic and cleavable polyfluorene for aqueous SWNT dispersion

**Abstract**

Non-covalent functionalization of SWNTs using conjugated polymers is a promising method to disperse nanotubes without altering their properties. However, the presence of the polymer backbone can impact the performance of the device by hindering the nanotube surface and therefore decreasing the conductivity. Here, we report our attempt to synthesize a cleavable fluorene-based polymer that contains an imine linker. The target polymer also bears amine groups at the end of the side-chains that can further react with 1,3-propanesultone to obtain a zwitterionic polymer to disperse SWNTs in water. The polymer can be synthesized via a polycondensation reaction of an aldehyde with an amine monomer. Therefore, both strategies to introduce either the aldehyde or the amine groups on the fluorene have been attempted but were not successful. However, control reactions on fluorene compounds that do not have any functional groups at the end of the side-chains were successful and confirmed that the presence of functional groups is not compatible with the formylation and the Buchwald-Hartwig reactions.

On the other hand, the synthesis of the non-cleavable analog polymer as a control sample was also attempted. Three strategies that consist of pre- or post-polymerization functionalization have been investigated. The first attempt was a post-functionalization of polyfluorene (PF-Br) to introduce the dimethylamine groups (PF-$NMe_2$) that would have further been reacted with 1,3-propanesultone. The second attempt was the Suzuki polycondensation of 6,6'-(2,7-dibromo-9H-fluorene-9,9-diyl)bis(N,N-dimethylhexan-1-amine) with

the diboronic ester analog monomer. Lastly, the introduction of the zwitterionic groups via copper-catalyzed azide-alkyne cycloaddition of polyfluorene PF-$N_3$ and sulfobetaine-alkyne was attempted. Unfortunately, none of these strategies resulted in the formation of the desired polymer.

## 5.1 Introduction

Among the dispersants used for the non-covalent functionalization of SWNTs, conjugated polymers (CPs) have received significant attention due to their facile structural tuning, such as the molecular weight, polymer backbone structure, and side-chain structure, to achieve different properties.[1–6] Although CPs are essential to disperse SWNTs, the presence of polymer backbone post-processing can be undesirable for SWNT-based devices as the polymer can hinder the surface of the nanotubes resulting in lower conductivity.[7] As a consequence, the removal of the polymer backbone after processing has received interest.[8–10] Different strategies have been employed that include polymers that can change their conformation,[11] supramolecular polymers,[9,12] as well as thermally-,[13] photo-[14,15] or acid-cleavable[8,10,16] polymers. Among the acid-cleavable polymers, polyimine-based polymers have recently attracted interest in the release of SWNTs. Indeed, imine bonds can be easily broken with a catalytic amount of acid.[17] As a result, some studies have shown the removable and recyclable advantages of these polymers.[8,10] Therefore, we were interested in the synthesis of a cleavable poly(*p*-phenyl-co-fluorene) containing imine linkers that would be used to disperse SWNT and fabricate

thin films. The resulting thin film would have been treated with acid to remove the polymer backbone and improve the conductivity.

In addition to its degradability, we wanted to develop a conjugated polymer that could be water-soluble. Usually, CPs are functionalized with hydrophobic side-chains resulting in SWNT dispersions in organic solvents such as THF or toluene.[18] However, these common solvents are not environmentally friendly. Therefore, developing a polymer-SWNT complex dispersed in water could be an alternative. To this end, our group has previously prepared polyfluorene derivatives containing azide groups in the side-chains. The resulting polyfluorenes were then functionalized using either copper-catalyzed azide–alkyne cycloaddition (CuAAC)[19,20] or strain-promoted azide–alkyne cycloaddition (SPAAC).[21,22] To achieve aqueous solubility, polyfluorene was functionalized pre- or post-SWNT dispersion with a series of polyethylene glycol (PEG) derivatives[19,21] or a mixture of PEG 5 kDa side-chains and small polar molecules such as D-mannose and zwitterionic sulfobetaine.[20] Post-dispersion functionalization of the polyfluorene with different PEG lengths showed that a minimal length of 2 kDa was required to effectively re-disperse SWNTs in water.[19] To minimize the side-chain length and explore other types of water-soluble CPs, we aimed to synthesize a zwitterionic CP. Zwitterionic CPs are polymers that contain both cationic and anionic groups and offer good solubility in polar solvents such as DMSO, water, and methanol.[23–26] In the literature, zwitterionic CPs have received attention in the development of devices such as polymer solar cells,[26] organic thin film transistors[24] and light-emitting

diodes.[23,25] They have also been investigated for biomedical applications, especially for their antifouling properties.[27–31]

Here, we report our attempt to synthesize two zwitterionic CPs to disperse SWNTs in water. The first polymer is a fluorene-based-conjugated polymer containing an imine linkage. The polymer also contains dimethylamine groups at the end of the side-chains that can then be functionalized with 1,3-propanesultone. The second polymer is the non-cleavable analog that can be used as a control sample.

## 5.2 Results and Discussion

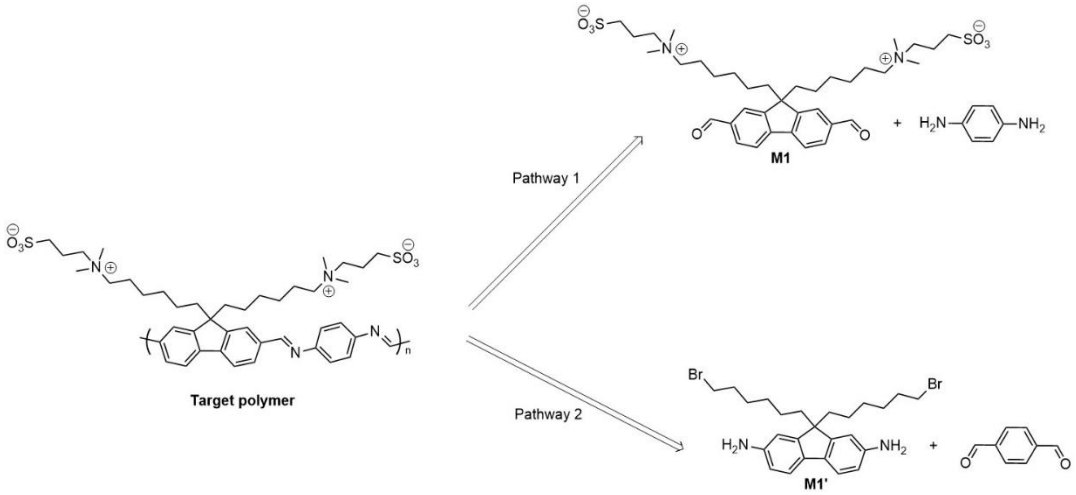


Scheme 5.1. Strategies for the synthesis of the target cleavable polymer.

**Cleavable polymer**. The first synthetic pathway to synthesize the polymer was via polycondensation of 9,9-bis(6-(dimethylamino)hexyl)-9H-fluorene-2,7-dicarbaldehyde with *p*-phenylenediamine. Commercial fluorene was first brominated using N-bromosuccinimide (NBS) to obtain precursor **1** (Scheme 5.2) followed by a phase-transfer alkylation with 1,6-dibromohexane to produce

compound **2**. The dimethyl amine groups were then introduced via nucleophilic substitution of compound **2** with dimethylamine to obtain compound **3**. Formylation was then performed on compound **3** with $^{n}$BuLi followed by the addition of DMF. Various conditions such as concentration and stoichiometry were investigated. Unfortunately, the desired compound **4** could not be isolated as too many unknown side reactions occurred. The reaction was also performed on compounds **1** and **2** resulting in similar observations. A control reaction was performed on 2,7-dibromo-9,9-dihexyl-9H-fluorene and showed the successful synthesis of the dicarbaldehyde product (see Supporting Information for details). We therefore concluded that the presence of the functional groups at the end of the side-chains results in too many side reactions that prevent the isolation of the desired product. As a consequence, another synthetic approach was investigated.

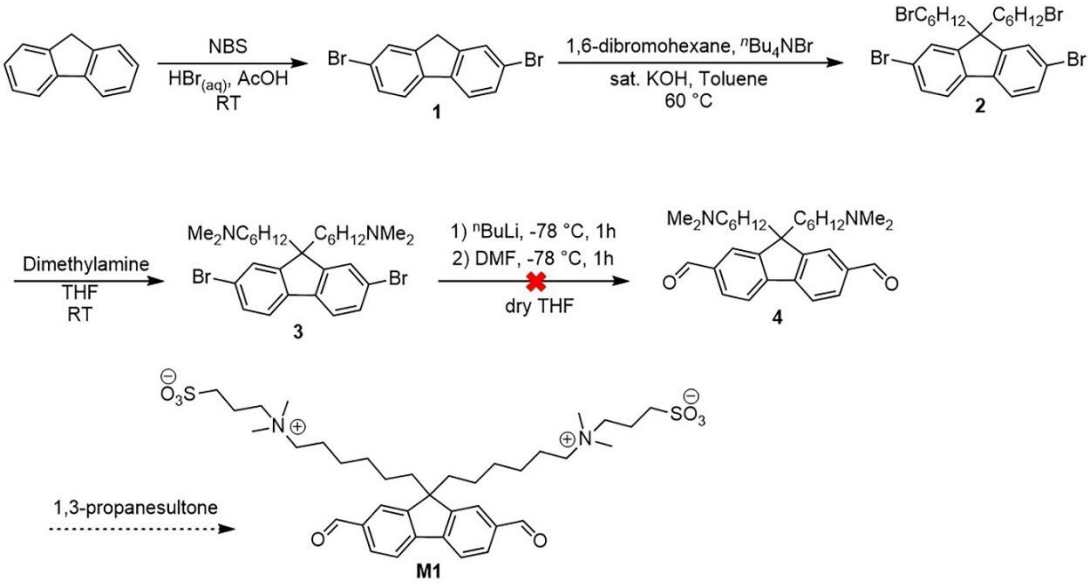


Scheme 5.2. Proposed synthesis of **M1.**

The second synthetic approach was to obtain the target polymer via polycondensation of 9,9-bis(6-bromohexyl)-9H-fluorene-2,7-diamine with terephtalaldehyde followed by post-polymerization functionalization to introduce the zwitterionic groups. The synthesis of the diamine monomer **M1'** was first attempted via a Buchwald-Hartwig cross-coupling reaction between compound **2** and benzophenone imine. The desired product could not be isolated mainly due to side reactions such as nucleophilic substitutions that occurred between benzophenone imine and the bromine at the end of the side-chains under basic conditions.

Another attempt was made with compound **1,** but it also resulted in too many unknown side reactions due to the acidic methylene protons on the fluorene bridge that can get deprotonated under basic conditions. Although this reaction has been attempted, this synthetic approach would have required additional steps such as the protection of the amine groups before the alkylation step and subsequent deprotection. Additionally, another method involving the use of nitro groups has been considered but it would have also required too many additional steps. Finally, a control reaction was performed with 2,7-dibromo-9,9-didodecyl-9H-fluorene and resulted in the successful synthesis of the diamine (see Supporting Information for details). This confirms that the presence of the functional groups at the end of the side-chains prevents the synthesis of our target compound. We therefore abandoned this approach.

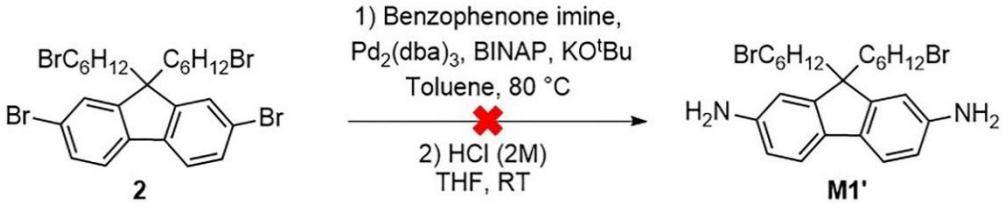


Scheme 5.3. Proposed synthesis of **M1'**.

**Control polymer**. Compound **2** was borylated using Miyaura conditions to afford diboronate **5.** Monomers **2** and **5** were then copolymerized using Suzuki polycondensation to obtain the homopolymer **PF-Br** (see Supporting Information). Gel permeation chromatography (GPC) revealed an $M_n$ of 39 kDa and a dispersity (Đ) of 2.9. The first strategy to obtain the control polymer was the functionalization of **PF-Br** via a nucleophilic substitution with dimethylamine. A precipitate was obtained during the reaction and could not be dissolved in either cold or hot organic solvents such as THF, toluene, DMSO, or DMF. This is most likely due to crosslinking reaction that can occur between the side-chains.

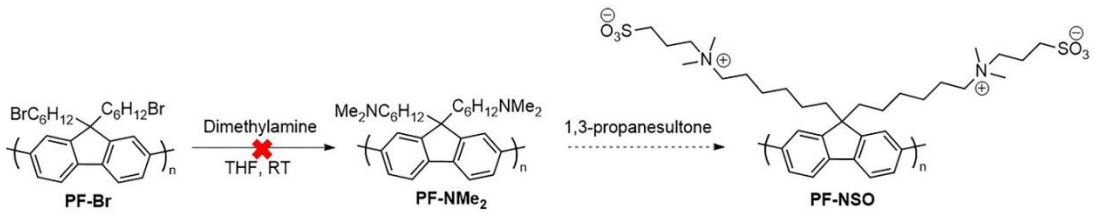


Scheme 5.4. Proposed synthesis of **PF-NMe$_2$** via post-polymerization functionalization of **PF-Br**

Since the post-polymerization functionalization was not successful, pre-polymerization functionalization was done to introduce the amine groups (Scheme 5.5). The boronate ester **5** was therefore treated with dimethylamine

to obtain compound **6** (See Supporting Information). Monomers **3** and **6** were then copolymerized using Suzuki polycondensation to obtain **PF-NMe$_2$**. The molecular weight could not be monitored using gel permeation chromatography (GPC) due to the adsorption of the polymer onto the stationary phase of the GPC column. UV-Vis absorption spectroscopy was therefore used during the reaction to confirm the formation of the polymer. As shown in Figure 5.1, a new peak at 370 nm was observed after 24h of reaction at 80 °C. A yellow solid was isolated and characterized by $^1$H-NMR spectroscopy. As an alternative to GPC, we used diffusion-ordered NMR spectroscopy (DOSY) to determine the average molecular weight.[32,33] DOSY is a tool that provides the diffusion coefficients of molecules which is related to their hydrodynamic radius ($r_h$) and the molecular weight ($M_w$).[33,34] $M_w$ using DOSY can be determined using calibration curves due to the linear correlation between the logarithm of the diffusion coefficients (log D) and the molecular weights (log $M_w$).[33] Recently, Junkers et al. have proposed a method of calibration using polystyrene (PS) and poly(ethylene glycol) standards for a variety of solvents.[34] We, therefore, followed their procedure to create a calibration curve using PS standards. DOSY was then performed on **PF-NMe$_2$** to obtain the diffusion coefficient which was then used in Equation 5.1 (see Supporting Information for details). The calculated $M_w$ of **PF-NMe$_2$** was 105 kDa. **PF-NMe$_2$** was then treated with 1,3-propanesultone in THF to obtain the zwitterionic polymer. A precipitate was obtained and isolated. The solid could not be characterized because it was only partially soluble in cold or hot organic and aqueous solvents. We also tried to dissolve the compound into a mixture of THF/$H_2O$ but it resulted in a cloudy

dispersion suggesting that some aggregation occurs. A quick experiment using a laser pointer to test the Tyndall Effect confirmed the presence of aggregation as the laser beam was observed through the solution. However, since the reaction could not be characterized, we could not be sure that the reaction went to completion. The solubility issue could be due to a partially functionalized polymer.

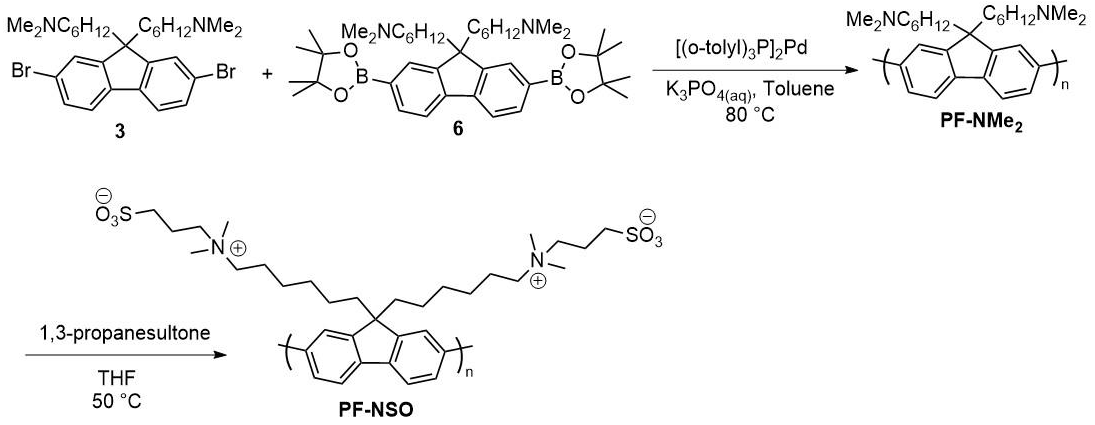


Scheme 5.5. Proposed synthesis of **PF-NSO**.

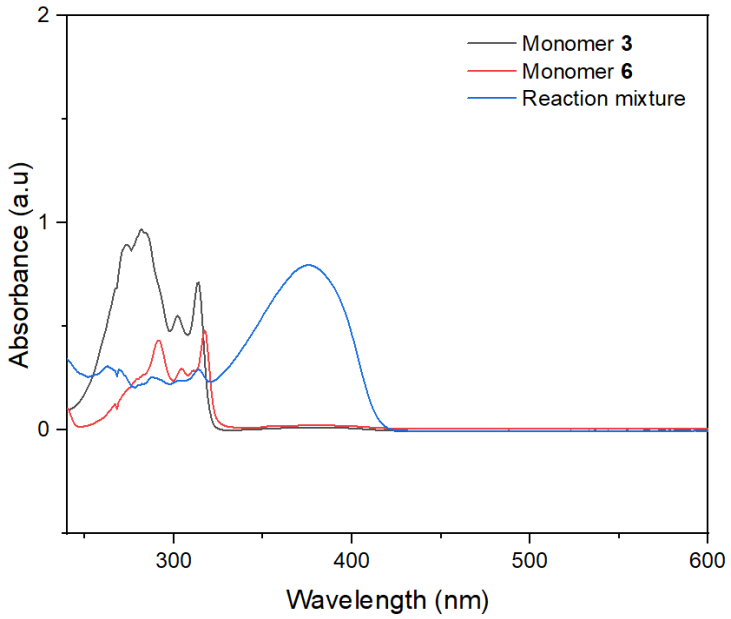


Figure 5.1. UV-Vis absorbance spectra overlays of monomer **3**, **6** and the reaction mixture of **PF-NSO.**

The last strategy used to synthesize the control polymer was the functionalization of PF-$N_3$ with sulfobetaine-alkyne via CuAAC. In comparison to the previous strategy, the reaction can be monitored by infrared spectroscopy (IR) via the disappearance of the azide stretch at 2090 $cm^{-1}$. **PF-$N_3$** was first prepared via a reaction between **PF-Br** and $NaN_3$ in the presence of $^{n}Bu_4NBr$. The substitution was confirmed via $^{1}$H-NMR spectroscopy with the presence of alkyl azides (3.15 ppm) in **PF-$N_3$** and the disappearance of the signal corresponding to the alkyl bromides (3.31 ppm) in **PF-Br**. Sulfobetaine-alkyne was prepared using dimethylamino-1-propyne and 1,3-propanesultone. **PF-$N_3$** was then functionalized with sulfobetaine-alkyne via CuAAC. The reaction was monitored via IR spectroscopy until the disappearance of the azide stretch. Similar to our previous attempt, the solid could not be fully dissolved into organic

and aqueous solvents and resulted in a cloudy suspension. The aggregation is most likely due to the strong dipole-dipole interactions between the zwitterionic groups.[29] Salts such as NaCl and KBr have also been added to the solution to improve the solubility but were unfortunately unsuccessful. We have considered this solution because it has been shown that zwitterionic polymer chains are more soluble in salt solution than in pure water.[35] Indeed, in pure water, zwitterionic chains tend to aggregate due to their strong interactions including dipole-dipole, charge-dipole and charge-charge interactions.[36] In contrast, in a salt solution, the presence of counterions weakens those interactions resulting in an extension of the chain and better solubility.[29,35–37] This effect called anti-polyelectrolyte depends on salt concentration and ion types.[36,37] Moreover, the structure of the zwitterionic groups especially the chain spacer length also plays an important role in the solubility.[29] Further investigations could have been performed to explore this but this would have been counterproductive relative to our initial goal of developing a printable ink, and we therefore decided to abandon this approach.

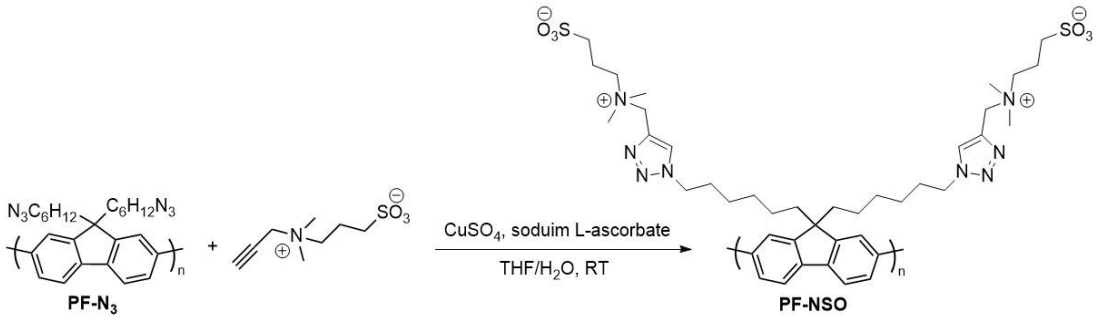


Scheme 5 6. Proposed synthesis to obtain **PF-NSO** via CuAAC.

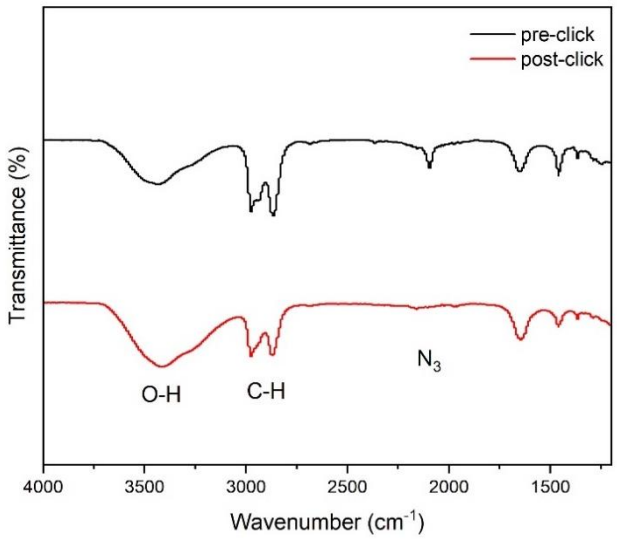


Figure 5.2. FT-IR overlay of the click reaction between **PF-$N_3$** and sulfobetaine-alkyne

## 5.3 Conclusion

Different strategies have been attempted to synthesize a water-soluble and degradable zwitterionic functionalized conjugated polymer. The target polymer was a fluorene-based-conjugated polymer containing imine linkages and bearing amine groups at the end of the side-chain that can then react with 1,3-propanesultone. Unfortunately, the presence of the functional groups at the end of the side-chain was incompatible with the introduction of either the aldehyde or amine groups on the fluorene monomer. On the other hand, the synthesis of a non-cleavable zwitterionic analog has also been investigated. Strategies including pre- and post-polymerization functionalization have been attempted. Although our last attempt showed a complete functionalization of PF-$N_3$ with sulfobetaine-alkyne via CuAAC, the resulting polymer was only partially soluble in organic, aqueous and a mixture of organic/aqueous solvents

due to aggregation. Despite the addition of salts, the resulting polymer remained insoluble in water.

## 5.4 Supporting Information

### 5.3.1 General

All reagents were purchased from commercial chemical suppliers and used as received. Flash chromatography was performed using a CombiflashRF200 by Teledyne ISCO. Unless otherwise noted, compounds were monitored using a variable wavelength detector at 254 nm. Solvent amounts used for gradient or isocratic elution were reported in column volumes (CV). Columns were prepared in Biotage® SNAP KP-Sil cartridges using 40 – 63 µm silica or 25 – 40 µm silica purchased from Silicycle. $^{1}$H-NMR spectra were recorded on Bruker Avance 600 MHz and shift-referenced to the residual solvent resonance. DOSY data were analyzed with Dynamic Centre 2.8.2. Polymer molecular weights and dispersities were analyzed (relative to polystyrene standards) via GPC using a Waters 2695 Separations Module equipped with a Waters 2414 refractive index detector and a TSKgel SuperHZM-N with 3 µm particle diameter. THF with 2% acetonitrile was used as the eluent at a flow rate of 0.3 mL/min.

## 5.3.2 Synthesis

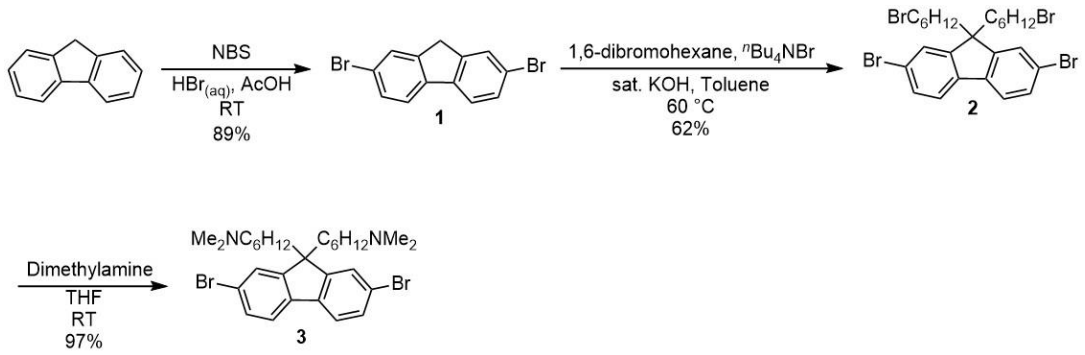


Scheme 5.7. Synthesis of compounds **1**, **2** and **3**.

Compounds **1** and **2** were prepared following literature procedures.[22]

**6,6'-(2,7-dibromo-9H-fluorene-9,9-diyl)bis(N,N-dimethylhexan-1-amine) (3)**[38]

A 100 mL round bottom flask equipped with a stir bar was charged with **2** (3 g, 4.6 mmol) in 15 mL of dry THF. Dimethylamine (2M in THF) (2.7 g, 60 mmol) was added dropwise. The reaction was stirred at RT overnight. Water (20 mL) was added to the reaction mixture and extracted with dichloromethane, washed with water and brine. The organic phase was then dried with $MgSO_4$ and concentrated to give **3** as a brown solid (2.6 g, 97%). $^1$H NMR (600 MHz, $CDCl_3$): δ 7.51 (m, 2H), 7.45-7.42 (m, 4H), 2.16 (s, 12H), 2.13 (m, 4H), 1.92-1.89 (m, 4H), 1.07 (m, 8H), 0.61-0.55 (m, 4H).

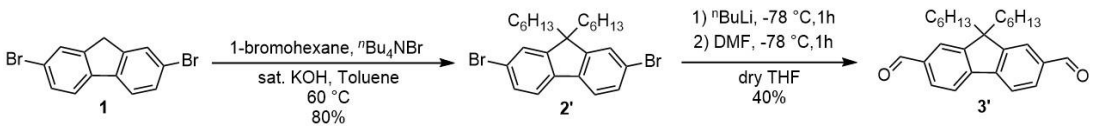


Scheme 5.8. Synthesis of the control formylation reaction.

**9,9-dihexyl-9H-fluorene-2,7-dicarbaldehyde (2')**[38]

A 50 mL round bottom flask equipped with a stir bar was charged with **1** (2 g, 6.2 mmol), 1-bromohexane (10 g, 62 mmol), $^{n}Bu_4NBr$ (0.4 g, 10 mmol), toluene (12 mL), and sat. $KOH_{(aq)}$ (12 mL). The reaction mixture was heated to 60 °C and stirred vigorously for 2 h under a nitrogen atmosphere. The biphasic mixture was allowed to separate, and the organic layer was isolated. The aqueous phase was extracted twice with diethyl ether (2 x 30 mL). The organic extracts were combined and concentrated *in vacuo*. Excess 1-bromohexane was removed using vacuum distillation (1 mbar, 80 °C) to obtain a green solid. The crude product was purified by flash chromatography (40 g column, 100% Hexanes) to afford **2'** as a yellowish solid (2.4 g, 80%). $^{1}$H-NMR (600 MHz; $CDCl_3$): δ 7.52 (m, 2H), 7.46-7.44 (m, 4H), 1.93-1.90 (m, 4H), 1.14-1.02 (m, 11H), 0.78 (t, *J* = 7.3 Hz, 6H), 0.61-0.56 (m, 4H).

**9,9-dihexyl-9H-fluorene-2,7-dicarbaldehyde (3')**[39]

A 500 mL round bottom flask equipped with a stir bar was charged with **2'** (1.85 g, 3.8 mmol) in 188 mL of dry THF. The solution was cooled down to - 78 °C and $^{n}$BuLi (2.5 M in Hexanes) (1.4 g, 23.0 mmol) was added dropwise. The solution was stirred for 1 h at -78 °C under $N_2$ followed by the addition of dry DMF ( 2.6 g, 38.0 mmol). The mixture was stirred for 30 min then allowed to warm up to RT and stirred for an additional 30 min. The reaction was quenched with water (40 mL) and extracted with $Et_2O$ (3 x 75 mL). The combined organic layers were then washed with water, brine and dried with $MgSO_4$. The crude product was purified by flash chromatography Hex/EtOAc (0% to 15%) to give

a colourless solid (0.6 g, 40%). $^1$H-NMR (600 MHz; $CDCl_3$): δ 10.10 (s, 2H), 7.94-7.90 (m, 6H), 2.08-2.05 (m, 4H), 1.09-0.99 (m, 12H), 0.74 (t, *J* = 7.3 Hz, 6H), 0.55 (m, 4H).

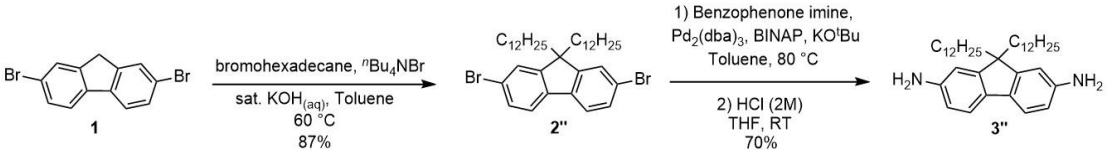


Scheme 5.9. Synthesis of the control Buchwald-Hartwig reaction.

Compound **2''** was synthesized following the literature procedure.[21]

**9,9-didodecyl-9H-fluorene-2,7-diamine (3'')**[8]

A 25 mL oven-dried Schlenck tube equipped with a stir bar was charged with $Pd_2(dba)_3$ (14 mg, 15.0 µmol, 0.5 mol%) and BINAP (29 mg, 46.2 µmol, 1.5 mol%), and purged with $N_2$. To the flask were added **2''** (1 g, 3.1 mmol), benzophenone imine (0.7 g, 4.0 mmol), KOtBu (0.5 g, 4.2 mmol) and toluene (8 mL). The reaction mixture was heated to 80 °C and stirred overnight. The reaction was diluted with DCM (20 mL), filtered through a celite plug and washed with DCM). The crude product was hydrolyzed with HCl (2M, 3 equiv.) in 1 mL of THF. The product was purified via flash chromatography Hex/$Et_2O$ 0% to 60 % to give a brown oil (0.55 g, 70%). $^1$H-NMR (600 MHz; $CDCl_3$): δ 7.38-7.29 (m, 2H), 6.74-6.50 (m, 4H), 3.74-3.57 (m, 4H), 1.84-1.79 (m, 4H), 1.30-1.01 (m, 36H), 0.90-0.86 (m, 6H), 0.66-0.63 (m, 4H).

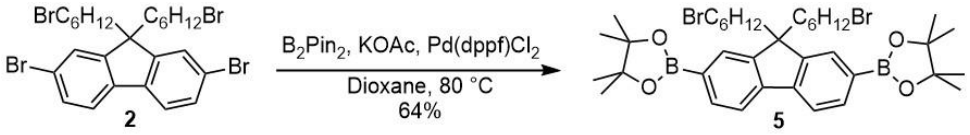


Scheme 5.10. Synthesis of compound **5**

Compound **5** was prepared following the literature procedure.[20]

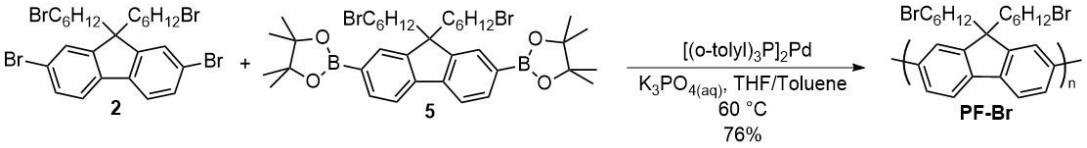


Scheme 5.11. Synthesis of **PF-Br**.

**Poly(bis(6-bromohexyl)fluorene) (PF-Br)**[20]

A Schlenk tube equipped with a stir bar was charged with **2** (0.5 g, 0.8 mmol), 5 (0.57 g, 0.8 mmol), THF (3.8 mL), toluene (3.8 mL), and 3M $K_3PO_{4(aq)}$ (7.7 mL). The reaction mixture was degassed by three freeze–pump–thaw cycles. The biphasic mixture was frozen under liquid nitrogen, then $[(o\text{-tol})_3P]_2Pd$ (8 mg, 0.1 µmol) was added under a positive pressure of nitrogen. The Schlenk tube was evacuated and backfilled three times, and the reaction was vigorously stirred at 60 °C for 3 h. The phases were allowed to separate, and the organic layer was filtered through a plug of celite and neutral alumina (1:1 composition). The plug was washed with THF, and the filtrate was concentrated *in vacuo*. The crude polymer was precipitated in MeOH (~ 150 mL) and filtered to afford **PF-Br** as a yellow solid (0.57 g, 76%). $^1$H–NMR (600 MHz; $CDCl_3$): δ 7.86 (m, 2H), 7.73–7.67 (m, 4H), 3.31–3.28 (m, 4H), 2.15 (m, 4H), 1.71–1.69 (m, 4H), 1.28–1.25 (m, 4H), 1.18 (m, 4H), 0.88 (m, 4H).

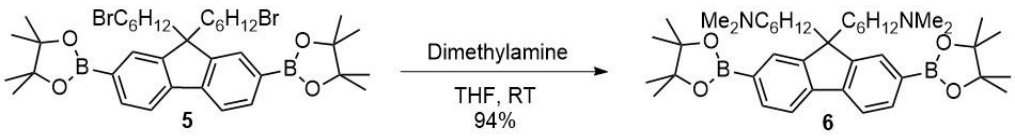


Scheme 5.12. Synthesis of monomer **6**.

**6,6'-(2,7-bis(4,4,5,5-tetramethyl-1,3,2-dioxaborolan-2-yl)-9H-fluorene-9,9-diyl)bis(N,N-dimethylhexan-1-amine) (6)**

A 25 mL round bottom flask equipped with a stir bar was charged with **5** (0.75 g, 1.0 mmol) in 8 mL of dry THF. Dimethylamine (2 M in THF) (0.68 g, 15.1 mmol) was added dropwise. The reaction was stirred at RT overnight. Water (8 mL) was added to the reaction mixture and extracted with dichloromethane, which was washed with water and brine. The organic phases were then dried with $MgSO_4$ and concentrated to give a brown solid (0.63 g, 94%). $^1$H-NMR (600 MHz; $CDCl_3$): δ 7.80-7.79 (m, 2H), 7.72-7.70 (m, 4H), 2.15 (s, 12H), 2.11 (m, 4H), 2.01-1.98 (m, 4H), 1.39 (s, 24H), 1.28-1.22 (m, 5H), 1.06-1.01 (m, 8H), 0.57-0.52 (m, 5H).

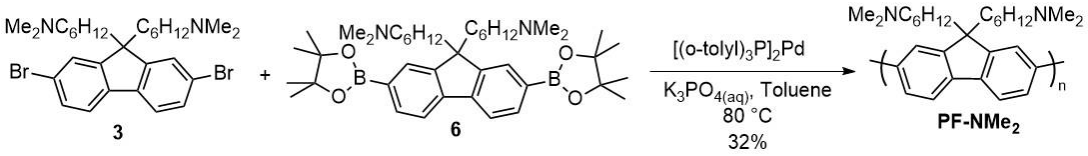


Scheme 5.13. Synthesis of **PF-NMe$_2$**.

**Polymer PF-NMe$_2$**

A Schlenk tube equipped with a stir bar was charged with **3** (0.43 g, 0.74 mmol), **6** (0.5 g, 0.74 mmol), toluene (7.4 mL), and 3M $K_3PO_{4(aq)}$ (7.4 mL). The reaction mixture was degassed by three freeze–pump–thaw cycles. The biphasic

mixture was frozen under liquid nitrogen, then $[(o\text{-tolyl})_3P]_2Pd$ (30 mg, 37.1 µmol) was added under a positive pressure of nitrogen. The Schlenk tube was evacuated and backfilled three times, and the reaction was vigorously stirred at 80 °C for 24 h. The phases were allowed to separate, and the organic layer was filtered through a plug of celite and neutral alumina (1:1 composition). The plug was washed with THF, and the filtrate was concentrated *in vacuo*. The crude polymer was precipitated in MeOH (~ 150 mL) and filtered to afford **PF-NMe$_2$** as a yellow solid (0.2 g, 32%). $^1$H-NMR (500 MHz; $CDCl_3$): δ 7.88-7.79 (m, 2H), 7.74-7.64 (m, 4H), 2.14 (s, 12H), 1.78-1.73 (m, 4H), 1.37-1.29 (m, 4H), 1.21-1.10 (m, 8H), 0.92-0.75 (m, 4H).

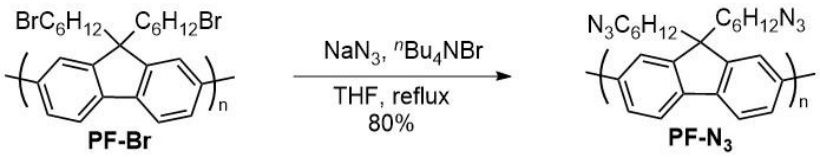


Scheme 5.14. Synthesis of **PF-N$_3$**.

**Poly(bis(6-azidohexyl)fluorene) (PF-N$_3$)**[20]

A round bottom flask equipped with a stir bar was charged with **PF-Br** (0.4 g, 0.81 mmol), $NaN_3$ (0.53 g, 8.1 mmol), $^n$Bu$_4$NBr (0.53 g, 1.3 mmol), and THF (82 mL). The reaction mixture was heated to reflux for 24 h. The reaction mixture was filtered through a neutral alumina plug, washed with THF, and precipitated in MeOH (~ 150 mL) to afford **PF-N$_3$** (0.26 g, 80%).$^1$H–NMR (600 MHz; $CDCl_3$): δ 7.87**–**7.85 (m, 2H), 7.72**–**7.68 (m, 4H), 3.16**–**3.14 (m, 4H), 2.15 (m, 4H), 1.46, 1.40 (m, 4H), 1.25**–**1.20 (m, 8H), 0.88**–**0.83 (m, 4H).


Scheme 5.15. Synthesis of **sulfobetaine-alkyne**.

Sulfobetaine-alkyne has been prepared following the literature procedure.[20]

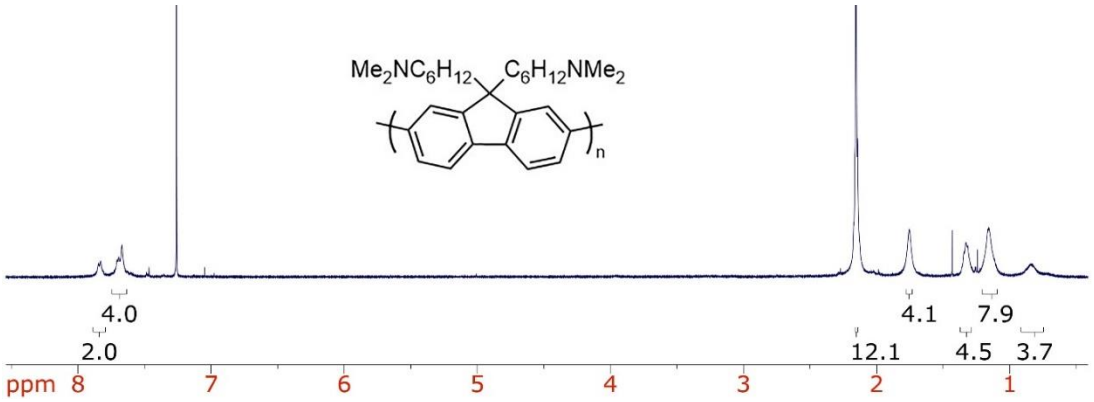


Figure 5.3. 1H-NMR of **PF-NMe2** in $CDCl_3$.

**DOSY calculations**

Equation 5.1:[34]

$$\log(D) + \log(\eta) = \log(c) - v\log(M)$$

Where D is the diffusion coefficient, Ƞ is the solvent bulk viscosity, c and v are proportionality parameters and M is the molecular weight. The calibration curve was created using PS standards with a molecular weight of 106 kDa, 66 kDa and 30 kDa and the new equation was:

$$\frac{\log(D) + \log(0.563) + 9.1201}{-0.1029} = \log(M)$$

With a diffusion coefficient of 4.10 x $10^{-10}$ $m^2.s^{-1}$, the molecular weight of **PF-$NMe_2$** is 105 kDa.

### 5.4 References

[1] W. Gomulya, G. D. Costanzo, E. J. F. De Carvalho, S. Z. Bisri, V. Derenskyi, M. Fritsch, N. Fröhlich, S. Allard, P. Gordiichuk, A. Herrmann, et al., *Adv. Mater.* **2013**, *25*, 2948–2956.

[2] S. K. Samanta, M. Fritsch, U. Scherf, W. Gomulya, S. Z. Bisri, M. A. Loi, *Acc. Chem. Res.* **2014**, *47*, 2446–2456.

[3] P. Imin, M. Imit, A. Adronov, *Macromolecules* **2011**, *44*, 9138–9145.

[4] P. Imin, F. Cheng, A. Adronov, *Polym. Chem.* **2011**, *2*, 1404–1408.

[5] N. A. Rice, A. V Subrahmanyam, S. E. Laengert, A. Adronov, *Polym. Chem.* **2015**, *53*, 2510–2516.

[6] D. Fong, W. J. Bodnaryk, N. A. Rice, S. Saem, J. M. Moran-Mirabal, A. Adronov, *Chem. Eur. J.* **2016**, *22*, 14560–14566.

[7] T. Lei, I. Pochorovski, Z. Bao, *Acc. Chem. Res.* **2017**, *50*, 1096–1104.

[8] L. Xu, M. Valášek, F. Hennrich, R. Fischer, M. M. Kappes, M. Mayor, *Macromolecules* **2021**, *54*, 4363–4374.

[9] F. Toshimitsu, N. Nakashima, *Nat. Commun.* **2014**, *5*, 1–9.

[10] T. Lei, X. Chen, G. Pitner, H. S. P. Wong, Z. Bao, *J. Am. Chem. Soc.* **2016**, *138*, 802–805.

[11] S. Liang, Y. Zhao, A. Adronov, *J. Am. Chem. Soc.* **2014**, *136*, 970–977.

[12] I. Pochorovski, H. Wang, J. I. Feldblyum, X. Zhang, A. L. Antaris, Z. Bao, *J. Am. Chem. Soc.* **2015**, *137*, 4328–4331.

[13] Z. Li, J. Ding, C. Guo, J. Lefebvre, P. R. L. Malenfant, *Adv. Funct. Mater.* **2018**, *28*, 1705568.

[14] F. Lemasson, J. Tittmann, F. Hennrich, N. Stürzl, S. Malik, M. M. Kappes, M. Mayor, *Chem. Commun.* **2011**, *47*, 7428–7430.

[15] W. J. Bodnaryk, K. Li, A. Adronov, *J. Polym. Sci.* **2020**, *58*, 1965–1972.

[16] W. Z. Wang, W. F. Li, X. Y. Pan, C. M. Li, L. Li, Y. G. Mu, J. A. Rogers, M. B. Chan-park, *Adv. Funct. Mater.* **2011**, *21*, 1643–1651.

[17] M. E. Belowich, J. F. Stoddart, *Chem. Soc. Rev.* **2012**, *41*, 2003–2024.

[18] D. Fong, A. Adronov, *Chem. Sci.* **2017**, *8*, 7292–7305.

[19] D. Fong, G. M. Andrews, A. Adronov, *Polym. Chem.* **2018**, *9*, 2873–2879.

[20] D. Fong, J. Yeung, E. Meichsner, A. Adronov, *ACS Appl. Polym. Mater.* **2019**, *1*, 797–803.

[21] D. Fong, J. Yeung, S. A. Mcnelles, A. Adronov, *Macromolecules* **2018**, *51*, 755–762.

[22] D. Fong, G. M. Andrews, S. A. McNelles, A. Adronov, *Polym. Chem.* **2018**, *9*, 4460–4467.

[23] C. Duan, L. Wang, K. Zhang, X. Guan, F. Huang, *Adv. Mater.* **2011**, *23*, 1665–1669.

[24] U. Scherf, *Angew. Chem., Int. Ed.* **2011**, 5016–5017.

[25] C. Duan, K. Zhang, X. Guan, C. Zhong, H. Xie, F. Huang, J. Chen, J. Peng, Y. Cao, *Chem. Sci.* **2013**, 1298.

[26] W. Zhang, C. Song, Y. Li, X. Liu, X. Wang, *Org. Electron.* **2017**, *47*, 94–101.

[27] T. Goda, Y. Miyahara, *Langmuir* **2019**, 1126–1133.

[28] H. Wu, C.-J. Lee, H. Wang, Y. Hu, M. Young, Y. Han, F.-J. Xu, H. Cong, G. Cheng, *Chem. Sci.* **2018**, 2540–2546.

[29] C. H. Lin, S. C. Luo, *Langmuir* **2022**, *38*, 7383–7399.

[30] B. Cao, Q. Tang, L. Li, C.-J. Lee, H. Wang, Y. Zhang, H. Castaneda, G. Cheng, *Chem. Sci.* **2015**, 782–788.

[31] B. Cao, C.-J. Lee, Z. Zeng, F. Cheng, F. Xu, H. Cong, Gang Cheng, *Chem. Sci.* **2016**, 1976–1981.

[32] P. Groves, *Polym. Chem.* **2017**, 6700–6708.

[33] W. Li, H. Chung, J. A. Johnson, R. H. Grubbs, *Macromolecules* **2012**, 9595–9603.

[34] P. Voorter, A. Mckay, J. Dai, O. Paravagna, N. R. Cameron, *Angew. Chem.* **2022**, e202114536.

[35] C. Lin, S. Luo, *Langmuir* **2021**, 12476–12486.

[36] S. Xiao, Y. Zhang, M. Shen, F. Chen, P. Fan, M. Zhong, B. Ren, J. Yang, J. Zheng, *Langmuir* **2018**, 97–105.

[37] K. Qu, Z. Yuan, Y. Wang, Z. Song, X. Gong, Y. Zhao, Q. Mu, Q. Zhan, W.

Xu, L. Wang, *ChemPhysMater* **2022**, *1*, 294–309.

[38] D. Tuncel, M. Artar, S. B. Hanay, *J. Polym. Sci. Part A Polym. Chem.* **2010**, *48*, 4894–4899.

[39] Y. Z. Su, J. T. Lin, Y. Tao, C. Ko, S. Lin, S. Sun, *Chem. Mater.* **2002**, 1884–1890.

# Chapter 6

# Overall conclusions and recommendations for future work

## 6.1 General conclusions

With their extraordinary electronic, mechanical, and optical properties, single-walled carbon nanotubes have received extensive interest in materials science for multiple applications. However, the heterogeneous mixture of semiconducting and metallic species as well as non-SWNT impurities generated during the production of SWNTs limit the incorporation of SWNTs into devices. Different techniques that involve covalent and non-covalent functionalization of SWNTs have been developed. Among them, the use of conjugated polymers has been a promising alternative to purify, process and extract specific SWNTs. This method has also proven to be a scalable and less expensive method for the purification of SWNTs. Conjugated polymers can be easily tuned to disperse specific SWNT species and obtain solubility in target solvents. Therefore, they are suitable as a purification technique for the fabrication of SWNT-based devices, especially in the area of printed electronics. However, the polymer backbone and the long and non-conductive side-chains could have an impact on the performance of the SWNT device by preventing good contact between the nanotubes.

The objective of this thesis was to develop different cleavable polymer-SWNT complexes to maximize the potential performance of printed devices post-precessing. We were also interested in the development of SWNT dispersions in green solvents that are compatible with printing processes such as inkjet printing.

In Chapter 2, we functionalized a polyfluorene with thermally cleavable side-chains and we investigated the impact on the conductivity of polymer-SWNT thin films upon the removal of the side-chains. The thermally cleavable side-chains used contain a carbonate linker which cleaves by decarboxylation when heating. We showed that the conductivity was an order of magnitude higher for the cleavable sample in comparison to the control sample after the removal of the side-chains. Moreover, to investigate the dispersion of SWNTs using green solvents, we functionalized the polyfluorene with larger and cleavable side-chains. We obtained stable SWNT dispersions in two green solvents: trimethylethylene glycol monomethyl ether and tetraethylene glycol dimethyl ether which are both suitable for inkjet printing.

In Chapter 3, we investigated a different type of side-chain and functionalized the polyfluorene with photocleavable side-chains. We were also interested in examing the impact on the conductivity after side-chain removal. The photocleavable side-chains contain an ortho-nitrobenzyl ether linker that can be cleaved by irradiation with a 365 nm light. We irradiated the polyfluorene-SWNT complex overnight which resulted in the precipitation of the nanotubes. Characterization using UV-Vis-NIR absorbance spectroscopy showed a broad absorption peak of the nanotubes indicating that the loss of side-chains eliminates steric stabilization of the nanotube dispersion. Despite the effective cleavage, conductivity measurements could not be performed. However, these results represent a proof-of-concept that can be used for the fabrication of SWNT devices.

In Chapter 4, we synthesized a functionalized and photocleavable polymer that contains a fluorene and an ortho-nitrobenzyl ether unit. The backbone of the polymer degrades when exposed to a 365 nm UV light and can release SWNTs. Characterization post-irradiation showed a decrease of 56% in polymer fraction from the surface of the nanotube. Functionalization of the polymer with hydrophilic polyethylene glycol side-chains produced SWNT dispersions in water. However, we could not demonstrate the SWNTs release concept in this solvent.

Finally, we attempted to synthesize a water-soluble and degradable zwitterionic functionalized conjugated polymer. The target cleavable polymer was a fluorene-based-conjugated polymer containing an imine linkage that can be easily cleaved by the addition of an acid. It also bears amine groups at the end of the side-chain that could react with 1,3-propanesultone to obtain a water-soluble degradable conjugated polymer. We also attempted to synthesize the non-cleavable analog polymer. We investigated different synthetic pathways but unfortunately, we could not achieve our goal. These results show that the development of SWNTs dispersion using water-soluble conjugated polymer remains challenging.

### 6.2 Recommendations for future work

As investigated in Chapter 2, the removal of the thermally cleavable side-chains leads to an order of magnitude higher conductivity than the control sample. This shows that this concept is a good alternative and can improve the performance of potential SWNT-based devices. However, the temperature (170

°C) and the heating time (17 h) are high. Moreover, the conductivity achieved is relatively low compared to traditional materials such as silver. After the removal of the thermally cleavable side-chains, small alkyl fragments remain at the surface of the nanotubes. Therefore, it would be interesting to develop cleavable side-chains that can be cleaved at the polymer backbone under milder conditions. At the time of this thesis, some projects in the Adronov group focus on this concept using self-immolative side-chains and polymer backbones. In addition, the polyfluorene used in this work does not selectively disperse specific SWNTs which prevents the use of these polymer-SWNT dispersions for devices. Since the improvement of conductivity was the main goal, the development of a conjugated polymer that can selectively disperse m-SWNTs and be degradable would be ideal.

As previously mentioned, most studies involve the dispersion of SWNTs in organic solvents such as THF and toluene. However, the need to minimize our environmental impact becomes imperative. We therefore should develop more environmentally friendly alternatives. This includes using green solvents to disperse SWNTs. Although I was able to obtain stable dispersion in two green solvents, my attempts at synthesizing water-soluble conjugated polymers highlight the current challenge. In Chapter 5, the target polymer was obtained but it was not soluble in aqueous solvents due to the aggregation of the zwitterionic groups. Redesigning the polymer by using a longer spacer between the two charged groups might reduce these aggregations and improve solubility.

Lastly, our polymers are mostly synthesized by Pd-catalyzed cross-coupling reactions. In the future, alternative techniques such as direct arylation polymerization could be envisaged to avoid the use of catalysts and make the overall synthesis process greener.